

Diss. ETH No. 21286

Prediction of Long Time Creep Rupture Properties of Welded Joints Using the Results of Short Duration Creep Crack Incubation Tests

A dissertation submitted to the
ETH Zurich

for the degree of
Doctor of Sciences

presented by
EHSAN HOSSEINI
MSc in Materials Engineering,
Sharif University of Technology, Tehran

born 2 May 1985
citizen of Iran

accepted on the recommendation of
Prof. Dr. E. Mazza, examiner
Dr. S.R. Holdsworth, coexaminer
Prof. Dr. R. Hurst, coexaminer

2013

Acknowledgement

I wish to express my sincere gratitude to

- Foremost, my advisers Dr. Stuart Richard Holdsworth and Prof. Dr. Edoardo Mazza for the continuous support of my study and research, for their patience, motivation, enthusiasm, and immense knowledge. Their guidance helped me in all the time of research and writing of this thesis.
- My co-examiners, Prof. Dr. Roger Hurst for carefully reviewing this thesis.
- All my colleagues at the laboratory of Mechanics for Modelling and Simulation and High Temperature Integrity group at Empa for support and good discussions, especially: Freddy Bürki, Michael Straessle, Dr. Thomas Mayer, Dr. Son Pham Minh, Erica Vacchieri, Dr. Marko Radosavljevic, Frank Ehrhardt, Benedikt Rentsch, Marco Frigerio, Wentao Yan, Dr. Valliappa Kalyanasundaram.
- All my friends all over the world helping me stay sane through these difficult years.
- Last but not least, my family, my parents for giving birth to me at the first place and supporting me spiritually throughout my life. My wife, Fereshteh, whose love and encouragement allowed me to finish this journey. She already has my heart, so I will just give her a heartfelt "thanks".

I thank all those who have helped me directly or indirectly in the successful completion of my thesis. Anyone missed in this acknowledgement is also thanked.

This work is dedicated to my family.

August 5, 2013
Ehsan Hosseini

Abstract

The aim of this research project is to examine the applicability of the LICON methodology for predicting the long-time creep rupture strength of a dissimilar metal weld.

The LICON methodology is an approach for predicting the lifetime of materials under creep loading conditions. The LICON method predicts long-time uniaxial creep strength using the results from several short duration creep crack incubation tests in conjunction with the outcome of a mechanical analysis on the testpiece (e.g. a reference stress solution). In the late 1990s, this method was successfully applied to advanced 9%Cr pipe steels (including their welded joints) and later, reports on applicability of the method for a high creep strength 1CrMoV were published.

This study has re-examined the previous application of the LICON methodology for 9%Cr and 1CrMoV steels. It has shown that application of the original LICON method (based on reference stress solutions) for certain materials is not appropriate. Application of reference stress solutions is limited to materials which achieve complete stress redistribution before the onset of crack extension (e.g. for advanced 9%Cr pipe steels). For 'non-reference stress' materials (creep brittle, notch sensitive materials such as high creep strength 1CrMoV) crack initiation occurs before complete stress redistribution. Application of the original LICON method (based on reference stress solutions) for such materials is therefore not recommended. This study has shown that application of the LICON method to 'non-reference stress' materials requires careful adoption of a more sophisticated mechanical analysis approach (e.g. finite element method).

Careful examination has shown that the creep finite element analysis of a structure can result in non-unique numerical representations if the assessment procedure has not been carefully defined. In particular, this study has highlighted the importance of considering a reliable stress regime dependent creep constitutive model for analysis of structures with a wide range of redistributing stresses. This study introduced a new (primary-secondary-tertiary)

creep constitutive model which considers a gradual change of creep deformation/damage accumulation mechanisms with stress variation. Application of the new constitutive model in finite element continuum damage mechanics could successfully reproduce creep deformation and damage accumulation in a series of creep crack incubation tests. The creep damage development formulation of the introduced constitutive model has been constructed based on the LICON concept and its successful demonstration was a new confirmation for the LICON concept, and from a new point of view, i.e. finite element continuum damage mechanics.

From the gathered experience with application of the LICON method to high creep strength 1CrMoV, this study has proposed a procedure for consideration of finite element analysis in the LICON method when it is to be applied for 'non-reference stress' materials. It has also been shown that although the newly proposed procedure was developed for application to 'non-reference stress' materials, it is equally applicable for 'reference stress' materials.

As the last part of this study, application of the LICON method for a dissimilar metal weld has been examined. The investigated material is part of an existing weldment of 1CrMoV and Alloy 625 with filler metal of Alloy 617 which had been a candidate to use for rotor constructions in new advanced power plants, i.e. AD700 power plants. A set of experiments including uniaxial creep, multiaxial creep crack incubation and uniaxial tensile tests and also microstructure examinations were conducted to generate the required information for examination of the LICON method application for this joint. Mechanical analysis of the creep crack incubation tests showed that the material did not achieve complete stress redistribution before the start of crack extension and hence, this joint can be regarded as a 'non-reference stress' material. Application of the LICON method to this joint therefore followed the newly proposed procedure and used finite element analysis for the mechanical analysis part of the approach. It has also been shown that the LICON method formulation for application to predict the creep rupture behaviour of uniaxially testpieces of dissimilar metal welds requires further development. The original LICON method formulas consider a homogeneous uniaxial stress state within a loaded uniaxial testpiece. This assumption is reasonable for homogeneous materials, for a dissimilar metal weld however, the different inelastic (creep) deformation behaviour of different sections (i.e. base material, heat affected zone and weld material) generates a non-uniform multiaxial stress state within the loaded uniaxial testpiece.

This study therefore proposed a new development for the LICON approach which uses finite element analysis to account for the generated multiaxial stress states within weld uniaxial testpieces. Application of the developed approach for predicting uniaxial creep rupture behaviour of the investigated joint showed an acceptable agreement with experimental observations which was not achievable without introducing the new development.

Zusammenfassung

Das Ziel dieser Forschungsarbeit ist die Anwendbarkeit der LICON Methode, zur prognostizierung der langzeit Kriechbruchfestigkeit von gemischten Metall-Verschweissungen, zu überprüfen. Die LICON Methode ist ein Verfahren zum prognostizieren der Lebensdauer von Materialien unter Kriechlast. Die Methode berechnet die Langzeit-Kriechbruchfestigkeit unter Verwendung mehrerer kurzzeit Kriech-Inkubationstests im Zusammenhang mit den Resultaten einer mechanischen Analyse des Probekörpers (z.B. eine Referenzspannungs-Lösung). Ende des 20. Jahrhunderts wurde diese Methode erfolgreich an fortschrittlichem 9%Cr Rohr Stahl (inklusive Schweißverbindung) angewandt. Später wurden Berichte zur Anwendbarkeit der Methode an 1CrMoV Stählen mit hoher Kriechbruchfestigkeit veröffentlicht.

Diese Arbeit prüfte die vorherige Anwendung der LICON Methode für 9%Cr und 1CrMoV Stahl nach. Es wurde gezeigt, dass die Anwendung der originalen LICON Methode (basierend auf Referenzspannungs-Lösungen) für gewisse Materialien nicht geeignet ist. Die Anwendbarkeit von Referenzspannungs-Lösungen ist auf Materialien beschränkt, welche vor Beginn der Rissausbreitung eine komplette Spannungsneuverteilung erlangen (z.B. fortgeschrittene 9%Cr Rohrstähe). Für nicht Referenzspannungsmaterialien (kriechspröd, kerbsensitive Materialien wie 1CrMoV) beginnt die Rissinitiation bevor der Neuverteilung der Spannungen. Die Anwendung der originalen LICON Methode (basierend auf nicht Referenzspannungslösungen) wird für solche Materialien nicht empfohlen. Diese Arbeit hat gezeigt, dass die Anwendungen der LICON Methode für nicht Referenzspannungsmaterialien eine anspruchsvollere mechanische Analyse benötigt (z.B. Finite Element Methode).

Vorsichtige Untersuchungen haben gezeigt, dass Finite-Element-Kriechanalysen einer Struktur in nicht singulären numerischen Repräsentationen enden können, falls das Beurteilungsverfahren nicht richtig definiert wurde. Diese Studie hat hervorgehoben, wie wichtig die Berücksichtigung eines zuverlässigen spannungsabhängigen konstitutiven Kriechmodells für die Analyse von Strukturen ist. In dieser Arbeit wird ein neues (primäres-sekundäres-tertiäres) konstitutives Kriechmodell eingeführt, welches die stufenweise Änderung von Kriechdeformation/Schadensakkumulationsmechanismen unter variierender Spannungen berücksichtigt. Durch Anwendung des neuen konstitutiven Modells in der Finite-Element-Kontinuumsschädigungsmechanik konnte die Kriechdeformation und Schade-

nakkumulation in Kriechriss-Inkubationstests reproduziert werden. Die Formulierung der Kriechschädigung des vorgestellten konstitutiven Modells basiert auf dem LICON Konzept und die erfolgreiche Anwendung ist eine neue Bestätigung der Funktionalität der LICON Methodik.

Mit der gesammelten Erfahrung aus der Anwendung der LICON Methode an 1CrMoV Stahl mit hoher Kriechfestigkeit, präsentiert diese Arbeit eine Vorgehensweise für die Finite-Element-Analyse mit der LICON Methode an Materialien welche nicht der Referenzspannung unterliegen. Obwohl dieses Verfahren für die Anwendung an nicht Referenzspannungsmaterialien entwickelt wurde, wurde unter anderem gezeigt, dass es ebenso anwendbar ist auf Referenzspannungsmaterialien.

Zum Abschluss dieser Arbeit wurde die Anwendung der LICON Methode an einer gemischten Metall-Verschweissung untersucht. Das beschriebene Material ist Teil einer bestehenden Verschweissung aus 1CrMoV und der Legierung 625 mit Füllmaterial aus der Legierung 617. Die Anwendung der Legierung 617 wurde für Rotorkonstruktionen in hochentwickelten Kraftwerken (z.B. AD700 Kraftwerke) in Erwägung gezogen. Zur Untersuchung der LICON Methode an dieser Schweissverbindung wurden uniaxial Kriechversuche, multiaxiale Kriechriss-Inkubationstests und uniaxial Zugversuche durchgeführt. Zudem wurden mikrostrukturelle Untersuchungen durchgeführt. Mechanische Analysen der Kriechriss-Inkubationstests haben gezeigt, dass das Material keine vollständige Spannungsneuverteilung vor Beginn der Rissausbreitung erreichte. Daher kann diese Verschweissung als nicht Referenzspannungsmaterial betrachtet werden. Die Anwendung der LICON Methode folgte daher der vorgeschlagenen Prozedur und nutze die Finite-Element-Methode für den mechanischen Teil der Analyse. Weiter wurde gezeigt, dass die Formulierung der LICON Methode zur Voraussage des Kriechbruchverhaltens von uniaxial Schweissproben weitere Entwicklung benötigt. Die Gleichungen der originalen LICON Methode berücksichtigen einen homogenen uniaxialen Spannungszustand mit einer belasteten uniaxialen Probe. Diese Annahme ist sinnvoll für homogene Materialien. Allerdings generiert das unterschiedliche inelastische (Kriechen) Deformationsverhalten der verschiedenen Sektoren (z.B. Basismaterial, Wärmeeinflusszone, und Schweissmaterial) einen nicht uniformen multiaxialen Spannungszustand in den belasteten, gemischten uniaxialen Schweissnahtproben.

Diese Arbeit schlägt daher eine Neuentwicklung der LICON Methode vor, welche die Finite-Element-Methode benutzt um den erzeugten multiaxialen Spannungszustand anzurechnen. Die Anwendung des entwickelten Verfahrens, zur Vorhersage vom uniaxialem Kriechrissverhalten der untersuchten Schweissnaht, zeigte eine akzeptable Übereinstimmung mit experimentellen Beobachtungen. Diese Übereinstimmung hätte ohne die Neuentwicklung nicht erfolgt.

Contents

Abstract	v
1 Introduction	1
References	4
2 Basic Concepts	5
2.1 Creep	5
2.2 Creep Deformation Mechanisms	6
2.3 Creep Failure Mechanisms	10
2.4 Creep Constitutive Modelling	12
2.4.1 Steady State Creep Modelling	14
2.4.2 Stress Regime Dependency	14
2.5 Creep Resistant Steels	15
2.5.1 Creep Resistant Weldments	19
2.6 Creep Life Prediction	23
2.6.1 Creep Life Prediction of Weldments	28
2.7 Creep Analysis of Structures	32
2.7.1 Reference Stress Approach	32
2.7.2 Finite Element Analysis	35
References	37

3	Articles	45
3.1	<i>Article One</i>	45
	Overview	45
	Experience with Using the LICON Methodology for Predicting Long Term Creep Behaviour in Materials	47
	Abstract	47
3.1.1	Introduction	48
3.1.2	LICON Methodology	51
3.1.3	Material and Experimental Details	53
3.1.4	FE Analyses	54
3.1.5	Concluding Remarks	60
	References	63
3.2	<i>Article Two</i>	65
	Overview	65
	Creep Constitutive Model Considerations for High Temperature Finite Element Numerical Simulations	67
	Abstract	67
3.2.1	Introduction	68
3.2.2	Creep Constitutive Models	69
3.2.3	Finite Element Analysis	71
3.2.4	Finite Element Results	73
3.2.5	Discussion	76
3.2.6	Concluding Remarks	79
	References	81
3.3	<i>Article Three</i>	83
	Overview	83
	Stress Regime Dependent Creep Model Consideration in Finite Element Continuum Damage Mechanics	85
	Abstract	85

3.3.1	Introduction	86
3.3.2	Stress Regime Dependent Creep Model	88
3.3.3	Creep Deformation/Damage Accumulation of 1CrMoV Alloy	92
3.3.4	Concluding remarks	101
	References	103
	Appendix	106
3.4	<i>Article Four</i>	109
	Overview	109
	The LICON Methodology for Predicting the Long Time Uniaxial Creep Rupture Strength of Materials	111
	Abstract	111
3.4.1	Introduction	112
3.4.2	LICON Methodology	114
3.4.3	Reference Stress Based LICON Application for HCS 1CrMoV	116
3.4.4	FEA Considerations for the LICON Methodology	117
3.4.5	FEA Based LICON Application for HCS 1CrMoV	120
3.4.6	FEA Based LICON Application for P91	123
3.4.7	FEA Based LICON Method for Newly Developed Alloys	124
3.4.8	Concluding Remarks	128
	References	130
	Appendix	132
3.5	<i>Article Five</i>	135
	Overview	135
	Exploring the Applicability of the LICON Methodology for the Creep Assessment of a Dissimilar Metal Weld	137
	Abstract	137
3.5.1	Introduction	138
3.5.2	Experiments	138
3.5.3	LICON Methodology Application for Dissimilar Metal Welds	147

3.5.4	Concluding Remarks	158
	References	159
4	Summary and Discussion	161
4.1	LICON Method Application for 1%Cr and 9%Cr steels	162
4.1.1	Reference Stress Solution Based LICON Methodology	163
4.1.2	Finite Element Analysis Based LICON Methodology	164
4.2	LICON Method Application for Dissimilar Metal Welds	171
	References	176
5	Conclusions and Future Work	177
5.1	Conclusions	177
5.1.1	Reference Stress Solutions/Materials	177
5.1.2	Creep Finite Element Analysis	178
5.1.3	LICON Method Application for Materials	180
5.1.4	LICON Method Application for Dissimilar Metal Welds	181
5.2	Future Work	182
	Appendix	185
	ABAQUS/Standard Solver Scheme	185
	Curriculum Vitae	193
	Nomenclature	197

Chapter 1

Introduction

One of the main challenges in the design of high temperature components such as those used in modern power generation plant is their lifetime prediction under creep conditions. It is important to be able to accurately predict the creep lifetimes of such structures, with due consideration of fitness-for-purpose, reliability, safety and cost effectiveness, and this has been a main topic of high temperature study for many years. In ideal circumstances, creep lifetime evaluation is based on strength values derived from experimental observations from a large quantity of long duration uniaxial tests for the material of interest, ideally for a number of different heats [1]. In circumstances for which such large datasets do not exist, long-time properties have to be predicted from the results of relatively short duration tests. While the latter approach can only be regarded as an interim compromise, and no substitute for the former approach with regards to accurate design life assessment, it is sometimes the only way to predict the long-time properties of new alloys in a relatively short-time scale and to thereby enable their early exploitation.

A number of approaches have been adopted for predicting long-time creep properties of materials from relatively short duration tests, e.g. extrapolating the results of high stress isothermal tests using for example the Larson–Miller formulation [2], iso-stress testing [3, 4], applying the theta projection concept [5, 6], stress relaxation testing [7, 8]. These methods might work well for materials with stable deformation and rupture mechanisms over a wide range of temperatures and stresses. However, experience with all of these techniques consistently indicates that none are effective in predicting long-time creep rupture properties when the rupture mechanism in the long-time regime is different to that in the short-time regime.

In the late 1990s, an iso-thermal extrapolation approach referred to as the LICON methodology was developed in an European Brite Euram project [9, 10]. This methodology relies on multiaxial loading conditions to bring forward the onset of long-time creep damage formation into the short-time rupture regime. The LICON method employs observations from several short-time creep crack incubation (CCI) tests in conjunction with the results of a mechanical analysis for the testpieces to predict the long-time uniaxial creep strength of a material. The approach provides similarity with the loading conditions experienced in real structures and enables a more accurate evaluation of the future in-service performance of materials for which no long term service experience exists.

This method was originally developed for predicting the long term creep rupture strength of advanced martensitic 9%Cr pipe steels (including their welded joints). Successful application of the method for P91, E911, P92 and their weldments has been reported in the early 2000s [9, 10]. More recently, the scope of applicability for the LICON method has been extended to low alloy creep resistant 1CrMoV steels [11, 12]. This study has examined the applicability of the LICON methodology for predicting the long term uniaxial creep strength of a dissimilar metal weld (DMW). The investigated weld had been a candidate to use for rotor constructions in new advanced power plants, i.e. AD700 power plants.

The advanced pulverised 700°C power plant or shortly AD700 power plant is a project started in 1994 with a large group of European power generators and equipment manufacturers. The mission for this group is to create a strategic and technological platform to convert coal to power with an efficiency of higher than 50% and, thereby contributes to reduction of CO₂ emissions [13].

Maximum steam temperature of the AD700 power plant would be around 720°C [13, 14]. The realisation of the AD700 project requires materials with 10⁵h rupture strength of 100MPa at 720°C, and therefore nickel based alloys have been called for application in the most severely exposed components [13, 15].

Turbine rotors supporting moving blades which are rotated by receiving high temperature steam experience a high temperature-stress condition [16]. Figure 1.1 illustrates the predicted temperature distribution within a rotor for the AD700 power plant.

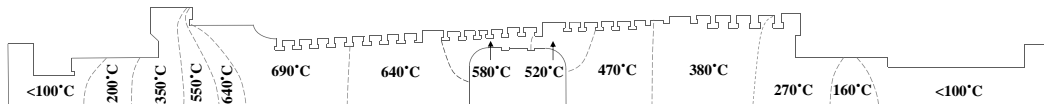


Figure 1.1: Expected temperature distribution within a rotor for AD700 power plant [17].

Construction of such a rotor from nickel based alloys is limited by the manufacturable upper size and the cost [16]. Nickel based alloys are much more expensive than alloyed steels and it is desirable that the nickel based alloys are used for only portions which must be made of the nickel base alloys and other portions are made of iron-steel materials. Welding technology allows the application of appropriate material where needed [15, 16].

One of the candidate designs for welded rotors applicable in AD700 power plants had been based on the use of Alloy 625 for the high temperature portion and 1CrMoV for the portions experiencing lower temperatures. The candidate filler metal was Alloy 617 [17]. Long-time creep behaviour predictions for such designs is critical to establish the technical feasibility of the new power plant concept [15]. One of the most important assessments is evaluation of long term creep strength of the welded parts.

This study therefore explores applicability of the LICON method for predicting the long term creep strength of the weldment of 1CrMoV and Alloy 625 with filler metal of Alloy 617.

References

- [1] S.R. Holdsworth. The ECCC approach to creep data assessment. *Journal of Pressure Vessel Technology*, 130:1–6, 2008.
- [2] F.R. Larson and J. Miller. A time–temperature relationship for rupture and creep stresses. *Transactions ASME*, 74(5):765–775, 1952.
- [3] K.N. Melton. The iso–stress extrapolation of creep rupture data. *Materials Science and Engineering*, 59(2):143–149, 1983.
- [4] O. Kanemaru, M. Shimizu, T. Ohba, K. Yagi, Y. Kato, and K. Hattori. Life prediction by the iso–stress method of boiler tubes after prolonged service. *International Journal of Pressure Vessels and Piping*, 48(2):167–182, 1991.
- [5] R.W. Evans and B. Wilshire. *Creep of Metals and Alloys*. Institute of Metals, 1985.
- [6] M. Evans. Predicting times to low strain for a 1CrMoV rotor steel using a 6– θ projection technique. *Journal of Materials Science*, 35(12):2937–2948, 2000.
- [7] D.A. Woodford. Accelerated testing for high temperature materials performance and remaining life assessment. *EPRI report*, 1999.
- [8] D.A. Woodford. Creep strength evaluation, design, and life management of 1CrMoV rotor steel using stress relaxation testing. In *Advances in Turbine Materials, Design and Manufacturing*, pages 613–624, 1997.
- [9] P. Auerkari, W. Bendick, S. Holdsworth, J.H. Rantala, R. Hurst, C. Coussement, and R. Hack. Predicting long term creep behaviour using the LICON methodology. In *Proceedings of the 3rd International Conference of Advances in Material Technology for Fossil Power Plants*, pages 329–339, 2001.
- [10] V.M. Martins and S.R. Holdsworth. The LICON methodology for predicting the long term service behaviour of new steels. *Materials at High Temperatures*, 19(2):99–103, 2002.
- [11] S.R. Holdsworth and E. Mazza. Exploring the applicability of the LICON methodology for a 1CrMoV steel. *Materials at High Temperatures*, 25(4):267–276, 2008.
- [12] S.R. Holdsworth and E. Mazza. Using the results of creep crack incubation tests on 1CrMoV steel for predicting long time creep rupture properties. *International Journal of Pressure Vessels and Piping*, 86(12):838–844, 2009.
- [13] R. Blum, S. Kjær, and J. Bugge. Development of a PF fired high efficiency power plant (AD700). In *Proceedings of the Riso International Energy Conference of Energy Solutions for Sustainable Development*, 2007.
- [14] J. Bugge, S. Kjær, and R. Blum. High-efficiency coal–fired power plants development and perspectives. *Energy*, 31(10):1437–1445, 2006.
- [15] R. Blum and R.W. Vanstone. Materials development for boilers and steam turbines operating at 700°C. In *6th International Charles Parsons Turbine Conference*, pages 489–510, 2003.
- [16] M. Hiegemann and M. Reigl. Rotor for a Steam Turbine, 2007. US Patent 7267525.
- [17] A. Pirscher. Alstom steam turbine designs for AD700 power plant. In *AD700 Conference Milan*, 2005.

Chapter 2

Basic Concepts

2.1 Creep

Creep of materials is classically regarded as the irreversible and time-dependent deformation of materials. Although creep can take place at all temperatures above absolute zero, traditionally creep refers to the time-dependent plastic deformation at elevated temperatures, often higher than roughly $0.4T_m$ (T_m is material melting temperature). A typical creep curve for an engineering steel is schematically shown in Figure 2.1. The instantaneous strain can be characterized by the strain value ε_0 which contains elastic strain and possibly plastic strain depending on the stress level [1, 2].

Following Andrade [3], textbooks generally consider three stages in a typical creep curve: the first stage (primary or transient creep), the second stage (secondary or stationary creep) and the third stage (tertiary or accelerated creep). During the primary creep stage, between t_0 and t_1 , the creep rate decreases with time due to strain hardening until it reaches a certain value (minimum or steady creep rate, $\dot{\varepsilon}_s$). In the secondary creep stage, between t_1 and t_2 , there is a balance between the strain hardening and thermal softening and the creep rate remains approximately constant at $\dot{\varepsilon}_s$. During the tertiary stage, the creep rate increases and finally at the end of the tertiary stage creep rupture of the specimen occurs. The increase in creep rate with time in the tertiary creep stage can arise from increasing stress (due to cross-section reduction in constant tensile loading) or from microstructure evolution including damage formation [1, 4].

The shape of the creep curve and the duration of the creep stages for a material depend strongly on creep testing conditions, namely stress and temperature [1, 4]. The creep curve

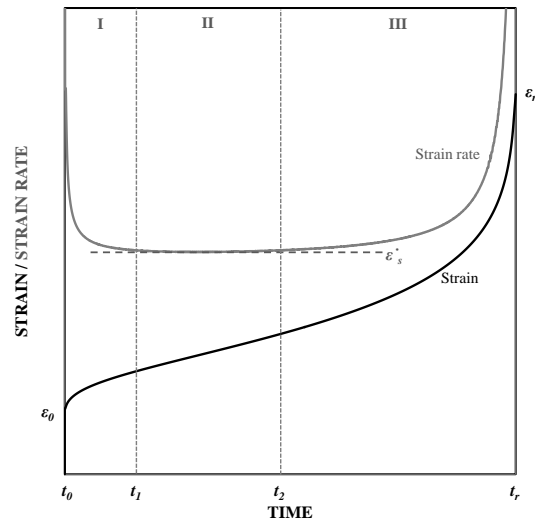


Figure 2.1: A typical creep curve for an engineering steel under constant tensile load and constant temperature.

dependencies on stress and temperature are shown in Figure 2.2.

2.2 Creep Deformation Mechanisms

Several mechanisms contribute to the creep deformation of engineering metals at elevated temperatures. Representatives of the mechanisms are [6]:

- diffusion creep controlled by volume diffusion (Nabarro–Herring creep)
- diffusion creep controlled by grain boundary diffusion (Coble creep)
- dislocation creep controlled by volume diffusion (at high homologous temperatures)
- dislocation creep controlled by pipe diffusion (at low homologous temperatures)

The four mentioned creep mechanisms are independent of each other and the creep strain arising from each mechanism contributes additively to the total creep strain. At a given stress and temperature, the mechanism giving the highest value of creep rate is the controlling mechanism [6].

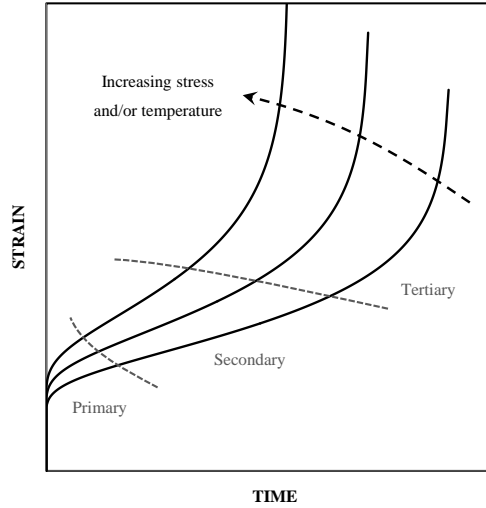


Figure 2.2: Influence of stress and temperature on material creep behaviour [5].

When secondary creep dominates, the Norton [7] creep model equation gives:

$$\dot{\epsilon}_s = A\sigma^n \quad (2.1)$$

Creep is a thermally activated process and its temperature dependency can be expressed with an Arrhenius-type expression [8]:

$$\dot{\epsilon}_s = A \exp\left(\frac{-Q_c}{RT}\right) \quad (2.2)$$

Combination of Equations 2.1 and 2.2 gives:

$$\dot{\epsilon}_s = A\sigma^n \exp\left(\frac{-Q_c}{RT}\right) \quad (2.3)$$

where A and n are constants, R is the universal gas constant and Q_c is the activation energy for creep. The values of n and Q_c are sensitive to the mechanism controlling creep deformation [9].

Plots of $\log \dot{\epsilon}_s$ vs. $\log \sigma$ for the majority of advanced heat resistant steels show at least one transition of creep exponent, n , depending on the level of stress (Figure 2.3) [10]. The change of n corresponds to a transition in dominant creep deformation mechanism. In general, plots of $\log \dot{\epsilon}_s$ vs. $\log \sigma$ (and/or $\log \dot{\epsilon}_s$ vs. $1/T$) provide useful information about the

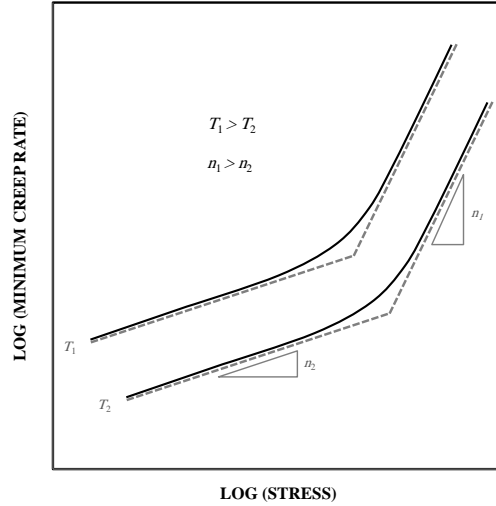


Figure 2.3: Schematic illustration of $\log \dot{\epsilon}_s$ vs. $\log \sigma$ [4, 6].

dominant creep mechanism and its changes due to change of creep condition.

The contribution of different mechanisms to the total deformation of a creeping material depends on the applied stress and temperature. To distinguish between different mechanisms involved in creep deformation processes under different creep conditions, Ashby [11] developed a compact method of representation called 'deformation mechanism map'. A schematic illustration of such a map is shown in Figure 2.4 in which the stress and temperature dependent regions with different dominant creep deformation mechanisms can be represented. The boundaries between two adjacent fields in the deformation mechanism map indicate the conditions under which two mechanisms contribute equally to the overall creep rate.

At stresses lower than the material yield stress, creep is controlled by the movement of dislocations (dislocation creep). Dislocation core diffusion (pipe diffusion) at low homologous temperatures and volume diffusion at high homologous temperatures control the movement of dislocations. Therefore, the dislocation creep region may be further divided into two fields: low and high temperature dislocation creep regions. The expected activation energy for this mechanism regime is Q_{SD} at high and Q_{CD} at low temperatures (Q_{SD} and Q_{CD} are self diffusion and dislocation core diffusion activation energies, respectively). The stress exponent of n for this mechanism region is larger than 5. Therefore, dislocation creep has a strong dependence on the applied stress [6, 9].

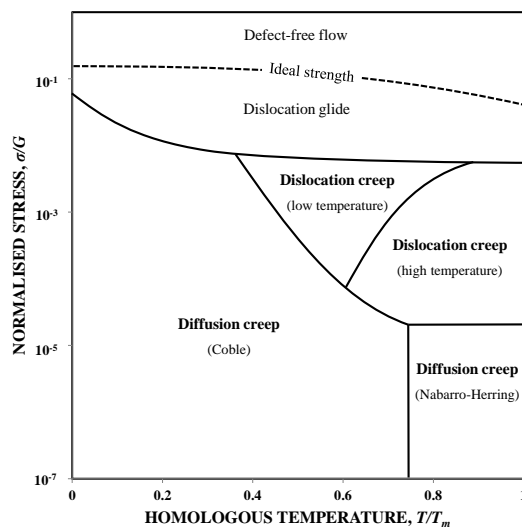


Figure 2.4: Schematic deformation mechanism map [1].

At even lower stresses, diffusion creep (Nabarro–Herring and Coble creep) dominate [12–14]. At higher homologous temperatures, atoms diffuse through the lattice causing grains to elongate along the stress axis. This results in a permanent creep strain through a Nabarro–Herring creep mechanism. At lower temperatures, the Coble mechanism represents the diffusion of atoms along the grain boundaries resulting in grain elongation in the direction of stress and occurrence of creep strain. The activation energies for this mechanism regime are Q_{SD} and Q_{BD} for the high and low homologous temperatures, respectively (Q_{BD} is grain boundary diffusion activation energy). Theoretically, the diffusion creep mechanisms take the stress exponent of $n = 1$ [9].

It should be noted that the consideration of a stress exponent equal to one ($n = 1$) in the low stress regime is still under consideration, e.g. [15–18]. Although fundamental creep deformation theory suggests a value of one in this mechanism regime, there are several reports of higher values, up to about three, e.g. Spigarelli et al. [19].

It is worthy of mention that the rate of dislocation creep is almost independent of grain size, but that of diffusion creep (Nabarro–Herring and Coble) increases with decreasing grain size. Therefore, the diffusion creep fields (especially the Coble creep field) expand with decreasing grain size.

First Ashby [11] provided the first global overview of deformation mechanisms maps. Later, they were widely promoted in the literature, e.g. [4, 20–22]. Currently, deformation mech-

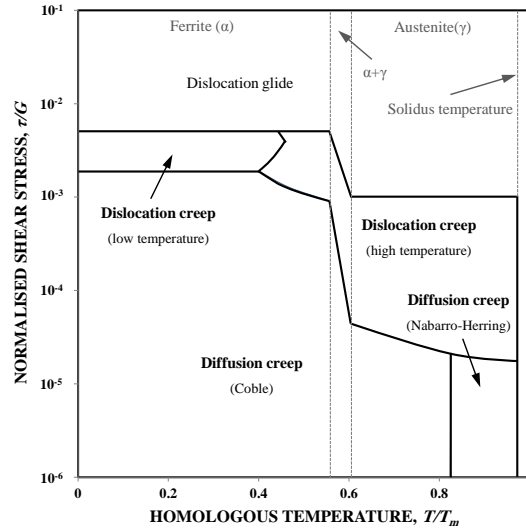


Figure 2.5: A typical deformation mechanism map for 1CrMoV alloy [23].

anism maps are available for various materials being useful in selecting materials for high temperature applications [23]. Figure 2.5 illustrates a deformation mechanism map for a 1CrMoV alloy with grain size of $100\mu\text{m}$.

2.3 Creep Failure Mechanisms

While creep at low temperature rarely leads to failure, creep at high temperature can terminate in fracture. An early indication of eventual fracture is usually the acceleration of creep rate at the onset of the tertiary stage.

High temperature fracture occurs by one of the two different modes, each based on the growth and coalescence of voids [10].

- transgranular creep fracture
- intergranular creep fracture

Transgranular or ductile creep fracture is typically accompanied by a relatively high elongation/reduction in area (necking). Transgranular creep fracture generally results from high applied stresses and fails by a void forming process similar to that of microvoid coalescence in room temperature dimple rupture [24, 25].

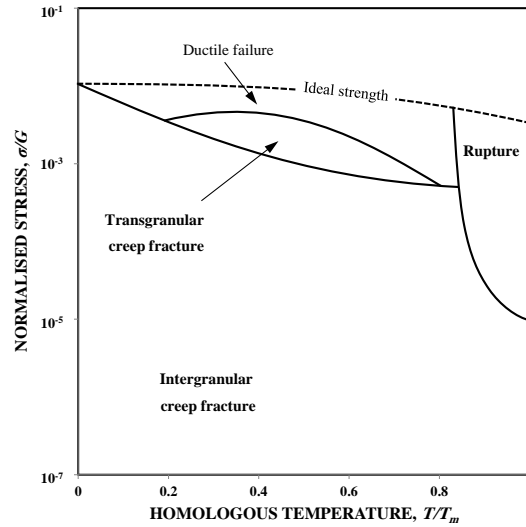


Figure 2.6: Schematic of a typical fracture mechanism map for a FCC metal [1, 26].

Intergranular creep fracture occurs at stresses and strain rates lower than those for transgranular creep fracture (long duration failure). In this condition, voids form on grain boundaries that are normal to the tensile axis and cause fracture. This mechanism is characterized by little to no reduction in area [24, 25].

By analogy with material deformation mechanism maps, fracture mechanism maps can also be devised. Fracture mechanism maps are also diagrams with tensile stress (or normalised tensile stress) as one axis and temperature (or homologous temperature) as the other which show the fields of dominance of a given fracture mechanism [26]. A typical fracture mechanism map for a FCC metal, reported by Ashby [26], is given in Figure 2.6.

Similar to creep deformation, creep failure is a stress–temperature dependent phenomenon. Orr–Sherby–Dorn model equation expresses the time to rupture as [27]:

$$t_f = A' \sigma^{-n'} \exp\left(\frac{-Q_c}{RT}\right) \quad (2.4)$$

where A' and n' are constants. Similar to that for creep deformation, a transition of n' , observed in plots of $\log t_f$ vs. $\log \sigma$ corresponds to a transition in dominant creep failure mechanism. Typically, creep failure with a low stress exponent (diffusion controlled) appears at low stresses, whereas it shows a high stress dependence (large stress exponent) at high stresses. There are several creep life prediction examples neglecting this mechanism.

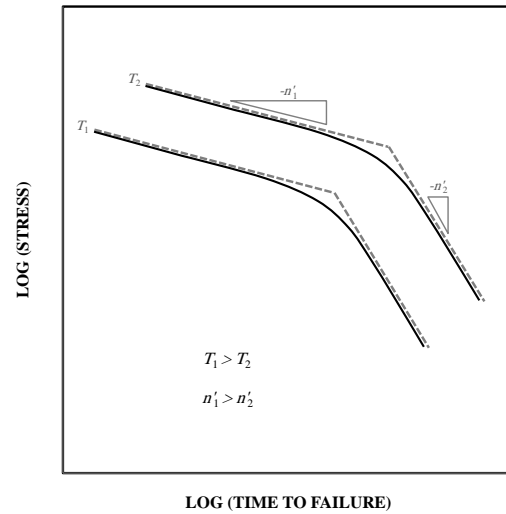


Figure 2.7: Schematic illustration of $\log \sigma$ vs. $\log t_f$ [4, 6].

transition which brought about overestimation of the long term failure life, a multi-region analysis of creep failure data is therefore recommended [28].

Figure 2.8 illustrates a creep fracture mechanism map for 1CrMoV, reported by Shinya et al. [29]. The region of practical importance for 1CrMoV steel in power plants is the long-time to failure region (e.g. $2-3 \times 10^5$ h time to failure) at temperatures of 550°C or lower, which belongs to the intergranular creep fracture field. This suggests that a good knowledge of the development of creep voids at grain boundaries during creep may contribute to the improvement of the reliability of creep life estimations for this alloy [1].

2.4 Creep Constitutive Modelling

A constitutive equation is a relation between two or more physical quantities that is specific to the material and represents the response of that material to external influences. The requirement for a knowledge of creep constitutive behaviour, $\varepsilon(t, T, \sigma)$ is no longer just for scientific interest or metallurgical understanding, this is now routinely a requirement for computer based finite element analysis (FEA) of engineering components loaded at elevated temperatures [30].

Many creep constitutive models have been developed during the last 100 years and a number

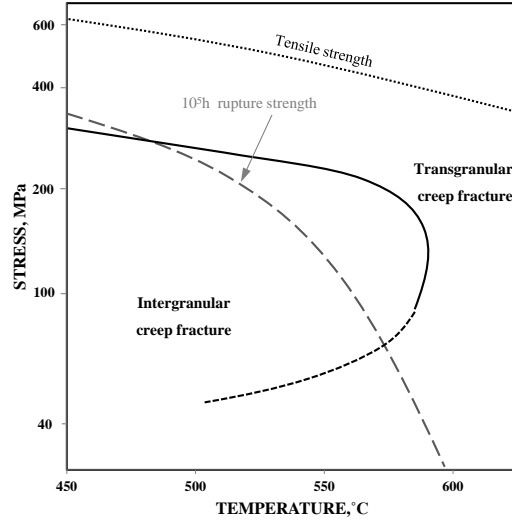


Figure 2.8: A typical fracture mechanism map for 1CrMoV alloy [29].

of these have recently been reviewed by Holdsworth [30]. Table 2.1 presents a number of classical representations of primary, secondary and tertiary creep deformation stages. A small number of the presented equations may be contained in creep constitutive models to represent the material behaviour over all three creep deformation stages. This can be simply achieved by summing up the expressions representing primary, secondary and tertiary creep strains:

$$\varepsilon_{\text{total}} = \varepsilon_{\text{primary}} + \varepsilon_{\text{secondary}} + \varepsilon_{\text{tertiary}} \quad (2.5)$$

Furthermore, a secondary creep model may be extended to primary and tertiary stages by introducing state variables representing primary and tertiary stages. The primary–secondary–tertiary creep model presented by Dyson and McClean [31] can be regarded as an extension of the secondary creep model of $\dot{\varepsilon}_s = A \sinh(B'\sigma)$ proposed originally by Nadai [32]:

$$\dot{\varepsilon} = A \sinh\left[\frac{B(1 - \mathcal{H})}{(1 - \varphi)(1 - \omega)}\right] \quad (2.6)$$

where state variable \mathcal{H} represents the strain hardening that occurs during primary creep, φ describes the evolution of the spacing of the precipitates which leads to a progressive loss in the creep resistance of particle hardened alloys and ω represents the effect of cavitation damage accumulation occurring during the tertiary creep stage [33].

Finally, it is worthy of mention that there is not a single universal constitutive equation applicable for all materials. The selection of creep constitutive model often depends on which model best represents the high temperature deformation characteristics of a specific material at the temperature and stress ranges under investigation [30].

2.4.1 Steady State Creep Modelling

For engineering components in service, the material should never enter the creep tertiary stage [42]. The ease of access to steady-state creep rate data for materials (e.g. NIMS Creep Data Sheet [43]) means that some engineering assessments neglect the primary creep deformation (as well as tertiary creep deformation) and focus only on steady state creep deformation and therefore use secondary creep models. Numerous applications of secondary creep models, e.g. Norton creep model [7] can be found in recent studies, e.g. [42, 44, 45].

2.4.2 Stress Regime Dependency

High temperature components can experience creep over a wide range of stresses (and temperatures). Analysis procedures for such components require creep models being representative of the creep behaviour of the material over a wide range of stresses.

Some creep models (e.g. the conventional Norton [7] equation) involve a general single formulation to describe the behaviour of materials for all stress regimes (i.e. single regime creep

Table 2.1: Classical representations of primary, secondary and tertiary creep stages [30].

Models	Mathematical formulations
Primary creep	
Logarithmic [34]	$\varepsilon = A \log(1 + Bt)$
Power [35]	$\varepsilon = At^c$
Exponential [36]	$\varepsilon = A[1 - \exp(-Bt)]$
Hyperbolic sine [37]	$\varepsilon = A \sinh(Bt^c)$
Secondary creep	
Power [7]	$\dot{\varepsilon}_s = A\sigma^n$
Exponential [32]	$\dot{\varepsilon}_s = A \exp(B\sigma)$
Hyperbolic sine [32]	$\dot{\varepsilon}_s = A \sinh(B\sigma)$
Tertiary creep	
Power [35]	$\varepsilon = At^c$
Exponential [38]	$\varepsilon = A[\exp(-Bt) - 1]$
Omega [39]	$\dot{\varepsilon} = \dot{\varepsilon}_0 \exp(-\Omega\varepsilon)$
Damage type [40, 41]	$\dot{\varepsilon} = A\sigma^{c_1}(1 - \omega)^{-c_2}$ where $\dot{\omega} = B\sigma^{c_3}(1 - \omega)^{-c_4}$

models). However, for many engineering alloys, the creep deformation mechanism exhibited at high stresses is not the same as that at lower stresses [10, 23]. Typically, at relatively high temperatures, dislocation creep controlled by dislocation climb and glide occurs at higher stresses (when the stress exponent is ≥ 5), whereas diffusion creep controlled by volume or grain boundary diffusion occurs at lower stresses (when the stress exponent is around three or, in the limit, unity). The consideration of single regime creep models cannot represent the effect of a creep mechanism transition due to a change of stress and ideally should not be used in applications involving a wide range of stresses.

Consideration of the conventional creep model formulations with different parameter sets for different stress regimes can be a possibility for consideration of creep mechanism transition. Extension of the conventional Norton creep model [7] to two mechanism regimes gives:

$$\dot{\epsilon}_s = \begin{cases} A_1 \sigma^{n_1} & \text{if } \sigma \geq \sigma^* \\ A_2 \sigma^{n_2} & \text{if } \sigma < \sigma^* \end{cases} \quad (2.7)$$

Where σ^* is the stress associated with a creep deformation mechanism change. The application of such formulations for application to a wide range of stresses is much more successful than that of single regime models. However in reality, the stress dependent creep mechanism change is not a sharp transition and considering a step change of creep mechanism at a critical stress is not a realistic assumption. The more physically acceptable solution is a gradual and continuous change of creep deformation mechanism with stress variation. Consideration of the overall creep rate as a summation of creep rates arisen from low and high stress creep deformation mechanisms can represent a continuous creep mechanism transition due to change of stress, e.g. for the Norton creep model [4]:

$$\dot{\epsilon}_s = A_1 \sigma^{n_1} + A_2 \sigma^{n_2} \quad (2.8)$$

Figure 2.9 shows a schematic comparison of the expected creep behaviours with different representation of the Norton creep model (i.e. Equations 2.1, 2.7 and 2.8) for a wide range of stresses.

2.5 Creep Resistant Steels

Creep resistant steels are steels designed to withstand loads at high temperatures and for long durations. The main application of creep resistant steels is in power generation and petrochemical plants. The efficiency of power plants can be improved by increasing the

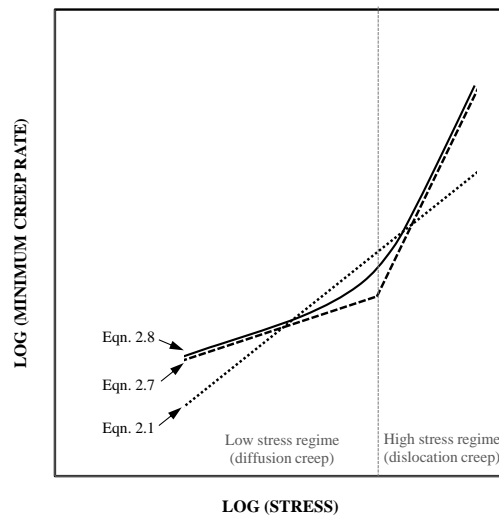


Figure 2.9: Schematic comparison of presented creep behaviours with Equations 2.1, 2.7 and 2.8.

maximum operating temperature and pressure and this was the major driving force behind the continuous development of creep resistant steels for application to higher temperatures and pressures [1, 46–50].

Up to the 1920s, non-alloyed steels were used for the components exposed to maximum temperatures of 350°C and pressures of about 15bar. At the beginning of the 1920s, development of low alloyed heat resistant steels improved the operating condition to a steam temperature of 450°C and a pressure of 35bar. Later, different low alloyed heat resistant steels with different chemical compositions were developed [46, 51]. The high creep resistance of low alloyed steels is attributed to precipitation and solid solution strengthening resulting from addition of alloying elements of Mo, Cr, V, Nb, Ti and B. Amongst the numerous steel versions developed, 1CrMoV has found worldwide acceptance for the manufacture of rotors, casings, valves and bolts for steam turbines [51]. Further information about this alloy is specifically provided in next section.

The maximum allowable temperature for conventional low alloyed heat resistant steels, for steam turbine rotor applications, is 565°C. Continuous development of heat resistant steels after the 1950s led to development of high strength 9–12%Cr ferritic–martensitic steels capable of operating in ultra super critical power plants with working temperatures of about 650°C [51]. The high creep resistance of the early developed 9–12%Cr steels was based on solution hardening and precipitation of Cr_{23}C_6 . In 1970s, an advanced steel referred to as

P91 was developed containing additive of Nb and a controlled amount of N. These additives form thermal stable precipitates of VN, Nb(C,N) during heat treatment which effectively increases the creep strength of the alloy. Further enhancement in creep resistance was achieved by the introduction of W and B for the P92 steel. While B prevents the coarsening of $\text{Cr}_{23}(\text{C,B})_6$ particles, W causes hardening due to both solid solution hardening and Laves phase particle formation. Later, creep resistance of this class of steels was further improved by increasing the Cr content from 9 to 11% in T/P122, NF12 and SAVE12 steels. This high Cr content increases the oxidation resistance of the steel for application at steam temperatures above 600°C. Future martensitic 9–10%Cr steels are under development for steam temperatures up to 650°C [46, 47, 51].

The development of austenitic steels for use in power plants operating at temperatures above 650°C was started in the 1980s. Austenitic creep resistant steels contain considerable amounts of Cr and Ni (18%Cr–8%Ni, e.g. AISI 316 and 304). The high Cr content increases the oxidation and corrosion resistances and with the austenitic stabilizing effect of Ni, this alloy shows both high strength and high ductility under creep loading condition. The presence of alloying element of Ti and Nb results in the formation of carbides and nitrides improving the creep resistance of these steels. Also, Mo and W cause hardening due to both solid solution hardening and the formation of Sigma and Laves phases. The limit for austenitic steels application is approximately 680°C for 350bar pressure plants. Development of austenitic steels with acceptable long term creep strength at a temperature of 700°C is a future desire. Nickel based alloys (e.g. Alloy 617, Alloy 625 and Haynes 230) can be used for applications at even higher temperatures, however the material cost for nickel based alloys is high compared with that for austenitic steels which limits the application of nickel based alloys [46, 51].

Figure 2.10 illustrates a schematic comparison of creep ruptures strength of different class of heat resistant alloys.

CrMoV Alloy

Amongst the numerous low alloyed steel versions developed, 1CrMoV has found worldwide acceptance for the use in power industry for components such as high pressure (HP) and intermediate pressure (IP) steam turbine rotors operating at temperatures up to 565°C [51, 52]. Depending on the component size and the location of the site of development, the chemical composition of the alloy is roughly 0.20–0.30%C, 1–1.5%Cr, 0.70–1.25%Mo, 0.25–0.35%V and 0.50–0.75%Ni [1, 53].

The high creep resistance of 1CrMoV originates from solid solution strengthening and precip-

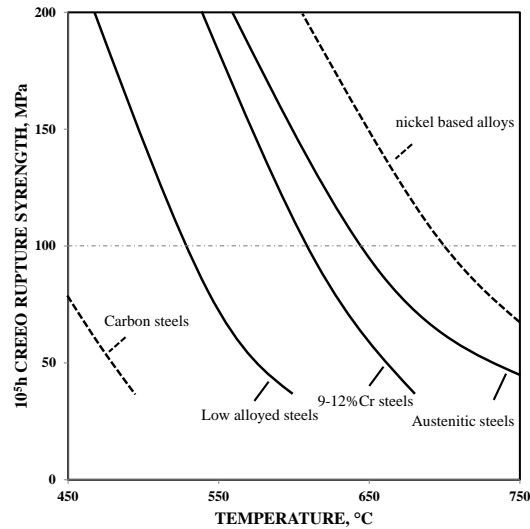


Figure 2.10: Schematic comparison of creep ruptures strength of heat resistant alloys [46, 51].

itation hardening. Interstitial and substitutional solute atoms (e.g. C, N and Mo) increase the matrix high temperature strength, however the high creep resistance of 1CrMoV is mainly due to the presence of fine and stable intragranular vanadium carbides which pin the dislocations and inhibit recovery [54].

The highest creep strength for 1CrMoV alloy relates to a microstructure consisting of upper bainite with fine and uniformly distributed precipitates of V_4C_3 . Such a structure however has low ductility and a tempering treatment should be conducted to increase the ductility [54–56].

Investigations have shown that composition and heat treatment can significantly affect the creep behaviour of 1CrMoV alloy [1, 55–57]. Higher austenitizing temperature and lower tempering parameters generally result in an increased creep strength with the cost of reduced toughness and high notch sensitivity. A typical heat treatment for 1CrMoV rotor steel comprises austenitization at $975^\circ\text{C}/12\text{h}/\text{oil}$ –quench and tempering at $700^\circ\text{C}/18\text{h}/\text{furnace}$ cool [55]. Table 2.2 gives optimised chemical compositions for HP and IP steam turbine rotors according to Norton and Strang [55].

Figures 2.11 and 2.12 indicate typical high temperature mechanical behaviour for 1CrMoV steel.

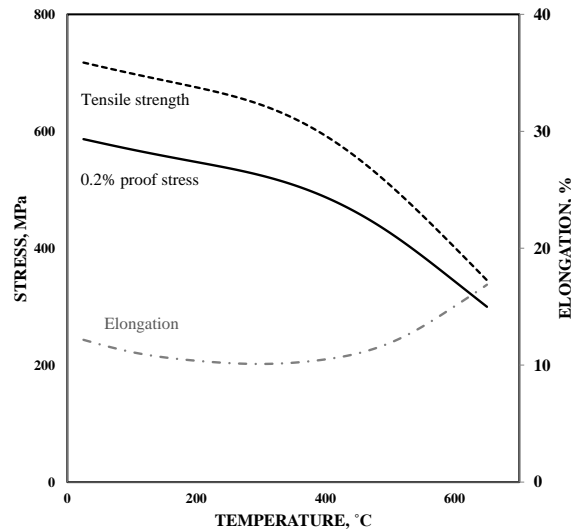


Figure 2.11: Variation of tensile properties of 1CrMoV with temperature [56, 58].

2.5.1 Creep Resistant Weldments

Welding is still the major joining technology for power plant components. The joint of components such as pipes and tubes can consist of similar metal welding (SMW) and dissimilar metal welding (DMW). Welding is mainly considered for economic design of components with application to a wide range of temperatures and corrosion conditions [59, 60].

The heat involved in the welding process strongly influences the microstructure and mechanical properties of creep resistant steels adjacent to the fusion line (FL). The influenced region is called heat affected zone (HAZ). The resulting microstructures and mechanical properties of the HAZ are governed by several parameters (e.g. the experienced peak temperature during welding, post-weld heat treatment (PWHT), etc.) [59, 60].

The microstructures of HAZs for low alloyed ferritic steels exhibit a gradient in characteristics. The HAZ can be divided in to different sections (Figure 2.13) [60]:

Table 2.2: Optimised chemical composition (in wt%) for HP and IP rotor forgings [55].

C	Cr	Mo	Ni	V	Si	Mn	P	S
0.24	0.98	0.65	0.60	0.27	0.17	0.74	0.007	0.009
0.31	1.15	1.08	0.76	0.36	0.27	0.81	0.003	0.019

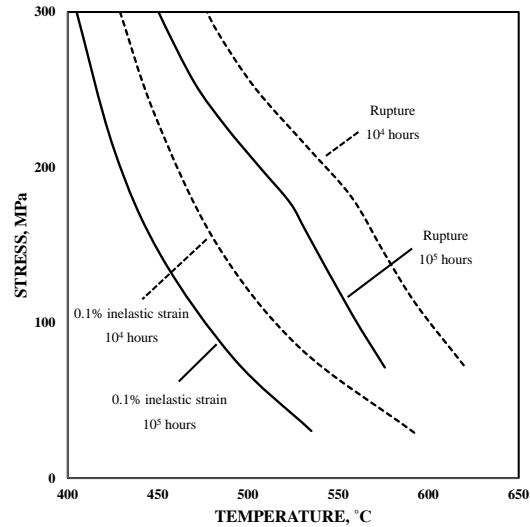


Figure 2.12: Variation of creep properties of 1CrMoV with temperature [56].

- Coarse grained HAZ (CGHAZ): the zone adjacent to the FL experiences very high temperatures during welding causing full austenitization and grain growth. The final structure therefore evolves from coarse austenite grains. The high temperatures experienced by this zone dissolves precipitates which could obstruct the growth of austenite grains.
- Fine grained HAZ (FGHAZ): lower peak temperature experiences of about 1100°C result in full austenitization, but not dissolution of precipitates. Presence of the precipitates acts as nucleation sites for new austenite grains and, at the same time, limits their growth. The final structure therefore evolves from fine austenite grains.
- Intercritical HAZ (ICHAZ): peak temperature experience between A_{c1} and A_{c3} transformation temperatures results in a partial austenitization of structure. While new austenite grains nucleate at favoured positions, the untransformed structure is simply tempered. The final structure therefore is a twofold microstructure consisting of newly formed, and the tempered original structure.
- Over tempered zone: with peak temperatures experienced below A_{c1} , the microstructure of this zone does not undergo any phase transformations, but the original microstructure is tempered at high temperatures which may result in precipitation coarsening.

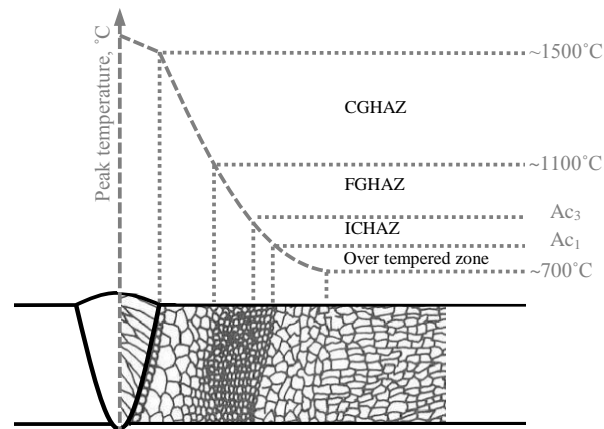


Figure 2.13: Schematic representation of the microstructure developed in HAZ for ferritic steels [60, 61].

It is worth mentioning that the resulting microstructures of multi-pass welds are more complicated. Additional heat input from subsequent welding passes affects the previously generated HAZ and weld deposit [60].

As mentioned above, the weld thermal cycle completely changes the optimised microstructure of parent material (PM), established as the result of a well specified manufacturing procedure. All these improper changes affect the creep strength of the materials surrounding the weld and make the weldments one of the most critical locations in high temperature components [59, 61].

Cracks in welded joints are classified depending on their location. Cracks arrested in the deposited weld metal (WM) are referred to as type I and cracks in the deposited WM which propagate into the HAZ or even into the PM are referred to a type II. These two cracking types are commonly associated with the welding process or stress relief during PWHT [62]. Improvements to the cleanliness of the weld deposit for weldments of ferritic steels has diminished the significance of these cracks. Type III cracks form in the CGHAZ and can extend in this zone as well as into the PM. This type of cracking, also called reheat or stress relief cracking, results when the relaxation strains occurring during the exposure of weldment to elevated temperature exceed the local ductility of the CGHAZ structure. Multi-pass welding refines the microstructure of prior CGHAZ and results in an increased rupture ductility for this zone and usually eliminates reheat cracking susceptibility. Type IV cracking, restricted to the FGHAZ and ICHAZ, is the major failure mechanism for ferritic steel weldments. The low creep resistance of FGHAZ and ICHAZ causes localization of the

creep deformation in these zones and generates a multiaxial stress condition in these zones. This accelerates the nucleation and growth of creep cavities [63], in particular subsurface, and leads to final failure. Investigations have demonstrated the beneficial effect of controlled additions of B to parent and weld materials for suppressing the formation of type IV cracking [64, 65].

In addition, cracks located at or very close to FL have been observed in DMWs. For DMWs, the mechanism of creep rupture can be complicated by chemical element transfer [66–68]. Solid state diffusion can occur during PWHT and/or service. The migration of carbon into the side containing strong carbide forming elements (e.g. austenitic steels with high Cr content) can produce a decarburized zone in the ferritic steels adjacent to the FL [69]. Regarding creep rupture properties, the carbon depleted zone is weak and is surrounded by zones of higher creep strength. This leads to localized premature damage in the decarburised HAZ located in the low alloyed steel part. Brett [70] assigned the term type IIIa cracking to this type of cracking which usually occurs after long-time service. A common preventative method for this type of cracking is to use nickel based filler metals as a diffusion barrier [71]. Service experience has shown that the nickel based joints perform better than those made with austenitic filler metals. However, it was later found that these fillers can only decrease the scale of diffusion and long-time service exposure of them (e.g. $\sim 70,000$ h at 600°C [68]) results in a strong susceptibility to low ductility cracking. The cracking in such conditions is close to the FL and is due to formation of semicontinuous M_{23}C_6 (Cr rich) and M_6C (Mo rich) particles in the ferritic steel, parallel and very close to FL ($1\mu\text{m}$) [66–68, 72]. Nicholson [73] explained that as a result of partial mixing during the welding process, a thin layer of martensite may form between the ferritic steel and the WM. Later during high temperature exposure, carbon migrates from the ferritic steel to the WM to compensate the chemical potential gradient. However, the presence of the martensite band, containing a relatively high chromium content at the interface introduces an intermediate step in the overall migration and forms carbides. Creep cavitation at the formed carbides may lead to low ductility creep failure [72].

Large differences in coefficients of thermal expansion of weld and parent materials, large creep strength mismatch and the formation of oxide notch at the interface are other promoting parameters in the creep failure of DMWs [74].

2.6 Creep Life Prediction

Elevated temperature components such as those used in modern power generation plant are designed using allowable stress under creep conditions. The allowable stress is usually estimated on the basis of 10^5 h creep rupture strength at the operating temperature [1]. One of the main challenges in the design process of such components is the prediction of long term creep strength.

In ideal circumstances, creep lifetime evaluation is based on strength values derived from experimental observations from a large quantity of long duration uniaxial tests for the material of interest, ideally for a number of different heats [75]. Recently, long term creep rupture test data beyond 10^5 h have become available for a number of creep resistant steels in several materials test institutions (e.g. NIMS, Japan [43]). In circumstances for which such large datasets do not exist, long term properties have to be predicted from the results of relatively short duration tests. While the latter approach can only be regarded as an interim compromise, and no substitute for the former approach with regards to accurate design life assessment, it is sometimes the only way to predict the long term properties of alloys in a relatively short-time scale. A number of approaches have been adopted for predicting long-time creep properties from relatively short duration tests. The advantages and disadvantages of each approach for application to different materials at different creep conditions have been reported in the literature (e.g. [1]). The following text shortly reviews some of the adopted approaches.

Time Temperature Parameters

Many attempts have been made to formulate dependency of creep life to operating temperature and stress. A promising approach has been the use of time-temperature parameters. All the various developed time-temperature parameters consist of a combination of time, temperature and suitable constants. With such parameters and for a given material, a single or master curve of stress against the parameter can be obtained and this is of a great value for extrapolating test results [76]. A few of the various developed time-temperature parameters are briefly presented here.

- Larson–Miller Parameter [77]:

$$\text{LMP} = f(\sigma) = T(C + \log t_r) \quad (2.9)$$

where C is a constant in the range of 15–35.

- Orr–Sherby–Dorn Parameter [27, 78]:

$$\text{OSDP} = f(\sigma) = \log t_r - \frac{Q}{RT} \quad (2.10)$$

where Q is the activation energy of creep process.

- Manson–Haferd Parameter [79]:

$$\text{MHP} = f(\sigma) = \frac{T - T_a}{\log t_r - \log t_a} \quad (2.11)$$

where T_a and t_a are material constants.

The general form for $f(\sigma)$ is [80]:

$$f(\sigma) = c_0 + c_1 \log(T) + c_2 \log(\sigma)^2 + c_3 \log(\sigma)^3 + c_4 \log(\sigma)^4 \quad (2.12)$$

It is worth mentioning that, similar to time–temperature parameters, algebraic models can be used for extrapolation of material creep rupture behaviour. The following represent two examples for the algebraic models, i.e. the so-called Soviet model (SM) [81] and simplified minimum commitment model (SMCM) [82]:

$$t_r = \exp[c_0 + c_1 \log(T) + c_2 \log(\sigma) + c_3/T + c_4\sigma/T] \quad \text{SM} \quad (2.13)$$

$$t_r = \sigma \exp[c_0 + c_1 \log(\sigma) + c_2] + c_3\sigma^2 + c_4T + c_5/T \quad \text{SMCM} \quad (2.14)$$

where c_{0-5} are constant values. During the 1970s, focus was more on the development of algebraic models which were less flexible than the time–temperature parameter approaches, but were more stable in extrapolation [83].

Monkman Grant Relationship [84]

The times to creep rupture for many alloy systems correlate with minimum (or steady) creep rates through the phenomenological Monkman–Grant relationship [84]:

$$(\dot{\epsilon})^m t_r = C \quad (2.15)$$

where the values of m and C are constants depending on the material and/or temperature. For metals and alloys originally examined by Monkman and Grant, the exponent m was between 0.8 and 0.95 and the constant C had the value of 3–20 [85].

Although the Monkman–Grant relationship was not originally intended for extrapolation [86], it can be used to estimate the rupture life from minimum creep rate obtained either from non-accelerated uniaxial tests (without the need for running to rupture) or stress relaxation test data.

The stress relaxation test based method for creep life prediction was proposed by Woodford [87]. The procedure involves loading a tensile specimen to a prescribed strain level at the desired temperature, and then holding the strain constant. The stress relaxes as elastic strain is replaced by inelastic creep strain and by using an appropriate value of elastic modulus the stress relaxation response may be converted to a creep strain rate (stress) formulation which can be used to predict rupture times for a wide range of stress values using the Monkman–Grant relationship [84].

Theta Projection Method

The theta projection concept assumes that creep is the result of a competition between hardening and softening processes and represents the creep behaviour of materials as a stress, temperature and time dependent equation set. Failure is determined by ductility exhaustion, a failure strain which again depends upon stress and temperature. The method can be described by the following empirically derived equation:

$$\varepsilon_r = \theta_1[1 - \exp(-\theta_2 t)] + \theta_3[\exp(\theta_4 t) - 1] \quad (2.16)$$

$$\varepsilon_r = C_1 + C_2 T + C_3 \sigma + C_4 \sigma T \quad (2.17)$$

where θ_1 and θ_2 define the primary and θ_3 and θ_4 describe the tertiary creep behaviours. $\log(\theta_i)$ is stress temperature dependent parameters parameters, usually in the form of $f(\sigma, T) = c_1^i + c_2^i T + c_3^i \sigma + c_4^i \sigma T$ (C_i, c_i are constant values). Determination of the 20 parameters of this equation set requires the results from a well distributed matrix of stress and temperature accelerated creep tests [88].

MPC Omega Method [39]

The MPC Omega method developed by Prager is based on the idea that current creep strain rate, along with a brief history of creep strain rates, can provide information on the past and future behaviour of a material under creep condition [39]. This method considers only tertiary creep and expresses the creep rate of a material as:

$$\dot{\varepsilon} = \dot{\varepsilon}_0 \exp(\Omega \varepsilon) \quad (2.18)$$

where $\dot{\epsilon}_0$ is initial tertiary creep rate and Ω is materials creep damage susceptibility parameter which should be determined experimentally. This gives rise to [89]:

$$\text{Life fraction consumed} = \frac{\dot{\epsilon}t\Omega}{1 + \dot{\epsilon}t\Omega} \quad (2.19)$$

Wilshire Method [90, 91]

In the early 2000s, Wilshire developed a methodology for predicting the long term creep lives, minimum creep rates and the times to various strains of materials. In this method, the applied stress is normalised through measured values of tensile stress at the creep temperature (σ_m) and then the multi-heat data is superimposed onto a sigmoidal master curve. For creep rupture durations:

$$\frac{\sigma}{\sigma_m} = \exp\{-k_1[t_r \exp(Q_{SD}/RT)]^u\} \quad (2.20)$$

where constant values of k_1 and u are different in the high and low stress regimes, determined from plots of $\log[t_r \exp(Q_{SD}/RT)]$ against $\log[\sigma/\sigma_m]$ and [91].

The LICON Method

In the late 1990s, an advanced iso-thermal extrapolation approach referred to as the LICON methodology was developed in an European Brite Euram project to predict the long term creep rupture behaviour of new generation steels from the results of relatively short duration multiaxial specimen tests [92, 93]. This methodology relies on multiaxial loading conditions to bring forward the onset of long-time creep damage formation into the short-time rupture regime to thereby enable extended extrapolation of rupture strength into the long-time fracture regime [94].

The LICON method is based on the formulation:

$$t_{i,x} = A(\bar{\sigma})^{-\nu}(H)^{-\gamma} \quad (2.21)$$

with $H = \sigma_1/\bar{\sigma}$, where σ_1 is the maximum principal stress and $\bar{\sigma}$ is the von Mises equivalent stress, and where A , ν and γ are constants determined for the material and temperature of interest and the associated multiaxial creep-rupture response. The LICON method characterises the material behaviour in different creep failure mechanism regimes. For the regime where creep failure is $\bar{\sigma}$ -controlled, $\gamma = 0$ and for condition where creep failure is σ_1 -controlled, $\gamma' \rightarrow \nu'$ [94, 95]. With a knowledge of $\bar{\sigma}$ and H values from the results of

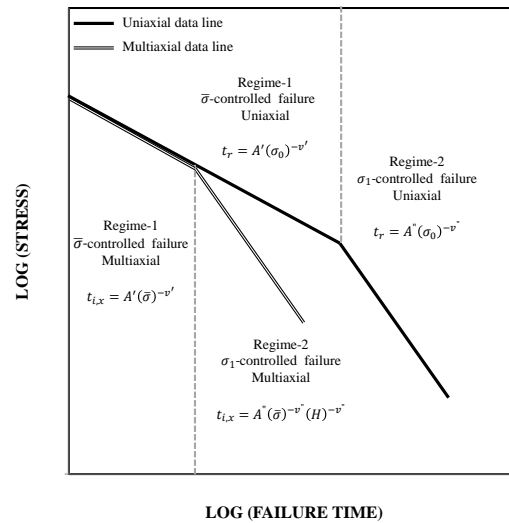


Figure 2.14: Schematic representation of the LICON concept.

mechanical analysis for the multiaxial testpieces and knowing the value of rupture criterion obeyed by the material (i.e. γ), the values of A and ν and eventually uniaxial creep rupture behaviour of material can be determined from the results of a series of short duration multiaxial tests. Figure 2.14 schematically represents the concept of LICON method.

Continuum Damage Mechanics

The continuum damage mechanics (CDM) approach was first introduced by Kachanov, based on a continuum mechanics concept [40]. On the microscale, material structure is discontinuous and inhomogeneous, because of the existence of micro-defects or damage. Continuum mechanics however considers a continuous representative volume element (RVE) for all properties that can be represented by homogenized variables [96]. CDM introduces a damage parameter which, in contrast to the traditional material mechanics concept of perfect or failed, points out an intermediate stage existing between perfect and failed material. The damage variable is 0 for perfect and 1 for failed and broken stages [96]. The variation of the damage parameter should be defined by a damage evolution equation. Several different damage evolution equations have been defined in the literature, from phenomenological to physically based, and with single or multi, scalar or tensorial damage variables [40, 96–99]. The damage variables may define cavity formation, precipitation growth or other material

degeneration phenomena. The predictability of this approach depends heavily on the choice of an appropriate damage evolution equation and accurate determination of the equation constants [97]. These are usually determined by means of dexterous trial and error and computationally expensive numerical optimizations. With the rapid development of modern computer technology and FEA, CDM has found considerable attentions during recent years [96]. Table 2.3 presents some literature reported damage evolution equations (the list is not exhaustive and only gives some examples of damage evolution equations).

There are other approaches for the prediction of creep life time of materials such as the initial strain method (ISM) [100] and the β -envelope method [101], etc. But these are not considered further.

2.6.1 Creep Life Prediction of Weldments

Weldment creep life can be affected by several different parameters such as weld imperfections, weld residual stresses, metallurgical transformations, etc. Furthermore, a weldment is a multi-material system (parent, HAZ and weld materials) and under creep loading conditions, each material creeps at a different rate [102] which results in development of complex multiaxial stress states.

In general, weldment creep rupture strength is lower than that of PM (Figure 2.15). Design codes therefore recommend to consider a weld strength factor (WSF) in the design of components with weldments. The WSF is defined as the ratio between creep rupture strength of weldment and PM [60, 103]. Design codes usually consider a constant (material, time and temperature independent) WSF factor, for example WSF= 0.8 by German AD2000–Merkblatt B0 [60, 104]. However, many researches have reported either higher but also significantly lower WSF factors dependent on several factors like material type, stress level, temperature, etc [61, 105–107]. The European Creep Collaborative Committee (ECCC) has

Table 2.3: Uniaxial creep damage evolution equations.

Equations	Mathematical formulations
Kachanov–Rabotnov [40, 41]	$\dot{\omega} = \frac{B\sigma^p}{(1+q)(1-\omega)^q}$
Liu–Murakami [98]	$\dot{\omega} = D \frac{1-\exp(-q)}{q} \sigma^p \exp(q\omega)$
Dyson–Osgerby [99]	$\dot{\omega}_1 = N c_1 \dot{\epsilon}, \dot{\omega}_2 = \frac{c_2}{3} (1 - \omega_2)^4$

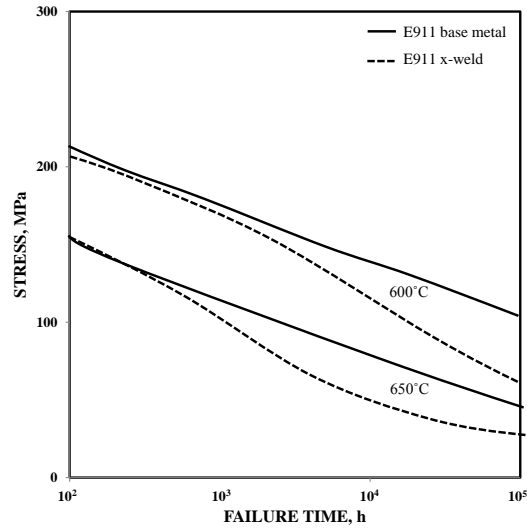


Figure 2.15: Comparison of base metal and cross-weld creep rupture strengths for E911 at different temperatures [105].

defined the WSF as follows [108]:

$$\text{WSF}_{t,T} = \frac{\sigma_{r,t,T}(\text{weldment})}{\sigma_{r,t,T}(\text{PM})} \quad (2.22)$$

where $\sigma_{r,t,T}$ is the creep rupture strength at time t and temperature T (other factors are also defined [108]).

Design of real components concerned with long-time applications needs WSF factors for long term conditions. Observations of significant reductions of WSF factor after long-times have highlighted the risk involved in extrapolation of long term WSF factor from short term creep rupture data. In the 1990s, the occurrence of several catastrophic failures of welded steam piping systems acted as a driving force for increasing research activities on creep failure of welded joints [60].

A weldment has different microstructural constituents with different creep deformation/failure behaviours. Creep behaviour characterisation of HAZ and WM is difficult and there is only limited data available in the literature. Figure 2.16 shows a comparison of the creep resistance of parent, HAZ and weld materials.

The overall creep lifetime of weldments may be simply defined as the minimum creep lifetime

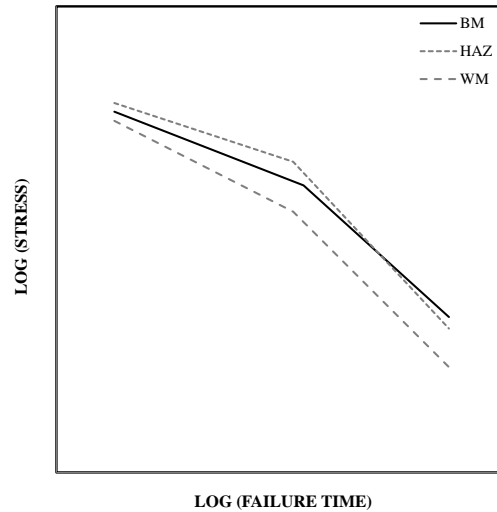


Figure 2.16: Schematic comparison of creep rupture strengths of PM, HAZ and WM in [109].

of the individual sections (i.e. weld, HAZ and parent materials) under the homogeneous reference stress determined for the component (the reference stress concept is explained in the next section). Despite the simplicity of the approach, the basic problem is that it does not account for the stress redistribution occurring within the weldment due to different creep deformation behaviours of the weldment constituent [110].

Coleman et al. [111] have shown that for a creep loaded weldment, the stress may distribute differently within the different sections of the weldment. To consider this effect, another approach may factor the global stress to give the stresses at the different constituents of weldments [112]. The overall creep lifetime of weldments is then defined from the minimum creep lifetime of individual sections at the correspondingly factored reference stresses. The factors however can vary for each specific weldment and creep condition and hence, their specification is difficult. As another approach, numerical analysis such as FEA may be used to determine the stationary stress state for weldments and determine the reference stress for each individual section of the weldment [110].

The above approaches determine the creep rupture life of a weldment based on an estimated stationary stress state. The basic assumption here is that for a loaded component, there are two distinct phases. In the first phase, without considerable damage formation, creep strains accumulate to distribute the stress and form a stationary stress state. In the second phase, it is assumed that, without further stress redistribution, the established stationary

stress state leads to creep damage accumulation and final failure [110]. Preservation of a stationary stress state during the second phase however is not a realistic assumption. During the second phase, when damage develops in some regions, the load bearing capacity of those regions reduces and consequently stress is off-loaded onto stronger (less-damaged) regions. It means that stress redistribution may start again in the second phase. Therefore, while the above approaches can be effective for conditions for which the stationary stress state is preserved for a large portion of creep life, more accurate analyses are required for other conditions.

Finite element continuum damage mechanics (FECDM) is generally a more accurate approach which considers continuous stress redistribution and damage formation within the whole life of a component [110]. The basis of CDM has already been explained in the previous section and FECDM is simply an implementation of the CDM concept into the material constitutive formulation of an FEA solver. Basically a successful application of FECDM for analysis of a structure, with or without welding, can predict not only the lifetime of a component, but also its deformation behaviour and failure location [110]. For example, Hall and Hayhurst [113] have used FECDM to predict the deformation, life time and failure location for a pressurised butt welded ferritic steel pipe. The generated predictions were in good agreement with experimental observations reported by Coleman et al. [111, 114].

The success of FECDM for analysis of a weldment significantly relies on the accuracy of the implemented material constitutive information. The use of FECDM methods demands accurate materials testing data to describe the deformation and rupture of different material sections of the weldment [109, 110]. In fact, the lack of accurate creep deformation and failure data for the HAZ and WM is the main drawback of this approach.

As another approach, the LICON method can be used to predict the creep rupture behaviour of weldments. The basis for the LICON method has been already explained in the previous section. Briefly, the LICON method predicts the long term creep failure behaviour of materials/weldments using the results from several short term creep crack incubation (CCI) tests. After demonstration of successful application of this method for predicting the creep life of advanced 9%Cr pipe steel cross-welds in late 1990s [93], this study examines the applicability of the method for a DMW (1CrMoV–Alloy 617–Alloy 625). It must be remarked that the effectiveness of the approach for application to welded structures of copper (SMW) is currently under investigation at VTT institute, Finland [115].

2.7 Creep Analysis of Structures

The creep analysis of structures is an important subject and has received increasing attention in engineering design [116]. The aim of such analyses is to reflect basic features of creep in engineering structures including inelastic deformation, stress redistribution as well as creep damage development and failure [117]. As a generality, the resolution of creep problems is more difficult than that of elastic–plastic problems, as the constitutive behaviour of material during creep deformation is very complicated [116]. Ideally, the mechanical analysis of a creeping structure needs extensive information concerning the creep behaviour of the material from which the structure is made (under different loading conditions) [118]. Engineering methods however try to minimise the amount of needed data. Therefore, while approaches such as reference stress methods approximate the creep behaviour of a structure with minimum data availability, numerical analyses such as FEA can potentially provide more accurate results but with a more extensive material data requirement. The following explains two methods which can be used to mechanically analyse a structure under creep loading condition.

2.7.1 Reference Stress Approach

The idea of a reference stress method was first introduced by Soderberg [119] and later improved by Mackenzie [120], Sim [121] and others. This approach, in certain conditions, can provide accurate predictions for the creep deformation and rupture behaviour of components under creep loading conditions and, because of its simplified nature, is widely used for analysis and design of engineering components [122].

For a component loaded under creep conditions, after instantaneous elastic and plastic deformation, creep begins, stresses redistribute and then, a stationary state is eventually reached [118]. The deformation behaviour of a structure under creep may therefore be expressed by:

$$\phi = \phi_i + \phi_c = \phi_i + (\phi_s + \phi_t) \quad \text{if } t > t_{red} \quad (2.23)$$

where ϕ is a general deformation parameter, ϕ_i is the initial deformation, ϕ_c is the creep deformation (including stationary and transient components, ϕ_s and ϕ_t , respectively) and t_{red} is the stress redistribution time (Figure 2.17) [118].

The stationary creep deformation part of equation 2.23 for a material with the creep gov-

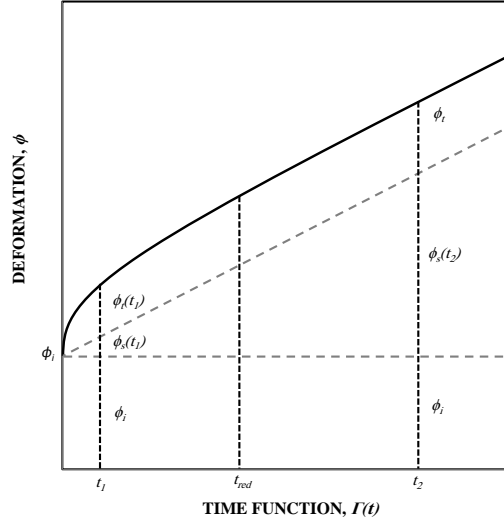


Figure 2.17: Deformation components of a structure under creep loading conditions [118].

erning law of $\varepsilon_c = \sigma^n \Gamma(t)$ can be expressed in the form of:

$$\begin{aligned}\phi_s &= (\sigma_{\text{nom}})^n F_n F_{\text{dim}} \Gamma(t) \\ &= \left[\frac{\sigma_{\text{nom}}}{\sigma_0} \right]^n F_n F_{\text{dim}} \varepsilon_0\end{aligned}\quad (2.24)$$

where F_n and F_{dim} are functions of stress exponent n and dimensions, respectively. The σ_{nom} is the nominal stress of the structure (proportional to the magnitude of applied load), σ_0 is an arbitrary stress and $\varepsilon_0 = \sigma_0 \Gamma(t)$ [118].

Anderson et al. [123] and Mackenzie [120] have investigated the stationary state creep deformation behaviour of several geometries and have shown that for a suitable choice of σ_0 , the function of $[\sigma_{\text{nom}}/\sigma_0]^n F_n$ is weakly dependent on n and, therefore to some extent on material creep behaviour. This value of σ_0 is called reference stress, σ_{ref} , hence [118]:

$$\phi_s = B F_{\text{dim}} \varepsilon_{\text{ref}} \quad (2.25)$$

where $B = [\sigma_{\text{nom}}/\sigma_{\text{ref}}]^n F_n$. Equation 2.25 illustrates the power of the reference stress approach which can express the stationary creep deformation behaviour of a structure in terms of uniaxial data for a single value of stress [118]. Marriott and Leckie [124] have shown that, only for some geometries, the reference stress can be identified with the stress

at a skeletal point for the structure where the stress remains constant during redistribution [118].

Later, Penny and Marriott [125] used the similarity of creep behaviour when $n = \infty$ with the rigid–perfectly plastic behaviour and showed:

$$\sigma_{\text{ref}} = \frac{P}{P_L} \sigma_y \quad (2.26)$$

where σ_y is the yield stress of the material, P is the magnitude of applied load [118]. P_L is the collapse load which has been determined for a range of simple geometries [126] and can numerically be calculated for any other geometry. Equation 2.26, being an upper bound for reference stress, gives an easily obtainable value for the reference stress [118].

For long durations, $t \gg t_{\text{red}}$, transient deformation, ϕ_t , can be neglected and the addition of instantaneous deformation (which can be determined from simple elastic–plastic analysis) and the stationary deformation is an approximation for the total deformation [118].

The reference stress concept is also applicable for rupture properties. Hayhurst et al. [127] have shown that for creep ductile materials with rupture obeying an equivalent shear stress criterion, the rupture reference stress is the same as that for creep deformation [118]. However, for creep brittle materials, the creep deformation reference stress is a lower bound for creep rupture reference stress and can therefore result in non-conservative lifetime predictions [128]. Sim [129] alleviated this shortcoming by assuming the creep rupture reference stress as a function of the principal stress and the equivalent stress [130]. Finally, R5 defined an empirical estimation for the rupture reference stress as [131–133]:

$$\sigma_{\text{ref}}^r = [1 + 0.13(\chi - 1)] \sigma_{\text{ref}} \quad (2.27)$$

where $\chi = (\bar{\sigma}^{\text{max}} / \sigma_{\text{ref}})$ is a stress concentration factor for the adjustment of reference stress and $\bar{\sigma}^{\text{max}}$ is the maximum value of the equivalent stress in the structure calculated from an elastic analysis [134].

Generally, it is doubtful if ideal reference stresses exist for real components and real materials. However for many real situations, an approximate reference stress which is insensitive to the material behaviour rather than independent of that, can be determined to predict the creep behaviour of structures to an acceptable degree of accuracy [118].

2.7.2 Finite Element Analysis

The design and life assessment of high temperature components increasingly rely on determinations of the creep stress/strain (rate) state at the critical locations. In principal, it is possible to calculate the stress and strain distributions throughout a structure provided that the constitutive behaviour of the material from which the structure is made is known [130]. As a generality, the resolution of creep problems is more difficult than that of elastic-plastic problems and hence, FEA appears to be the only practical solution to this type of problems [116]. The underlying premise of FEA is that an approximate solution to any complex engineering analysis can be obtained by subdividing the problem into smaller (finite) elements where complex non-linear equations can be reduced to a set of linear equations.

Most time-dependent non-linear FEAs are based on determining small increments of strain (displacement) over small time increments. The procedure starts with the assumption of an increment of strain (displacement) to be accumulated over a small increment of time. The code should then determine the increment of inelastic strain. This can be calculated using a constitutive law for the material, but it requires an assumption that the stress is constant during the increment. the determination of inelastic strain can be based on the stress value at the start of the increment or, in an iterative procedure, at the end of increment. By either of the solution, it is possible to determine the stress at the end of the increment. An accuracy check then examines the validity of assuming a constant stress over the increment and if it fails, the process is repeated with a smaller increment. For the implicit FEA, a second check is also conducted to assure that the structure is in equilibrium at the end of the increment. When both checks are passed, the codes starts a new time increment and the process repeats until the final time is reached, and the final strains, displacements and stresses are determined. This simplified procedure, shown in Figure 2.18, is adequate to accurately analyse a structure provided a reasonable set of tolerances is used.

Determination of creep strain using a constitutive law may consider either a strain or a time hardening assumption. In the time hardening assumption, the creep strain increment is assumed to depend on the current stress and time, whereas in the strain hardening assumption, the creep strain increment depends on the current stress and the accumulated creep strain. The more realistic assumption is strain hardening although time hardening is often convenient to use in situations of constant or nearly constant stress [135].

A number of general purpose finite element (FE) codes (e.g. ABAQUS, ANSYS, NASTRAN, COMSOL, MARC, ADINA, etc) have been developed which can be used to solve creep problems [117]. They usually offer several options for solving strategy, constitutive behaviour definition, time incrementation, etc. The user should be aware of their characteristics to

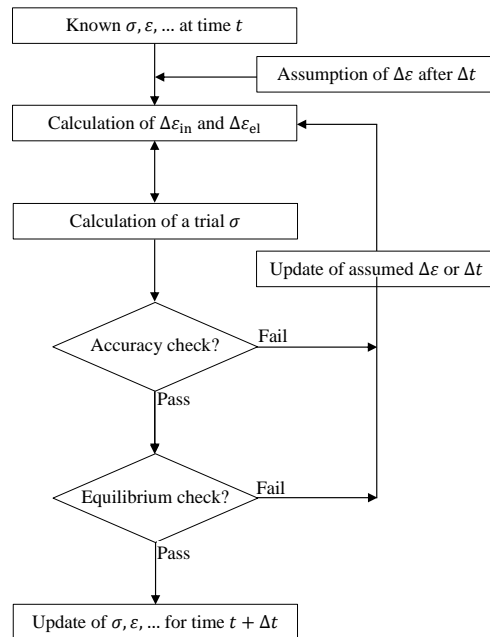


Figure 2.18: Displacement-based FEA procedure (implicit).

be able to choose the appropriate option or, if required, to develop an appropriate option. For example, commercial FE codes adopt sophisticated procedures incorporating automatic adjustment of the time increment. However, more sophisticated procedures should be implemented by the user if the tertiary creep stage is modelled. Similarly, the commercial codes are usually able to consider only a few simple creep constitutive models, e.g. Norton creep model. The user may therefore need to write a user-defined material subroutine to implement more sophisticated creep models with several internal state variables (e.g. damage), special types of stress and temperature functions, etc. [117, 135].

References

- [1] F. Abe, TU. Kern, and R. Viswanathan. *Creep Resistant Steels*. Woodhead Publishing; CRC Press, Cambridge, England, 2008.
- [2] M.E. Kassner and M.T. Pérez-Prado. *Fundamentals of Creep in Metals and Alloys*. Elsevier Science, 2004.
- [3] E.N.C. Andrade. On the viscous flow in metals, and allied phenomena. *Proceedings of the Royal Society of London. Series A*, 84(567):1–12, 1910.
- [4] K. Naumenko and H. Altenbach. *Modelling of Creep for Structural Analysis*. Springer, 2007.
- [5] Y. Gorash. *Development of a Creep Damage Model for Non-isothermal Long Term Strength Analysis of High Temperature Components Operating in a Wide Stress Range*. PhD thesis, National Technical University, Kharkiv, Ukraine, 2008.
- [6] K. Maruyama. *Creep Resistant Steels*, chapter Fundamental aspects of creep deformation and deformation mechanism map, pages 265–278. Woodhead Publishing; CRC Press, Cambridge, England, 2008.
- [7] F.H. Norton. *The Creep of Steel at High Temperatures*. McGraw–Hill book company, 1929.
- [8] O.D. Sherby and P.M. Burke. Mechanical behaviour of crystalline solids at elevated temperature. *Progress in Materials Science*, 13:323–390, 1968.
- [9] G.A. Webster and R.A. Ainsworth. *High Temperature Component Life Assessment*. Springer, 1994.
- [10] R.W. Evans and B. Wilshire. *Introduction to Creep*. Institute of Materials, London, 1993.
- [11] M.F. Ashby. A first report on deformation–mechanism maps. *Acta Metallurgica*, 20(7):887–897, 1972.
- [12] F.R.N. Nabarro. Deformation of crystals by the motion of single ions. In *Physical Society Bristol Conference Report*, pages 75–90, 1948.
- [13] C. Herring. Diffusional viscosity of a polycrystalline solid. *Journal of Applied Physics*, 21(5):437–445, 1950.
- [14] R.L. Coble. A model for boundary diffusion controlled creep in polycrystalline materials. *Journal of Applied Physics*, 34(6):1679–1682, 1963.
- [15] M.S. Mostafa and F.A. Mohamed. Correlation between creep stress exponent and ductility in Al–10%Zn. *Metallurgical and Materials Transactions A*, 17(2):365–366, 1986.
- [16] O.A. Ruano, J. Wadsworth, J. Wolfenstine, and O.D. Sherby. Evidence for Nabarro–Herring creep in metals: fiction or reality? *Materials Science and Engineering A*, 165(2):133–141, 1993.
- [17] D.M. Owen and T.G. Langdon. Low stress creep behavior: an examination of Nabarro–Herring and Harper–Dorn creep. *Materials Science and Engineering A*, 216(1):20–29, 1996.
- [18] L. Kloc, V. Sklenicka, and J. Fiala. Problems in theories of low stress creep mechanisms. In *Proceedings of the 10th International Metallurgical and Materials Conference*, 2001.
- [19] S. Spigarelli, M. El Mehtedi, and A. Di Salvia. Constitutive models for the description of creep and plasticity of cast and wrought Mg–Al and Mg–Zn alloys. In *IUTAM Symposium on Advanced Materials Modelling for Structures, April 23–27*, 2012.
- [20] M. Ashby and D.R.H. Jones. *Engineering Materials 1: an Introduction to their Properties and Applications*. Butterworth Heinemann, 1996.

- [21] M.F. Ashby, H. Shercliff, and D. Cebon. *Materials: Engineering, Science, Processing and Design*. Butterworth–Heinemann, 2007.
- [22] F.R.N. Nabarro and H.L. Villiers. *The Physics of Creep: Creep and Creep Resistant Alloys*. Taylor & Francis (London and Bristol, Pa.), 1995.
- [23] H.J. Frost and M.F. Ashby. *Deformation Mechanism Maps: the Plasticity and Creep of Metals and Ceramics*. Pergamon, 1982.
- [24] F.C. Campbell. *Elements of Metallurgy and Engineering Alloys*. ASM International, 2008.
- [25] T.H. Courtney. *Mechanical Behaviour of Materials*. McGraw–Hill, 1990.
- [26] M.F. Ashby, C. Gandhi, and D.M.R. Taplin. Fracture–mechanism maps and their construction for fcc metals and alloys. *Acta Metallurgica*, 27(5):699–729, 1979.
- [27] R.L. Orr, O.D. Sherby, and J.E. Dorn. Correlations of rupture data for metals at elevated temperatures. *Translation ASM*, 46:113–128, 1954.
- [28] K. Maruyama. *Creep Resistant Steels*, chapter Fracture mechanism map and fundamental aspects of creep fracture, pages 350–364. Woodhead Publishing; CRC Press, Cambridge, England, 2008.
- [29] N. Shinya, J. Kyono, and H. Kushima. Creep fracture mechanism map and creep damage of CrMoV turbine rotor steel. *ISIJ International*, 46(10):1516–1522, 2006.
- [30] S.R. Holdsworth. *Creep Resistant Steels*, chapter Constitutive equations for creep curves and predicting service life, pages 403–420. Woodhead Publishing; CRC Press, Cambridge, England, 2008.
- [31] F.B. Dyson and M. McLean. Microstructural evolution and its effects on the creep performance of high temperature alloys. In *Microstructural Stability of Creep Resistant Alloys for High Temperature Plant Applications*, pages 371–379. Institute of Materials, Minerals and Mining, London, 1998.
- [32] A. Nadai. *The Influence of Time upon Creep, the Hyperbolic Sine Creep Law*. Stephen Timoshenko Anniversary. Macmillan, New York, 1938.
- [33] I.J. Perrin and D.R. Hayhurst. Creep constitutive equations for a 0.5Cr0.5Mo0.25V ferritic steel in the temperature range 600–675 °C. *The Journal of Strain Analysis for Engineering Design*, 31(4):299–314, 1996.
- [34] P. Phillips. The slow stretch in indiarubber, glass, and metal wires when subjected to a constant pull. *Proceedings of the Physical Society of London*, 19(1):491–513, 1903.
- [35] A. Graham and K.F.A. Wallis. Relations between long and short time properties of commercial alloys. *Journal of Iron and Steel Institute*, 179:105–120, 1955.
- [36] P.G. McVetty. Factors affecting the choice of working stresses for high temperature service. *Transactions ASME*, 55:13–99, 1933.
- [37] J.B. Conway and M.J. Mullikin. An evaluation of various first stage creep equations. In *Proceedings AIME Conference, Detroit, Michigan*, 1962.
- [38] D. McHenry. A new aspect of creep in concrete and its application to design. In *ASTM Proceedings*, volume 43, pages 1069–1084, 1943.
- [39] M. Prager. Development of the MPC Omega method for life assessment in the creep range. *Journal of Pressure Vessel Technology*, 117(2):95–103, 1995.
- [40] L.M. Kachanov. On the time to failure under creep conditions. *Izvestiya Akadeil Nauk SSR*, 8:26–31, 1958.
- [41] I.U.N. Rabotnov and F.A. Leckie. *Creep Problems in Structural Members*. North–Holland series in applied mathematics and mechanics. North–Holland Publication Company, 1969.

-
- [42] B.G. Kim, J.L. Rempe, D.L. Knudson, K.G. Condie, and B.H. Sencer. In-situ creep testing capability development for advanced test reactor. Technical report, Idaho National Laboratory, 2010.
- [43] NIMS. *Data Sheet 9B, Data sheets on the elevated temperature properties of 1Cr-1Mo-0.25V steel forgings for turbine rotors and shafts*. National Research Institute for Metals, Tokyo, Japan, 1990.
- [44] T. Ogata, T. Sakai, and M. Yaguchi. Damage characterization of a P91 steel weldment under uniaxial and multiaxial creep. *Materials Science and Engineering A*, 510:238–243, 2009.
- [45] A.V. Shutov, H. Altenbach, and K. Naumenko. Steady-state creep analysis of pressurized pipe weldments by perturbation method. *International Journal of Solids and Structures*, 43(22):6908–6920, 2006.
- [46] Z.F. Hu. *Thermal Power Plants*, chapter Heat resistant steels, microstructure evolution and life assessment in power plants, pages 195–226. InTech, 2012.
- [47] D. Kopeliovich. Creep resistant steels, <http://www.substech.com>, 2012.
- [48] P.J. Ennis and A. Czyrska-Filemonowicz. Recent advances in creep resistant steels for power plant applications. *Sadhana Academy Proceedings in Engineering Sciences*, 28(3):709–730, 2003.
- [49] A. Nagode, L. Kosec, B. Ule, and G. Kosec. Review of creep resistant alloys for power plant applications. *Metalurgija*, 50(1):45–48, 2011.
- [50] H. Bhadeshia. Design of ferritic creep resistant steels. *ISIJ International*, 41(6):626–640, 2001.
- [51] K.H. Mayer. *Creep Resistant Steels*, chapter The development of creep resistant steels, pages 15–77. Woodhead Publishing; CRC Press, Cambridge, England, 2008.
- [52] R.L. Bodnar, J.R. Michael, S.S. Hansen, and R.I. Jaffee. Progress in the design of an improved high temperature 1CrMoV rotor steel. In *30th Mechanical Working and Steel Processing Conference*, volume 26, pages 173–194, 1988.
- [53] R.M. Curran. The development of improved forgings for modern steam turbines. In *Proceedings of ASTM Symposium on Steel, Stainless Steel and Related Alloys*, pages 9–32. ASTM Special Technical Publication, 1984.
- [54] D. Sidey. The high temperature creep and fracture behaviour of a 1CrMoV rotor steel. *Metallurgical and Materials Transactions A*, 7(11):1785–1791, 1976.
- [55] J.F. Norton and A. Strang. Metallurgical developments in manufacture of large 1CrMoV steam turbine rotor forgings. *English Electric Journal*, 23(6):20–28, 1968.
- [56] Branch G.D., Marriot J.B., and Murphy M.C. The creep and creep-rupture properties of six CrMoV rotor forgings for high temperature steam turbines. In *Proceedings of the International Conference on Properties of Creep Resistant Steels*, Düsseldorf, 1972, Paper VII, I.
- [57] G.J.P. Buchi, J.H.R. Page, and M.P. Siedey. Creep properties and precipitation characteristics of 1CrMoV steel. *Journal of the Iron and Steel Institute*, 203:291–298, 1965.
- [58] N.S. Cheruvu. Degradation of mechanical properties of CrMoV and 2.25Cr-1Mo steel components after long term service at elevated temperatures. *Metallurgical and Materials Transactions A*, 20(1):87–97, 1989.
- [59] J.A. Williams. The high temperature performance of austenitic-ferritic dissimilar welds. In *Proceedings of International Conference on Integrity of High Temperature Welds*, pages 3–4, 1998.
- [60] H. Cerjak and P. Mayr. *Creep Resistant Steels*, chapter Creep strength of welded joints of ferritic steels, pages 472–503. Woodhead Publishing; CRC Press, Cambridge, England, 2008.

- [61] P. Mayr. *Evolution of microstructure and Mechanical Properties of the Heat Affected Zone in B-Containing 9% Chromium Steels*. PhD thesis, Mechanical Engineering of the Graz University of Technology, 2007.
- [62] C.D. Lundin, J.F. Henry, and F.V. Ellis. *Failure Analysis of a Service Exposed Hot Reheat Steam Line in a Utility Steam Plant*. Welding Research Council, 1990.
- [63] I.J. Perrin and D.R. Hayhurst. Continuum damage mechanics analyses of type IV creep failure in ferritic steel crossweld specimens. *International journal of pressure vessels and piping*, 76(9):599–617, 1999.
- [64] M. Tabuchi, K. Masayuki, K. Kubo, and S.K. Albert. Improvement of type IV creep cracking resistance of 9%Cr heat resisting steels by boron addition. *Operation Maintenance and Materials Issue*, 3(3):1–11, 2004.
- [65] S.K. Albert, M. Kondo, M. Tabuchi, F. Yin, K. Sawada, and F. Abe. Improving the creep properties of 9Cr–3W–3Co–NbV steels and their weld joints by the addition of boron. *Metallurgical and Materials Transactions A*, 36(2):333–343, 2005.
- [66] D.I. Roberts, R.H. Ryder, and R. Viswanathan. Performance of dissimilar welds in service. *Journal of Pressure Vessel Technology*, 107(3):247–254, 1985.
- [67] R.D. Nicholson. Effect of aging on interfacial structures of nickel based transition joints. *Metals Technology*, 11:115–124, 1984.
- [68] R.D. Nicholson. Creep rupture properties of nickel base transition joints after long term service. *Materials Science and Technology*, 2(7):686–692, 1986.
- [69] V.M. Radhakrishnan. *Welding Technology & Design*. New Age International, 2005.
- [70] S.J. Brett. Type IIIa cracking in 0.5CrMoV steam pipework systems. *Science and Technology of Welding & Joining*, 9(1):41–45, 2004.
- [71] R.L. Klueh and J.F. King. Austenitic stainless steel–ferritic steel weld joint failures. Technical report, Oak Ridge National Laboratory, 1982.
- [72] J.D. Parker and G.C. Stratford. Review of factors affecting condition assessment of nickel based transition joints. *Science and Technology of Welding & Joining*, 4(1):29–39, 1999.
- [73] R.D. Nicholson. Effect of post-weld heat treatment on development of interfacial structures in nickel based transition joints. *Materials Science and Technology*, 1(3):227–233, 1985.
- [74] J.N. DuPont and R.E. Mizia. Review of dissimilar metal welding for the NGNP helical–coil steam generator. Technical report, Idaho National Laboratory (INL), 2010.
- [75] S.R. Holdsworth. The ECCC approach to creep data assessment. *Journal of Pressure Vessel Technology (ASME)*, 130:1–6, 2008.
- [76] G.J. Heimerl. Time–temperature parameters and an application to rupture and creep of aluminum alloys. Technical report, Langley Aeronautical Laboratory, 1954.
- [77] F.R. Larson and J. Miller. A time–temperature relationship for rupture and creep stresses. *Transactions ASME*, 74(5):765–775, 1952.
- [78] O.D. Sherby and J.E. Dorn. On the correlation between creep and tensile properties of dilute alpha solid solutions of aluminum. Technical report, Institute of Engineering Research, 1951.
- [79] S.S. Manson and A.M. Haferd. A linear time–temperature relation for extrapolation of creep and stress–rupture data. Technical report, Lewis Flight Propulsion Laboratory, 1953.
- [80] BSI PD 6605. *Guidance on Methodology for the Assessment of Stress Rupture Data*. British Standards Institution, 1997.

-
- [81] I.I. Trunin, N.G. Golobova, and E.A. Loginov. New method of extrapolation of creep test and long time strength results. In *Proceedings of the 4th International Symposium on Heat Resistant Metallic Material*, 1971.
- [82] S.S. Manson and U. Muraldihan. Analysis of creep rupture data for five multi-heat alloys by minimum commitment method using double heat term centring technique. *EPRI*, 1981.
- [83] S.R. Holdsworth. Advances in the assessment of creep data. In *Proceedings of 9th Liege Conference: Materials for Advanced Power Engineering*, pages 946–947, 2010.
- [84] F.C. Monkman and N.J. Grant. An empirical relationship between rupture life and minimum creep rate in creep–rupture tests. *ASTM Proceedings*, 56:593–620, 1956.
- [85] D.C. Dunand, B.Q. Han, and A.M. Jansen. Monkman–Grant analysis of creep fracture in dispersion–strengthened and particulate–reinforced aluminum. *Metallurgical and Materials Transactions A*, 30(13):829–838, 1999.
- [86] E.J.R. Davis and ASM International Handbook Committee. *Heat Resistant Materials*. ASM International, 1997.
- [87] D.A. Woodford. Accelerated testing for high temperature materials performance and remaining life assessment. *EPRI Report*, 1999.
- [88] M. Evans. Predicting times to low strain for a 1CrMoV rotor steel using a $6-\theta$ projection technique. *Journal of Materials Science*, 35(12):2937–2948, 2000.
- [89] M. Prager. The Omega method: an engineering approach to life assessment. *Journal of Pressure Vessel Technology*, 122(3):273–280, 2000.
- [90] B. Wilshire and P.J. Scharning. Prediction of long term creep data for forged 1Cr–1Mo–0.25V steel. *Materials Science and Technology*, 24(1):1–9, 2008.
- [91] B. Wilshire and P.J. Scharning. Extrapolation of creep life data for 1Cr–0.5Mo steel. *International Journal of Pressure Vessels and Piping*, 85(10):739–743, 2008.
- [92] P. Auerkari, W. Bendick, S. Holdsworth, J.H. Rantala, R. Hurst, C. Coussement, and R. Hack. Predicting long term creep behaviour using the LICON methodology. In *3rd International Conference of Advances in Material Technology for Fossil Power Plants, Swansea, UK*, pages 329–339. Institute of Materials, Minerals and Mining, 2001.
- [93] V.M. Martins and S.R. Holdsworth. The LICON methodology for predicting the long term service behaviour of new steels. *Materials at High Temperatures*, 19(2):99–103, 2002.
- [94] S. Holdsworth and E. Mazza. Exploring the applicability of the LICON methodology for a 1CrMoV steel. *Materials at High Temperatures*, 25(4):267–276, 2008.
- [95] B.J. Cane. Creep cavitation and rupture in 2.25CrMo steel under uniaxial and multiaxial stresses. In *Proceedings of 3rd International Conference on Mechanical Behaviour of Materials*, volume 2, pages 173–182, 1979.
- [96] H.T. Yao, F.Z. Xuan, Z. Wang, and S.T. Tu. A review of creep analysis and design under multiaxial stress states. *Nuclear Engineering and Design*, 237(18):1969–1986, 2007.
- [97] J.W. Ju. Damage mechanics of composite materials: constitutive modelling and computational algorithms. Technical report, DTIC Document, 1991.
- [98] Y. Liu and S. Murakami. Damage localization of conventional creep damage models and proposition of a new model for creep damage analysis. *JSME International Journal A*, 41:57–65, 199.
- [99] B.F. Dyson and S. Osgerby. *Modelling and Analysis of Creep Deformation and Fracture in a 1Cr–0.5Mo Ferritic Steel*. NPL report. National Physical Laboratory, 1993.

- [100] S.K. Oh and S.U. Jeong. Long-time creep strength and life prediction of steam turbine rotor steel by initial strain method. *Transaction of ASME*, 17(6):1321–1329, 1993.
- [101] V.M. Radhakrishnan. The relationship between minimum creep rate and rupture time in Cr–Mo steels. *Journal of Materials Engineering and Performance*, 1(1):123–128, 1992.
- [102] J. Jelwan, M. Chowdhry, and G. Pearce. Creep life forecasting of weldment. *Journal of Solid Mechanics*, 2011.
- [103] C.F. Etienne and J.H. Geerings. Evaluation of the influence of welding on creep resistance. *Steel research*, 65(5):187–196, 1994.
- [104] AD 2000 MERKBLATT B0 Design Of Pressure Vessels, Technical Rule. 2008.
- [105] S.R. Holdsworth and A. Klenk. ECCC guidelines for generation and assessment of weld creep data. In *MPA-Seminar "Werkstoff & Bauteilverhalten in der Energie & Anlagentechnik"*, Stuttgart, 2007.
- [106] R. Sandström and S.T. Tu. The effect of multiaxiality on the evaluation of weldment strength reduction factors in high temperature creep. *Journal of Pressure Vessel Technology*, 116(1), 1994.
- [107] M. Tabuchi and Y. Takahashi. Evaluation of creep strength reduction factors for welded joints of modified 9Cr–1Mo steel. *Journal of Pressure Vessel Technology*, 134(3), 2012.
- [108] P.F. Morris. Terms and terminology for weld creep testing. In *ECCC Recommendations*, volume 2(Iib), 2001.
- [109] Z.P. Wang and D.R. Hayhurst. Materials data for high temperature design of ferritic steel pressure vessel weldments. *International Journal of Pressure Vessels and Piping*, 55(3):461–479, 1993.
- [110] I.J. Perrin, D.R. Hayhurst, and R.A. Ainsworth. Approximate creep rupture lifetimes for butt welded ferritic steel pressurised pipes. *European Journal of Mechanics A*, 19(2):223–258, 2000.
- [111] M.C. Coleman, J.D. Parker, and D.J. Walters. The behaviour of ferritic weldments in thick section 0.50Cr0.50Mo0.25V pipe at elevated temperature. *International Journal of Pressure Vessels and Piping*, 18(4):277–310, 1985.
- [112] R.A. Ainsworth and P.J. Budden. Design and assessment of components subjected to creep. *The Journal of Strain Analysis for Engineering Design*, 29(3):201–207, 1994.
- [113] F.R. Hall, D.R. Hayhurst, F.R. Hall, and D.R. Hayhurst. Continuum damage mechanics modelling of high temperature deformation and failure in a pipe weldment. *Proceedings of the Royal Society of London A*, 433(1888):383–403, 1991.
- [114] M.C. Coleman, J.D. Parker, D.J. Walters, and J.A. Williams. The deformation behaviour of thick walled pipes at elevated temperatures. In *Proceedings of 3rd International Conference on Mechanical Behaviour of Materials*, volume 2, pages 193–202, 1979.
- [115] J. Rantala, P. Auerkari, J. Salonen, S. Holmström, A. Laukkanen, and T. Saukkonen. Mechanical performance and life prediction for canister copper. Technical report, VTT Technical Research Centre of Finland, 2010.
- [116] G.G. Chen and T.R. Hsu. A mixed explicit–implicit algorithm for creep stress analysis. *International Journal for Numerical Methods in Engineering*, 26(2):511–524, 1988.
- [117] K. Naumenko. *Modelling of High Temperature Creep for Structural Analysis Applications*. PhD thesis, Martin Luther Universität Halle Wittenberg, 2006.
- [118] T.H. Hyde. *Experimental Reference Stress Techniques for the Prediction of Creep Deformation Using Lead Alloy Models*. PhD thesis, University of Nottingham, 1976.
- [119] C.R. Soderberg. Interpretation of creep tests on tubes. *Transactions ASME*, 63(8):737–748, 1941.

-
- [120] A.C. Mackenzie. On the use of a single uniaxial test to estimate deformation rates in some structures undergoing creep. *International Journal of Mechanical Sciences*, 10(5):441–453, 1968.
- [121] R.G. Sim. *Creep of Structures*. PhD thesis, University of Cambridge, 1968.
- [122] G. Rayner. *Creep of Welded Branched Pipes*. PhD thesis, University of Nottingham, 2004.
- [123] R.G. Anderson, L.R.T. Gardner, and W.R. Hodgkins. Deformation of uniformly loaded beams obeying complex creep laws. *Journal of Mechanical Engineering Science*, 5(3):238–244, 1963.
- [124] D.L. Marriott and F.A. Leckie. Some observations on the deflections of structures during creep. In *Proceedings of the Institution of Mechanical Engineers*, volume 178, pages 115–125, 1963.
- [125] R.K. Penny and D.L. Marriott. *Design for Creep*. Springer, 1995.
- [126] S. Al Laham, S.I. Branch, and R.A. Ainsworth. Stress Intensity Factor and Limit Load Handbook. *British Energy Generation*, 1999.
- [127] D.R. Hayhurst, D.A. Kelly, F.A. Leckie, C.J. Morrison, A.R.S. Ponter, and J.J. Williams. Approximate design methods for creeping structures. In *International Conference on Creep and Fatigue in Elevated Temperature Applications*, 1973.
- [128] I.W. Goodall and R.D.H. Cockroft. On bounding the life of structures subjected to steady load and operating within the creep range. *International Journal of Mechanical Sciences*, 15(3):251–263, 1973.
- [129] R.G. Sim. Reference stress concepts in the analysis of structures during creep. *International Journal of Mechanical Sciences*, 12(6):561–573, 1970.
- [130] J. Jelwan, M. Chowdhury, and G. Pearce. Creep life design criterion and its applications to pressure vessel codes. *Materials Physics and Mechanics*, 11:157–182, 2011.
- [131] R5. Assessment Procedure for the High Temperature Response of Structures. *British Energy Generation*, 3, 2003.
- [132] D.R. Hayhurst. Creep rupture under multi-axial states of stress. *Journal of the Mechanics and Physics of Solids*, 20(6):381–382, 1972.
- [133] B.J. Cane. Creep cavitation and rupture in 2.25Cr1Mo steel under uniaxial and multiaxial stresses. In K.J. Miller and R.F. Smith, editors, *Proceedings of 3rd International Conference on Mechanical Behaviour of Materials*, pages 173–182, 1980.
- [134] P.F. Morris. High Temperature Component Analysis Overview of Assessment and Design Procedures. *ECCC Recommendations*, 9(II), 2005.
- [135] A.A. Becker, T.H. Hyde, and L. Xia. Numerical analysis of creep in components. *The Journal of Strain Analysis for Engineering Design*, 29(3):185–192, 1994.

Chapter 3

Articles

3.1 *Article One*

Overview

This section contains a reprint of the article: E. Hosseini, S.R. Holdsworth, E. Mazza, Experience with using the LICON methodology for predicting long term creep behaviour in materials, International Journal of Pressure Vessels and Piping, 2012, Volume 92, 70–76, with permission from Elsevier.

Background Motivation

Investigation of the applicability of the LICON methodology for welded joints, as the main objective of this research project, requires understanding of the previous applications of the method for other material types. Re-examination of the LICON method application to a low alloy creep resistant steel (i.e. 1CrMoV) has highlighted some undiscussed details about the mechanical analysis part of the LICON method which require further consideration.

Summary

This article re-examined the applicability of the LICON methodology for a high creep strength 1CrMoV alloy when different assumptions in the mechanical analysis part of the method (i.e. finite element analysis) were considered. The focus was on examination of

different assumptions for finite element model mesh configuration and adopted creep constitutive model. Finally, the sensitivity of the LICON approach prediction to the evaluated conditions are discussed.

Main Conclusions, Link to the Next Article

The conclusion was that the LICON method long term creep rupture strength predictions are sensitive to input conditions for the associated finite element analysis used to evaluate creep crack incubation tests. It has been shown that special care should be considered in designing the finite element model mesh configuration. Moreover, it was found that the consideration of different types of creep constitutive model in the mechanical analysis part of the LICON method might provide different long term creep rupture strength predictions for the material under investigation. The next article further explains the sensitivity of creep finite element analysis to the adopted creep constitutive model.

Experience with Using the LICON Methodology for Predicting Long Term Creep Behaviour in Materials¹

Abstract

The LICON methodology is a newly developed approach for predicting the lifetime of materials under creep loading condition. The LICON method has gained attention for application to newly developed materials, for which there is little existing creep–rupture data, and for their welded structures. The LICON method predicts long term uniaxial creep strength using the results from several short duration creep crack incubation (CCI) tests in conjunction with the outcome of a mechanical analysis (e.g. involving finite element analysis (FEA), at least initially for a new material and/or multiaxial specimen geometry). In this study, the sensitivity of results from the LICON method to input conditions for the associated FEA is investigated. Two important considerations for creep FEAs are the mesh configuration and the type of creep constitutive model used. In order to evaluate the sensitivity of the outcome of the approach to finite element (FE) mesh condition, twelve different configurations in terms of size, geometry and interpolating formulation are examined. Moreover, to examine the sensitivity of the outcome of the approach to the type of creep equation employed, three constitutive models have been evaluated. Finally, the sensitivity of the LICON approach to the evaluated conditions have been discussed with reference to the information contained in a comprehensive creep–rupture database available for a high creep strength (HCS) 1CrMoV steel at 550°C.

Keywords:

Finite element analysis; Mesh configuration; Creep constitutive model; 1CrMoV.

¹E. Hosseini, S.R. Holdsworth, E. Mazza, *International Journal of Pressure Vessels and Piping* 92 (2012), 70–76

3.1.1 Introduction

One of the main challenges in the design of high temperature components such as those used in modern power generation plant is their lifetime prediction under creep conditions. It is important to be able to accurately predict the creep lifetimes of such structures, with due consideration of fitness-for-purpose, reliability, safety and cost effectiveness, and this has been a main topic of high temperature study for many years. In ideal circumstances, creep lifetime evaluation is based on strength values derived from experimental observations from a large quantity of long duration uniaxial tests for the material of interest, ideally for a number of different heats [1]. In circumstances for which such large datasets do not exist, long term properties have to be predicted from the results of relatively short duration tests. While the latter approach can only be regarded as an interim compromise, and no substitute for the former approach with regards to accurate design life assessment, it is sometimes the only way to predict the long term properties of new alloys in a relatively short-time scale.

A number of approaches have been adopted for predicting long-time creep properties from relatively short duration tests, and some of these are reviewed in the following text. Initially, it was common practice to simply extrapolate the results of high stress (short duration) tests out to long durations using, for example, a Larson–Miller type parameter (e.g. [2]), but it was soon recognised that such an approach could be responsible for non-conservative predictions because it did not account for strain enhanced thermal ageing effects which could influence creep deformation and rupture mechanisms at long times, in particular for metallurgically complex steels (e.g. [3]). Subsequently, the iso-stress test method was adopted to accelerate strain enhanced thermal ageing effects (e.g. [4] and [5]). In this approach, the creep-rupture times at the temperature of interest are extrapolated from the results of a number of iso-stress tests performed at progressively higher temperatures. The disadvantage of this approach is that thermal enhancement in this way can change the material microstructure, and subsequent deformation and rupture mechanisms, in a way that does not occur at the temperature of interest at long creep-rupture durations.

In 1985, Evans & Wilshire introduced a methodology involving both stress and temperature acceleration for predicting long duration creep-rupture behaviour [6]. The 'theta projection' concept assumes that creep is the result of a competition between hardening and softening processes and represents the creep behaviour of material as a stress, temperature and time dependent equation set. Determination of the parameters for this equation set requires the results from a well distributed matrix of stress and temperature accelerated creep tests, and has been shown to work well for materials with balanced primary and tertiary creep strain characteristics which are stable in terms of their deformation and rupture mechanisms

over a wide T , σ regime. In practice, these conditions are not fulfilled for many engineering materials, although more recent improvements have extended the applicability of the concept [7].

In 1993, a stress relaxation based accelerated testing method was proposed by Woodford [8]. The procedure involves loading a tensile specimen to a prescribed strain level at the desired temperature, and then holding the strain constant for around 20h during which time the stress relaxes as elastic strain is replaced by inelastic creep strain. The test material can be in either the virgin, long-time thermally exposed or service exposed condition. By using an appropriate value of elastic modulus the stress relaxation response may be converted to a creep strain rate (stress) formulation which can be used for example to predict rupture times for a wide range of stress values (e.g. using the Monkman–Grant relationship [9]). It was said that the approach could be effective for predicting the long-time properties of high strength nickel base alloys [8], but was less effective for other material classes such as low alloy steels [10].

Experience with all of these techniques consistently indicated that none were effective in predicting long-time creep–rupture properties from the results of relatively short duration tests when the rupture mechanism in the long-time regime was different to that in the short-time regime.

In the late 1990s, an iso-thermal extrapolation approach referred to as the LICON methodology was developed in an European Brite Euram project to predict long term creep strength values for a new generation of advanced martensitic 9%Cr pipe steels (including their weldments) [11, 12]. This methodology relied on multiaxial loading conditions to bring forward the onset of long-time creep damage formation into the short-time rupture regime. More recently, the applicability of this method for low alloy creep resistant 1CrMoV steels was confirmed [13, 14] and, currently, the effectiveness of the approach for application to welded structures of 1CrMoV steel and copper is being investigated by the authors and others (e.g. [15]).

The LICON method employs observations from several short term creep crack incubation (CCI) tests (e.g. using compact tension (CT) specimens) in conjunction with the results of a mechanical analysis of the testpieces to predict the long term uniaxial creep strength of a material. The original concept was for the mechanical analysis part to only involve finite element analysis (FEA) to establish the necessary creep stress state parameters in the first evaluation of a new material type and/or testpiece geometry, and thereafter to rely on these initial findings ideally in the form of more approximate solutions (e.g. [16]). One purpose of the present study was to re-examine the feasibility of this approach. While several studies (e.g. [11–15]) have evaluated the LICON method and its application to different

materials and multiaxial geometries, the sensitivity of the approach to FEA input conditions has not been systematically investigated. Two important input conditions for creep FEAs are the mesh configuration and the type of creep constitutive model adopted for the simulation. The sensitivity of the LICON approach to the adopted FEA input conditions has been investigated in the present study by using an available comprehensive uniaxial and multiaxial creep database for a high creep strength (HCS) 1CrMoV at 550°C. Twelve mesh constructions with different configurations in terms of size (coarse, medium and fine), geometry (tetrahedral and hexahedral) and interpolating formulation (linear and quadratic) have been examined to provide an indication of their influence on the analytical outcome.

In order to reveal the sensitivity of the LICON approach to creep constitutive equation type, three models have been evaluated, namely two-regime Norton (2RN), Norton–Bailey+2RN and Bartsch. The 2RN model simply acknowledges that the parameters in the conventional Norton equation [17], for a given material, are different for different deformation mechanism regimes, i.e.

$$\dot{\varepsilon} = \begin{cases} A_1 \sigma^{n_1} & \text{if } \sigma \geq \sigma^* \\ A_2 \sigma^{n_2} & \text{if } \sigma < \sigma^* \end{cases} \quad \text{2RN model} \quad (3.1.1)$$

where σ^* is the stress below which there is a change in the deformation mechanism, reflected by a change in the constant and the stress exponent (e.g. Figure 3.1.1). In Figure 3.1.1, the $\dot{\varepsilon}(\sigma)$ creep data for 1CrMoV extracted from [18] clearly exhibit bi-linear characteristics, and the 2RN model constants have been set to reflect this for the MMS001 heat of the steel under investigation.

While the Norton equation only represents secondary creep deformation, combining the model with the Norton–Bailey (NB) model [19] enables both primary and secondary creep deformation to be characterized, i.e.

$$\varepsilon = \begin{cases} B\sigma^b t^c + A_1 \sigma^{n_1} t & \text{if } \sigma \geq \sigma^* \\ B\sigma^b t^c + A_2 \sigma^{n_2} t & \text{if } \sigma < \sigma^* \end{cases} \quad \text{NB+2RN model} \quad (3.1.2)$$

The Bartsch model [20] provides an alternative representation of primary and secondary creep deformation, i.e.

$$\begin{aligned} \varepsilon &= A_1 \exp(a_1 \sigma) \sigma^{b_1} t^c \\ &+ A_2 \exp(a_2 \sigma) \sigma^{b_2} t \end{aligned} \quad \text{Bartsch model} \quad (3.1.3)$$

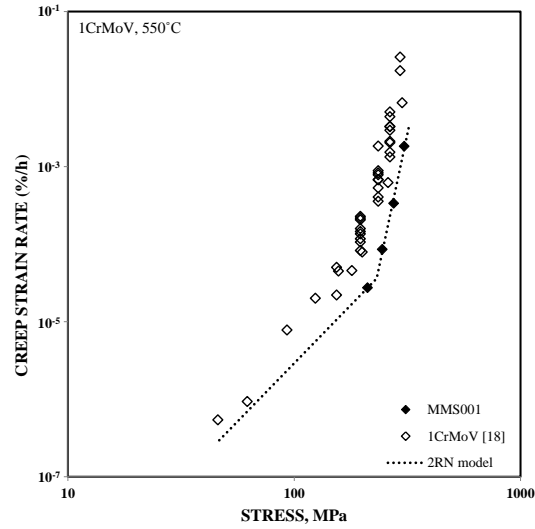


Figure 3.1.1: Minimum creep strain rate (stress) diagram showing the basis of the 2RN model used for the heat of 1CrMoV steel (MMS001) under investigation.

The models reviewed above represent either primary–secondary or secondary (only) creep deformation behaviour. Tertiary creep models (e.g. [21, 22]) were not considered for the purpose of this study. While this could be regarded as an omission in a consideration of constitutive equations for the assessment of service component remaining life, this is not the case for the determination of creep stress distribution ahead of the crack starter of a CT testpiece as part of the LICON procedure.

The sensitivity of the outcome of the LICON approach to FEA mesh configuration and the creep model used in the simulation is examined in the following sections.

3.1.2 LICON Methodology

The original LICON development is based on the formulation:

$$t_{i,x} = A(\bar{\sigma})^{-\nu}(H)^{-\gamma} \quad (3.1.4)$$

with $H = \sigma_1/\bar{\sigma}$, where σ_1 is the maximum principal stress and $\bar{\sigma}$ is the relevant von Mises effective stress, and where A , ν and γ are constants determined for the material and temperature of interest and the associated multiaxial creep–rupture response. Typically γ varies

between zero for $\bar{\sigma}$ -controlled rupture and ν for σ_1 -controlled rupture [13, 23]. In its original formulation, the LICON model equations characterised the rupture behaviour in two mechanism regimes. In regime-1, the damage mechanism for ferritic steels is typically void nucleation due to particle/matrix decohesion, and rupture is $\bar{\sigma}$ -controlled (i.e. with $\gamma' \rightarrow 0$), such that:

$$t_r = A'(\sigma_0)^{-\nu'} \quad \text{uniaxial} \quad (3.1.5)$$

$$t_{i,x} = A'(\bar{\sigma}_{CT})^{-\nu'} \quad \text{multiaxial (e.g. CT specimen)} \quad (3.1.6)$$

In regime-2, for ferritic steels, creep damage nucleates and develops at grain/lath boundaries and rupture is σ_1 -controlled (i.e. with $\gamma'' \rightarrow \nu''$ [13]), such that:

$$t_r = A''(\sigma_0)^{-\nu''} \quad \text{uniaxial} \quad (3.1.7)$$

$$t_{i,x} = A''(\bar{\sigma}_{CT})^{-\nu''} (H_{CT})^{-\gamma''} \quad \text{multiaxial (e.g. CT specimen)} \quad (3.1.8)$$

The LICON equation set is specifically defined above for predicting long duration uniaxial rupture times from relatively short duration CCI tests using CT specimens. It may also be used for determining the lifetimes of components with multiaxial features [13, 14], but this application is not considered here. In Equations 3.1.6 and 3.1.8, reference is made to the crack initiation criterion, x . The crack initiation criterion adopted here for 1CrMoV steel is $\Delta a=0.5\text{mm}$, following the experience reviewed in [24]. Equations 3.1.5–3.1.8 are schematically presented in Figure 3.1.2.

Having determined the values of $A''(H_{CT})^{-\gamma''}$ and ν'' from the results of a series of CCI tests using CT specimens, and with a knowledge of the appropriate reference stress $\bar{\sigma}_{CT}$ and H_{CT} values (e.g. from the results of FEA), the long-time uniaxial rupture behaviour can be predicted using Equation 3.1.7. More accurate predictions may be made with a knowledge of the actual value of rupture criterion obeyed by the material (e.g. $\gamma'' = 0.74\nu''$ for 1CrMoV [13]).

In the original LICON development applied to three advanced 9%Cr steels [11, 12], the initial FEA indicated that $\bar{\sigma}_{CT}$ (or a von Mises equivalent stress [16]) and H_{CT} at a distance of 0.5mm ahead of the notch root could be regarded as representative reference quantities for the CT specimen geometries. This reference distance conveniently coincided with the adopted crack initiation criterion ($\Delta a=0.5\text{mm}$). In the subsequent investigation of 1CrMoV steel [13, 14], the initial FEA also indicated that the determined quantities for $\bar{\sigma}_{CT}$ (or von Mises equivalent stress [16]) and H_{CT} at the same reference distance could also be regarded as representative quantities for the CT specimen geometry. However, there was a significant

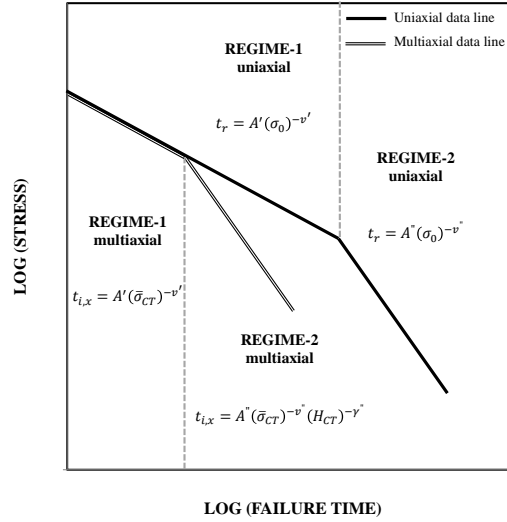


Figure 3.1.2: Schematic representation of the LICON concept.

difference between the analyses for the two material classes which is worthy of note. H_{CT} for the 9%Cr steels was determined to be ~ 3.6 [12], whereas for the 1CrMoV steels it was determined to be ~ 3.1 [13]. It should be acknowledged that in the first study a traditional (single regime) Norton model was used in the FEA evaluation, while in the second study, the Bartsch model (Equation 3.1.3) was adopted. It was unknown if the determined difference in H_{CT} was a function of material or creep model. In this study, the sensitivity of H_{CT} to creep model is investigated.

3.1.3 Material and Experimental Details

The focus of the present study is a high creep strength (HCS) 1CrMoV steel (heat MMS001, Table 3.1.1). For this particular heat of the steel, there were uniaxial creep–rupture data for stresses (σ_0) in the range 211–306MPa at 550°C ($1.2 < t_r < 33.6$ kh, Figures 3.1.1 and 3.1.3 [13]) and CT specimen CCI data for loads in the range 11.2–25.5kN ($0.3 < t_{i,x} < 3.7$ kh [14]).

Table 3.1.1: Material details for MMS001 heat of 1CrMoV.

C, wt%	Cr, wt%	Mo, wt%	Ni, wt%	V, wt%	$R_{p0.2}$, MPa	R_m , MPa	E , GPa
0.25	0.880	0.76	0.69	0.33	640	780	220

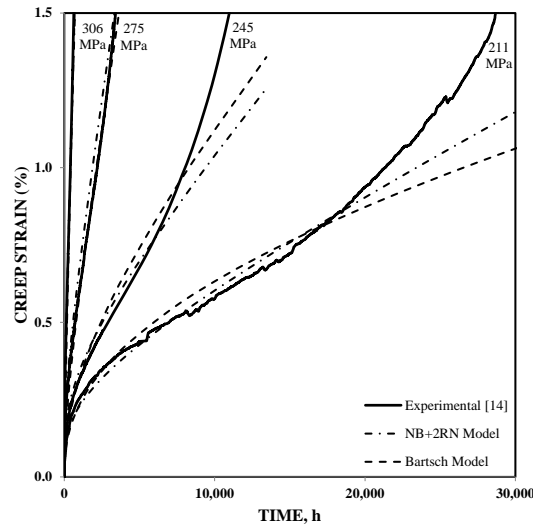


Figure 3.1.3: Creep strain data for 1CrMoV steel at 550°C with model fits using NB+2RN and Bartsch creep equations.

Constant load CCI tests were performed, where appropriate, in accordance with [25] using fully instrumented 25mm thick CT testpieces with side grooves. Full experimental details are given elsewhere [13, 14].

3.1.4 FE Analyses

Overview

In the present study, the elastic–plastic–creep FE analysis of a CT testpiece using 1/4 model symmetry conditions was used to calculate the values of $\bar{\sigma}_{CT}$ and H_{CT} at the reference point (Figure 3.1.4). The geometry shown is representative of the CT testpiece used in the experimental test programmed [13, 14]. Five load conditions in the range 11.2–25.5kN were simulated. The FE code employed a non-linear kinematic hardening plasticity model to represent the rate independent flow characteristics of the material, while uniaxial creep strain response was represented by model fits to uniaxial experimental data available for the 1Cr–MoV steel under investigation at 550°C. The formulations for the three evaluated creep models are defined by Equations 3.1.1–3.1.3, and the ECCC fitting approach [1] was used to determine the numerical constants of the formulations. The model fits of the NB+2RN and Bartsch equations to the experimental data are shown in Figure 3.1.3. The constitu-

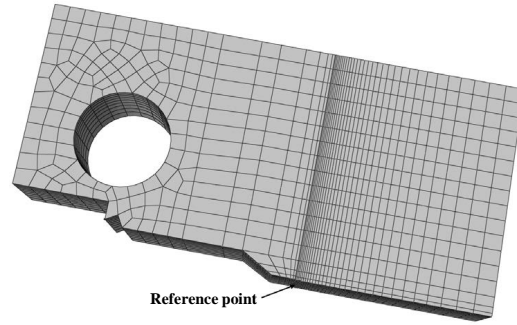


Figure 3.1.4: Optimised FE mesh configuration.

tive models were implemented in the commercially available FE code of ABAQUS through FORTRAN subroutines assuming strain hardening in their formulation.

In order to investigate the sensitivity of the calculated values of $\bar{\sigma}_{CT}$ and H_{CT} at the reference point to the FE mesh configuration, twelve different mesh configurations for the load level of 25.5kN were evaluated using the Bartsch model. The details of the twelve mesh configurations are given in Table 3.1.2. Having determined an optimized mesh configuration, the sensitivity to creep constitutive model type of reference $\bar{\sigma}_{CT}$ and H_{CT} values, and then, LICON method predicted uniaxial creep-rupture strength curves was investigated for different load levels.

Table 3.1.2: Details of the considered FE models.

No.	Name	Description	Node spacing*
1	Coarse (TL)	29,578 tetrahedral elements with linear interpolation	234 μm
2	Coarse (TQ)	29,578 tetrahedral elements with quadratic interpolation	234 μm
3	Coarse (HL)	25,405 hexahedral elements with linear interpolation	234 μm
4	Coarse (HQ)	25,405 hexahedral elements with quadratic interpolation	234 μm
5	Medium (TL)	53,571 tetrahedral elements with linear interpolation	157 μm
6	Medium (TQ)	53,571 tetrahedral elements with quadratic interpolation	157 μm
7	Medium (HL)	34,934 hexahedral elements with linear interpolation	157 μm
8	Medium (HQ)	34,934 hexahedral elements with quadratic interpolation	157 μm
9	Fine (TL)	90,762 tetrahedral elements with linear interpolation	118 μm
10	Fine (TQ)	90,762 tetrahedral elements with quadratic interpolation	118 μm
11	Fine (HL)	55,804 hexahedral elements with linear interpolation	118 μm
12	Fine (HQ)	55,804 hexahedral elements with quadratic interpolation	118 μm

* Node spacing at the crack tip

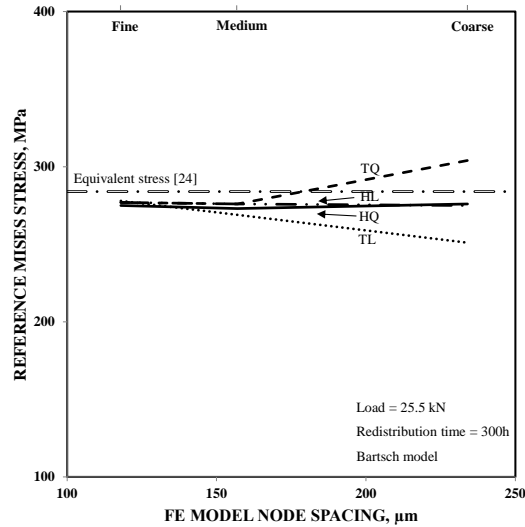


Figure 3.1.5: Effect of mesh configuration characteristics on the FE analysis predicted creep reference effective stress (see Table 3.1.2 for key to element and interpolation types).

FE Mesh Configuration Sensitivity

It is generally recognised that reducing the element size improves FEA solution accuracy. However, the use of extremely fine mesh in the FE model can result in excessive computation times and computer memory demands, which can significantly influence the efficiency of the simulation. An evaluation of mesh sensitivity, and a consideration of the optimum conditions for a LICON stress analysis of a CT specimen have therefore been conducted.

The mesh sensitivity analysis was performed using the Bartsch creep equation (i.e. Equation 3.1.3). The results of reducing node spacing, for various element and node interpolation types, on the reference $\bar{\sigma}_{CT}$ and H_{CT} values for the CT testpiece are respectively shown in Figures 3.1.5 and 3.1.6. The results show that hexahedral elements with quadratic interpolation, even with the coarse mesh configuration, can represent acceptable values for stress components at the reference point of CT testpiece. It can also be seen that the H_{CT} value is the most sensitive parameter to variations in the mesh configuration characteristics. On the basis of the evidence in Figures 3.1.5 and 3.1.6, it was concluded that future $\bar{\sigma}_{CT}$ and H_{CT} determinations should involve the use of hexahedral elements with quadratic interpolation, with a convergence check on node spacing to ensure that convergence had been achieved for H_{CT} .

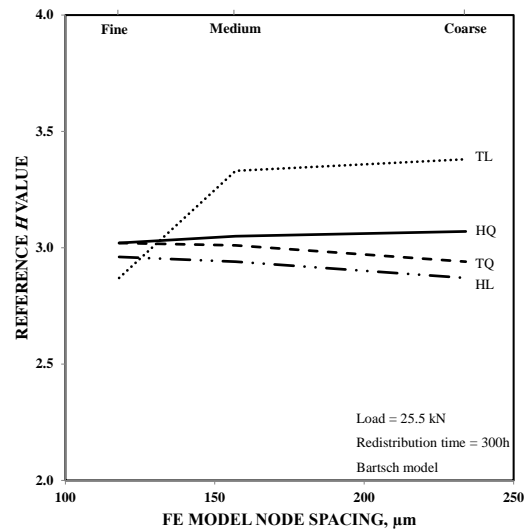


Figure 3.1.6: Effect of mesh configuration characteristics on the FE analysis predicted creep reference H_{CT} value (see Table 3.1.2 for key to element and interpolation types).

Creep Constitutive Model Type Sensitivity

Using the optimized mesh configuration (i.e. quadratic hexahedral elements with a node spacing of 157mm at the crack tip), the influence of load on the reference $\bar{\sigma}_{CT}$ and H_{CT} values for the CT testpiece at 550°C is shown in Figures 3.1.7 and 3.1.8. The $\bar{\sigma}_{CT}$ reference stresses determined using the three creep models increase approximately in line with the plane stress von Mises equivalent reference stress [16], although there are significant differences between the respective values shown (Figure 3.1.7). Interestingly, there are notable difference in the magnitudes of $\bar{\sigma}_{CT}$ determined by the two creep equations modelling both primary and secondary behaviour (i.e. NB+2RN and Bartsch), despite the fact that their respective fits to the source uniaxial experimental data are comparable (Figure 3.1.3). A comparison of the predicted creep strain behaviour at 100MPa using these two models (i.e. well outside the uniaxial experimental stress range of 211–306MPa) indicates significant differences (Figure 3.1.9). This demonstrated the levels of uncertainty which can be encountered when extending the use of creep models to stress levels well below the experimental range for which they were determined.

At loads greater than 22kN the level of H_{CT} appears to be independent of the creep model used. However, with decreasing load below 22kN, there is a deviation in the value of the stress triaxiality factor determined using different creep models (Figure 3.1.8). As before,

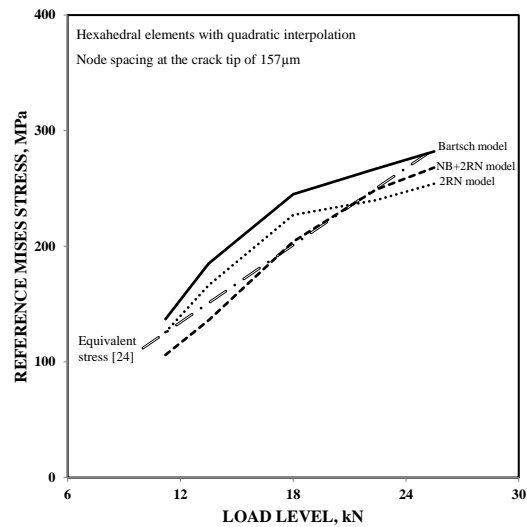


Figure 3.1.7: Sensitivity of the creep reference equivalent stress to the type of creep constitutive model used, as a function of load level.

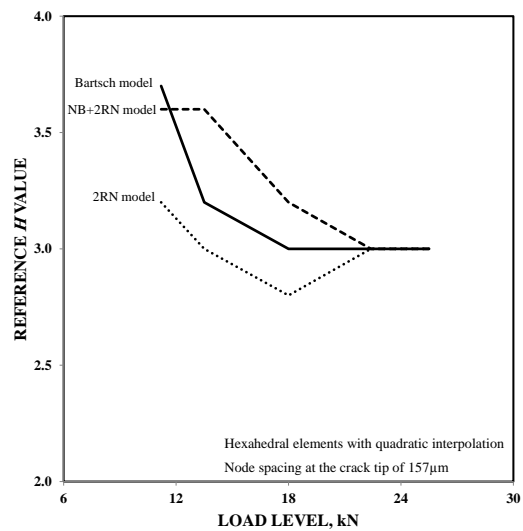


Figure 3.1.8: Sensitivity of the creep reference stress multiaxiality factor to the type of creep constitutive model used, as a function of load level.

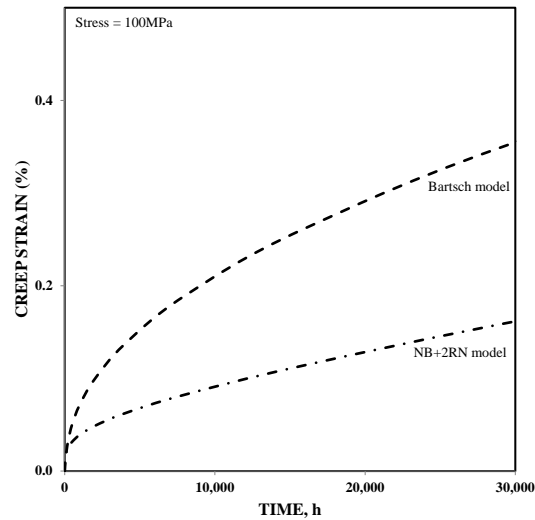


Figure 3.1.9: Creep strain behaviour at 100MPa predicted by the NB+2RN and Bartsch constitutive models.

this is regarded as a reflection of the change in the creep deformation characteristics of 1CrMoV for stresses below ~ 200 MPa, and the ability of the different models to extrapolate into the lower stress regime.

LICON predictions

The reference $\bar{\sigma}_{CT}$ and H_{CT} values shown in Figures 3.1.7 and 3.1.8 were used to form the basis of LICON predicted Regime-2 uniaxial rupture strength values using the 2RN (Figure 3.1.10), NB+2RN (Figure 3.1.11) and Bartsch (Figure 3.1.12) creep models. When compared with the existing experimentally determined long-time creep-rupture strength values available for the heat of 1CrMoV steel under investigation, it can be seen that good agreement is achieved with the 2RN secondary creep model based prediction (Figure 3.1.10), while conservative and non-conservative predictions are respectively determined using the two primary-secondary creep models (i.e. Figures 3.1.11 and 3.1.12 respectively).

The original concept of the LICON approach was to only employ fully inelastic FEA initially to establish the steady-state creep reference H value and identify the appropriate reference stress solution for a new material type and/or multiaxial testpiece geometry (it was originally believed that the creep reference H value would only depend on material and geometry).

Thereafter, mechanical analysis was to involve the use of the reference stress solution (e.g. [16]) and H established for the conditions of interest without the need for repeated FEA. Importantly, the evidence presented here has shown that the creep reference H value is not independent of load (e.g. Figure 3.1.8). In these circumstance, it is therefore recommended that the mechanical analysis part of the LICON approach is always based on the results of fully inelastic FE analysis performed in accordance with the guidance given in the paper. In performing this FE analysis care should be taken in the choice of the creep model and parameters used, in particular to ensure representative predictions of deformation behaviour beyond the range of the source experimental data (e.g. Figure 3.1.1).

3.1.5 Concluding Remarks

The LICON approach was initially developed as a means of predicting long-time creep-rupture strength values from the results of relatively short duration CCI tests involving fracture mechanics type compact tension (CT) specimens. The use of a multiaxial testpiece accelerates the onset of creep damage encountered after long times, but requires fully inelastic finite element analysis (FEA) to characterize the creep reference stress state. The paper has evaluated the sensitivity of LICON predicted rupture strength values to various

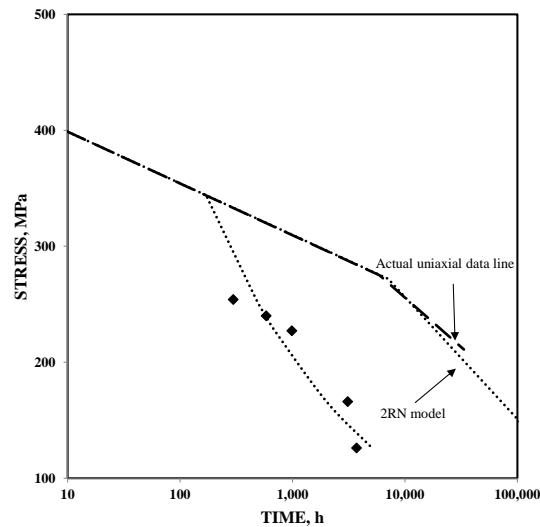


Figure 3.1.10: Comparison of actual and LICON predicted regime-2 uniaxial rupture strength data lines for HCS 1CrMoV at 550°C (prediction using the 2RN creep model, Equation (3.1.1)).

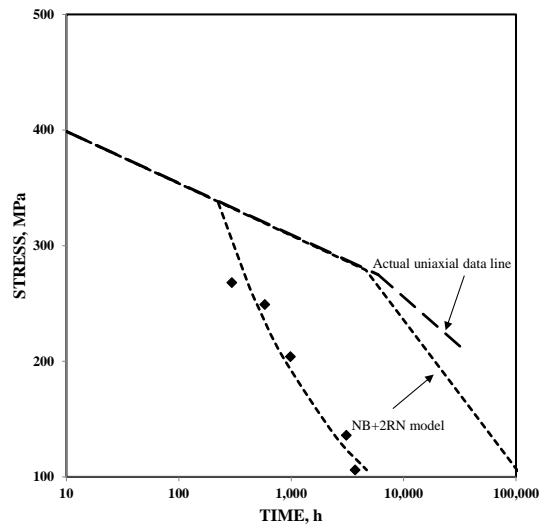


Figure 3.1.11: Comparison of actual and LICON predicted regime-2 uniaxial rupture strength data lines for HCS 1CrMoV at 550°C (prediction using the NB+2RN creep model, Equation (3.1.2)).

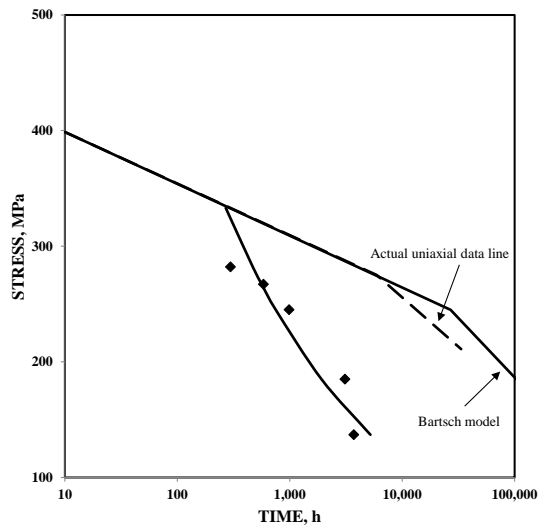


Figure 3.1.12: Comparison of actual and LICON predicted regime-2 uniaxial rupture strength data lines for HCS 1CrMoV at 550°C (prediction using the Bartsch creep model, Equation (3.1.3)).

FEA input conditions, with the following conclusions.

- It is shown that care is required in the choice of FEA mesh configuration for characterising the creep stress state ahead of the notch root of a CT specimen. The evidence indicates that reproducible results are determined using hexahedral elements with quadratic interpolation, and an element size which has been optimized to give convergence of the stress multiaxiality factor.
- The LICON predicted rupture strength is sensitive to the creep model used in FEA simulations to determine creep stress state ahead of the notch root of a CT specimen. It is not only important to consider which type of creep equation is most appropriate (in terms of its ability to represent primary, secondary and/or tertiary deformation behaviour), but it is also necessary to evaluate how well the constitutive model is likely to represent the deformation characteristics at stress levels significantly below the experimental range of stresses for which it was established.

References

- [1] S.R. Holdsworth. The ECCC approach to creep data assessment. *Journal of Pressure Vessel Technology*, 130:1–6, 2008.
- [2] F.R. Larson and J. Miller. A time–temperature relationship for rupture and creep stresses. *Transactions ASME*, 74(5):765–775, 1952.
- [3] P. Greenfield, J.B. Marriott, and K. Pithan. *A Review of the Properties of 9–12%Cr Steels for Use as HP/IP Rotors in Advanced Steam Turbines: Cost*. Official Publications of the European Communities, 1989.
- [4] K.N. Melton. The iso–stress extrapolation of creep rupture data. *Materials Science and Engineering*, 59(2):143–149, 1983.
- [5] O. Kanemaru, M. Shimizu, T. Ohba, K. Yagi, Y. Kato, and K. Hattori. Life prediction by the iso–stress method of boiler tubes after prolonged service. *International Journal of Pressure Vessels and Piping*, 48(2):167–182, 1991.
- [6] R.W. Evans and B. Wilshire. *Creep of Metals and Alloys*. Institute of Metals, 1985.
- [7] M. Evans. Predicting times to low strain for a 1CrMoV rotor steel using a 6– θ projection technique. *Journal of Materials Science*, 35(12):2937–2948, 2000.
- [8] D.A. Woodford. Accelerated testing for high temperature materials performance and remaining life assessment. Technical report, EPRI Project TR-114045, 1999.
- [9] F.C. Monkman and N.J. Grant. An empirical relationship between rupture life and minimum creep rate in creep–rupture tests. *ASTM Proceedings*, 56:593–620, 1956.
- [10] D.A. Woodford and K. Iijima. Creep strength evaluation, design, and life management of 1CrMoV rotor steel using stress relaxation testing. In *Advances in Turbine Materials, Design and Manufacturing*, pages 613–624, 1997.
- [11] P. Auerkari, W. Bendick, S.R. Holdsworth, J.H. Rantala, R. Hurst, C. Coussement, and R. Hack. Predicting long term creep behaviour using the LICON methodology. In *Proceedings of 3rd International Conference of Advances in Material Technology for Fossil Power Plants*, pages 329–339, 2001.
- [12] V.M. Martins and S.R. Holdsworth. The LICON methodology for predicting the long term service behaviour of new steels. *Materials at High Temperatures*, 19(2):99–103, 2002.
- [13] S.R. Holdsworth and E. Mazza. Exploring the applicability of the LICON methodology for a 1CrMoV steel. *Materials at High Temperatures*, 25(4):267–276, 2008.
- [14] S.R. Holdsworth and E. Mazza. Using the results of creep crack incubation tests on 1CrMoV steel for predicting long time creep rupture properties. *International Journal of Pressure Vessels and Piping*, 86(12):838–844, 2009.
- [15] J. Rantala, P. Auerkari, J. Salonen, S. Holmström, A. Laukkanen, and T. Saukkonen. Mechanical performance and life prediction for canister copper. Technical report, VTT Technical Research Centre of Finland, 2010.
- [16] A.G. Miller. Review of limit loads of structures containing defects. *International Journal of Pressure Vessels and Piping*, 32(1–4):197–327, 1988.
- [17] F.H. Norton. *The Creep of Steel at High Temperature*. McGraw–Hill book company New York, 1929.
- [18] NIMS. *Data Sheet 9B, Data sheets on the elevated–temperature properties of 1Cr–1Mo–0.25V steel forgings for turbine rotors and shafts*. National Research Institute for Metals, Tokyo, Japan, 1990.

-
- [19] R.W. Bailey. The utilisation of creep test data in engineering design. *Proceedings of the Institution of Mechanical Engineers*, 131:131–349, 1935.
- [20] H. Bartsch. New creep equation for ferritic and martensitic steels. *Steel Research*, 66(9):384–388, 1995.
- [21] M. Prager. Development of the MPC Omega method for life assessment in the creep range. *Journal of Pressure Vessel Technology*, 288:401–421, 1994.
- [22] L.M. Kachanov. Time of the rupture process under creep conditions. *Izvestiya Akademii Nauk SSSR. Otdelenie Tekhnicheskikh Nauk*, 8:26–31, 1958.
- [23] B.J. Cane. Creep cavitation and rupture in 2.25CrMo steel under uniaxial and multiaxial stresses. *Proceedings Conference on Mechanical Behaviour of Materials*, 2:173–182, 1979.
- [24] S.R. Holdsworth. Initiation and early growth of creep cracks from pre-existing defects. *Materials at High Temperatures*, 10(2):127–137, 1992.
- [25] ASTM Standard E1457. Standard test method for measurement of creep crack growth rates in metals, Annual Book of ASTM Standards, volume 3.1.

3.2 *Article Two*

Overview

This section contains a reprint of the article: E. Hosseini, S.R. Holdsworth, E. Mazza, Creep constitutive model considerations for high temperature finite element numerical simulations, *Journal of Strain Analysis for Engineering Design*, 2012, Volume 47(6), 341–349, with permission from SAGE.

Background Motivation

In the previous paper, it was illustrated that LICON method long term creep strength predictions are sensitive to the input conditions for the finite element analysis used for evaluation of creep crack incubation tests. It was shown that results of finite element calculations on generated stress states ahead of the notch of compact tension specimens might vary when different considerations for creep constitutive behaviour of the material were adopted. This article has further discussed the sensitivity of finite element calculation for high temperature components to the adopted creep constitutive model.

Summary

This article has used the finite element method to simulate the behaviour of fracture mechanics compact tension specimens made of 1CrMoV in a series of creep crack incubation tests. The simulations used five different creep constitutive models fitted to a set of experimental uniaxial creep curves for 1CrMoV at 550°C. Comparison of the resulting finite element analysis representations from consideration of different creep constitutive models clearly demonstrated the sensitivity of high temperature finite element analyses of structures to the adopted creep constitutive model. This article has presented discussions on the source of this sensitivity and recommended prior benchmark examination for checking the effectiveness of finite element simulation procedures for critical high temperature components.

Main Conclusions, [Link to the Next Article](#)

This article has demonstrated the potential sensitivity of high temperature finite element analyses of structures to the type of creep constitutive model adopted, and to the scope of the experimental data from which the model is derived. Important for the LICON method application, it has been shown that the finite element calculated stress state distributions

ahead of the notch of compact tension specimens exhibit a strong sensitivity to the type of creep model adopted. This study has also highlighted the need for adoption of stress regime dependent creep constitutive models for consideration in finite element analyses of structures with a wide range of redistribution stresses. This topic has been further explained in the next article.

Creep Constitutive Model Considerations for High Temperature Finite Element Numerical Simulations¹

Abstract

Finite element modelling is increasingly used as an integral part of creep analyses for the integrity assessment of high temperature structures. An important consideration in such finite element (FE) simulations is the constitutive model used to represent the creep strain response of the component material as a function of temperature, stress and time. There are a variety of creep models which can be chosen by the analyst for implementation in FE codes. In this study, five different creep models have been fitted to a set of experimental uniaxial creep curves for a 1CrMoV turbine rotor steel at 550°C. Subsequently, the derived constitutive equations have been implemented in FE model representations of a series of fracture mechanics compact tension (CT) specimens manufactured from the same heat of the steel and loaded at the same temperature. The outcome clearly demonstrates the potential sensitivity of high temperature numerical analyses of structures to the type of creep model adopted, and to the scope of the experimental data from which the model is derived. This is shown by comparing the load point displacement (LPD) records from a number of CT specimen creep crack incubation (CCI) tests with the results of FE simulations employing the different creep deformation models. FE calculated steady-state creep stress/strain distributions ahead of the notches of CT specimens can also exhibit a strong sensitivity to the type of creep model adopted. Prior benchmarking the effectiveness of FE simulation procedures for critical high temperature components with the selected material creep model equation is therefore strongly recommended.

Keywords:

Creep Finite element analysis; Creep constitutive model; Compact tension test; 1CrMoV.

¹E. Hosseini, S.R. Holdsworth, E. Mazza, *Journal of Strain Analysis for Engineering Design* 47(6) (2012), 341–349

3.2.1 Introduction

Increasingly the design and remaining life assessments of high temperature components rely on determinations of the creep stress/strain (rate) state at the critical location using non-linear finite element (FE) analysis, irrespective of whether the analysis procedure is concerned with the consideration of defect-free or defective structures. For example, defect-free assessments can involve the application of phenomenological or physical based modelling [1–9]. In particular, continuum damage mechanics (CDM) may consider the local creep damage intensity to be proportional to the time integration of creep strain rate and stress multiaxiality factor [7, 8]. Alternatively, defect assessments requiring a knowledge of creep crack incubation (CCI) and growth times can depend on a knowledge of C^* [10, 11], a parameter which characterises the stress and strain rate fields at a crack tip [12–15]. While the potential advantages of physical based modelling have been promoted for many years [6–8], the application of such models is still essentially limited to research study and their adoption for practical (industrial) application is not commonplace. There is therefore still a place for the judicious use of phenomenological modelling [16].

The onset of creep crack growth (CCG) from a pre-existing (manufacturing) defect is generally preceded by an incubation period during which time sufficient creep damage is generated at the crack tip for initiation to occur. The duration of the incubation period is determined by the creep ductility of the material, and can occupy a significant proportion of life in the case of creep ductile materials [17]. CCI and CCG properties are typically determined in tests involving compact tension (CT) testpieces [18, 19]. CCI test data determined using this specimen geometry were investigated in the present study for a high creep strength (HCS) 1CrMoV turbine rotor steel identified as MMS001 (for which material details and uniaxial creep properties are given in Ref. [20]).

The results of CCI tests can be used to form the basis of $t_i(C^*)$ diagrams [10, 17, 19], time-dependent failure assessment diagrams [10, 11], and for estimating long time uniaxial creep rupture strength values [20]. Observations from a research project evaluating the effectiveness of using CCI test results for the latter application [20, 21] provide the background to this consideration of creep constitutive models for high temperature FE numerical simulation in the present paper.

The specific aim of this paper is to reveal the sensitivity of FE numerical creep analyses to the creep constitutive model adopted. Using available creep data for a 1CrMoV turbine rotor steel at 550°C, the parameters for five creep constitutive models have been determined to evaluate the states of stress and strain generated in fracture mechanics CT specimens forming part of a series of CCI tests for the same material and temperature [20].

3.2.2 Creep Constitutive Models

Creep constitutive models represent the creep strain response of a material as a function of temperature, stress and time. Many models have been developed during the last 100 years [22], and a number of these have recently been reviewed [23]. The Norton equation is the most commonly used, describing the secondary (or minimum) creep rate as a power law function of stress [1] (Table 3.2.1). Secondary (or minimum) creep rates are commonly available for many engineering materials, and consequently there is extensive use of this model. This formulation implies a single power law creep deformation mechanism for all stresses in a specified range of application.

For many engineering alloys, the creep deformation mechanism exhibited at high stresses is not the same as that at lower stresses [4, 16]. As an alternative to the conventional Norton equation, a two-regime form of the model may therefore be adopted [21], with different parameter sets for high and low stress regimes. Typically, at relatively high temperatures, creep is controlled by dislocation glide and climb (high temperature power law creep) at higher stresses (when the stress exponent is ≥ 5), whereas diffusion creep controlled by volume diffusion occurs at lower stresses (when the stress exponent approaches unity). Parameter fitting for models such as the two-regime Norton (2RN) equation requires experimental creep strain data from low stress (long duration) creep tests which are not usually available for most materials. Indeed, the basis for the 2RN model parameters adopted for the MMS001 heat of 1CrMoV [20] in the present study also exploited the long duration test data published in the NIMS Data Sheet for 1CrMoV steel [24], Figure 3.2.1. This experimental dataset indicated that the stress exponent in the low stress regime for the low alloy creep resistant steel at 550°C was 3 rather than unity (as was assumed by Naumenko et al. [16]). The two Norton model equation variants are based on secondary creep, and neglect primary

Table 3.2.1: Creep constitutive model parameters for HCS 1CrMoV (MMS001) at 550°C.

Models	Mathematical formulations
Norton [1]	$\dot{\epsilon} = 2.0 \times 10^{-33} \sigma^{11}$
2RN [21]	$\dot{\epsilon} = \begin{cases} 2.9 \times 10^{-14} \sigma^{03} & \sigma^* < 235 \\ 1.2 \times 10^{-39} \sigma^{13} & \sigma^* \geq 235 \end{cases}$
Bartsch [5]	$\epsilon = 4.9 \times 10^{-07} \sigma \exp(1.3 \times 10^{-3} \sigma) t^{0.4} + 1.3 \times 10^{-15} \sigma \exp(5.7 \times 10^{-2} \sigma) t$
NB+2RN [21]	$\epsilon = \begin{cases} 1.4 \times 10^{-09} \sigma^{2.3} t^{0.3} + 2.4 \times 10^{-14} \sigma^{03} t & \sigma^* < 235 \\ 1.4 \times 10^{-09} \sigma^{2.3} t^{0.3} + 2.1 \times 10^{-43} \sigma^{15} t & \sigma^* \geq 235 \end{cases}$
2RSinh	$\dot{\epsilon} = 1.8 \times 10^{-09} \sinh(0.06\sigma(1 - \mathcal{H})) + 1.7 \times 10^{-14} \sinh(0.15\sigma(1 - \mathcal{H}))$ $\dot{\mathcal{H}} = 0.1\sigma^2 \dot{\epsilon} (1 - \mathcal{H}/0.54)$

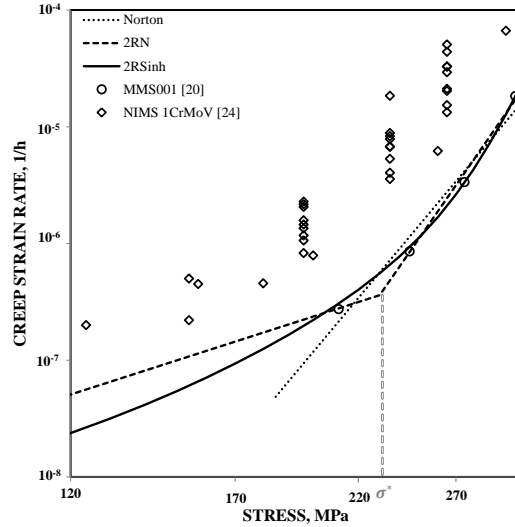


Figure 3.2.1: Secondary (or minimum) creep rate (stress) diagram for MMS001 at 550°C (including a comparison of experimental data with creep model representations).

creep deformation. However, if the available dataset includes complete creep strain–time curves, the adoption of primary+secondary models is also possible. The full Bartsch equation [5] may be adopted as a model with only primary and secondary terms [20]. It is used here in the same way as the conventional Norton equation (assuming a single creep mechanism for all stresses) but, like the 2RN model, it may also be formulated with different parameter sets for high and low stress regimes. The fourth model equation investigated in this study (Table 3.2.1) is the combination of a simple primary creep power law [2] with the 2RN model to enable the implementation of a two–regime primary+secondary model (i.e. NB+2RN) [21]. This formulation provides a primary and secondary creep representation assuming different deformation mechanisms in high and low stress regimes. The simultaneous contribution of more than one creep mechanism can be summed in a continuous way by adopting a two–term hyperbolic sine expression in conjunction with a hardening parameter (\mathcal{H}) to account for primary creep behaviour (Table 3.2.1). The two–regime hyperbolic sine expression formulated here is referred to as the 2RSinh model, and originates from the single term variant [7, 8]. The first and second terms in the 2RSinh model formula relate to high stress and low stress regime creep mechanisms, respectively. Figure 3.2.1 summarises the considered creep data for 1CrMoV in terms of secondary (or minimum) creep rate as a function of stress. It can be seen that the MMS001 heat of the steel [20] is significantly more resistant to creep than the NIMS heats of 1CrMoV [24]. This is because the alloy

composition of MMS001 had been intentionally adjusted to have HCS at the top of the scatter-band for 1CrMoV rotor steels. It can also be seen in Figure 3.2.1 that a single regime model (i.e. simple Norton or Bartsch equation) representation of the creep properties of MMS001 does not accurately represent the creep resistance of the steel in the low stress regime. Influenced by the two-regime characteristics exhibited by the NIMS heats, it was possible to formulate a 2RN (& NB+2RN) model representation for MMS001, but with a sharp transition from the high to the low stress regime at a stress of ~ 235 MPa. The 2RSinh model provides an alternative representation with a continuous transition from high to low stress creep response.

Whereas the Norton creep equation is a standard option in most FEA software applications, it was necessary to write special subroutines for FE implementation of the primary+secondary creep models adopted in this study. The considered hardening rule for Bartsch and NB+2RN model implementations was strain-hardening, while the internal state variable concept employed by Hayhurst et al. [8] was used for the 2RSinh model implementation.

The mathematical formulations for the five creep models are summarised in Table 3.2.1. The material parameters were determined for the 1CrMoV rotor steel at 550°C using a uniaxial creep strain to rupture dataset which had been previously established for the MMS001 heat for rupture times of up to ~ 33.5 kh [20]. Model-fitting within the range of the experimental data for MMS001, and with reference to the NIMS dataset [24] in the low stress regime, was achieved using the MATLAB optimisation toolbox [25]. Ultimately, model-fit acceptability was checked using a procedure recommended by ECCC [22, 23]. The model parameters determined by this approach are included in Table 3.2.1. The model fits of the three primary+secondary creep models to the experimental data are shown in Figure 3.2.2.

The multiaxial generalisation of the creep equations used for the FE numerical simulation is included as a footnote to Table 3.2.1.

3.2.3 Finite Element Analysis

For the FE analysis of the CT testpiece, a three-dimensional (3D) elastic-plastic-creep FE model using 1/4 model symmetry conditions was designed to be solved using the commercially available code of ABAQUS [26]. The adopted mesh detail involving 21770 elements (20-node hexahedral elements with quadratic interpolation) is shown in Figure 3.2.3 (a detailed discussion on mesh discretisation of the model is provided elsewhere [21]). This arrangement was used to simulate the states of stress and strain in a series of CCI tests performed on a 1CrMoV rotor steel at 550°C , with loading levels of 11.2, 13.5, 18.0, 22.4 and

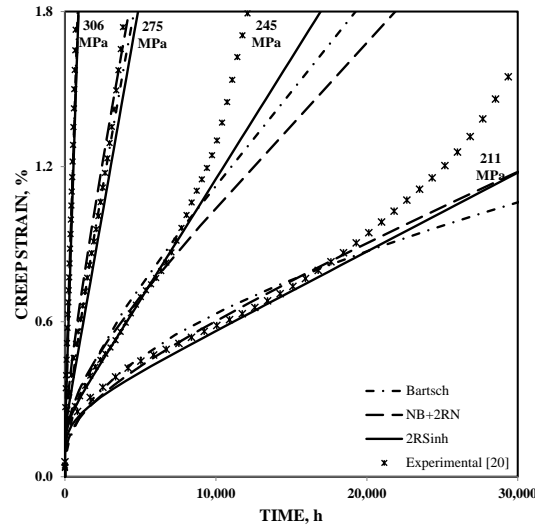


Figure 3.2.2: Creep strain data for MMS001 at 550°C with model fits using NB+2RN, Bartsch, and 2RSinh creep equations.

25.5kN. The FE code employed a non-linear kinematic hardening plasticity model [21] to represent the rate independent flow characteristics of the material. Plasticity model parameters were determined using tensile test data at 550°C, while uniaxial creep strain response was represented by model fits to uniaxial experimental data available for the 1CrMoV steel under investigation at 550°C (Table 3.2.1). The adopted multiaxial generalisations of the creep equations are also given in Table 3.2.1. Simulations were stopped at the experimentally observed CCI times. The onset of creep crack extension was identified from the test records of continuous crack monitoring using DC electrical potential instrumentation [20].

Prior to the onset of creep cracking in CCI tests, there is an incubation period while sufficient creep damage develops immediately ahead of the crack starter [17]. Tertiary creep deformation occurs in the local process zone, which for this steel is less than 2–3 grain diameters [17]. Typically for the 1CrMoV steel, crack initiation occurs at around or before the stress redistribution time (as approximated by $K^2/[EC^*(n+1)]$), but still while approximately steady-state creep conditions dominate in the remaining ligament of the CT testpiece. As the focus of this study was on the stress/strain state beyond the boundary of the process zone, the analyses did not include the consideration of tertiary creep deformation.

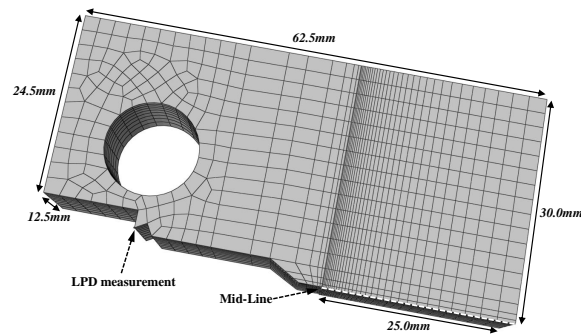


Figure 3.2.3: FE mesh detail of CT testpiece.

3.2.4 Finite Element Results

Figure 3.2.4 shows the FE simulated maximum principal stress (σ_1), von Mises equivalent stress ($\bar{\sigma}$), and stress multiaxiality factor ($\sigma_1/\bar{\sigma}$) distributions along the centre line ahead of the stress concentration, at the mid-thickness plane of the CT specimen geometry, determined with the five different creep constitutive model implementations. Figure 3.2.5 shows the equivalent creep strain distributions. The figures show the situation for two load levels of 11.2 and 25.5kN at 550°C. Figures 3.2.4 and 3.2.5 clearly indicate that FE simulations of creep stress/strain state are very sensitive to the constitutive model adopted, and to the scope of the $\varepsilon(T, \sigma)$ data to which the model is fitted, in particular for the lower load level of 11.2kN.

FE simulations were performed of uniaxial specimen deformation at high and low stresses (Figure 3.2.6). The simulations compared the responses obtained using the three primary+secondary creep constitutive models. The results showed that there was good agreement between the predictions of the different creep equations at the high stress of 250MPa. The same conclusion can be derived from Figure 3.2.2 which also shows the good consistency of different creep model predictions with the experimental observations at stresses in the range of 211 to 306MPa. However, for lower stress levels of 190 and 130MPa (for which there was no experimental data) for the MMS001 heat, the predictions diverge significantly.

During CCI tests, the load point displacement (LPD) of the CT specimen evolves in an analogous way to the total strain in a uniaxial creep test [17, 19, 20]. On loading a CT specimen at high temperature, there is an instantaneous LPD response, followed by an increase in magnitude with time due to the accumulation of primary and then secondary

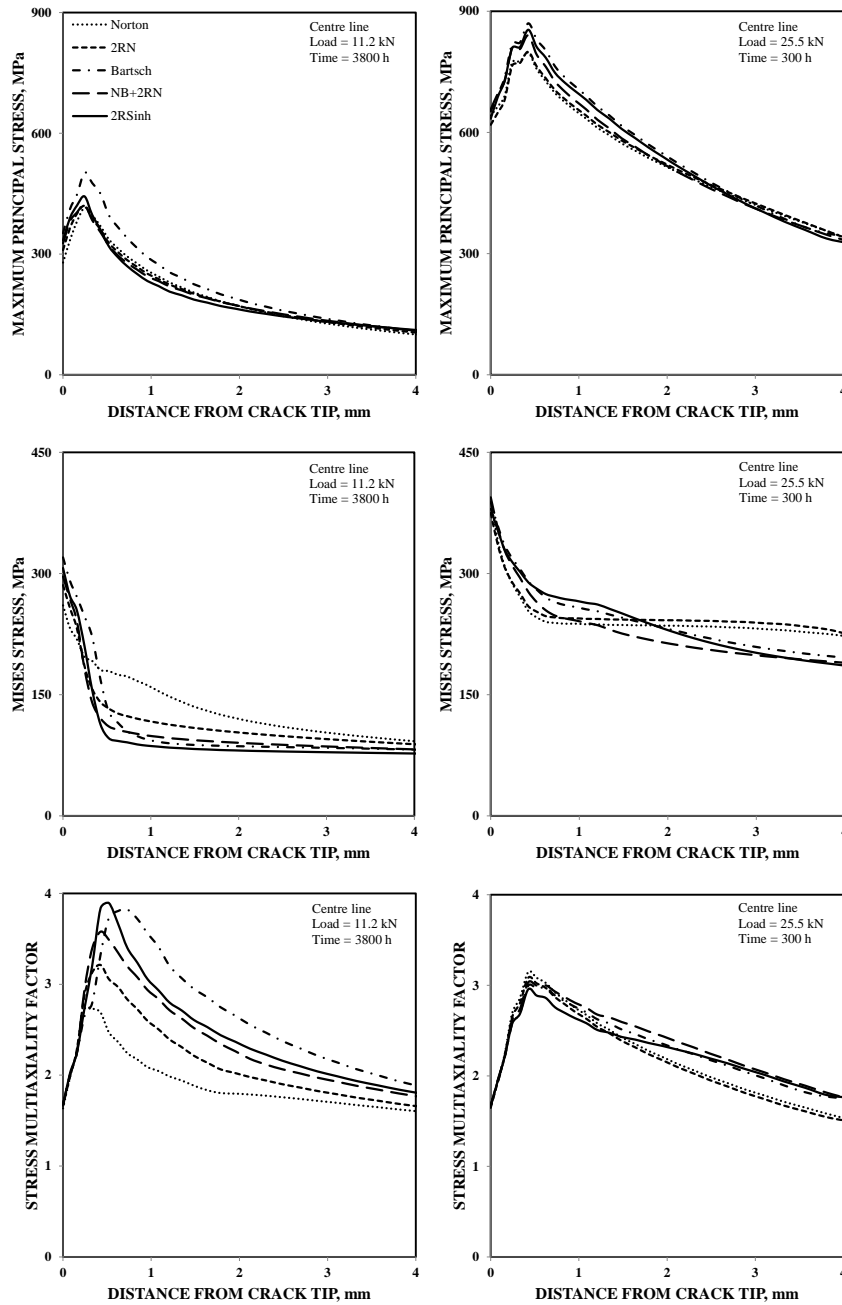


Figure 3.2.4: Sensitivity of FE simulated stress field distribution to the type of implemented creep model (MMS001 at 550°C, CT testpiece).

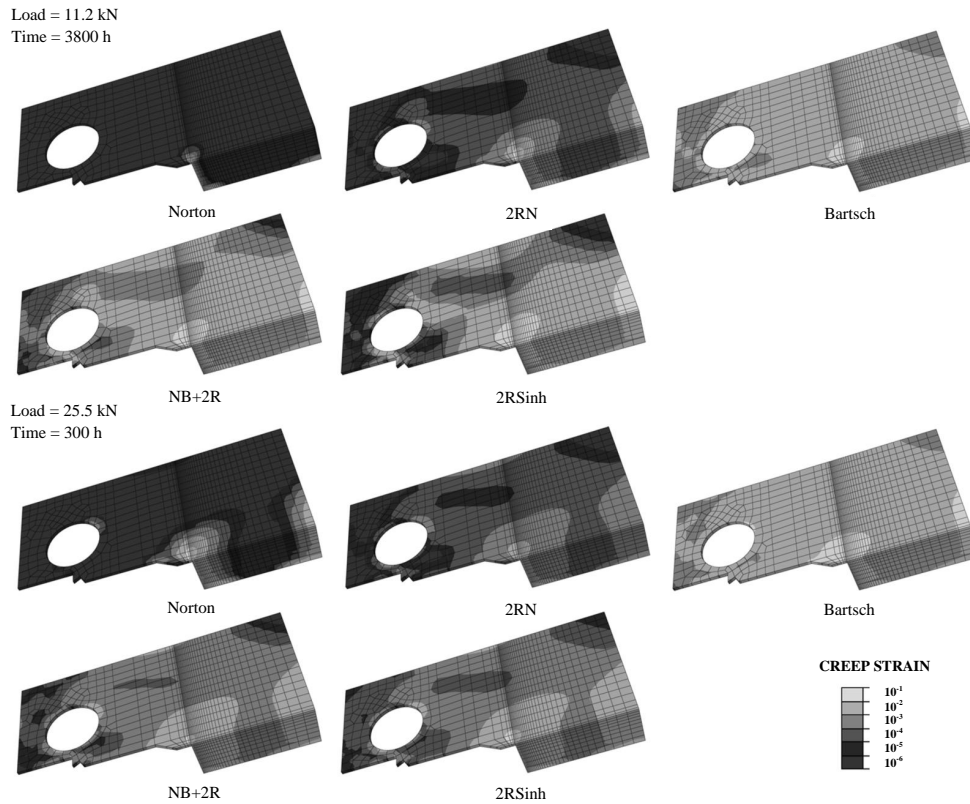


Figure 3.2.5: Sensitivity of FE simulated creep strain distribution to the type of implemented creep model (MMS001 at 550°C, CT testpiece).

creep deformation. The effectiveness of the five creep models to reproduce such behaviour for the five CCI tests by FE simulation has been evaluated, and the results are shown in Figure 3.2.7. The secondary creep models consistently underestimated LPD development in the CCI tests, while the primary+secondary models were more successful (depending on the applied load level). The 2RSinh and NB+2RN models most consistently represented the experimental data.

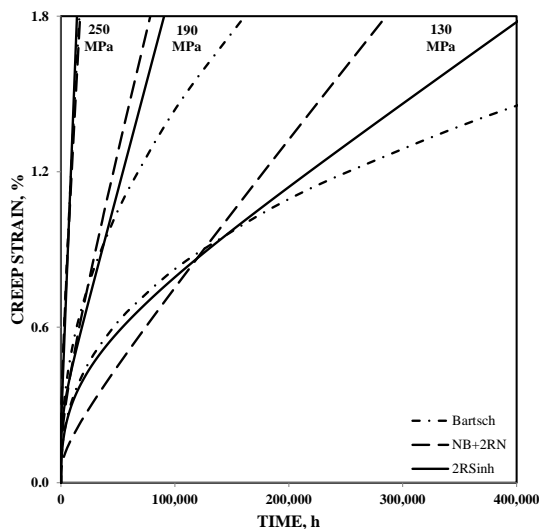


Figure 3.2.6: predicted creep strain responses of MMS001 at 550°C at different stress levels using primary+secondary creep equations.

3.2.5 Discussion

The sensitivity of FE numerical creep analyses to the adopted creep constitutive model has been evaluated using experimental uniaxial and CT specimen CCI data for a HCS 1CrMoV turbine rotor steel at 550°C. It has been shown that stress/strain state predictions of experimental behaviour at 550°C are dependent not only on the type of constitutive model used to represent the steels creep response, but also on the respective scopes of: (a) the test stresses providing the data to underpin the creep model, and (b) the stress distribution in the simulated components.

Model Type

Two categories of model have been evaluated, one representing only secondary creep deformation behaviour and one representing both primary and secondary creep strain accumulation characteristics. Secondary creep deformation behaviour is modelled by conventional and two-regime versions of the Norton equation (Table 3.2.1). Primary+secondary creep strain accumulation characteristics are modelled using three types of formulations, i.e. Bartsch [5], NB+2RN [21] and a new 2RSinh model.

The observed differences between the FE predictions using the secondary and primary+ sec-

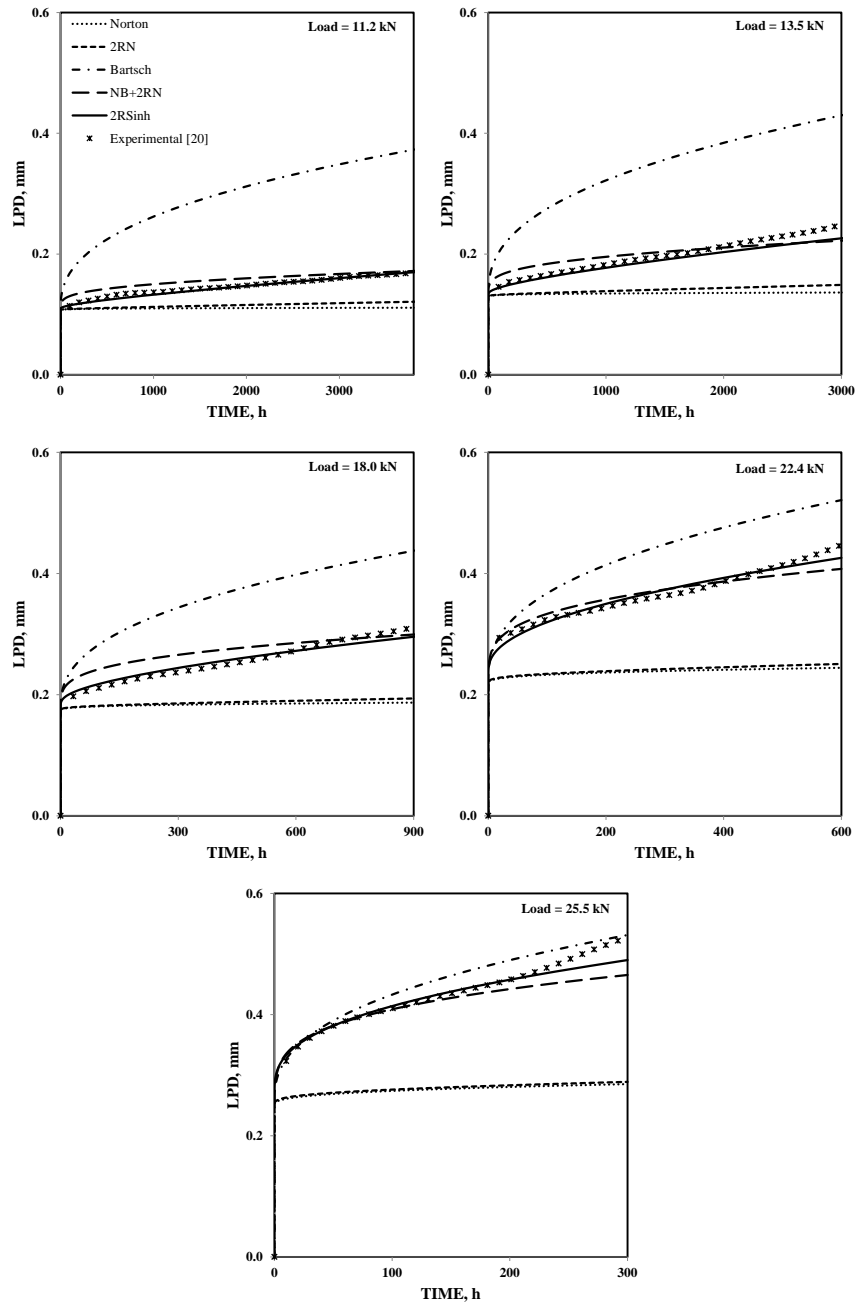


Figure 3.2.7: Comparison of FE predicted LPD responses using the five creep models with the observed behaviour in CCI tests (MMS001 at 550°C).

ondary creep model implementations are not surprising when applied to a material exhibiting significant primary creep. Since the secondary models neglect the incidence of primary creep deformation, they inevitably underestimate the extent of stress relaxation and redistribution within the crack near field relative to that predicted with primary+secondary creep models. The consequence of this is the prediction of higher stresses and lower creep strains in the vicinity of the crack tip (e.g. Figures 3.2.4 and 3.2.5) in such materials. The explanation for the observed differences between FE predictions using the different primary+secondary creep models (or different secondary creep models) is complex and is examined in the next section.

It is important to acknowledge that there is not a single model capable of representing the creep response of all materials. For example, unlike 1CrMoV at 550°C, some materials do not exhibit significant primary creep deformation under certain conditions and, for these, the adoption of a primary plus secondary model is unnecessary. Model selection should therefore be based on the deformation characteristics of the material under evaluation.

Stress Regime

The 2RN equation was proposed to overcome a problem associated with modelling $\dot{\epsilon}(\sigma)$ data in high and low stress regimes in a relatively simple way [21]. Even though the conventional Norton model fit was based on uniaxial creep strain data for stresses in the range 211 to 306MPa [20], reference to the NIMS 1CrMoV dataset [24] indicated that there was a mechanism change (reflected by a significant change in stress exponent) at stress between 200–235MPa, dependent to the relative creep strength of steel [21]. It is believed that the 2RSinh model describes this creep mechanism change in a more realistically continuous way (Figure 3.2.1). The model form in Naumenko et al. [16] also represents the creep strain rate dependence on stress in a continuous way, but only for secondary deformation rates.

The different ways in which the creep behaviour of the MMS001 heat of the 1CrMoV steel was represented were responsible for the very different predictions of stress/strain state in the remaining ligaments of CT specimens during CCI tests.

The situation is illustrated in Figure 3.2.6 for uniaxial creep strain predictions using the three primary+secondary creep models. At a stress of 250MPa, predictions of primary+secondary creep strain are consistent (same condition was observed for four other stress levels of 211, 245, 275 and 306MPa (Figure 3.2.2) which also confirmed the consistency of different models with the experimental observations). At lower stresses of 190 and 130MPa (well below the minimum uniaxial creep test stress for this heat of 1CrMoV), the agreement between predictions is not so good. The extrapolation characteristics of these three models beyond

the range of the experimental input data are significantly different.

In complex loaded structures such as the CT specimen geometry, the component material experiences a wide range of effective stresses, from very high to very low, with increasing distance ahead of the critical feature. The prediction of different creep strain behaviour by different creep models for the low stress regime results in the representation of different stress/strain states in the remaining ligaments of CT specimens during CCI tests. The analyst must therefore recognise that the constitutive models used in FE numerical simulations should adequately represent creep deformation behaviour throughout the full range of application stresses of interest. When this is not possible, the prediction uncertainties must be acknowledged.

Increasing the applied load on CT specimens increases the magnitudes of ligament (reference) stresses closer to the stress levels applied in the uniaxial tests thereby resulting in more consistent FE results from the different creep model implementations at high load levels (e.g. Figures 3.2.4, 3.2.5 and 3.2.7).

It has been shown that more reliable FE predictions can be achieved using two-regime creep model implementations accounting for different creep response characteristics in different stress (mechanism) regimes (i.e. using the 2RSinh and NB+2RN models). This finding is similar to that of Naumenko et al. who also employed a stress regime dependent creep model to more effectively predict stress relaxation in a number of engineering structures [16].

In the absence of a fully validated creep constitutive equation, it is strongly recommended to benchmark model effectiveness using for example the LPD results from CT specimen CCI tests, as shown in Figure 3.2.7. In this case, for example, it is demonstrated that use of the 2RSinh and NB+2RN models provides the most consistent representation of creep response in 1CrMoV steel CT specimen CCI tests conducted for a range of load (stress) levels at 550°C.

3.2.6 Concluding Remarks

The aim of the paper has been to highlight the sensitivity of finite element (FE) numerical creep analyses to the adopted creep constitutive model. It has been shown that even when different creep models are carefully fitted to the same experimental uniaxial dataset, very different predictions of stress/strain distributions can be determined. This emphasises the need for benchmarking creep FE simulations before using the results to predict time-dependent behaviour at critical locations of high temperature components.

The evaluation has employed the results of uniaxial creep to rupture tests and creep crack

incubation (CCI) tests using compact tension (CT) specimens on the same heat of a 1CrMoV turbine rotor steel at 550°C. From the uniaxial creep to rupture test data, parameters have been determined for five constitutive model equations, namely a conventional Norton model, a two-regime variant of the Norton model (i.e. the 2RN model), the Bartsch model, the NB+2RN model (where NB stands for Norton–Bailey) and a new two-regime hyperbolic sine (2RSinh) model. The first two of these models represent secondary creep behaviour only, while the second three represent primary plus secondary creep deformation behaviour. Creep behaviour predictions for 1CrMoV at 550°C are sensitive to whether the constitutive model represents secondary creep deformation or primary plus secondary creep deformation. However this may not be true for all materials at all temperatures and stresses, and model selection should be determined by the deformation characteristics of the alloy under evaluation.

There is also an important sensitivity to stress, in particular if the stress for which predictions are needed is responsible for a deformation mechanism which is different to that relating to the stress regime in which model underpinning experimental observations were generated.

References

- [1] F.H. Norton. *The Creep of Steel at High Temperature*. McGraw–Hill book company New York, 1929.
- [2] R.W. Bailey. The utilisation of creep test data in engineering design. *Proceedings of the Institution of Mechanical Engineers*, 131:131–349, 1935.
- [3] D.R. Hayhurst, D.A. Lavender, N.G. Worley, and A. Salim. An assessment of the θ -projection method for the representation and extrapolation of creep data for a 0.5Cr0.5Mo0.25V steel tested at 565°C. *International Journal of Pressure Vessels and Piping*, 20(4):289–317, 1985.
- [4] R.W. Evans and B. Wilshire. *Introduction to Creep*. Institute of Materials, 1993.
- [5] H. Bartsch. New creep equation for ferritic and martensitic steels. *Steel Research*, 66(9):384–388, 1995.
- [6] F.B. Dyson and M. McLean. Microstructural evolution and its effects on the creep performance of high temperature alloys. In *Microstructural Stability of Creep Resistant Alloys for High Temperature Plant Applications*, pages 371–379, 1998.
- [7] I.J. Perrin and D.R. Hayhurst. Creep constitutive equations for a 0.5Cr0.5Mo0.25V ferritic steel in the temperature range 600–675°C. *The Journal of Strain Analysis for Engineering Design*, 31(4):299–314, 1996.
- [8] R.J. Hayhurst, R. Mustata, and Hayhurst D.R. Creep constitutive equations for parent, Type IV, R-HAZ, CG-HAZ and weld material in the range 565–640°C for CrMoV weldments. *International Journal of Pressure Vessels and Piping*, 82(2):137–144, 2005.
- [9] J.L. Bolton. A characteristic strain model for creep. In *Proceedings of ECCC Conference on Creep and Fracture in High Temperature Components: Design and Life assessment Issues*, pages 456–477, 2005.
- [10] G.A. Webster and R.A. Ainsworth. *High Temperature Component Life Assessment*. Chapman & Hall, London, 1994.
- [11] R5. Assessment Procedure for the High Temperature Response of Structures. volume 3, 2003.
- [12] D.R. Hayhurst, P.R. Brown, and Morrison C.J. The role of continuum damage in creep crack growth. *Philosophical Transactions of the Royal Society A*, 311(1516):131–158, 1984.
- [13] H. Riedel. *Fracture at High Temperatures*. Springer–Verlag, Berlin, New York, 1987.
- [14] F.R. Hall and D.R. Hayhurst. Modelling of grain size effects in creep crack growth using a non-local continuum damage approach. *Proceedings of the Royal Society of London A*, 433(1888):405–421, 1991.
- [15] C.J. Hyde, T.H. Hyde, W. Sun, and A.A. Becker. Damage mechanics based predictions of creep crack growth in 316 stainless steel. *Engineering Fracture Mechanics*, 77(12):2385–2402, 2010.
- [16] K. Naumenko, H. Altenbach, and Y. Gorash. Creep analysis with a stress range dependent constitutive model. *Archive of Applied Mechanics*, 79(6):619–630, 2009.
- [17] S.R. Holdsworth. Initiation and early growth of creep cracks from pre-existing defects. *Materials at High Temperatures*, 10(2):127–137, 1992.
- [18] ASTM Standard E1457. Standard test method for measurement of creep crack growth rates in metals, Annual Book of ASTM Standards, volume 3.1.
- [19] S.R. Holdsworth. Creep crack growth in low alloy steel weldments. *Materials at High Temperatures*, 15(3–4):203–209, 1998.
- [20] S.R. Holdsworth and E. Mazza. Exploring the applicability of the LICON methodology for a 1CrMoV steel. *Materials at High Temperatures*, 25(4):267–276, 2008.

- [21] E. Hosseini, S.R. Holdsworth, and E. Mazza. Experience with using the LICON methodology for predicting long term creep behaviour in materials. *International Journal of Pressure Vessels and Piping*, 92:70–76, 2012.
- [22] S.R. Holdsworth. Advances in the assessment of creep data. In *Proceedings of 9th Liege Conference on Materials for Advanced Power Engineering*, 2010.
- [23] S.R. Holdsworth. *Creep Resistant Steels*, chapter Constitutive equations for creep curves and predicting service life, pages 403–420. Woodhead Publishing; CRC Press, Cambridge, England, 2008.
- [24] NIMS. *Data Sheet 9B, Data sheets on the elevated temperature properties of 1Cr–1Mo–0.25V steel forgings for turbine rotors and shafts*. National Research Institute for Metals, Tokyo, Japan, 1990.
- [25] Optimisation toolbox, MATLAB version 7.10.0 (R2010a). Natick, Massachusetts: The MathWorks Inc. 2010.
- [26] ABAQUS. User’s Manual, Version 6.10, Hibbit, Karlsson and Sorenson, Pawtucket, RI, USA, 2011.

3.3 *Article Three*

Overview

This section contains a reprint of the article: E. Hosseini, S.R. Holdsworth, E. Mazza, Stress regime dependent creep constitutive model consideration in finite element continuum damage mechanics, International Journal of Damage Mechanics, 2013, with permission from SAGE.

Background Motivation

For many engineering alloys, the creep deformation/damage accumulation mechanisms exhibited at high stresses is not the same as that at lower stresses. Previous articles explained the need for consideration of stress regime dependent creep constitutive models in finite element analyses of structures with a wide range of redistribution stresses. This article has introduced a new creep constitutive model, applicable for particle hardened alloys over a wide range of stresses, which considers a gradual change of creep deformation/damage accumulation mechanism with stress variation.

Summary

This article has introduced a new (primary–secondary–tertiary) stress regime dependent creep constitutive model. The creep deformation part of this model has been based on the Garofalo creep model and viscous glide creep considerations. The creep damage development part of the model has been constructed based on the LICON method concept. Application of the introduced creep model in finite element continuum damage mechanics for simulating the creep deformation/damage accumulation in a series of creep crack incubation tests involving fracture mechanics compact tension specimens made of 1CrMoV has been shown to be successful.

Main Conclusions, [Link to the Next Article](#)

This article has shown that, in particular for analysis of components with a wide range of redistributing stresses, it is crucial to adopt creep constitutive models which consider stress regime dependency of creep deformation/damage accumulation behaviour of materials. The newly developed creep constitutive model which considers a gradual change of creep deformation/damage accumulation mechanisms with stress variation could successfully reproduce

the deformation and damage accumulation behaviours of 1CrMoV in a series of creep crack incubation tests. The creep damage accumulation part of this model has been constructed based on the LICON method formulation and successful demonstration of it provided a new confirmation for the LICON formulation, and from a different point of view, i.e. finite element continuum damage mechanics. The next article has summarised the gathered knowledge about creep finite element analysis and LICON method application for 1CrMoV.

Stress Regime Dependent Creep Constitutive Model Consideration in Finite Element Continuum Damage Mechanics¹

Abstract

Structural analysis and the design of high temperature components require the consideration of material inelastic deformation and damage accumulation characteristics for a wide range of stresses and temperatures. For many engineering alloys, the creep deformation/damage accumulation mechanism exhibited at high stresses are not the same as those at lower stresses. This paper explains the importance of considering this stress regime dependency in the creep model formulations and introduces a new (primary–secondary–tertiary) creep model which considers a gradual change of creep deformation/damage accumulation mechanism with stress variation. Application of the new stress regime dependent creep model formulation in finite element continuum damage mechanics (FECDM) to simulate creep deformation/damage accumulation in a series of creep crack incubation (CCI) tests involving fracture mechanics compact tension (CT) specimens showed a good agreement with experimental observations which was not achievable by considering conventional single regime creep model equations.

Keywords:

Stress regime dependent creep behaviour; Creep constitutive model; Finite element continuum damage mechanics; Creep crack development; 1CrMoV alloy.

¹E. Hosseini, S.R. Holdsworth, E. Mazza, *International Journal of Damage Mechanics* 22(5) (2013), xxx–xxx

3.3.1 Introduction

Many important components of power generation plant are subjected to high temperatures and complex loading conditions over a long period of time. Design procedures for the life assessment of such components can require the consideration of material inelastic deformation and damage accumulation characteristics for a wide range of stresses and temperatures. Structural analysis under creep conditions requires a reliable constitutive model which reflects time-dependent deformation and accompanying processes like hardening/recovery and damage accumulation. A creep model should therefore represent the creep deformation/damage accumulation of a material over a wide range of stresses and temperatures. Many creep constitutive models have been developed during the last 100 years and a number of these have recently been reviewed by Holdsworth [1].

Some creep deformation models (e.g. the conventional Norton equation [2] or the version of the Bartsch equation [3] used by Holdsworth and Mazza [4]) involve a general single formulation to describe the behaviour of material for all stress regimes (i.e. single regime creep models). However, for many engineering alloys, the creep deformation mechanism exhibited at high stresses is not the same as that at lower stresses [5, 6] and such creep models cannot represent the effect of a creep mechanism transition due to a change of stress.

Typically, at relatively high temperatures, dislocation creep controlled by dislocation climb and glide (high temperature power law creep) occurs at higher stresses (when the stress exponent is ≥ 5), whereas diffusion creep controlled by volume or grain boundary diffusion occurs at lower stresses (when the stress exponent is around three or, in the limit, unity). Some creep models like two-regime Norton (2RN) provide a bi-linear formulation with different parameter sets for high and low stress regimes and therefore need experimental creep data from both stress regimes to fit the creep model parameters [7]. The application of such formulations for a wide range of stresses is much more successful. However in reality, the stress dependent creep mechanism change is not a sharp transition and considering a sudden change of creep mechanism at a critical stress is not a realistic assumption. In addition, consideration of two different sets of equations for the creep constitutive model introduces numerical difficulties in the simulation of complex stress states and demands increased numerical effort. The more physically acceptable and numerically efficient solution is a gradual and continuous change of creep deformation mechanism with stress variation (i.e. the formulation proposed in this study).

The same statement is valid for creep damage accumulation. While in a high stress regime, creep damage arises mainly due to $\bar{\sigma}$ -controlled mechanisms, σ_1 -controlled mechanisms are

responsible for creep damage in a low stress regime. For example, for ferritic steels of the type considered in this work, at high stresses, the damage mechanism is predominantly void formation due to particle/matrix decohesion ($\bar{\sigma}$ -controlled) while at lower stresses, damage nucleates and develops at grain/lath boundaries (σ_1 -controlled) [4]. Consequently, as for creep deformation model equations, creep damage equations are therefore expected to cover multiple mechanism regimes and represent a gradual and continuous change of creep damage mechanism with stress variation.

In this paper, a modification to the primary–secondary version of a single regime creep model proposed by Dyson and Osgerby [8] (originating from the Garofalo creep model equation [9]) is presented. The new creep model considers a stress regime dependent creep deformation mechanism change with stress variation. Furthermore, influenced by the LICON method formulation proposed by Auerkari et al. [10], a stress regime dependent creep damage accumulation function is derived. This function is then introduced to the developed primary–secondary creep constitutive model to extend it for covering the tertiary creep regime.

The effectiveness of the developed creep constitutive (stress regime dependent primary–secondary–tertiary) model is later examined for reproducing experimental observations from a series of creep crack incubation (CCI) tests. The considered CCI tests, conducted by Holdsworth and Mazza [4], involve fracture mechanics compact tension (CT) specimens made of 1CrMoV turbine rotor steel loaded at 550°C. In general, CCI tests are specifically performed to observe the time to the onset of creep crack extension and are not creep crack growth tests. Typically, the creep crack initiation criterion adopted for such tests is 0.5mm (or 0.2mm) crack extension. The tests are intentionally stopped before the development of significantly long cracks and the specimens are then used to metallurgically investigate early creep damage development characteristics.

The prediction of creep deformation in CT specimens provides an appropriate challenge for any new creep model because of the wide range of stresses (from high to low) redistributing across the remaining ligament ahead of the sharp notch crack starter of this geometry. The effectiveness of the new creep constitutive model is therefore independently checked with respect to experimental observations from the CCI tests on 1CrMoV at 550°C reported by Holdsworth and Mazza [4]. For this reason, the creep model is applied in a finite element continuum damage mechanics (FECMD) implementation to predict deformation/damage accumulation in the CCI tests. The application of the new creep model formulation is shown to be successful in predicting creep deformation and early damage accumulation in the CCI tests, thus confirming the applicability of the proposed creep constitutive model.

3.3.2 Stress Regime Dependent Creep Model

Ferritic steels of the type considered in this work, are strengthened primarily by carbide precipitates. Originating from the Garofalo creep model equation [9], Dyson and Osgerby proposed the creep rate of an alloy with an interparticle distance of l to be [8]:

$$\dot{\epsilon}_{Dis} = \dot{\epsilon}_0 \sinh \frac{\sigma}{\sigma_0} \quad (3.3.1)$$

where $\dot{\epsilon}_{Dis}$ is the creep rate resulting from dislocation glide/climb, $\dot{\epsilon}_0$ is a stress-independent coefficient, σ is the applied stress, $\sigma_0 = 5kTf(V_p)/b^2l$ and k , T , V_p and b are Boltzmann's constant, temperature, volume fraction of precipitates and Burger's vector, respectively. Following the approach of Dyson and Osgerby [8], the state variable of $\varphi = 1 - l_0/l$ is introduced, where l_0 is the initial interparticle distance:

$$\dot{\epsilon}_{Dis} = A_1 \sinh \left[b_1 \frac{\sigma}{(1 - \varphi)} \right] \quad (3.3.2)$$

A_1 and b_1 are material-temperature dependent constants.

For particle-strengthened alloys, the above formulation applies, in particular for moderate to high stress regimes. However, other creep deformation mechanisms (e.g. diffusion creep mechanisms) which are less influential at higher stresses may significantly affect the material creep deformation behaviour in the low stress regime. Hence, the consideration of these for creep analyses over wide ranges of stresses is essentially required.

At low stresses, diffusion creep may occur because the chemical potential of vacancies in grain boundaries are affected by the stress direction with respect to the boundary plane, leading to diffusional mass fluxes from boundaries orientated along the tensile axis to those normal to the direction of applied stress, with the result that permanent creep strain may occur. The flow of vacancies may take place either through the crystalline lattice (Nabarro-Herring diffusion creep [11, 12]) or along the grain boundaries (Coble diffusion creep [13]). They give:

$$\dot{\epsilon}_{N-H} = b_{N-H} \frac{D_l V}{d^2 k T} \sigma \quad (3.3.3)$$

$$\dot{\epsilon}_{Cob} = b_{Cob} \frac{\delta D_{gb} V}{d^3 k T} \sigma \quad (3.3.4)$$

where b_{N-H} and b_{Cob} are constants, D_l and D_{gb} are the coefficients for lattice and grain boundary diffusion and δ , V and d are respectively the effective width of the grain boundary for vacancy diffusion, the atomic volume and the grain size.

These creep deformation mechanisms are assumed to act independently to each other and

the creep strain produced by each mechanism to contribute additively to the total creep strain [14, 15]. The overall material creep rate can therefore be written as:

$$\dot{\epsilon} = \dot{\epsilon}_{Dis} + \dot{\epsilon}_{N-H} + \dot{\epsilon}_{Cob} \quad (3.3.5)$$

$$\dot{\epsilon} = A_1 \sinh\left[b_1 \frac{\sigma}{(1-\varphi)}\right] + \frac{\Omega}{kT} \left[b_{N-H} \frac{D_l}{d^2} + b_{Cob} \frac{\delta D_{gb}}{d^3} \right] \sigma \quad (3.3.6)$$

$$\dot{\epsilon} = A_1 \sinh\left[b_1 \frac{\sigma}{(1-\varphi)}\right] + b_2 \sigma^n \quad (3.3.7)$$

where b_2 is a material-temperature dependent constant and $n = 1$. The summation of the two expressions can therefore provide a reliable continuous representation of the creep behaviour of a material for a wide range of stresses. Such a continuous transition in creep deformation mechanism is a more plausible assumption than that represented by bi-linear creep models (e.g. 2RN [7]). Moreover, it is much easier for numerical simulations to deal with a gradual behaviour transition than with the sharp change presented by bi-linear models. Equation 3.3.7 may be compared with the one proposed by Naumenko et al. [16] which assumed the minimum creep rate to be the sum of linear and power law functions.

It should be noted that adoption of a stress exponent equal to one ($n = 1$) for low stress regime models (such as Equation 3.3.7) is still under review, e.g. [17–20]. Although fundamental creep deformation theory suggests a value of one in this mechanism regime, there are several reports of higher values, up to about three, e.g. [21]. For 1CrMoV at 550°C, Sidey reported a creep stress exponent of about 3 at stresses lower than 230MPa, while it was about 16 at higher stresses [22]. This study therefore considers also the implementation of Equation 3.3.7 with a stress exponent of three, $n = 3$.

Dyson and Osgerby, using 'standard coarsening theory', implemented the following equation for interparticle spacing evolution [8]:

$$\dot{\varphi} = \frac{C_2}{3} (1-\varphi)^4 \quad (3.3.8)$$

where C_2 is a material-dependent rate function varying exponentially on temperature and inversely with l_0^3 . Equation 3.3.8, defining φ between zero and unity, is a first approximation for modelling the evolution of interparticle spacing. Increasing interparticle spacing (and/or particle growth) is mainly a diffusion controlled process. The diffusion coefficient of a material can increase with applied stress [23], and therefore, in a more accurate definition, the evolution of φ should also depend on applied stress. Observations for 1CrMoV, reported by Roberts and Strang [24], on the different magnitudes of hardness drop in the gauge sections and grip ends of uniaxial specimens after creep testing clearly demonstrate

the dependency of particle coarsening (interparticle distance evolution) on stress, time and temperature. It should be noted that while for relatively short thermal exposure durations, the particle state is likely to remain unchanged and $\varphi \simeq 0$, application of the creep model to long-time behaviour prediction certainly needs to consider the evolution of strengthening particles, i.e. with $\varphi \neq 0$

The extension of the creep model to the primary creep regime can be achieved in a manner similar to that proposed by Ion et al. [25] and employed by others [8, 26, 27]. Introducing the internal state variable $\mathcal{H}(= \sigma_i/\sigma$, where σ_i is the 'internal' stress growing during primary creep, as a hardening parameter, the primary creep included version of the proposed creep model is given by the following equation-set [28]:

$$\begin{aligned}\dot{\varepsilon} &= A_1 \sinh\left[B_1 \frac{(1-\mathcal{H})}{(1-\varphi)}\sigma\right] + B_2[(1-\mathcal{H})\sigma]^n \\ \dot{\mathcal{H}} &= \frac{C_1}{\sigma^\alpha} \left[1 - \frac{\mathcal{H}}{\mathcal{H}^*}\right] \dot{\varepsilon} \\ \dot{\varphi} &= \frac{C_2}{3} (1-\varphi)^4\end{aligned}\tag{3.3.9}$$

where B_1 , B_2 , C_1 and \mathcal{H}^* are material-temperature dependent constants and α defines the dependency of primary creep strain on the stress magnitude. The state variable \mathcal{H} is initially zero and takes the saturated value of \mathcal{H}^* when the material enters the secondary creep regime. The original formulation introduced an inverse linear dependency for \mathcal{H} parameter evolution on stress, i.e. $\dot{\mathcal{H}} \propto \sigma^{-1}$ [8, 25]. Evolution of the \mathcal{H} parameter defines the primary creep deformation behaviour of the material. As previously revealed [29], the stress dependency of primary creep deformation for 1CrMoV at 550°C cannot be reproduced with the above assumption. Updating the relationship to the form of $\dot{\mathcal{H}} \propto \sigma^{-\alpha}$, the α value can be determined from a best fit of the creep model to experimental uniaxial primary creep strains for different stress conditions.

The extension of the creep model to the tertiary creep regime is possible by introducing a third state variable ω to represent creep damage intensity. The damage parameter represents the effective area reduction due to the formation of microscopic cracks and cavities [30–32]. As mentioned earlier, different creep damage mechanisms may be considered for high and low stress regimes. After Hayhurst [33], Cane [34], Lonsdale and Flewitt [35] and as cited in the LICON method formulation by Martins and Holdsworth [36], the rupture behaviour of material for each damage (failure) mechanism regime can be presented by:

$$t_{f_i} = c_i \bar{\sigma}^{-\nu_i} H^{-\gamma_i}\tag{3.3.10}$$

where c_i , ν_i and γ_i are temperature–material dependent parameters and $H = \sigma_1/\bar{\sigma}$. Typically for ferritic steels, two damage mechanisms are involved, void nucleation due to particle/matrix decohesion at high stresses ($\bar{\sigma}$ -controlled, $\gamma_i \rightarrow 0$) and nucleation and development of creep damage at grain/lath boundaries at low stresses (σ_1 -controlled, $\gamma_i \rightarrow \nu_i$) [4]:

$$\begin{aligned} t_{f1} &= c_1 \bar{\sigma}^{-\nu_1} && \text{particle/matrix decohesion} \\ t_{f2} &= c_2 \bar{\sigma}^{-\nu_2} H^{-\gamma_2} && \text{grain/lath boundary cavitation} \end{aligned} \quad (3.3.11)$$

Based on a time fraction linear damage summation consideration [37], the overall behaviour can be written as:

$$\begin{aligned} \frac{1}{t_f} &= \frac{1}{t_{f1}} + \frac{1}{t_{f2}} \\ \frac{1}{t_f} &= \frac{\bar{\sigma}^{\nu_1}}{c_1} + \frac{\bar{\sigma}^{\nu_2}}{c_2} H^{\gamma_2} \end{aligned} \quad (3.3.12)$$

The evolution of damage intensity can be estimated to be:

$$\dot{\omega} = \frac{1}{t_f} \frac{(1 - e^{-q})}{q} e^{q\omega} \quad (3.3.13)$$

where q is a parameter introduced by Liu and Murakami [38]. Substituting 3.3.12 in 3.3.13, while $C_{3,4}$ are $1/c_{1,2}$, gives:

$$\dot{\omega} = (C_3 \bar{\sigma}^{\nu_1} + C_4 \bar{\sigma}^{\nu_2} H^{\gamma_2}) \frac{(1 - e^{-q})}{q} e^{q\omega} \quad (3.3.14)$$

Therefore, the uniaxial and multiaxial representations of the proposed creep model are:

$$\begin{aligned} \dot{\epsilon} &= A_1 \sinh[B_1 \frac{(1 - \mathcal{H})}{(1 - \varphi)(1 - \omega)} \sigma] + B_2 [\frac{(1 - \mathcal{H})}{(1 - \omega)} \sigma]^n \\ \dot{\mathcal{H}} &= \frac{C_1}{\sigma^\alpha} [1 - \frac{\mathcal{H}}{\mathcal{H}^*}] \dot{\epsilon} \\ \dot{\varphi} &= \frac{C_2}{3} (1 - \varphi)^4 \\ \dot{\omega} &= (C_3 \sigma^{\nu_1} + C_4 \sigma^{\nu_2}) \frac{(1 - e^{-q})}{q} e^{q\omega} \end{aligned} \quad (3.3.15)$$

and:

$$\begin{aligned}
\dot{\epsilon}_{ij} &= \frac{3S_{ij}}{2\bar{\sigma}} \left\{ A_1 \sinh \left[B_1 \frac{(1-\mathcal{H})}{(1-\varphi)(1-\omega)} \bar{\sigma} \right] + B_2 \left[\frac{(1-\mathcal{H})}{(1-\omega)} \bar{\sigma} \right]^n \right\} \\
\dot{\mathcal{H}} &= \frac{C_1}{\bar{\sigma}^\alpha} \left[1 - \frac{\mathcal{H}}{\mathcal{H}^*} \right] \dot{\epsilon}_e \\
\dot{\varphi} &= \frac{C_2}{3} (1-\varphi)^4 \\
\dot{\omega} &= N (C_3 \bar{\sigma}^{\nu_1} + C_4 \bar{\sigma}^{\nu_2} H^{\gamma_2}) \frac{(1-e^{-q})}{q} e^{q\omega}
\end{aligned} \tag{3.3.16}$$

where $\bar{\sigma}$ and $\dot{\epsilon}_e$ are the von Mises equivalent stress and strain rate values, S_{ij} and $\dot{\epsilon}_{ij}$ are the deviatoric stress and the creep strain rate tensor components and $N = 1$ if $\sigma_1 > 0$, otherwise $N = 0$.

3.3.3 Creep Deformation/Damage Accumulation of 1CrMoV Alloy

To examine the applicability of the proposed creep model, it is used to represent a series of experimental creep curves of a high creep strength (HCS) 1CrMoV turbine rotor steel, identified as MMS001 ($d = 60\mu\text{m}$), at 550°C . The creep behaviour observations from four uniaxial creep tests at stress levels of 306, 275, 245 and 211MPa (rupture times of 1–34kh [4]) in conjunction with the test data published in the NIMS Data Sheet [39] were used to underpin the creep model for the MMS001 alloy. It was necessary to complement the MMS001 1CrMoV creep data with those from the NIMS Data Sheet [39] for the turbine rotor steel because MMS001 was a strong production heat for which there was only high stress regime data (Figure 3.3.1 and 3.3.3). The NIMS lower creep strength (higher creep rate) data provided the necessary basis for the low stress regime model representation.

In order to evaluate the predictive capability of the proposed creep deformation/damage accumulation formulation, the creep model was applied in a FECDM implementation to reproduce the load point displacement (LPD) and creep crack development records for five CCI tests. The constant load CCI tests involved fully instrumented 25mm thick specimen with sidegrooves ($a_0/W = 0.5$) made of MMS001 and loaded at 550°C to five different load levels of 25.5, 22.4, 18.0, 13.5 and 11.2kN (testing times of 0.5–6kh). More information concerning the experimental details is available elsewhere [4].

Determination of Model Parameters

From Equation 3.3.16, it can be seen that the parameters which are required to be obtained are A_1 , B_1 , B_2 , n , C_1 , α , \mathcal{H}^* , C_2 , C_3 , ν_1 , C_4 , ν_2 , γ_2 and q_2 . The numerical values of these parameters are summarised in Table 3.3.1 and the methodologies for obtaining them are described as follows:

Secondary Creep Model Parameters (A_1 , $B_1(1 - \mathcal{H}^*)$, $B_2(1 - \mathcal{H}^*)^n$ and n) In the secondary creep regime: $\mathcal{H} = \mathcal{H}^*$ and $\varphi = \omega = 0$ (where the assumption of $\varphi = 0$ is only valid if the times to secondary creep of the considered experiments are relatively short). Following the approach of Kowaleski et al. [40], the expressions A_1 , $B_1(1 - \mathcal{H}^*)$ and $B_2(1 - \mathcal{H}^*)^n$ were estimated from the variation of the minimum creep strain rate with stress while two assumptions for the n value were considered ($n = 1, 3$) (Figure 3.3.1).

Versions of Equation 3.3.16 with values of $n = 1$ and $n = 3$ are compared in Figure 3.3.1 with respect to the NIMS data [39] to indicate the appropriateness of a stress exponent of three, similar to [21]. Furthermore, consideration of the creep model with $n = 1$ in the FE analysis of the CCI tests resulted in unacceptable creep deformation representations for the CT specimens (shown in Section 3.3.3). The consideration of $n = 3$ is therefore followed here.

Figure 3.3.1 also shows the line calculated from the original creep model equation (single regime creep model) [8]:

$$\dot{\epsilon} = A'_1 \sinh[B'_1(1 - \mathcal{H}^*)\sigma] \quad (3.3.17)$$

As can be seen, the single regime creep model underestimates the amount of deformation at low stresses. This illustrates the advantage of the considered formulation over the original formulation by Dyson and Osgerby [8]. This has been further explained in Section 3.3.3.

Primary Creep Model Parameters (C_1 , α and \mathcal{H}^*) In the primary creep regime: $\varphi = \omega = 0$ and the parameters C_1 , α and \mathcal{H}^* were defined to have optimum fit for primary creep strains at all the uniaxial tested stresses for MMS001 (Figure 3.3.2).

Interparticle Spacing Evolution Parameters (C_2) The second state variable, φ , describes the evolution of the spacing of the carbide precipitates which is known to lead to a progressive loss in the creep resistance of particle hardened alloys. For long term creep response, carbide evolution can significantly affect the creep resistance of materials and the evolution of φ is an important part of the formulation. However, in relatively short

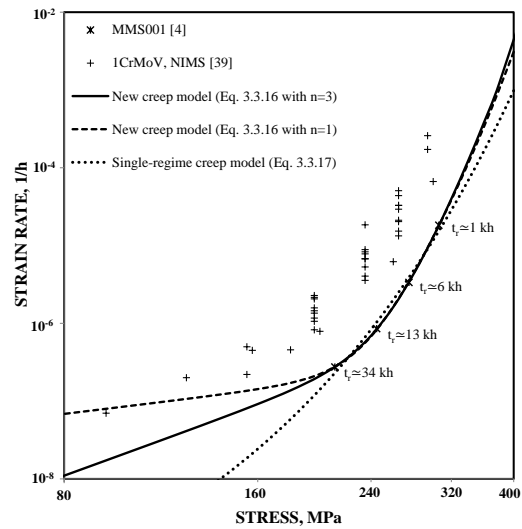


Figure 3.3.1: Secondary (or minimum) creep rate (stress) diagram for 1CrMoV steel at 550°C including a comparison of experimental uniaxial data with the creep models representations.

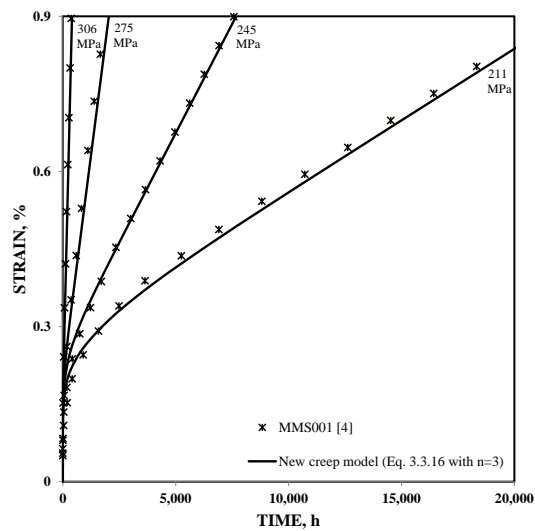


Figure 3.3.2: Uniaxial creep strain representation of the creep model for HCS 1CrMoV steel at 550°C in comparison with the experimental records (primary and secondary creep regimes).

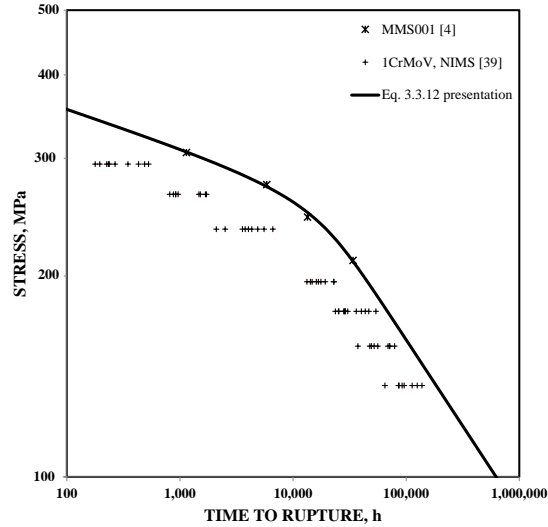


Figure 3.3.3: Rupture time (stress) diagram for 1CrMoV steel at 550°C including a comparison of experimental data with the assumed formulation (Equation 3.3.12).

term creep application, the extent of carbide evolution is negligible ($\varphi \simeq 0$). For 1CrMoV at 550°C, the carbide condition changes only significantly after ~ 20 kh [24] which is much longer than the adopted CCI benchmark tests (≤ 6 kh). The simulation presented in this study therefore neglected the effect of carbide evolution ($C_2 = 0$).

Creep Damage Evolution Parameters (C_3 , ν_1 , C_4 , ν_2 , γ_2 and q) Under uniaxial testing conditions, $H = 1$, and according to Equation 3.3.12, $C_{3,4}$ and $\nu_{1,2}$ can be determined from a fit on uniaxial creep rupture times at different stresses (Figure 3.3.3). Then, all the constants required in the uniaxial version of the creep model are known except for the q value. The q value was therefore defined to have the optimum fit for the tertiary creep strains at all the uniaxial tested stresses (Figure 3.3.4). Finally, the reported value by Holdsworth and Mazza [4] of γ_2 for 1CrMoV steel at 550°C was considered in this study ($\gamma_2 = 0.74\nu_2$) to implement the effect of stress multiaxiality in the creep damage evolution.

FECDM Results

After determination of the constitutive model parameters, Equation 3.3.16 was implemented into an ABAQUS [41] FE analysis using the mesh shown in Figure 3.3.5 to simulate the creep

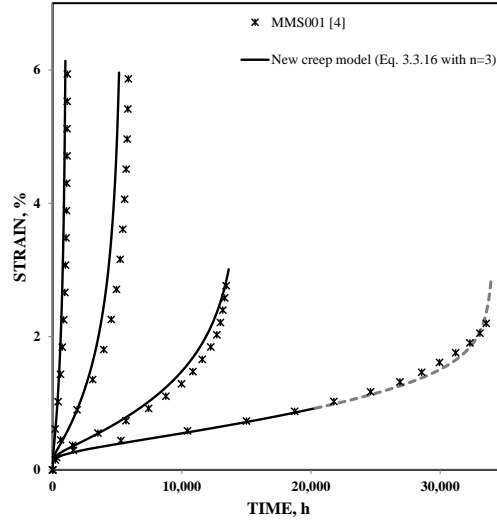


Figure 3.3.4: Uniaxial creep strain (primary–secondary–tertiary) representation of the new creep model in comparison with the experimental records for HCS 1CrMoV steel at 550°C.

deformation/damage accumulation of MMS001 at 550°C in the series of CCI tests. The main calculations was performed with a FE mesh involving 21770 quadratic hexahedral elements (element size of 100 μ m at the notch root of the CT specimen), and CREEP+USDFLD subroutines were used to implement the new constitutive model in to the code. The elastic modulus was updated according to the value of damage parameter, $E = E_0/(1 - \omega)$, and no rate-independent plasticity was considered in the calculations. As explained in Appendix, the presented simulations employed a new programming procedure to overcome the commonly occurring numerical instabilities experienced in FE calculations concerned with continuum damage mechanics.

Figures 3.3.6 and 3.3.7 present the results of FECDM calculations which illustrate an acceptable agreement between simulation and experimental CCI test results for LPD and

Table 3.3.1: Creep constitutive model parameters for the HSC 1CrMoV (MMS001) at 550°C.

Parameters	A_1	B_1	B_2	n	C_1	α	\mathcal{H}^*
Values	8.2×10^{-13}	0.12	2.2×10^{-13}	3.00	1.2×10^{-2}	-2.00	0.54
Parameters	C_2	C_3	ν_1	C_4	ν_2	γ_2	q
Values	0.00	2.8×10^{-47}	17.5	2.8×10^{-14}	3.87	$0.74 \times \nu_2$	13.0

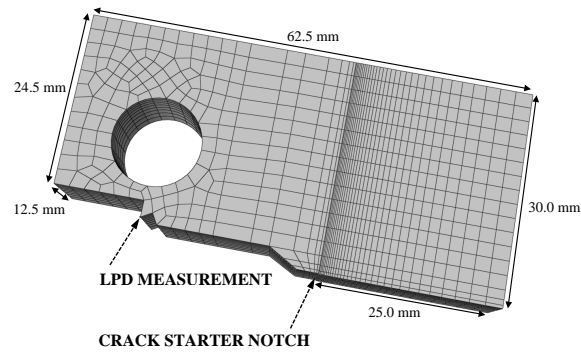


Figure 3.3.5: The adopted FE mesh for 25mm thick CT specimen.

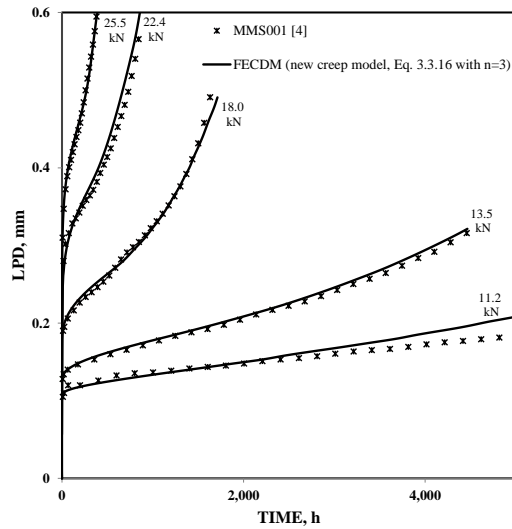


Figure 3.3.6: Comparison of FECDM predicted LPD responses with the observed behaviour for 1CrMoV CT specimens at 550°C.

crack development (except for the load level of 13.5kN). While there is a good agreement between predicted and observed LPD results for the 13.5kN CCI test, there is currently no satisfactory explanation for the inconsistency in the crack development comparison. Figure 3.3.8 compares the FECDM predicted crack development pattern with that of one of the experiments, both images representing a plane strain crack development pattern.

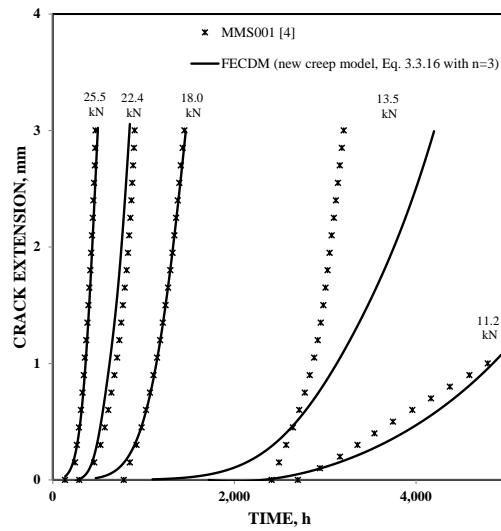


Figure 3.3.7: Comparison of FECDM predicted crack extension with the observed behaviour for 1CrMoV CT specimens at 550°C.

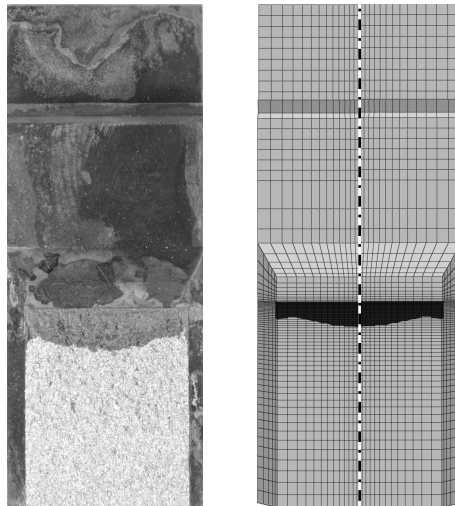


Figure 3.3.8: Comparison of FECDM predicted crack growth pattern with the observed pattern for a 1CrMoV CCI test at 550°C

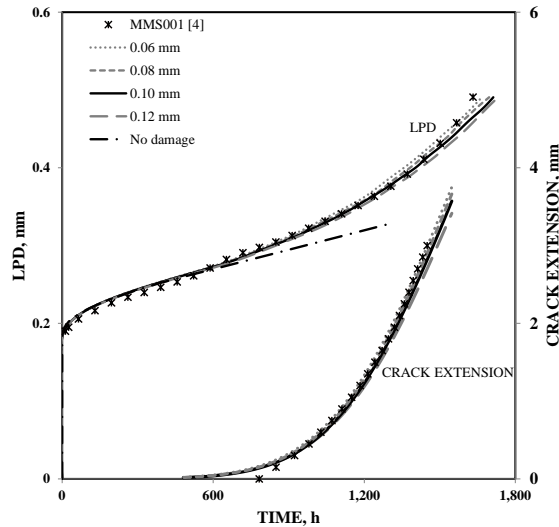


Figure 3.3.9: Sensitivity of LPD and crack extension predictions to the FE mesh size (element sizes of 60, 80, 100, 120 μm at the crack tip, load level of 18.0kN, new creep model consideration (Equation 3.3.16) with $n = 3$).

Sensitivity Analysis of FECDM Calculations

FECDM analyses of notch containing structures can be sensitive to the adopted FE model configuration. Two main causes of the mesh dependence of FECDM calculations are the stress singularity in front of the crack tip and the stress sensitivity of damage equations [38, 42]. Figure 3.3.9 shows the mesh sensitivity of calculated LPD and creep crack development responses for the performed FECDM calculations obtained with the proposed creep model formulation when element size at the crack tip varies between 60–120 μm (60, 80, 100, 120 μm). Furthermore, Figure 3.3.10 examines the same sensitivity for the calculated von Mises stress and creep strain evolutions at a position close to the notch root of the CT specimen. The weak mesh sensitivity observed for the FECDM results obtained from consideration of the proposed creep model is in line with the findings reported in [38, 43]. These works also implemented an evolution equation for the damage variable dependent on $\sigma \exp(q\omega)$ rather than as, usually for Kachanov-type damage models [44], on $\sigma/(1 - \omega)$.

In addition to the mesh sensitivity, this study has examined the accuracy of explicit creep integrations for the performed FECDM calculations. The accuracy of the creep integration in the ABAQUS FE code is controlled by an accuracy tolerance term called CETOL which is the maximum allowed difference between the creep strain increments calculated with stress

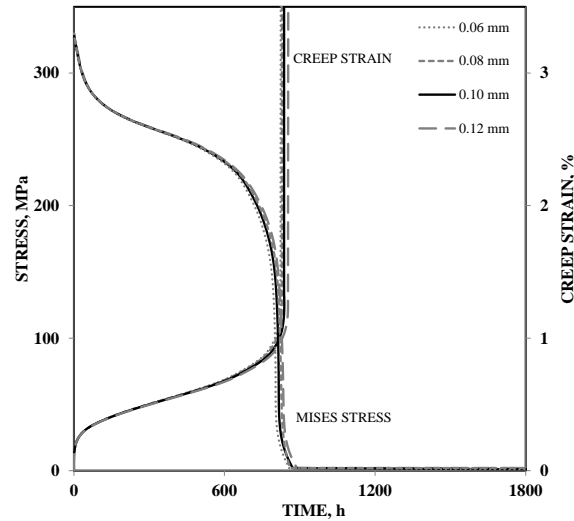


Figure 3.3.10: Sensitivity of stress/strain evolutions predictions at 0.5mm from the notch root in mid-thickness plane of the CT testpiece to the FE mesh size (element sizes of 60, 80, 100, 120 μ m at the crack tip, load level of 18.0kN, new creep model consideration (Equation 3.3.16) with $n = 3$).

states at the current and previous time increments [41]. The chosen CETOL parameter in the presented FECDM calculations was 10^{-4} . Figure 3.3.11 shows the sensitivity of performed FECDM calculations to the chosen value for CETOL. Observations of the negligible sensitivity of the FECDM results to the chosen value of CETOL in the range of 10^{-3} and 10^{-5} confirm accuracy of the performed FECDM calculations in this study (with CETOL of 10^{-4}).

Stress Regime Dependency

Previous studies have indicated the need to consider the stress regime dependency of secondary creep rates [7, 16]. The creep model developed in this study (Equation 3.3.16) has extended the consideration of stress dependency to the primary and tertiary creep regimes. The effectiveness of the model is demonstrated in simulations of creep deformation in CT specimens which provide an appropriate challenge because of the wide range of stresses (from high to low in magnitude) redistributing across the remaining ligament ahead of the sharp notch crack starter.

An example of the effectiveness of the model in simulations of creep deformation in CT

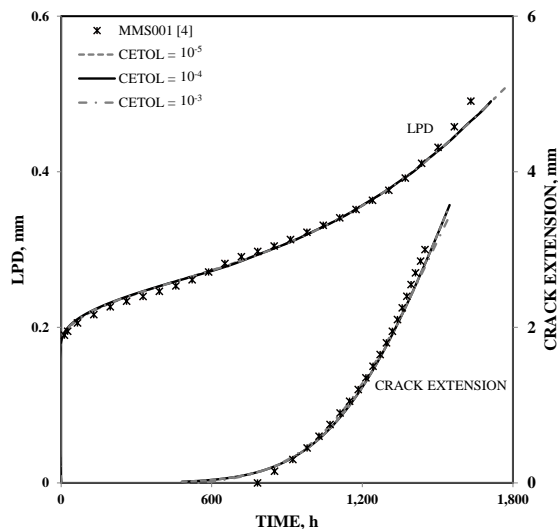


Figure 3.3.11: Sensitivity of LPD and crack extension predictions to the chosen accuracy tolerance parameter of CETOL (load level of 18.0kN, new creep model consideration (Equation 3.3.16) with $n = 3$).

specimens is shown in Figure 3.3.12. The results in Figure 3.3.12 show good agreement between observed and predicted LPD using Equation 3.3.16 with $n = 3$. Using an exponent of $n = 1$ gives an LPD prediction which is significantly overestimating the actual behaviour. This provides further justification for adopting an exponent of $n = 3$ for 1CrMoV steel in the low stress regime.

The primary–secondary part of the proposed constitutive model (i.e. Equation 3.3.16 with $\omega = 0$) is a modification to the primary–secondary version of the single regime creep model proposed by Dyson and Osgerby [8]. Comparison of the FE simulation results obtained from the application of the Dyson and Osgerby creep model [8] and the new creep model ($n = 3$) in Figure 3.3.12 clearly demonstrates the importance of stress regime dependent creep deformation consideration in the developed constitutive model formulation.

3.3.4 Concluding remarks

In this study, the need for consideration of the stress dependent deformation/damage accumulation of materials in creep model formulations is demonstrated, not just in the secondary creep regime, but also in the primary and tertiary regimes. A new stress regime dependent creep model formulation is proposed which considers a gradual change of creep deforma-

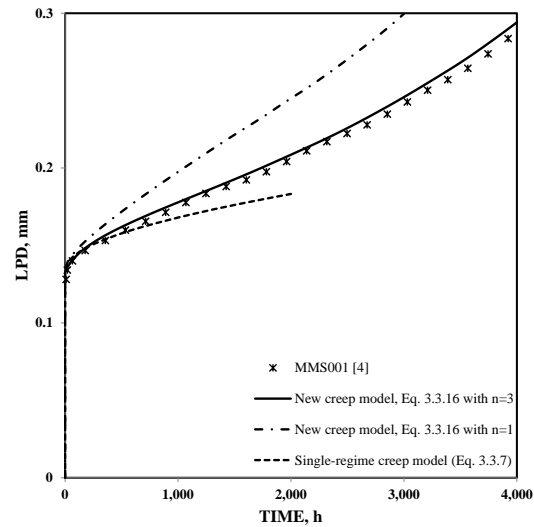


Figure 3.3.12: Comparison of the early LPD behaviour during CCI test predicted with different primary–secondary creep constitutive model consideration ($\omega = 0$) (CT specimen made of HCS 1CrMoV, loaded at 550°C and 13.5kN).

tion/damage accumulation mechanism with stress variation. The application of the new proposed creep model through finite element continuum damage mechanics (FECMD) to represent the deformation/damage accumulation behaviour exhibited in a series of creep crack incubation (CCI) tests involving fracture mechanics compact tension (CT) specimens made of a high creep strength (HCS) 1CrMoV turbine rotor steel loaded at 550°C has successfully confirmed the effectiveness of the proposed creep model (CT specimens being selected because of the wide range of stresses redistributing across the remaining ligament ahead of the sharp notch crack starter).

References

- [1] S.R. Holdsworth. *Creep-resistant Steels*, chapter Constitutive equations for creep curves and predicting service life, pages 403–420. Woodhead Publishing; CRC Press, Cambridge, England, 2008.
- [2] F.H. Norton. *The Creep of Steel at High Temperature*. McGraw–Hill, 1929.
- [3] H. Bartsch. A new creep equation for ferritic and martensitic steels. *Steel Research*, 66(9):384–388, 1995.
- [4] S.R. Holdsworth and E. Mazza. Exploring the applicability of the LICON methodology for a 1%CrMoV steel. *Materials at High Temperatures*, 25(4):267–276, 2008.
- [5] R.W. Evans and B. Wilshire. *Introduction to Creep*. Institute of Materials, London, 1993.
- [6] H.J. Frost and M.F. Ashby. *Deformation Mechanism Maps: the Plasticity and Creep of Metals and Ceramics*. Oxford, Oxfordshire, Pergamon Press, New York, 1982.
- [7] E. Hosseini, S.R. Holdsworth, and E. Mazza. Experience with using the LICON methodology for predicting long term creep behaviour in materials. *International Journal of Pressure Vessels and Piping*, 92:70–76, 2012.
- [8] B.F. Dyson and S. Osgerby. *Modelling and Analysis of Creep Deformation and Fracture in a 1Cr0.5Mo Ferritic Steel*. NPL report. National Physical Laboratory, 1993.
- [9] F. Garofalo. *Fundamentals of Creep and Creep Rupture in Metals*. Macmillan Series in Materials Science. Macmillan, 1965.
- [10] P. Auerkari, W. Bendick, S.R. Holdsworth, J.H. Rantala, R. Hurst, C. Coussement, and R. Hack. Predicting long term creep behaviour using the LICON methodology. In *Proceedings of 3rd International Conference of Advances in Material Technology for Fossil Power Plants*, pages 329–339, 2001.
- [11] F.R.N. Nabarro. Deformation of crystals by the motion of single ions. In *Physical Society Bristol Conference Report*, pages 75–90, 1948.
- [12] C. Herring. Diffusional viscosity of a polycrystalline solid. *Journal of Applied Physics*, 21(5):437–445, 1950.
- [13] R.L. Coble. A model for boundary diffusion controlled creep in polycrystalline materials. *Journal of Applied Physics*, 34(6):1679–1682, 1963.
- [14] M.F. Ashby. A first report on deformation–mechanism maps. *Acta Metallurgica*, 20(7):887–897, 1972.
- [15] K. Maruyama. *Creep-resistant Steels*, chapter Fundamental aspects of creep deformation and deformation mechanism map, pages 265–278. Woodhead Publishing; CRC Press, Cambridge, England, 2008.
- [16] K. Naumenko, H. Altenbach, and Y. Gorash. Creep analysis with a stress range dependent constitutive model. *Archive of Applied Mechanics*, 79(6–7):619–630, 2009.
- [17] M. Mostafa and F. Mohamed. Correlation between creep stress exponent and ductility in Al–10%Zn. *Metallurgical and Materials Transactions A*, 17:365–366, 1986.
- [18] O.A. Ruano, J. Wadsworth, J. Wolfenstine, and O.D. Sherby. Evidence for Nabarro–Herring creep in metals: fiction or reality? *Materials Science and Engineering A*, 165(2):133–141, 1993.
- [19] D.M. Owen and T.G. Langdon. Low stress creep behaviour: An examination of Nabarro–Herring and Harper–Dorn creep. *Materials Science and Engineering A*, 216(1–2):20–2, 1996.
- [20] L. Kloc, V. Sklenicka, and J. Fiala. Problems in theories of low stress creep mechanisms. In *Proceedings of the 10th International Metallurgical and Materials Conference, Metal*, 2001.

- [21] S. Spigarelli, M. El Mehtedi, and A. Di Salvia. Constitutive models for the description of creep and plasticity of cast and wrought Mg–Al and Mg–Zn alloys. In *IUTAM Symposium on Advanced Materials Modelling for Structures*, 2012.
- [22] D. Sidey. The high temperature creep and fracture behaviour of a 1CrMoV rotor steel. *Metallurgical and Materials Transactions A*, 7(11):1785–1791, 1976.
- [23] M.A. Korhonen, P. Børgesen, K.N. Tu, and C.Y. Li. Stress evolution due to electromigration in confined metal lines. *Journal of Applied Physics*, 73(8):3790–3799, 1993.
- [24] B.W. Roberts and A. Strang. Metallurgical aspects of turbine component life extension. In *Refurbishment and Life Extension of Steam Plant, Institution of Mechanical Engineers, London 1987*, pages 205–213, 1987.
- [25] J.C. Ion, A. Barbosa, M.F. Ashby, B.F. Dyson, and M. McLean. Modelling of creep for engineering design—I. Report, National Physical Laboratory, Teddington, UK, 1986.
- [26] I.J. Perrin and D.R. Hayhurst. Creep constitutive equations for a 0.5Cr–0.5Mo–0.25V ferritic steel in the temperature range 600–675°C. *Journal of Strain Analysis for Engineering Design*, 31(4):299–314, 1996.
- [27] F. Vakili-Tahami and D.R. Hayhurst. Failure of a welded pressure vessel due to creep: damage initiation, evolution and reheat cracking. *Philosophical Magazine*, 87(28):4383–4419, 2007.
- [28] A. Miller. An inelastic constitutive model for monotonic, cyclic, and creep deformation I. equations development and analytical procedures. *Journal of Engineering Materials and Technology*, 98:97–105, 1976.
- [29] E. Hosseini, S.R. Holdsworth, and E. Mazza. Creep constitutive model considerations for high-temperature finite element numerical simulations. *The Journal of Strain Analysis for Engineering Design*, 47(6):341–349, 2012.
- [30] F.R. Hall, D.R. Hayhurst, and P.R. Brown. Prediction of plane-strain creep-crack growth using continuum damage mechanics. *International Journal of Damage Mechanics*, 5(4):353–383, 1996.
- [31] T.E. Lacy, D.L. McDowell, P.A. Willice, and R. Talreja. On representation of damage evolution in continuum damage mechanics. *International Journal of Damage Mechanics*, 6(1):62–95, 1997.
- [32] Z. Wohua and S. Valliappan. Continuum damage mechanics theory and application—part I: Theory. *International Journal of Damage Mechanics*, 7(3):250–273, 1998.
- [33] D.R. Hayhurst. Creep rupture under multi-axial states of stress. *Journal of the Mechanics and Physics of Solids*, 20(6):381–382, 1972.
- [34] B.J. Cane. Creep cavitation and rupture in 2.25Cr1Mo steel under uniaxial and multiaxial stresses. In K.J. Miller and R.F. Smith, editors, *Proceedings of 3rd International Conference on Mechanical Behaviour of Materials*, pages 173–182, 1980.
- [35] D. Lonsdale and P.E.J. Flewitt. The effect of hydrostatic pressure on the uniaxial creep life of a 2.25Cr1Mo steel. *Proceedings of the Royal Society of London A*, 373(1755):491–509, 1981.
- [36] V.M. Martins and S.R. Holdsworth. The LICON methodology for predicting the long term service behaviour of new steels. *Materials at High Temperatures*, 19(2):99–103, 2002.
- [37] E.L. Robinson. Effect of temperature variation on the creep strength of steels. *ASME Transaction*, 60(3):25–259, 1938.
- [38] Y. Liu and S. Murakami. Damage localization of conventional creep damage models and proposition of a new model for creep damage analysis. *JSME International Journal, Series A*, 41:57–65, 1998.

- [39] NIMS. *Data Sheet 9B, Data sheets on the elevated-temperature properties of 1Cr-1Mo-0.25V steel forgings for turbine rotors and shafts*. National Research Institute for Metals, Tokyo, Japan, 1990.
- [40] Z.L. Kowaleski, D.R. Hayhurst, and B.F. Dyson. Mechanisms-based creep constitutive-equations for an aluminum-alloy. *Journal of Strain Analysis for Engineering Design*, 29(4):309–316, 1994.
- [41] ABAQUS. User's Manual, Version 6.10, Hibbit, Karlsson and Sorenson, Pawtucket, RI, USA, 2011.
- [42] S. Murakami and Y. Liu. Mesh-dependence in local approach to creep fracture. *International Journal of Damage Mechanics*, 4:230–250, 1995.
- [43] C.J. Hyde, T.H. Hyde, W. Sun, and A.A. Becker. Damage mechanics based predictions of creep crack growth in 316 stainless steel. *Engineering Fracture Mechanics*, 77(12):2385–2402, 2010.
- [44] L. M. Kachanov. *Introduction to Continuum Damage Mechanics*. Boston, M. Nijhoff, 1986.

Appendix

Numerical instability is one of the main problems encountered when implementing creep damage equations in finite element (FE) codes, in particular for commercial FE codes such as ABAQUS [41]. The existing procedure for creep strain increment calculation in the FE code of ABAQUS is shown in Figure 3.3.13(a).

For the conventional creep damage theories (independent on whether the damage variable increases with $\sigma/(1 - \omega)$ [44], or with $\sigma \exp(q\omega)$ [38]) there is a strong-mutual dependency between the rates of creep strain and damage development. Typically when a material element is severely damaged and its damage parameter reaches a high value (usually greater

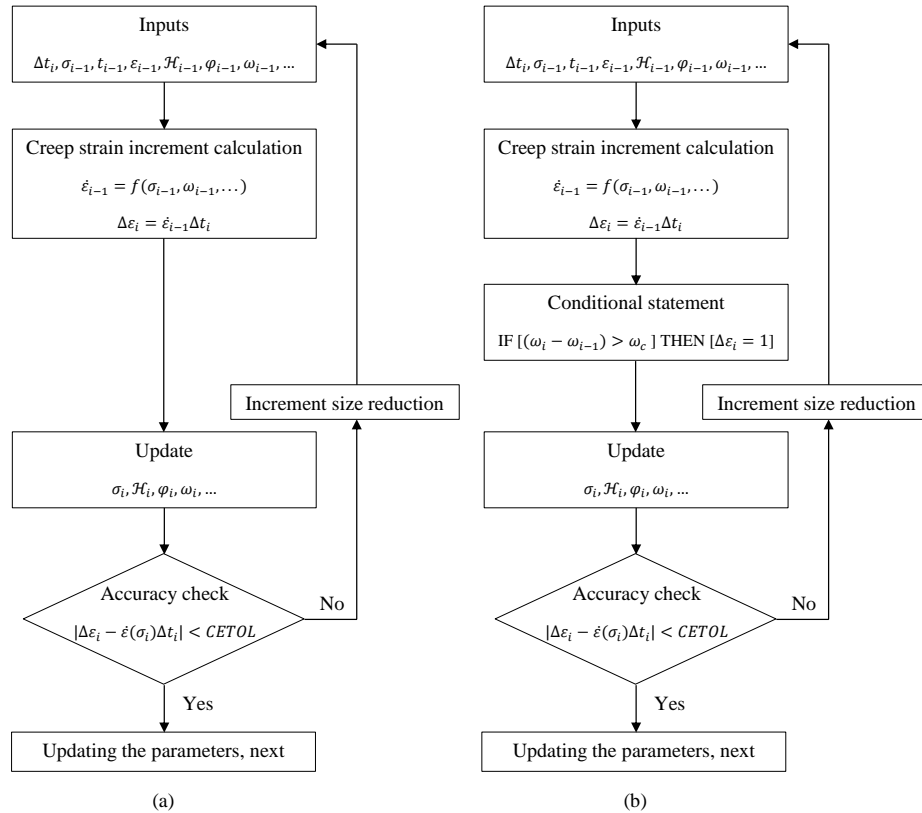


Figure 3.3.13: The procedure used by ABAQUS code to calculate the creep strain increment; (a) the original formulation and (b) the modified formulation.

than 0.5), there is a rapid growth of the damage parameter causing an over-acceleration of the creep strain rate which stops the simulation with a convergence error report. To solve this problem, a new conditional statement has been added to the code which guarantees a smooth damage parameter growth for the elements (see Figure 3.3.13(b), in which ω_c is a critical creep damage growth increment which is set to 1% in this study).

This statement forces the code to cutback the time increment if it involves a large damage parameter increment. In the modified formulation, damage development is checked to grow slowly. Such a moderate damage development allows the elastic and inelastic strain developments to gradually release the stress from the damaged elements and permit further progress of the simulation.

The ideal ultimate value for the damage parameter of a failed element, ω_{max} , is unity ($\overline{0.99}$). However, some studies arbitrarily decrease this value to remove the mentioned convergence error. By applying the adopted formulation, consideration of $\omega_{max} = 0.99$ was possible for the present constitutive model formulation without any convergence error report.

3.4 *Article Four*

Overview

This section contains a reprint of the article: E. Hosseini, S.R. Holdsworth, E. Mazza, The LICON methodology for predicting the long time uniaxial creep rupture strength of materials, International Journal of Pressure Vessels and Piping, 2013, with permission from Elsevier.

Background Motivation

The first article re-examined the LICON method application to 1CrMoV and reported some undiscussed details about the mechanical analysis part of the method. The second and third articles focused on the mechanical analysis of a series of creep crack incubation tests involving fracture mechanics compact tension specimens made of 1CrMoV and reported some important observations about creep constitutive model consideration in finite element analysis of high temperature structures. This article has used those findings and, in a more general point of view, discussed the details of mechanical analysis consideration for the LICON method.

Summary

This article has summarised the previous findings about application of the LICON methodology to different types of material. In the original LICON method development, it was aimed to use approximate reference stress solutions as the mechanical analysis part of the approach. It has been shown that the application of reference stress solutions to some conditions such as creep crack incubation examinations of high creep strength 1CrMoV is not appropriate. The recommendation of this study for such conditions is to consider a more sophisticated mechanical analysis tool (i.e. finite element analysis). This study has explained the details of a successful procedure for consideration of finite element analysis in the LICON method, when it is to applied for 'non-reference stress' materials.

Main Conclusions, Link to the Next Article

This article has shown that the behaviour of materials in creep crack incubation examinations can be classified in two categories. Creep ductile, notch insensitive materials achieve complete stress redistribution before any crack extension and hence, a reference stress solu-

tion is applicable for them (i.e. 'reference stress' materials such as P91). On the other hand, for creep brittle, notch sensitive materials with fast creep crack initiation, crack extension starts before complete stress redistribution and application of reference stress solutions for them is not appropriate (i.e. 'non-reference stress' materials such as high creep strength 1CrMoV). This article has concluded that application of either a reference stress solution based or finite element analysis based LICON method for 'reference stress' materials is appropriate. However, application of the LICON method to 'non-reference stress' materials requires careful consideration of an advanced mechanical analysis (e.g. finite element analysis). The next article has taken advantages of the already gathered knowledge and examined the applicability of the LICON methodology to a dissimilar metal weld.

The LICON Methodology for Predicting the Long Time Uniaxial Creep Rupture Strength of Materials¹

Abstract

The LICON methodology is an approach for predicting the lifetime of materials under creep loading conditions. The LICON method predicts long-time uniaxial creep strength using the results from several short duration creep crack incubation (CCI) tests in conjunction with the outcome of a mechanical analysis on the testpiece. This method was first applied to creep ductile, notch insensitive materials for which a reference stress solution was appropriate (e.g. advanced 9%Cr pipe steels). The original concept for the mechanical analysis part of the methodology was therefore to adopt reference stress solutions. This study explains the challenges involved in application of the reference stress based LICON method to creep brittle, notch sensitive materials and identifies the need for a careful implementation of advanced mechanical analyses (i.e. finite element analysis, FEA) for this application. Details are presented for the consideration of FEA in the LICON methodology, and the demonstration of a successful application of the FEA based LICON method for creep life assessment of a 'non-reference stress' material, i.e. high creep strength (HCS) 1CrMoV steel.

Keywords:

LICON methodology; Reference stress solutions; Finite element analysis; 1CrMoV; P91

¹E. Hosseini, S.R. Holdsworth, E. Mazza, *International Journal of Pressure Vessels and Piping* (2013)

3.4.1 Introduction

One of the main challenges in the design of high temperature components such as those used in modern power generation plant is their lifetime prediction under creep conditions. It is important to be able to accurately predict the creep lifetimes of such structures, with due consideration of fitness-for-purpose, reliability, safety and cost effectiveness, and this has been a main topic of high temperature study for many years. In ideal circumstances, creep lifetime evaluation is based on strength values derived from experimental observations from a large quantity of long duration uniaxial tests for the material of interest, ideally for a number of different heats [1]. In circumstances for which such large datasets do not exist, long-time properties have to be predicted from the results of relatively short duration tests. While the latter approach can only be regarded as an interim compromise, and no substitute for the former approach with regards to accurate design life assessment, it is sometimes the only way to predict the long-time properties of new alloys in a relatively short-time scale and to thereby enable their early exploitation.

A number of approaches have been adopted for predicting long-time creep properties from relatively short duration tests, e.g. extrapolating the results of high stress isothermal tests using the Larson–Miller formulation [2], iso-stress testing [3, 4], applying the ‘theta projection’ concept [5, 6], stress relaxation testing [7, 8], etc. (a review of these approaches can be found in [9]). These methods might work well for materials with stable deformation and rupture mechanisms over a wide range of temperatures and stresses. However, experience with all of these techniques consistently indicates that none are effective in predicting long-time creep rupture properties when the rupture mechanism in the long-time regime is different to that in the short-time regime.

In the late 1990s, an iso-thermal extrapolation approach referred to as the LICON methodology was developed in an European Brite Euram project [10, 11]. This methodology relies on multiaxial loading conditions to bring forward the onset of long-time creep damage formation into the short-time rupture regime. Here, the LICON method employs observations from several short-time creep crack incubation (CCI) tests (using fracture mechanics compact tension (CT) specimens) in conjunction with the results of a mechanical analysis of the testpieces to predict the long-time uniaxial creep strength of a material. In practice, other multiaxial specimen geometries may be employed, such as circumferentially grooved round bar or tubular specimen loaded in tension and/or torsion [10, 11]. The approach provides similarity with the loading conditions experienced in real structures and enables a more accurate evaluation of the future in-service performance of materials for which no long term service experience exists.

The LICON method was first applied to creep ductile, notch insensitive materials for which a reference stress creep rupture data analysis approach was appropriate. The original concept for the mechanical analysis part of the LICON methodology was therefore to adopt reference stress solutions. It was envisaged that it would only be necessary to employ finite element analysis (FEA) to establish the necessary stress–state parameters in the first evaluation of a new material type and/or testpiece geometry, and thereafter to rely on these initial findings ideally as a means to underpin an existing reference stress solution (e.g. [12]).

Early reports on successful application of the LICON method to advanced martensitic 9%Cr pipe steels (including their weldments) were published in 2001 [10, 11]. However, later studies exploring the applicability of the LICON methodology to low alloy creep resistant steels revealed several challenges, in particular for a high creep strength (HCS) heat of 1CrMoV [9, 13, 14].

Careful evaluation has indicated that HCS 1CrMoV does not have the necessary characteristics to be examined with the LICON approach in its original form. HCS CrMoV is a notch sensitive (creep brittle) material exhibiting relatively short CCI durations. Creep crack initiation in such a material occurs before ‘complete stress redistribution’ and HCS 1CrMoV is therefore an example of a ‘non-reference stress’ material [15]. Simple application of the reference stress based LICON method to this sort of material is not recommended.

‘Reference stress’ materials are typically creep ductile and notch insensitive for which a reference stress solution may be applied to multiaxial specimens (structures) for predicting creep–rupture times from the results of uniaxial tests [16]. In contrast, ‘non-reference stress’ materials are typically creep brittle and notch sensitive, such that multiaxial creep rupture stresses may not be simply predicted using reference stress solutions and uniaxial creep rupture data (e.g. [15]).

This study introduces a procedure for extending the applicability of the LICON methodology to ‘non-reference stress’ materials. The modified procedure recommends a careful implementation of advanced mechanical analysis (i.e. FEA) instead of simply considering a reference stress solution. The application of this modified procedure for the creep life assessment of HCS 1CrMoV alloy, as an example of a ‘non-reference stress’ material, is shown to be successful.

Adoption of an appropriate FEA for this application requires a creep model representing the steady–state creep behaviour of the material over a wide range of stresses. Some creep deformation models (e.g. the conventional Norton equation [17] or the version of the Bartsch equation [18] used in [13, 14]) involve a general single formulation to describe the behaviour of the material for all stress regimes (i.e. single regime creep models). However, for many

engineering alloys, the creep deformation mechanism exhibited at high stresses is not the same as that at lower stresses [19, 20] and such creep models cannot represent the effect of a creep mechanism transition due to a change of stress. Recent studies by the authors [9, 21, 22] have adopted a number of stress regime dependent creep model equations (i.e. two-regime Norton (2RN), two-regime hyperbolic sine (2RSinh) and hyperbolic sine+Norton (Sinh+N)) and highlighted the advantages resulting from consideration of these over conventional single regime models [21]. The proposed FEA based LICON method procedure therefore considers a stress regime dependent creep model equation (e.g. 2RN model) rather than a single regime creep model, as has previously been applied in [13, 14].

The remaining challenge is however that the required creep data for underpinning stress regime dependent creep models and building an appropriate finite element (FE) model for application to the LICON method includes information from steady-state creep rates of the material at low stresses. Such information was available for HCS 1CrMoV using available creep databases for 1CrMoV at 550°C [13, 23]. However, when the LICON method is applied to a newly developed alloy, the available creep data is usually limited to the high stress regime, and implementation of the proposed procedure is more challenging. Ways to overcome this problem are explored.

After a short introduction to the LICON methodology, the article examines the challenges associated with application of the reference stress based LICON method to HCS 1CrMoV. Sections 3.4.4 and 3.4.5 describe a procedure for applying the LICON methodology to HCS 1CrMoV at 550°C, as an example of a 'non-reference stress' material. Section 3.4.6 examines application of the proposed procedure to a 'reference stress' material (i.e. P91 at 600°C). It demonstrates that although the newly proposed procedure is developed for application to 'non-reference stress' materials, it is equally applicable for 'reference stress' materials. Section 3.4.7 explains the remaining challenge for application of the FEA based LICON method to materials with limited available creep information and proposes a potential solution to overcome the difficulty. Finally, the last section summarises the main findings of this study.

3.4.2 LICON Methodology

The LICON methodology is based on the formulation:

$$t_{i,x} = A(\bar{\sigma})^{-\nu}(H)^{-\gamma} \quad (3.4.1)$$

with $H = \sigma_1/\bar{\sigma}$, where σ_1 is the maximum principal stress and $\bar{\sigma}$ is the von Mises effective stress, and where A , ν and γ are constants determined for the material and temperature of

interest and the associated multiaxial creep–rupture response. Typically γ varies between zero for $\bar{\sigma}$ –controlled rupture and ν for σ_1 –controlled rupture [13, 14, 24]. The LICON model equations characterise the rupture behaviour in two mechanism regimes. In regime–1, the damage mechanism for ferritic steels is typically void nucleation due to particle/matrix decohesion, and rupture is $\bar{\sigma}$ –controlled (i.e. with $\gamma' \rightarrow 0$), such that:

$$t_r = A'(\sigma_0)^{-\nu'} \quad \text{uniaxial} \quad (3.4.2)$$

$$t_{i,x} = A'(\bar{\sigma}_{CT})^{-\nu'} \quad \text{multiaxial (e.g. CT specimen)} \quad (3.4.3)$$

In regime–2, for ferritic steels, creep damage nucleates and develops at grain/lath boundaries and rupture is mainly σ_1 –controlled (i.e. with $\gamma'' \rightarrow \nu''$, e.g. for 1CrMoV: $\gamma'' = 0.74\nu''$ [13, 14]), such that:

$$t_r = A''(\sigma_0)^{-\nu''} \quad \text{uniaxial} \quad (3.4.4)$$

$$t_{i,x} = A''(\bar{\sigma}_{CT})^{-\nu''} (H_{CT})^{-\gamma''} \quad \text{multiaxial (e.g. CT specimen)} \quad (3.4.5)$$

where $\bar{\sigma}_{CT}$ and H_{CT} are reference von Mises stress and reference stress multiaxiality factor for the CT testpiece [9, 13, 14]. In Equations 3.4.3 and 3.4.5, reference is made to the crack initiation criterion, x . Following the experience reviewed in [25], the crack initiation criterion of $\Delta a=0.5\text{mm}$ is conventionally used in LICON method applications (e.g. for 9%Cr [10, 11] and 1CrMoV steels [13, 14]). Equations 3.4.2 to 3.4.5 are schematically presented in Figure 3.4.1.

The LICON equation set is specifically defined above for predicting long duration uniaxial rupture times from relatively short duration CCI tests using CT specimens (a general form of the LICON method has been applied in conjunction with a continuum damage mechanics analysis to predict creep damage accumulation in [22]).

Prediction of the long–time uniaxial rupture behaviour (i.e. defining the values of A'' and ν'') from the results of a series of CCI tests needs determination of the values of $\bar{\sigma}_{CT}$ and H_{CT} using mechanical analysis. The LICON method was first applied to advanced 9%Cr pipe steels which coincidentally were also reference stress (creep ductile, notch insensitive) materials. The original concept for the mechanical analysis part of the approach was therefore to consider a reference stress solution for determination of von Mises equivalent stress and to use tabulated stress multiaxiality factors for the common multiaxial creep testing geometries (or to involve FEA to determine it in the first evaluation of a new testpiece geometry). It was intended that users of the LICON methodology would not need to perform FEA for laboratory testpieces as long as they used the standard configuration characterised within

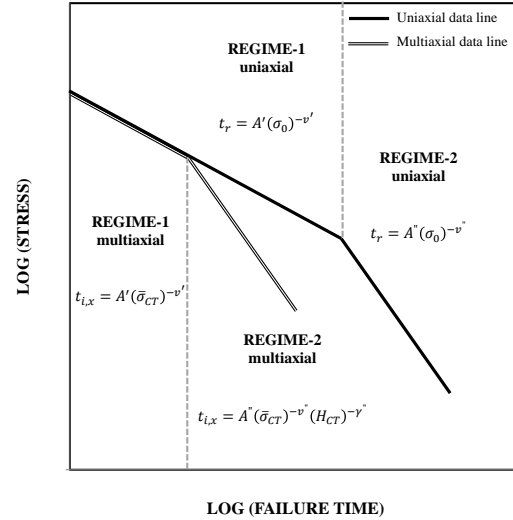


Figure 3.4.1: Schematic representation of the LICON concept.

the LICON project [10, 11]. For example, the introduced formulation for determination of the required stress state parameters for the CT specimen includes: $\bar{\sigma}_{CT} = P/(m^*B_nW)$ and $H_{CT} = 3.6$ (where P is the applied load, B_n is the specimen net section, W is the specimen width and m^* is the yield load ratio) [10, 11]. Consideration of the above expressions for the LICON method application to advanced 9%Cr pipe steels was successful which demonstrated the applicability of the original LICON concept for 'reference stress' materials. However, as shown in the next section, application of the LICON method to HCS 1CrMoV is not so straightforward.

3.4.3 Reference Stress Based LICON Application for HCS 1CrMoV

Figure 3.4.2 shows the LICON long-time predictions resulting from consideration of an acknowledged CT specimen reference stress solution for HCS 1CrMoV at 550°C, i.e. $\bar{\sigma}_{CT} = P/(m^*B_nW)$ and $H_{CT} = 3.6$ [10, 11] or 3.1, [13, 14]. As can be seen, although such an approach was successful for advanced 9%Cr pipe steels [10, 11], the long-time LICON predictions resulting from this consideration is not acceptable for HCS 1CrMoV at 550°C.

Figure 3.4.3 shows the FEA result on the evolution of von Mises stress at the reference position of the CT testpiece (0.5mm from the notch root in the mid-thickness plane [10,

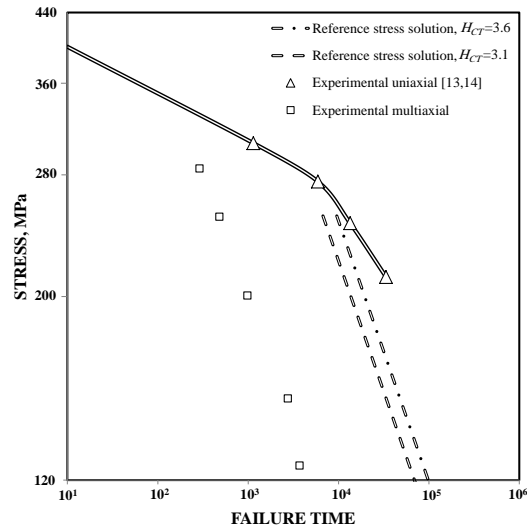


Figure 3.4.2: Comparison of experimental and LICON predicted regime-2 uniaxial rupture strength for HCS 1CrMoV at 550°C (predictions using consideration of reference stress solution and $H_{CT} = 3.6$ [10, 11] and 3.1 [13, 14]).

11, 13, 14]). This shows that HCS 1CrMoV does not exhibit the necessary characteristics to be examined with the reference stress based LICON method. HCS 1CrMoV is a notch sensitive (creep brittle) material exhibiting relatively short CCI durations at 550°C. Creep crack initiation in such materials occurs before 'complete stress redistribution' and HCS 1CrMoV is thereby an example of a 'non-reference stress' material. The application of the LICON method to this sort of material is not recommended without the adoption of suitable analytical tools.

3.4.4 FEA Considerations for the LICON Methodology

This section considers the adoption of more advanced analytical tools as an alternative to the use of approximate reference stress solutions for the mechanical analysis part of the LICON approach when it is to be applied to 'non-reference stress' materials (e.g. HCS 1CrMoV). The representation of non-uniform creep redistributing stress and strain states throughout a testpiece/component/structure is a challenging problem, and FEA is likely to be the most effective solution for this type of problem. FEA is therefore proposed for the mechanical analysis part of the LICON method, in particular when it is to be applied to 'non-reference stress' materials.

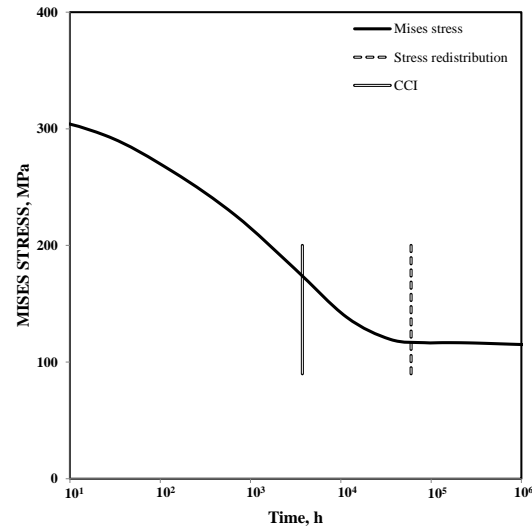


Figure 3.4.3: FEA calculated stress-state evolution at reference position of CT testpiece (HCS 1CrMoV at 550°C, load: 11.2kN, creep constitutive model: 2RN, Equation 3.4.6).

Creep FEA to determine the stress-state in a high temperature testpiece/structure can result in non-unique numerical representations if the analysis procedure (e.g. creep model selection) has not been carefully defined [21]. Defining such a procedure for consideration of FEA for the mechanical analysis part of the LICON approach involves: a) describing the characteristics of the FE model to be used and b) defining the reference position and time for determining $\bar{\sigma}_{CT}$ and H_{CT} . Without careful definition, the uncertainty associated with the LICON long duration rupture time predictions can be unacceptable for a given set of analysis input conditions.

FE model characteristics such as geometrical dimensions, loads, notch length, notch root radius, etc. are influential parameters and should be representative of the tested specimens and conducted experiments. Furthermore, recent studies by the authors have examined the sensitivity of creep FEA for the CT testpiece to the adopted constitutive model and size of FE elements [9, 21]. The results demonstrated the sensitivity of the calculated stress-state quantities (e.g. $\bar{\sigma}_{CT}$ and H_{CT}) to the chosen constitutive model and FE mesh configuration. According to the findings reported in [9], the best choice for the element type, for this application, is the hexahedral element in conjunction with a quadratic interpolating formulation. To determine the optimum size of elements, a check on mesh discretisation for H parameter convergence is recommended. For the constitutive model, the gathered

experience with the LICON application for HCS 1CrMoV indicated that FE consideration of an elastic–plastic–(secondary) creep constitutive model, where the creep model is a good representation of the material steady–state creep rate over a wide range of stresses, can provide good LICON long–time predictions (more details are provided in the next section when the LICON method application for HCS 1CrMoV is described).

The FEA calculated stress–state (e.g. $\bar{\sigma}$ and H) in a loaded CT testpiece is a function of position and varies with time. Determination of $\bar{\sigma}_{CT}$ and H_{CT} from FEA calculations therefore needs to be specified for a reference position and reference time. The original assumption of the LICON approach for reference position–time, when the CT testpiece was first analysed for determination of the H_{CT} value, was to consider 0.5mm from the notch root as the reference position and the time to ‘complete stress redistribution’ as the reference time. This consideration of reference position was coincident with the adopted crack initiation criterion of $\Delta a=0.5\text{mm}$.

As shown in Figure 3.4.3, ‘complete stress redistribution’ for creep brittle materials with relatively short CCI times does not occur until after crack initiation. Consideration of the stress redistribution time as the reference time in the LICON method application of such materials relates to a time–condition which cannot be achieved and an alternative assumption has to be introduced.

The recommendation of this study is therefore to keep the coincidence of reference position and crack initiation criterion at 0.5mm, but to replace ‘complete stress redistribution’ time with the CCI time as the reference time (Figure 3.4.4).

In summary, the recommendations of this study for consideration of FEA for the mechanical analysis part of the LICON methodology are:

- to adopt an elastic–plastic–(secondary) creep constitutive model, with the creep model being representative of the material behaviour over a wide range of stresses, i.e. the adoption of a stress regime dependent secondary creep model.
- to adopt 0.5mm from the notch root (in the mid–thickness plane of the CT testpiece) as the reference position and the CCI time as the reference time, with 0.5mm crack extension being the considered crack initiation criterion.
- to adopt a sufficiently refined mesh configuration for the FE model (quadratic hexahedral elements with converged H_{CT} value).

It should be acknowledged that an important aim for the LICON approach was for it to be readily applicable. This was achieved with the original LICON description through using

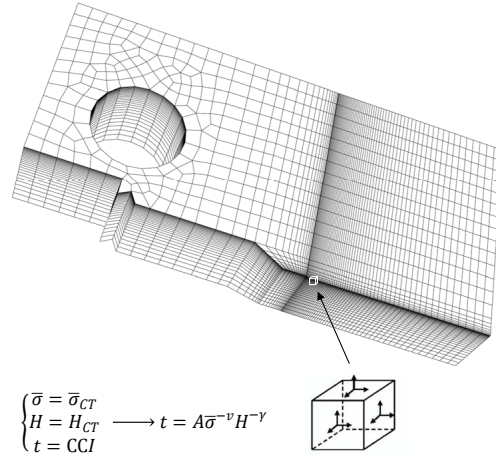


Figure 3.4.4: Representation of the proposed procedure for FEA consideration for the LICON method.

established reference stress solutions and tabulated H values (i.e. avoiding extensive use of FEA). This study therefore acknowledges the ongoing aim of the LICON concept to have simple applicability, but introduces the need for the use of FEA for the mechanical analysis part of the approach for certain materials.

3.4.5 FEA Based LICON Application for HCS 1CrMoV

This section explains the application of the LICON methodology for HCS 1CrMoV when the procedure proposed in Section 3.4.4 is used for the mechanical analysis part of the approach.

The adopted FE code for analysis of CCI tests employed a non-linear kinematic hardening plasticity model to represent the rate independent flow characteristics of the material. Plasticity model parameters were determined using tensile test data at 550°C. The representation of rate dependent plasticity (creep) behaviour of the material was based on adoption of stress regime dependent secondary creep models. As shown in Figure 3.4.5, the results of four uniaxial creep tests [13, 14] with reference to the published NIMS [23] low stress steady-state creep rate data for different heats of 1CrMoV at 550° were used to underpin the 2RN creep model (Equation 3.4.6). The numerical values of the creep model parameters

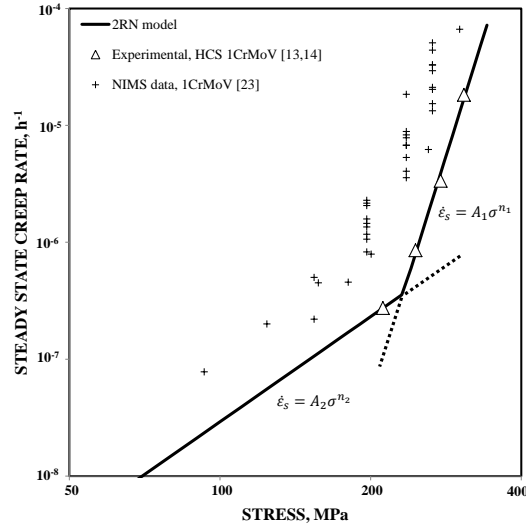


Figure 3.4.5: Steady-state creep rate (stress) diagram for 1CrMoV at 550°C including a comparison of experimental data with the 2RN creep model representation.

can be found in Table 3.4.1.

$$\dot{\epsilon}_s = \begin{cases} A_1 \sigma^{n_1} & \text{if } \sigma \geq \sigma^* \\ A_2 \sigma^{n_2} & \text{if } \sigma < \sigma^* \end{cases} \quad \text{2RN model [9]} \quad (3.4.6)$$

The 2RN creep model is implemented into pre-designed FE codes [9] representing a series of CCI tests for HCS 1CrMoV at 550°C (five load levels of 11.2, 13.5, 18.0, 22.4 and 25.5kN). Consistent with the proposed procedure in Section 3.4.4, the results of FEA for reference stress-state were considered in the LICON formulation to predict the long-time uniaxial rupture strength of the alloy (Figure 3.4.6). The conclusion was that the proposed procedure for the FEA consideration in the LICON approach is successful for HCS 1CrMoV at 550°C (this study only presents the outcome of a 2RN creep model implementation, although other stress regime dependent secondary creep models such as Sinh+N and 2RSinh [21, 22] are equally applicable for the FEA based LICON method).

Table 3.4.1: 2RN creep model parameters for HCS 1CrMoV at 550°C (Equation 3.4.6).

Parameter	A_1	n_1	A_2	n_2	σ^*
Value	1.16×10^{-39}	13.74	2.92×10^{-14}	3.00	231.29

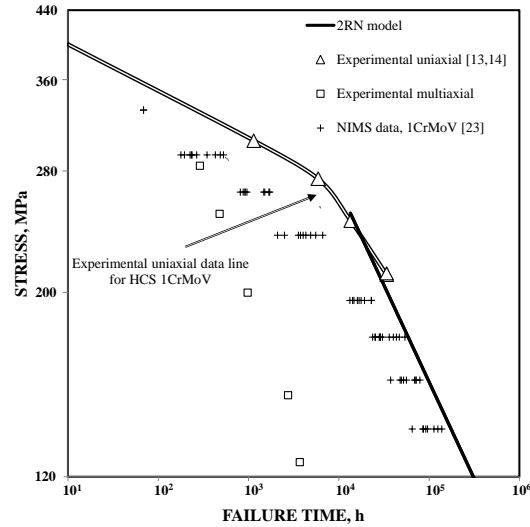


Figure 3.4.6: Comparison of experimental and LICON predicted regime-2 uniaxial rupture strength for 1CrMoV at 550°C (predictions using 2RN creep model, Equation 3.4.6). Note: The investigated heat of 1CrMoV in this study is significantly more resistant to creep than the NIMS heat of 1CrMoV and hence referred to as HCS 1CrMoV.

It should be noted that a combination of reference stress solution and FEA (based on a single regime creep model equation) for the mechanical analysis part of the LICON method was employed in earlier studies [13, 14] to predict long term creep strength of HCS 1CrMoV using CCI tests data at load levels of 13.5, 18.0, 22.4 and 25.5kN. Implementation of the later generated CCI test result for a load level of 11.2kN showed that the predictions can be effectively improved by implementation of the procedure proposed in this study, i.e. FEA based LICON method based on a stress regime dependent secondary creep model.

Figure 3.4.7 shows the LICON long-time predictions for HCS 1CrMoV at 550°C resulting from implementation of a conventional (single regime) Norton [17] creep model. As can be seen, the accuracy of LICON long-time predictions considerably decreases when the stress regime dependency of creep deformation behaviour is neglected. Of more concern, such predictions can be non-conservative. Therefore for this application, the consideration of stress regime dependency in creep constitutive model is essentially required, otherwise, the uncertainty associated with the LICON long duration rupture time predictions can be unacceptable.

It should be mentioned that for the evaluated HCS CrMoV steel at 550°C, the available

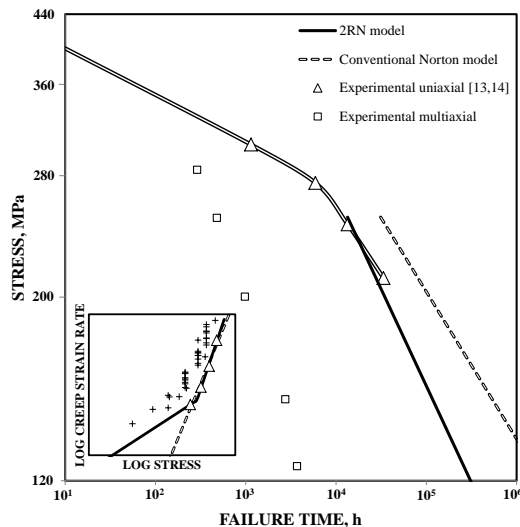


Figure 3.4.7: Comparison of experimental and LICON predicted regime-2 uniaxial rupture strength for HCS 1CrMoV at 550°C (predictions using 2RN and conventional Norton models).

uniaxial dataset [13, 14] in conjunction with the published NIMS data [23] provided the possibility to underpin stress regime dependent creep models. However, when the LICON method is applied to a newly developed alloy, the available creep data is usually limited to the high stress regime and underpinning a stress regime dependent creep model is more challenging. Resolving this problem is currently under investigation and a potential solution is proposed in Section 3.4.7.

3.4.6 FEA Based LICON Application for P91

Alloy P91 can be regarded as a reference stress (creep ductile, notch insensitive) material. Application of the LICON method for this material using a standard reference stress solution ($\bar{\sigma}_{CT} = P/(m^*B_nW)$ and $H_{CT} = 3.6$) has already been demonstrated [10, 11] and this section examines the applicability of the FEA based LICON method for this material.

Performed FE calculations for CCI tests using CT specimens made of P91 at 600°C considered a 2RN creep constitutive model and the reference quantities of stress-state were determined according to the procedure defined in Section 3.4.4. As mentioned earlier, in contrast to HCS 1CrMoV, P91 exhibits relatively fast stress redistribution characteristics and the von Mises stress at the reference position is completely redistributed before the start

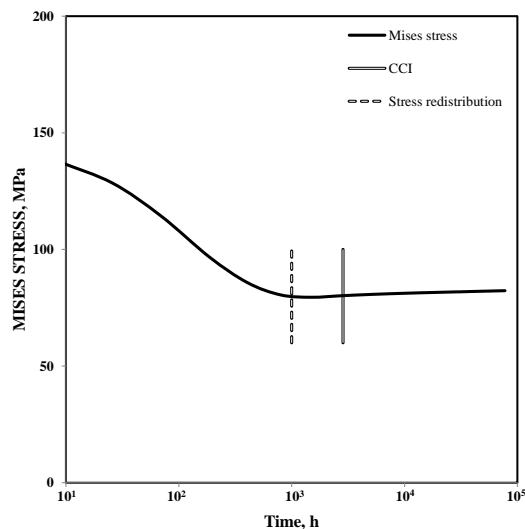


Figure 3.4.8: Von Mises stress evolution at reference position of CT testpiece (P91 at 600°C, load: 9.8kN, creep constitutive model: 2RN, Equation 3.4.6).

of the creep crack extension (Figure 3.4.8). Figure 3.4.9 shows the results of the LICON prediction for P91 at 600°C. As can be seen, the LICON predicted low stress rupture times are reasonable using either FEA or reference stress calculations.

3.4.7 FEA Based LICON Method for Newly Developed Alloys

It was demonstrated in the previous sections that the successful implementation of a FEA based LICON approach for creep life assessment of a material requires a steady-state creep rate model for the material over a wide range of stresses. This is a significant challenge for the LICON methodology, because the LICON method was originally developed to predict long term creep strength of materials with little existing creep data (e.g. for newly developed alloys). For such materials, the available creep data is usually limited to high stress (short duration) tests and developing an effective FE solution for LICON method application is not guaranteed. This section proposes a potential way to resolve this problem.

Figure 3.4.10 shows a typical variation of $\log \dot{\epsilon}_s$ vs. $\log \sigma$ exhibiting different regimes with $n > 8$ at high stresses and $2 < n < 6$ at lower stresses. At very low stresses (very long durations), fundamental creep deformation theory predicts a third regime with $n = 1$ [19, 20, 27].

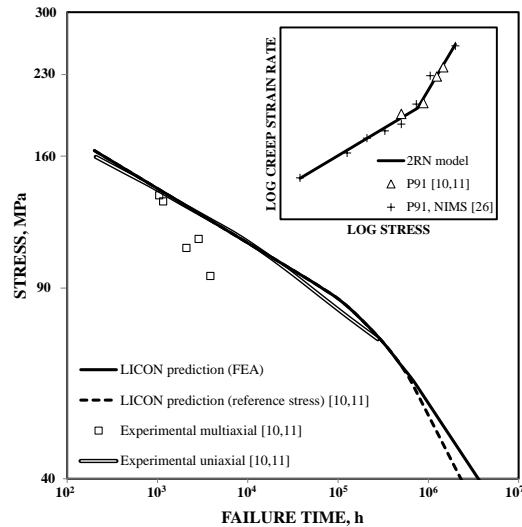


Figure 3.4.9: Comparison of experimental and LICON predicted regime-2 uniaxial rupture strength for P91 at 600°C (predictions using either FEA or the reference stress solution [10, 11, 26]).

Figures 3.4.11 and 3.4.12 summarise experimentally measured steady-state creep rates for a range of heat resistant alloys. Evaluation shows:

- There are only two regimes for the practical range of stresses considered, and a third regime with $n = 1$ is not encountered. Earlier investigations have also examined the existence of the regime with $n = 1$ for the studied range of stresses [28–32]. It is therefore concluded that even though such a regime may exist for very low stresses, it can be neglected for the stresses responsible for life durations of 200–300kh, i.e. typical design life durations for high temperature components.
- While in the high stress regime (i.e. the power-law breakdown regime) very different n values have been observed, the variation of n in the viscous-glide stress regime is limited to 2.5–5.2.
- Time independent yield properties, e.g. 0.2% proof stress ($R_{p0.2}$) and limit of proportionality (LP, σ_{LP}) can be used to approximate the transition stress for the steady-state creep rate behaviour of materials. Normalising the transition stress with respect to 0.2% proof stress and LP for the evaluated alloys reveals that, in particular, LP is a potential parameter to be used for determination of the transition stress with an acceptable accuracy.

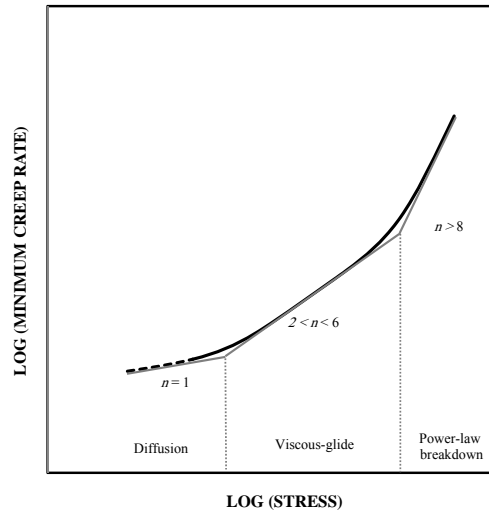


Figure 3.4.10: Schematic representation of steady-state creep rate vs. stress.

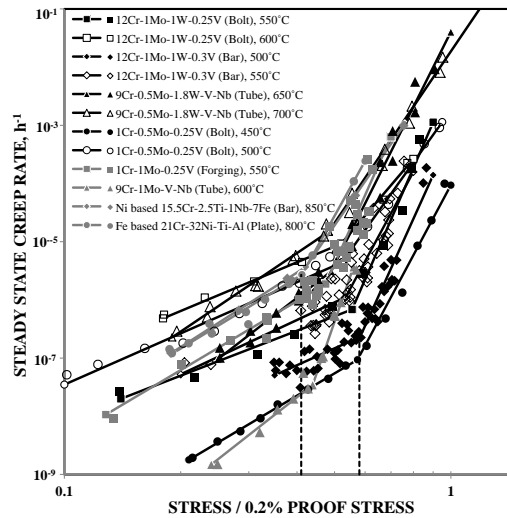


Figure 3.4.11: Steady-state creep rate as function of normalised stress with respect to 0.2% proof stress for different heat resistant alloys [10, 11, 23, 26, 33–37]

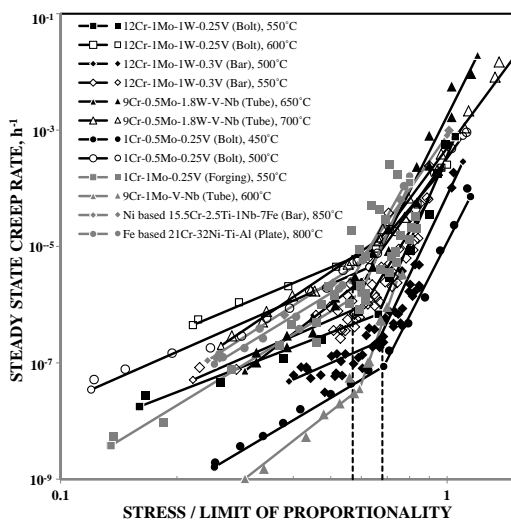


Figure 3.4.12: Steady-state creep rate as function of normalised stress with respect to LP for different heat resistant alloys [10, 11, 23, 26, 33–37] (LP values are estimated based on available information for 0.2% proof stress ($R_{p0.2}$) and tensile strength (R_m), see Appendix).

This study concludes that for a newly developed alloy with only high stress creep and short term tensile data available, adoption of 2RN creep model with consideration of $\sigma^* = 63\% \sigma_{LP}$ and $n = 3.54$ (Table 3.4.2) can be used as an early approximation for the steady-state creep

Table 3.4.2: 2RN creep model equation parameters for the viscous glide stress regime for different heat resistant alloys.

Material	Temperature	$\sigma^*/R_{p0.2}$	σ^*/σ_{LP}	n_2
12Cr1Mo1W0.25V [33]	550°C	56%	66%	2.57
12Cr1Mo1W0.25V [33]	600°C	52%	65%	2.78
12Cr1Mo1W0.3V [34]	500°C	58%	66%	2.96
12Cr1Mo1W0.3V [34]	550°C	53%	61%	3.01
9Cr0.5Mo1.8WVNb [35]	650°C	49%	62%	5.15
9Cr0.5Mo1.8WVNb [35]	700°C	48%	67%	4.63
1Cr0.5Mo0.25V [33]	450°C	58%	68%	3.95
1Cr0.5Mo0.25V [33]	500°C	52%	63%	2.93
1Cr1Mo0.25V [23]	550°C	47%	60%	3.98
9Cr1MoVNb [10, 11, 26]	600°C	43%	59%	5.21
Ni based 15.5Cr2.5Ti1Nb7Fe [36]	850°C	42%	59%	4.25
Fe based 21Cr32NiTiAl [37]	800°C	41%	57%	4.05
95% confidence bounds		(50±3.4)%	(63.0±2.0)%	3.54±0.68

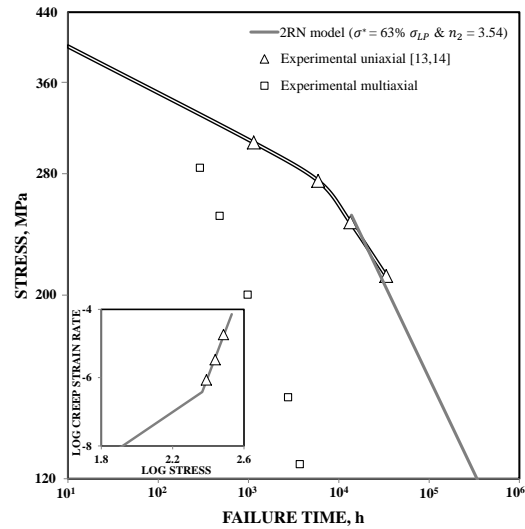


Figure 3.4.13: Comparison of experimental and LICON predicted regime-2 uniaxial rupture strength for HCS 1CrMoV at 550°C (predictions using 2RN model where $\sigma^* = 63\% \sigma_{LP}$ and $n_2 = 3.54$).

rate behaviour of the material in the viscous-glide stress regime. The appropriateness of the presented approximation for application to creep life assessment of HCS 1CrMoV steel using a FEA based LICON approach is now examined.

The calculations described in Section 3.4.5 have been repeated. The steady-state creep rates observed in three high stress uniaxial tests (i.e. at 306, 275 and 245 MPa) were used to determine the 2RN creep model parameters in the high stress regime (A_1, n_1). The viscous-glide stress regime parameters are calculated with considerations of $n_2 = 3.54$ and $\sigma^* = 63\% \sigma_{LP}$. Figure 3.4.13 shows the generated LICON predictions which demonstrate the potential applicability of the proposed approximation for the FEA based LICON approach. The study therefore introduces this approximate method as a potential solution for application of the LICON method to new materials with little/no existing low stress creep data, but also acknowledge the involved uncertainty. Improvement of this method is currently under investigation.

3.4.8 Concluding Remarks

In this paper, the application of the LICON methodology for different types of materials has been re-examined. This method was first applied to creep ductile, notch insensitive

materials for which a reference stress solution was appropriate (e.g. advanced 9%Cr pipe steels). The original concept for the mechanical analysis part of the methodology was therefore to adopt reference stress solutions. This study shows that extending the scope of applicability of the LICON method to creep brittle, notch sensitive (non-reference stress) materials requires the adoption of a more sophisticated mechanical analysis (i.e. advanced finite element analysis (FEA)). The details of a proposed procedure to consider FEA as the mechanical analysis part of the LICON method when it is to be applied for 'non-reference stress' materials has been described. It is explained that, in such circumstances, construction of an appropriate FE model for application to the LICON method requires knowledge of steady-state creep rates of the material over a wide range of stresses (from high to low stresses). The successful application of the proposed procedure for creep life assessment of the high creep strength (HCS) 1CrMoV alloy, as an example of a 'non-reference stress' material, has been demonstrated. Examination of the FEA based LICON approach for application to a 'reference stress' material (i.e. P91 at 600°) indicates the methodology is also appropriate for this purpose. This study proposes a viable approximate method to estimate the creep rates of newly developed alloys in the viscous-glide stress regime based on time independent yield properties as a solution to the problem of applying the FEA based LICON method to a newly developed alloy with little existing low stress creep data.

References

- [1] S.R. Holdsworth. The ECCC approach to creep data assessment. *Journal of Pressure Vessel Technology*, 130:1–6, 2008.
- [2] F.R. Larson and J. Miller. A time–temperature relationship for rupture and creep stresses. *Transactions ASME*, 74(5):765–775, 1952.
- [3] K.N. Melton. The iso–stress extrapolation of creep rupture data. *Materials Science and Engineering*, 59(2):143–149, 1983.
- [4] O. Kanemaru, M. Shimizu, T. Ohba, K. Yagi, Y. Kato, and K. Hattori. Life prediction by the iso–stress method of boiler tubes after prolonged service. *International Journal of Pressure Vessels and Piping*, 48(2):167–182, 1991.
- [5] R.W. Evans and B. Wilshire. *Creep of Metals and Alloys*. Institute of Metals, 1985.
- [6] M. Evans. Predicting times to low strain for a 1CrMoV rotor steel using a 6– θ projection technique. *Journal of Materials Science*, 35(12):2937–2948, 2000.
- [7] D.A. Woodford. Accelerated testing for high temperature materials performance and remaining life assessment. *EPRI Report*, 1999.
- [8] D.A. Woodford. Creep strength evaluation, design, and life management of 1CrMoV rotor steel using stress relaxation testing. In *Advances in Turbine Materials, Design and Manufacturing*, pages 613–624, 1997.
- [9] E. Hosseini, S.R. Holdsworth, and E. Mazza. Experience with using the LICON methodology for predicting long term creep behaviour in materials. *International Journal of Pressure Vessels and Piping*, 92:70–76, 2012.
- [10] P. Auerkari, W. Bendick, S. Holdsworth, J.H. Rantala, R. Hurst, C. Coussement, and R. Hack. Predicting long term creep behaviour using the LICON methodology. In *Proceedings of the 3rd International Conference of Advances in Material Technology for Fossil Power Plants*, pages 329–339, 2001.
- [11] V.M. Martins and S.R. Holdsworth. The LICON methodology for predicting the long term service behaviour of new steels. *Materials at High Temperatures*, 19(2):99–103, 2002.
- [12] A.G. Miller. Review of limit loads of structures containing defects. *International Journal of Pressure Vessels and Piping*, 32(1–4):197–327, 1988.
- [13] S.R. Holdsworth and E. Mazza. Exploring the applicability of the LICON methodology for a 1CrMoV steel. *Materials at High Temperatures*, 25(4):267–276, 2008.
- [14] S.R. Holdsworth and E. Mazza. Using the results of creep crack incubation tests on 1CrMoV steel for predicting long time creep rupture properties. *International Journal of Pressure Vessels and Piping*, 86(12):838–844, 2009.
- [15] D.J. Gooch, S.R. Holdsworth, and P.R. McCarthy. The influence of net section area on the notched bar creep rupture lives of three power plant steels. In *Proceedings of the 3rd International Conference on Creep and Fracture of Engineering Materials and Structures*, pages 441–457, 1987.
- [16] R.K. Penny and D.L. Marriott. *Design for Creep*. McGraw–Hill London, 1971.
- [17] F.H. Norton. *The Creep of Steel at High Temperatures*. McGraw–Hill book company, 1929.
- [18] H. Bartsch. A new creep equation for ferritic and martensitic steels. *Steel Research*, 66(9):384–388, 1995.
- [19] R.W. Evans and B. Wilshire. *Introduction to Creep*. Institute of Materials, London, 1993.

-
- [20] H.J. Frost and M.F. Ashby. *Deformation Mechanism Maps: the Plasticity and Creep of Metals and Ceramics*. Oxford, Oxfordshire, Pergamon Press, New York, 1982.
- [21] E. Hosseini, S.R. Holdsworth, and E. Mazza. Creep constitutive model considerations for high-temperature finite element numerical simulations. *The Journal of Strain Analysis for Engineering Design*, 47(6):341–349, 2012.
- [22] E Hosseini, S.R. Holdsworth, and E. Mazza. Stress-regime dependent creep constitutive model consideration in finite element continuum damage mechanics. *International Journal of Damage Mechanics*, doi:10.1177/1056789513479810, 2013.
- [23] NIMS. *Data Sheet 9B, Data sheets on the elevated-temperature properties of 1Cr-1Mo-0.25V steel forgings for turbine rotors and shafts*. National Research Institute for Metals, Tokyo, Japan, 1990.
- [24] B.J. Cane. Creep cavitation and rupture in 2.5CrMo steel under uniaxial and multiaxial stresses. In *Proceedings of Conference on Mechanical Behaviour of Materials*, pages 173–182, 1979.
- [25] S.R. Holdsworth. Initiation and early growth of creep cracks from pre-existing defects. *Materials at High Temperatures*, 10(2):127–137, 1992.
- [26] NIMS. *Data Sheet 43, Data sheets on the elevated-temperature properties of 9Cr-1Mo-V-Nb steel tubes for boilers and heat exchangers and 9Cr-1Mo-V-Nb steel plates for boilers and pressure vessels*. National Research Institute for Metals, Tokyo, Japan, 1996.
- [27] K. Naumenko and H. Altenbach. *Modelling of Creep for Structural Analysis*. Springer, 2007.
- [28] O.A. Ruano, J. Wadsworth, J. Wolfenstine, and O.D. Sherby. Evidence for Nabarro–Herring creep in metals: fiction or reality? *Materials Science and Engineering A*, 165(2):133–141, 1993.
- [29] M. Mostafa and F. Mohamed. Correlation between creep stress exponent and ductility in Al–10%Zn. *Metallurgical and Materials Transactions A*, 17:365–366, 1986.
- [30] D.M. Owen and T.G. Langdon. Low stress creep behaviour: An examination of Nabarro–Herring and Harper–Dorn creep. *Materials Science and Engineering A*, 216(1–2):20–2, 1996.
- [31] L. Kloc, V. Sklenicka, and J. Fiala. Problems in theories of low stress creep mechanisms. In *Proceedings of the 10th International Metallurgical and Materials Conference, Metal*, 2001.
- [32] S. Spigarelli, M. El Mehtedi, and A. Di Salvia. Constitutive models for the description of creep and plasticity of cast and wrought Mg–Al and Mg–Zn alloys. In *IUTAM Symposium on Advanced Materials Modelling for Structures*, 2012.
- [33] NIMS. *Data Sheet 44, Data sheets on the elevated-temperature stress relaxation properties of 1Cr-0.5Mo-0.25V steel and 12Cr-1Mo-1W-0.25V steel bolting materials for high temperature service*. National Research Institute for Metals, Tokyo, Japan, 1997.
- [34] NIMS. *Data Sheet 10B, Data sheets on the elevated-temperature properties of 18Cr-12NiMo stainless steel plates for reactor vessels*. National Research Institute for Metals, Tokyo, Japan, 1988.
- [35] NIMS. *Data Sheet 48A, Data sheets on the elevated-temperature properties of 9Cr-0.5Mo-1.8W-V-Nb steel tube for power boilers and 9Cr-0.5Mo-1.8W-V-Nb steel pipe for high temperature service*. National Research Institute for Metals, Tokyo, Japan, 2012.
- [36] NIMS. *Data Sheet 49A, Data Sheets on the Elevated-Temperature Properties of Nickel Base 16Cr-8.5Co-3.5Al-3.5Ti-2.6W-1.8Mo-0.9Nb superalloy Casting for Gas Turbine components*. National Research Institute for Metals, Tokyo, Japan, 2012.
- [37] NIMS. *Data Sheet 27B, Data sheets on the elevated-temperature properties of iron base 21Cr-32Ni-Ti-Al alloy plates for corrosion and heat resistant applications*. National Research Institute for Metals, Tokyo, Japan, 2000.
- [38] W. Ramberg and W.R. Osgood. Description of stress–strain curves by three parameters. Technical report, National Advisory Committee for Aeronautics, 1943.

Appendix

For a material under uniaxial tensile testing conditions, the limit of proportionality (LP, σ_{LP}) is the maximum stress for which strain remains proportional to stress. The exact position of this limit is sometimes difficult to determine from experimental stress strain curves. The accepted approach is therefore to use an offset method and to determine σ_{LP} as the stress required to produce a permanent strain of 0.02% (or 0.005%).

The NIMS reported tensile properties for heat resistant alloys do not include σ_{LP} and only provide 0.2% proof stresses ($R_{p0.2}$) and tensile strengths (R_m). The following describes a method to approximate σ_{LP} from a knowledge of $R_{p0.2}$ and R_m .

The Ramberg–Osgood model describes the non-linear relationship between stress and strain [38]:

$$\varepsilon_p = K_{ro} \left(\frac{\sigma}{E} \right)^{n_{ro}} = K'_{ro} \sigma^{n_{ro}} \quad (3.4.7)$$

where ε_p is the plastic strain, E is the elastic modulus, K_{ro} , K'_{ro} and n_{ro} are material constants. For σ_{LP} and $R_{p0.2}$, it gives:

$$0.02\% = K'_{ro} (\sigma_{LP})^{n_{ro}} \quad (3.4.8)$$

$$0.2\% = K'_{ro} (R_{p0.2})^{n_{ro}} \quad (3.4.9)$$

and hence:

$$\sigma_{LP} = (0.1)^{1/n_{ro}} R_{p0.2} \quad (3.4.10)$$

Therefore, for a known n_{ro} , $R_{p0.2}$ can be used to determine σ_{LP} .

The tensile strength of a material, R_m , is equal to the maximum force during the uniaxial tensile test divided by the initial cross section area of the specimen (engineering stress).

Therefore:

$$\sigma \Big|_{Max\ Force} = R_m \exp(\varepsilon_p) \Big|_{Max\ Force} \quad (3.4.11)$$

At the maximum force:

$$dF = 0 \quad (3.4.12)$$

$$= \sigma dS + d\sigma S \quad (3.4.13)$$

where F is the force and S is the specimen cross section area. Volume constancy gives:

$$\frac{dS}{S} = -\frac{dl_g}{l_g} = -d\varepsilon_p \quad (3.4.14)$$

where l_g is the specimen gauge length. Combination of 3.4.13 and 3.4.14 results in:

$$\left. \frac{d\varepsilon_p}{d\sigma} \right|_{Max\ Force} = \left. \frac{1}{\sigma} \right|_{Max\ Force} \quad (3.4.15)$$

$d\varepsilon_p/d\sigma$ can also be calculated from the Ramberg–Osgood model equation:

$$\frac{d\varepsilon_p}{d\sigma} = n_{ro} K'_{ro} \sigma^{n_{ro}-1} = \frac{n_{ro}}{\sigma} \varepsilon_p \quad (3.4.16)$$

From Equations 3.4.15 and 3.4.16:

$$n_{ro} = \left. \frac{1}{\varepsilon_p} \right|_{Max\ Force} \quad (3.4.17)$$

Combination of Equations 3.4.17 and 3.4.11 gives:

$$\left. \sigma \right|_{Max\ Force} = R_m \exp\left(\frac{1}{n_{ro}}\right) \quad (3.4.18)$$

and from the Ramberg–Osgood model equation:

$$\frac{1}{n_{ro}} = K'_{ro} \left(R_m \exp\left(\frac{1}{n_{ro}}\right) \right)^{n_{ro}} \quad (3.4.19)$$

Combination of Equation 3.4.9 and 3.4.19 gives:

$$\frac{0.2\%}{1/n_{ro}} = \left[\frac{R_{p0.2}}{\left(R_m \exp\left(\frac{1}{n_{ro}}\right) \right)} \right]^{n_{ro}} \quad (3.4.20)$$

Resolution of Equation 3.4.20 defines the value of n_{ro} and then σ_{LP} can be determined from Equation 3.4.10.

3.5 *Article Five*

Overview

This section contains a reprint of the article: E, Hosseini, S.R. Holdsworth, E. Mazza, Exploring the applicability of the LICON methodology for a dissimilar metal weld, International Journal of Pressure Vessels and Piping, 2013, with permission from Elsevier.

Background Motivation

The main objective of this PhD project is to examine the applicability of the LICON methodology for predicting the long term creep rupture strength of a dissimilar metal weld. Previous articles have re-examined early applications of the LICON method for bainitic 1%Cr and martensitic 9%Cr steels and reported some undiscussed, but important, details about mechanical analysis considerations in the method. This article takes the advantage of already gathered knowledge and deals with the main objective of this research project, i.e. examination of the LICON method applicability for a dissimilar metal weld.

Summary

This article has reported details of experimental and analytical efforts made for examination of the LICON method applicability to a dissimilar metal weld. The investigated material is part of an existing weldment of 1CrMoV and Alloy 625 with filler metal of Alloy 617 which had been a candidate to use for rotor constructions in new advanced power plants. Mechanical analysis of the conducted creep crack incubation tests for the weldment has shown that this joint, similar to the high creep strength 1CrMoV, is an example of 'non-reference stress' materials. The LICON method application to this joint therefore requires consideration of an advanced mechanical analysis, i.e. finite element analysis. The proposed procedure in the previous article for consideration of finite element analysis in the LICON method application for 'non-reference stress' materials has been followed in this article.

Main Conclusions

This article has examined the applicability of the LICON method for the weldment of 1CrMoV and Alloy 625 with filler metal of Alloy 617. Beside the conducted analytical/numerical analyses, experimental examinations including uniaxial and multiaxial creep testing and microstructural investigations have been performed to provide the required information for

examination of the LICON method. It has also been shown that the LICON method formulation for application to predict the creep rupture behaviour of dissimilar metal weld uniaxial testpieces requires further development. This study therefore proposed a new development for the LICON approach which uses finite element analysis to account for the generated multiaxial stress states within weld uniaxial testpieces. Application of the developed approach for predicting uniaxial creep rupture behaviour of the investigated joint showed an acceptable agreement with experimental observations which was not achievable without introducing the new development.

Exploring the Applicability of the LICON Methodology for the Creep Assessment of a Dissimilar Metal Weld¹

Abstract

The LICON methodology is an approach for predicting the lifetime of materials under creep loading conditions. The LICON method predicts long-time uniaxial creep strength using the results from several short duration creep crack incubation (CCI) tests in conjunction with the outcome of a mechanical analysis for the adopted multiaxial specimen geometry. The applicability of the methodology for long term creep strength prediction of martensitic 9%Cr and bainitic 1%Cr steels has already been demonstrated. This study has examined the applicability of the procedure for predicting long term uniaxial creep strengths for a dissimilar metal weld (DMW). It has required new developments to the original formulation. Application of the developed formulation for predicting uniaxial creep rupture behaviour of the investigated DMW shows an acceptable agreement with experimental observations which was not previously achievable.

Keywords:

LICON methodology; Dissimilar metal weld; Long term creep strength; Finite element analysis; 1CrMoV; Alloy 617/625

¹E, Hosseini, S.R. Holdsworth, E. Mazza, *International Journal of Pressure Vessels and Piping* (2013)

3.5.1 Introduction

The LICON methodology was originally developed in the late 1990s to predict the long-time creep rupture behaviour of new generation steels, including their welded joints, from the results of relatively short duration multiaxial specimen tests. The methodology relies on the acceleration of creep damage development under multiaxial loading conditions to enable extended extrapolation of rupture strength into the long-time rupture regime. The approach provides similarity with the loading conditions experienced in real structures and enables a more accurate evaluation of the future in-service performance of components made of new-generation materials for which no long-time service experience exists.

After recent reports on successful application of the methodology for martensitic 9%Cr pipe steels (including their weldments) [1, 2] and 1CrMoV alloys [3–6], this study examines the applicability of the methodology for prediction of the long term creep strength of a dissimilar metal weld (DMW).

3.5.2 Experiments

Experimental Procedure

The investigated material in this study is part of an existing weldment of 1CrMoV and Alloy 625 with Alloy 617 filler metal which was considered as a candidate to use for rotor constructions in advanced 700°C power plants (AD700) [7–9].

Figure 3.5.1 presents an optical image of the as-received DMW under investigation. The figure illustrates five different zones: 1CrMoV parent material (PM), 1CrMoV heat affected zone (HAZ), Alloy 617 weld material (WM), Alloy 625 HAZ and Alloy 625 PM. The creep strengths of Alloy 625 (PM/HAZ) and Alloy 617 WM are much higher than that of the 1CrMoV (PM/HAZ) at the maximum applicable temperature and hence, occurrence of creep failure in these zones is less probable.

Mechanical Testing Uniaxial constant load creep tests were conducted at 550°C using round bar testpieces for cross-weld (x-weld), 1CrMoV PM and Alloy 617 WM property determinations. Figure 3.5.2a shows the used uniaxial creep specimen configuration (8mm diameter with 42mm gage length). Table 3.5.1 provides details of the performed uniaxial creep tests.

Constant load creep crack incubation (CCI) tests at 550°C were performed using fully instrumented 25mm-thick compact tension (CT) testpieces with side-grooves (Figure 3.5.2b).

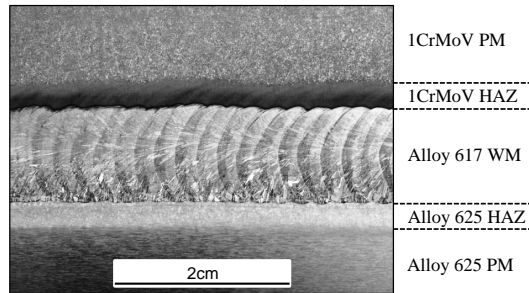


Figure 3.5.1: Different microstructural zones in joint of 1CrMoV/Alloy 617/Alloy 625 (as received, etchant: Marble's Reagent).

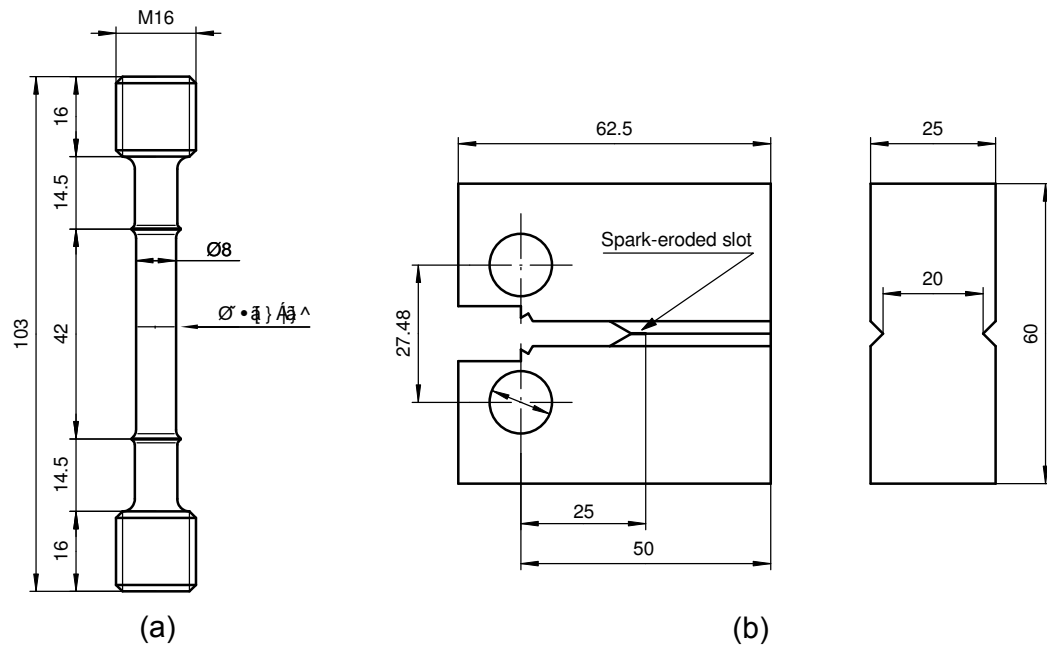


Figure 3.5.2: (a) Uniaxial creep and (b) CT specimens.

The crack starter was located in the middle of the 1CrMoV HAZ and its final part was a spark-eroded slot. Five load levels of 17.8, 13.7, 8.4, 8.0 and 6.0kN have been examined. Load point displacement (LPD) was recorded using a clip-on type mechanical extensometer attached to the testpiece integral knife edge. In addition, creep crack development was continuously monitored using electrical direct current potential drop (DCPD) instrumentation.

The tests were run to the attainment of creep crack extensions larger than 0.5mm. A central 3mm-thick slice for metallographical examination was extracted from the testpiece by spark erosion, prior to final fracture at room temperature to reveal the full extent of creep crack extension [3, 4]. Physical measurement of the actual extent of creep cracking at the end of test complemented and verified the online crack extension results determined by the DCPD instrumentation.

Uniaxial tensile tests at 550°C were conducted for characterisation of the time independent mechanical behaviour of 1CrMoV PM and Alloy 617 WM.

Microstructural Investigations Samples from crept specimens were prepared by standard metallographic techniques for microstructural investigations. Different techniques were used to investigate the material microstructure. Optical microscopy was initially used to observe the microstructure of the material. While Marble’s Reagent was used to reveal the Alloy 617/625 microstructures, Nital was used to reveal the microstructures of 1CrMoV (PM/HAZ). Also, Vilella’s Reagent was used to expose prior austenitic grain boundaries in the 1CrMoV steel.

As a part of post-test examination of the crept specimens, it was important to define the location of developed creep cavities with respect to the grain boundaries. Employment of the CCI test results within the LICON method requires a knowledge of the corresponding creep crack development mechanisms (e.g. by particle/matrix decohesion or grain boundary cavitation). Optical examination of etched specimens however could not provide confident observations for the responsible creep failure mechanism in the fine grained structure of the 1CrMoV HAZ. More detailed microstructural investigation was therefore performed using an electron channelling contrast (ECC) imaging technique. This technique uses back scatter electrons (BSE) in a scanning electron microscopy (SEM) to identify grain/subgrain boundaries in un-etched specimens to a much higher resolution than that using optical microscopy. The high sensitivity of 1CrMoV to pitting corrosion, in particular when connected to a more noble alloy (i.e. Alloy 617), introduced difficulties associated with the observation of creep

Table 3.5.1: Uniaxial creep tests description.

Testpiece	x-weld	x-weld	x-weld	x-weld	x-weld	Alloy 617
Stress, MPa	220	200	120	80	50	440
Status	ruptured	ruptured	ruptured	ruptured	interrupted	interrupted
Testpiece	1CrMoV	1CrMoV	1CrMoV	1CrMoV	1CrMoV	1CrMoV
Stress, MPa	300	280	260	200	180	160
Status	ruptured	ruptured	ruptured	interrupted	interrupted	interrupted

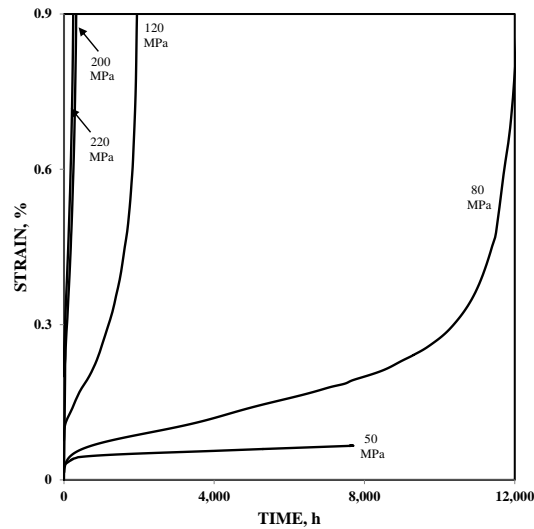


Figure 3.5.3: Constant load uniaxial creep test results for the DMW at 550°C.

cavities in etched samples, and using un-etched samples with an ECC imaging technique was therefore an advantage.

Since discrimination between low-angle subgrain and high-angle grain boundaries was not possible in ECC images, electron backscatter diffraction (EBSD) analysis was conducted as a complementary technique.

Experimental Results

Mechanical Testing Figure 3.5.3 shows the results of constant load uniaxial creep tests at 550°C for cross-weld specimens. The results were used for *a*) indicating the secondary creep deformation behaviour of the DMW and *b*) providing data for evaluation of the LICON method uniaxial creep strength predictions.

Figure 3.5.4 shows the results of constant load uniaxial creep tests at 550°C for 1CrMoV PM and Alloy 617 WM specimens. The results were only to indicate the secondary creep deformation behaviour of the materials and therefore, some of the tests were interrupted after reaching the steady-state creep deformation condition (secondary creep). The test for Alloy 617 WM at the high stress level of 440MPa demonstrated the high creep resistance of this alloy at 550°C. For the same stress level, creep deformation of Alloy 617 in comparison with that of 1CrMoV is negligible and therefore, calculations described in the following

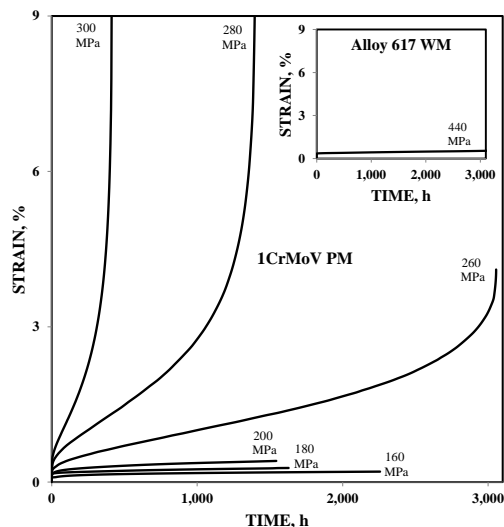


Figure 3.5.4: Constant load uniaxial creep test results for 1CrMoV PM and Alloy 617 WM at 550°C.

sections neglected the creep deformation for Alloy 617 WM and, similarly, for Alloy 625 (PM/HAZ).

Figure 3.5.5 shows the uniaxial tensile test results for 1CrMoV PM and Alloy 617 WM at 550°C. The results were used to underpin non-linear kinematic hardening plasticity models for 1CrMoV (PM/HAZ) and Alloy 617 WM. The approximation assuming the behaviour of 1CrMoV HAZ to be the same as that for 1CrMoV PM is acknowledged. As is explained later, the stresses developed for Alloy 625 (PM/HAZ) during the conducted creep tests in this study were much less than its yield strength and therefore, characterisation of the plastic behaviour of Alloy 625 was not required.

Figure 3.5.6 shows the evolution of LPD and creep crack extension for the performed CCI tests at 550°C. As can be seen, the LPD increases with time in a similar way to the creep strain accumulation observed in a uniaxial testpiece. The tests were intentionally stopped before the development of significantly long cracks and the specimens were then used to metallurgically investigate early creep damage development characteristics. The presented creep crack extension records in Figure 3.5.6 (inset) show that prior to the onset of creep cracking, there is an incubation period during which time sufficient creep damage develops ahead of the crack starter to initiate creep crack extension. This stage is followed by creep crack growth until final rupture. Time durations to a crack extension of 0.5mm were considered as CCI times for later application to the LICON methodology [3, 4].

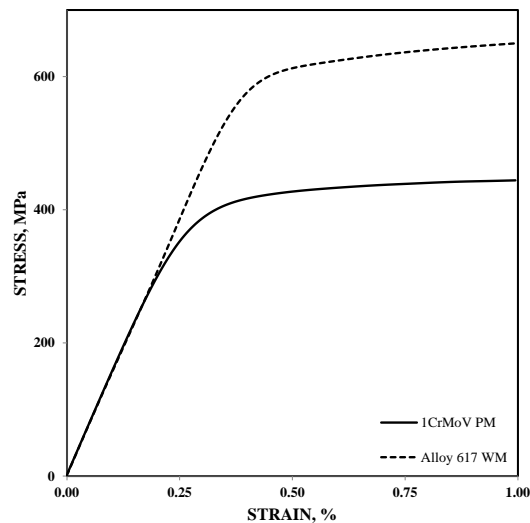


Figure 3.5.5: Uniaxial tensile test results for 1CrMoV PM and Alloy 617 WM at 550°C.

Microstructural Observations Figure 3.5.7 shows the optical microstructures of the DMW. As can be seen, 20–80 μm sized grains were observed in 1CrMoV PM. The microstructural transition to the 1CrMoV HAZ section can be seen in Figure 3.5.7b in the form of some fine recrystallised grains located at the prior austenite grain boundaries (intercritical HAZ, ICHAZ). Figure 3.5.7c shows the central region of the 1CrMoV HAZ comprising a very fine structure (fine grain HAZ, FGHAZ) and finally, Figure 3.5.7d illustrates the interface between 1CrMoV HAZ and Alloy 617 WM. The weld has been deposited in a way to give almost 100% FGHAZ adjacent to the fusion line (FL).

Figure 3.5.8 shows the results of preliminary trials to reveal the mechanism of creep damage development experienced in the performed CCI tests. Confident judgement on the location of creep cavities with respect to grain boundaries using the shown micrographs was not possible, because the very fine structure was not easily resolvable using optical microscopy.

More detailed microstructural investigation was performed using an ECC imaging technique. This technique used BSE signals in a SEM to determine the orientation of different grain/subgrains and could define the location of boundaries in an un-etched specimen to a much higher resolution than that of the optical microscope. Figure 3.5.9 shows the results of ECC imaging of samples from CT specimens and shows that the nucleation of creep cavities has occurred at fine grain boundaries.

Figure 3.5.10 shows the results of the EBSD analysis which confirmed that the majority of

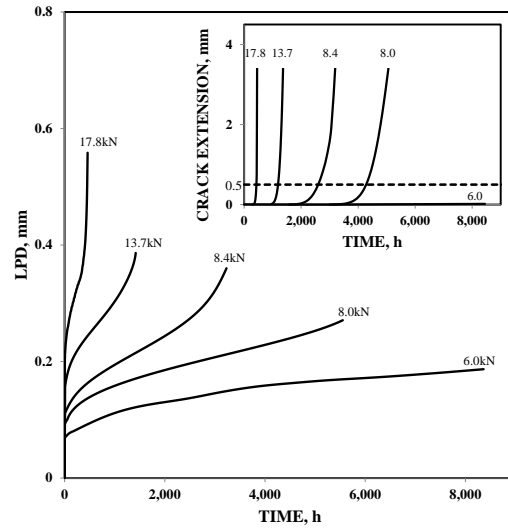


Figure 3.5.6: LPDs and creep crack extensions for of the conducted CCI tests for the DMW at 550°C.

observed boundaries in ECC images were high-angle grain boundaries. This demonstrated that the sites of creep cavity nucleation were located at grain boundaries and that the mechanism of creep crack development, even for the highest examined load and the shortest CCI test, was grain boundary cavity nucleation, growth and coalescence and this is the damage mechanism anticipated after long-time creep. The CCI test data can therefore be used by the LICON method formulation for predicting the long-time creep rupture behaviour of DMW uniaxial testpieces.

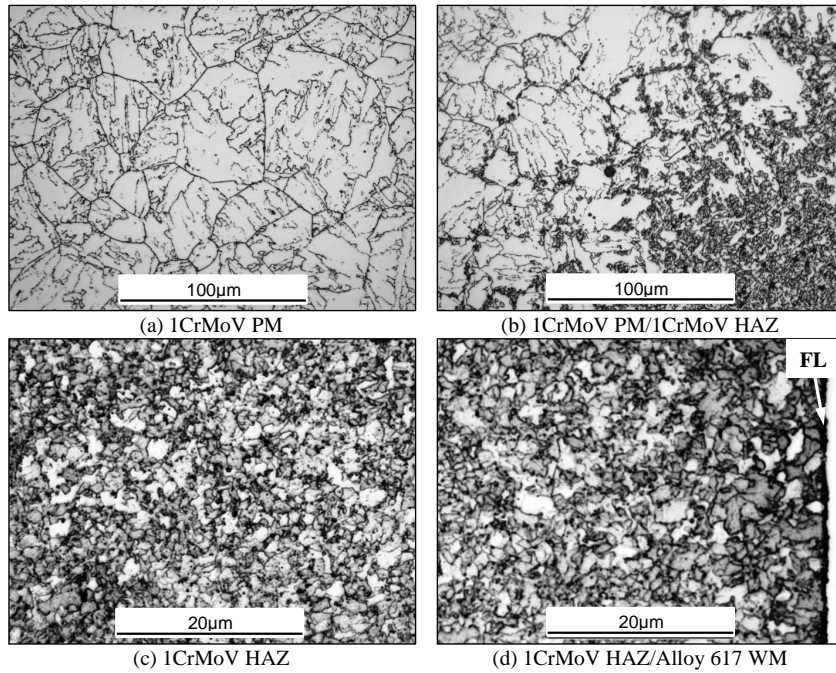


Figure 3.5.7: Microstructure of the DMW (Etchant: Vilella's Reagent).

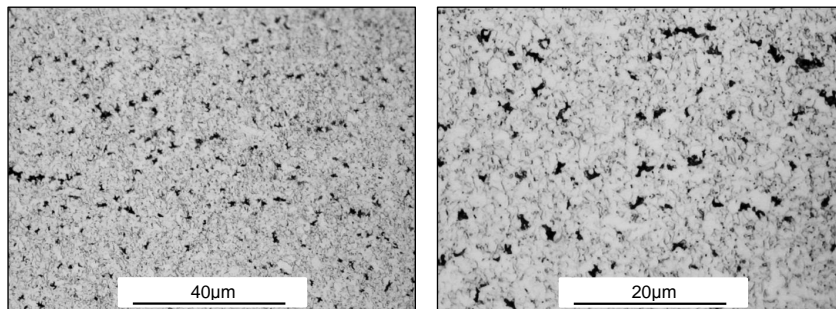


Figure 3.5.8: Microstructure of the DMW after CCI test at load level of 8.0kN at 550°C (Etchant: Nital).

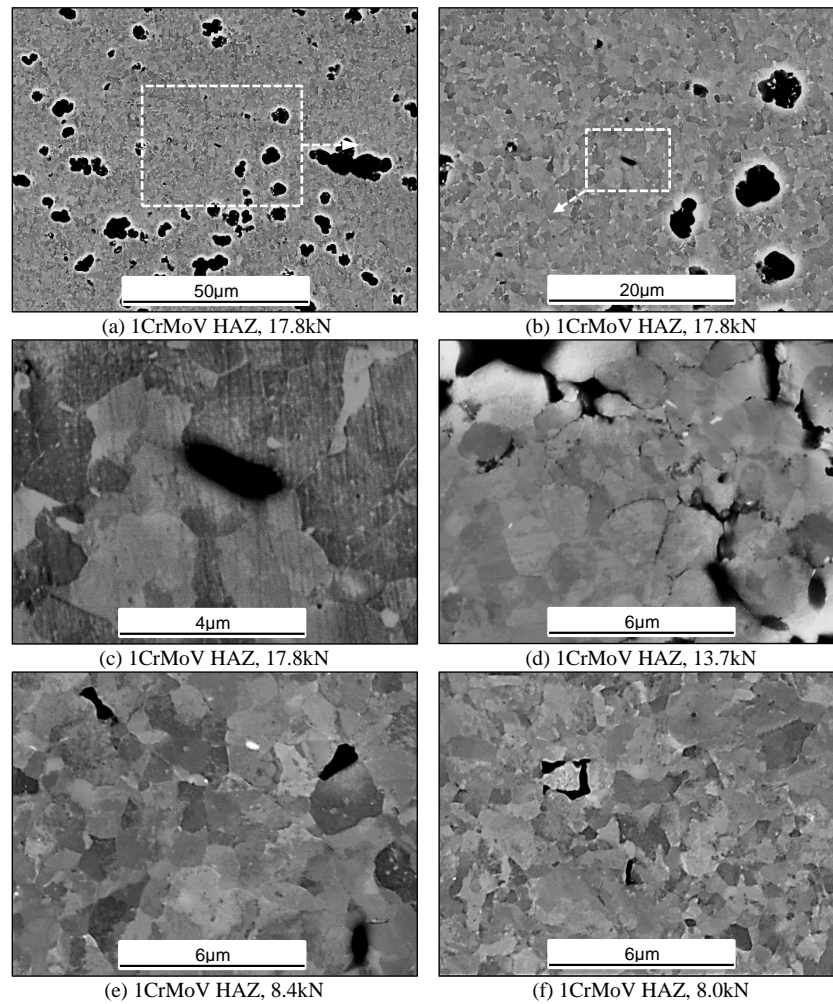


Figure 3.5.9: ECC images for the DMW after CCI tests at 550°C ((a,b,c): 17.8kN, (d): 13.7kN, (e): 8.4kN and (f): 8.0kN).

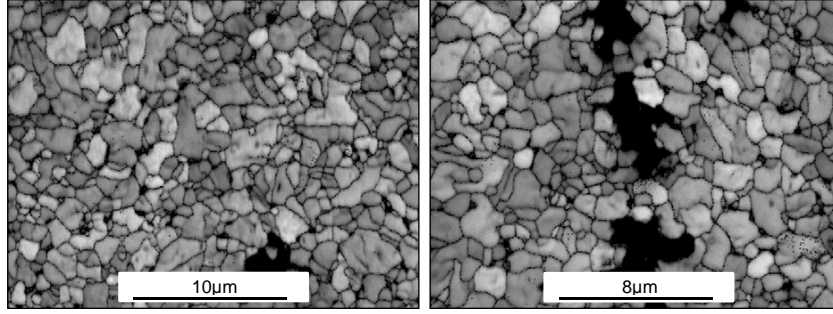


Figure 3.5.10: EBSD results for the DMW after CCI test at the load level of 8.0kN (550°C) presenting high-angle grain boundaries in 1CrMoV HAZ.

3.5.3 LICON Methodology Application for Dissimilar Metal Welds

LICON Methodology

The LICON methodology is currently based on the formulation:

$$t_{i,x} = A(\bar{\sigma})^{-\nu}(H)^{-\gamma} \quad (3.5.1)$$

with $H = \sigma_1/\bar{\sigma}$, where σ_1 is the maximum principal stress and $\bar{\sigma}$ is the von Mises equivalent stress, and where A , ν and γ are constants determined for the material and temperature of interest and the associated multiaxial creep rupture response. Typically γ varies between zero for $\bar{\sigma}$ -controlled rupture and ν for σ_1 -controlled rupture [3, 10]. The LICON method equations characterise the rupture behaviour in two mechanism regimes. In regime-1, the damage mechanism for ferritic steels is typically void nucleation due to particle/matrix decohesion, and rupture is $\bar{\sigma}$ -controlled (i.e. with $\gamma' \rightarrow 0$), such that [3, 4]:

$$t_r = A'(\sigma_0)^{-\nu'} \quad \text{uniaxial} \quad (3.5.2)$$

$$t_{i,x} = A'(\bar{\sigma}_{CT})^{-\nu'} \quad \text{multiaxial (e.g. CT specimens)} \quad (3.5.3)$$

In regime-2, for ferritic steels, creep damage nucleates and develops at grain/lath boundaries and rupture is mainly σ_1 -controlled (i.e. with $\gamma'' \rightarrow \nu''$), such that [3, 4]:

$$t_r = A''(\sigma_0)^{-\nu''} \quad \text{uniaxial} \quad (3.5.4)$$

$$t_{i,x} \approx A''(\bar{\sigma}_{CT})^{-\nu''}(H_{CT})^{-\nu''} \quad \text{multiaxial (e.g. CT specimen)} \quad (3.5.5)$$

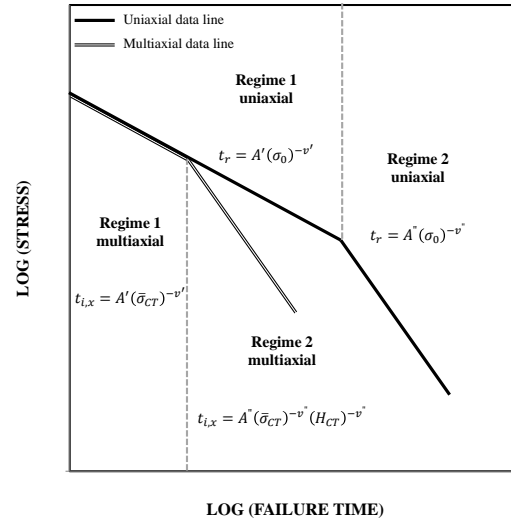


Figure 3.5.11: Schematic representation of the LICON concept.

where $\bar{\sigma}_{CT}$ and H_{CT} are respectively reference von Mises stress and reference stress multiaxiality factor for the CT testpiece. Following the experience reviewed in [11], the crack initiation criterion of $\Delta a=0.5\text{mm}$ is conventionally used in LICON applications (e.g. for 9%Cr [1, 2] and 1CrMoV steels [3, 4]). Equations 3.5.2 to 3.5.5 are schematically presented in Figure 3.5.11.

The LICON equation set is specifically defined above for predicting long duration uniaxial rupture times from relatively short duration CCI tests using CT specimens. Prediction of the long-time uniaxial rupture behaviour (i.e. defining the values of A'' and v'') from the results of a series of CCI tests needs determination of the values of $\bar{\sigma}_{CT}$ and H_{CT} using a mechanical analysis.

The LICON method was first developed for application to advanced 9%Cr pipe steels which coincidentally were creep ductile and notch insensitive materials. The original concept for the mechanical analysis part of the approach was therefore to consider a reference stress solution for determination of a net section representative von Mises stress and to use tabulated stress multiaxiality factors for the common multiaxial creep testing geometries (or to employ finite element analysis (FEA) to determine their values in a first evaluation for a new testpiece geometry). It was intended that users of the LICON methodology would not need to perform FEA for laboratory testpieces as long as they used one of the standard configuration characterised within the LICON project [1, 2]. For example, the introduced

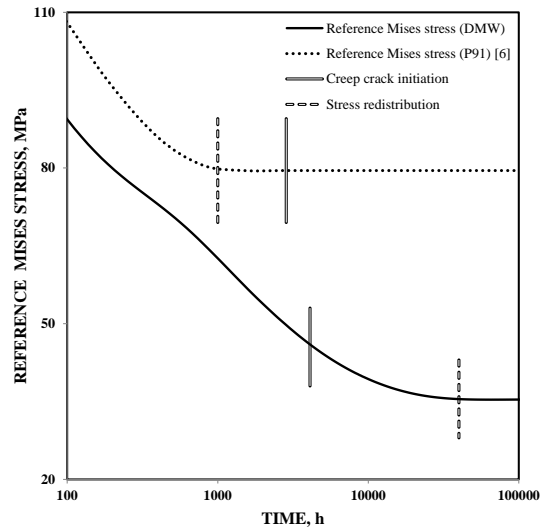


Figure 3.5.12: Reference von Mises stress evolution for CT specimens made of the DMW and P91 loaded at 8.0kN and 9.8kN, respectively [6].

formulation for determination of the required stress state parameters for the CT specimen included: $\bar{\sigma}_{CT} = P/(m^*B_nW)$ and $H_{CT} = 3.6$ (where P is the applied load, B_n is the specimen net section, W is the specimen width and m^* is the yield load ratio as defined in [12, 13]) [1, 2]. Consideration of the above expressions for the LICON method application to advanced 9%Cr pipe steels was successful which demonstrated the applicability of the original LICON concept (based on reference stress solutions). However, later studies exploring the applicability of the LICON methodology to a low alloy creep resistant steels (1CrMoV) revealed several challenges, in particular for high strength heats (e.g. high creep strength (HCS) 1CrMoV) [3–5]. Careful evaluation has indicated that HCS 1CrMoV does not have the essential characteristics to be examined with the original LICON approach (based on reference stress solutions) [6]. In contrast with 9%Cr steels which experience complete stress redistribution before the start of crack extension ('reference stress' materials [6]), HCS Cr-MoV, and similarly the investigated DMW, do not achieve complete stress redistribution before the onset of crack extension (Figure 3.5.12). Reference stress solutions are only appropriate after the occurrence of complete stress redistribution, and therefore HCS 1CrMoV and the DMW under investigation are examples of 'non-reference stress' material. In these circumstances, application of the original LICON method procedure (based on reference stress solutions) is not appropriate.

Extending the applicability of the LICON method to 'non-reference stress' materials requires the consideration of a more sophisticated mechanical analysis approach (e.g. involving FEA). The details of a proposed procedure for involving FEA as the mechanical analysis part of the LICON method when applied to a 'non-reference stress' material includes [6]:

- the adoption of an elastic–plastic–(secondary) creep constitutive model, with the creep rate formulation being representative of the material behaviour over a wide range of stresses, i.e. the adoption of a stress regime dependent secondary creep model.
- the adoption of a location 0.5mm from the notch root (in the mid-thickness plane of the CT testpiece) as the stress/strain state reference position, and the CCI time as the reference time, with 0.5mm crack extension being the considered crack initiation criterion.
- the adoption of a sufficiently refined mesh configuration for the FE model (quadratic hexahedral elements with converged H_{CT} value).

Employment of this procedure for application of the LICON methodology to the HCS 1Cr-MoV steel was successful [6]. Furthermore, examination of the proposed procedure for the LICON method application to a 9%Cr steel showed that the procedure is equally applicable for 'reference stress' materials (e.g. 9%Cr steels) [6]. This study therefore adopts the modified procedure for application of the LICON methodology to the DMW under investigation.

Application of the LICON method formulation to predict the creep rupture behaviour of DMW uniaxial testpieces has required further development. In particular, Equation 3.5.4 assumes a uniformly distributed stress state with $H=1$, for predicting long–time uniaxial strength values. This assumption is reasonable for homogeneous material conditions. In contrast, for a DMW, different inelastic (creep) deformation behaviours exhibited by different microstructural constituents (e.g. PM, HAZ, WM) generate non-uniform multiaxial stress states within the testpiece and $H \neq 1$. Development of the LICON method formulation for predicting the uniaxial creep rupture strength of a DMW has involved rewriting Equation 3.5.4 to become:

$$t_{r,DMW} \approx A''(\sigma_0)^{-\nu''} (H_{DMW})^{-\nu''} \quad \text{uniaxially loaded DMW} \quad (3.5.6)$$

Equation 3.5.6 takes into consideration that although loaded in a uniaxial stress state in the 1CrMoV and Alloy 625 parts of the testpiece, the stress state at the interface of DMW constituents is multiaxial. Consistent with general expressions introduced in [3, 4], the present study has considered H_{DMW} to be the maximum FEA calculated stress multiaxiality factor within the loaded DMW uniaxial testpiece.

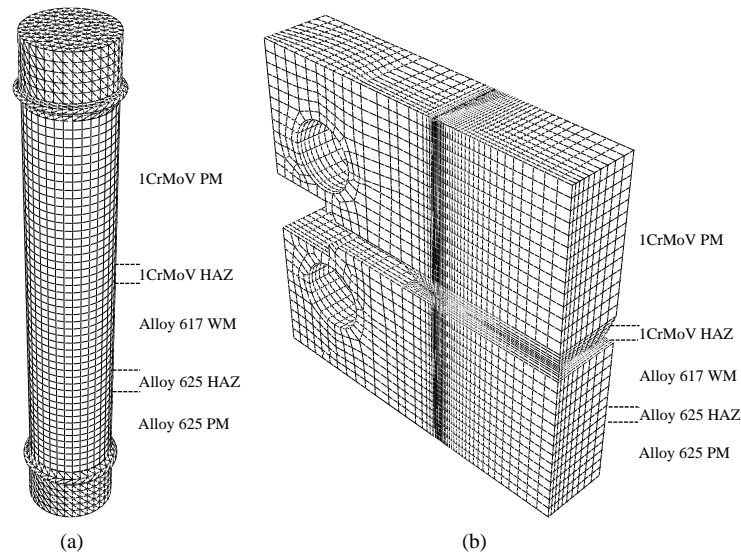


Figure 3.5.13: Designed FE models for (a) uniaxial and (b) CT specimens made of the DMW.

FE Modelling

The designed FE meshes used to simulate the conducted (a) uniaxial and (b) CCI tests for the DMW are shown in Figure 3.5.13. The models include five different material sections: 1CrMoV PM, 1CrMoV HAZ, Alloy 617 WM, Alloy 625 HAZ, Alloy 625 PM. The size of each section was generated according to physical observations from the actual DMW shown in Figure 3.5.1.

The representative model for the uniaxial tests (Figure 3.5.13a) involved 8948 elements (20-node hexahedral elements with quadratic interpolation) and was used to simulate the uniaxial DMW creep tests at stress levels of 220, 200, 120 and 80MPa, at 550°C, for the corresponding rupture durations.

The adopted model for the CT testpiece used a 1/2 model symmetry condition and involved 18390 elements (20-node hexahedral elements with quadratic interpolation). Consistent with the used specimens, the notch was located in the middle of the 1CrMoV HAZ section of the adopted FE model. The model was employed to simulate the conducted CCI tests at the five load levels of 17.8, 13.7, 8.4, 8.0 and 6.0kN, at 550°C, for the corresponding CCI durations.

The described FE models were solved using the commercially available code of ABAQUS [14].

The quality of the mesh configurations were checked according to the procedure described in [5, 6].

Constitutive Behaviour Modelling This section describes details of the constitutive material behaviour adopted within the FE model. Following the approach introduced in [6], this study considered an elastic–plastic–(stress regime dependent secondary) creep rate formulation for representing the constitutive behaviour of each material section.

A linear elastic model was used to represent the elastic behaviour of the material sections. While a previously reported E modulus value was adopted for Alloy 625 PM [15], results of tensile tests at 550°C (Figure 3.5.5) were used for E moduli values of 1CrMoV PM and Alloy 617 WM. This study assumed the elastic properties of the HAZs to be the same as their respective PMs.

Uniaxial tensile test data (Figure 3.5.5) was used to represent the non–linear loading characteristics of the 1CrMoV PM and Alloy 617 WM. The adopted plasticity model for 1CrMoV PM was also used for the 1CrMoV HAZ. Plasticity models were not required for Alloy 625 PM and HAZ (the maximum von Mises stresses developed in these microstructural sections were much less than the yield strength of Alloy 625).

Alloy 617 and Alloy 625 at 550°C are extremely creep resistant and uniaxial creep test results for Alloy 617 WM at the high stress level of 440MPa, shown in Figure 3.5.4, illustrate negligible creep deformation in comparison with that of 1CrMoV at much lower stresses. This study therefore neglected any creep deformation of Alloy 617 WM, and similarly, Alloy 625 (PM/HAZ). The stress regime dependent secondary creep model given by Equation 3.5.7 was used to represent the creep behaviour of 1CrMoV PM and HAZ:

$$\dot{\epsilon}_s = A_1 \sinh(B_1 \sigma) + A_2 \sigma^{n_2} \quad \text{Sinh+N model [16]} \quad (3.5.7)$$

where $\dot{\epsilon}_s$ is the steady creep rate and A_1 , B_1 , A_2 are numerical constants determined from uniaxial creep data. n_2 is the stress exponent in the creep rate equation of the material for low stresses which is 3 for 1CrMoV [5, 17]. More information related to the model is given in [16].

The uniaxial creep test results for 1CrMoV PM (Figure 3.5.4) were used to underpin the creep model for this parent material. The secondary creep behaviour of 1CrMoV HAZ was extracted from the uniaxial creep test results for the DMW in the following way. Assuming a composite structure and neglecting the interactions between different microstructural

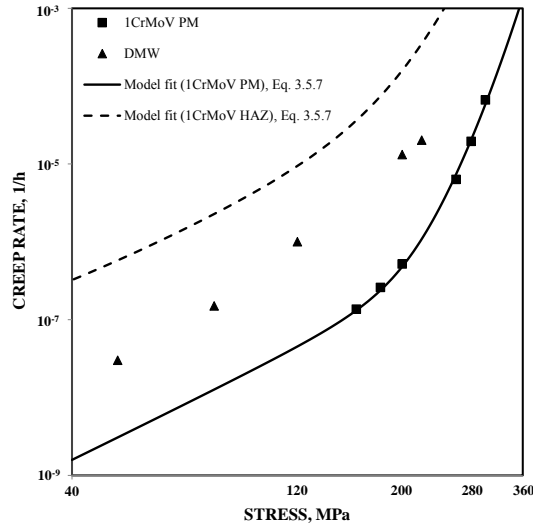


Figure 3.5.14: Steady creep rate (stress) diagram for 1CrMoV (PM/HAZ) and DMW at 550°C.

sections, the steady-state creep rate of the DMW can be estimated using [18, 19]:

$$(\dot{\epsilon}_s)_{(DMW)} = \frac{1}{L_{DMW}} \times \sum_{i=1}^5 L_i \times (\dot{\epsilon}_s)_i \quad (3.5.8)$$

where L_i is the length of each section.

Consideration of $(\dot{\epsilon}_s)_{Alloy\ 617(WM)} = (\dot{\epsilon}_s)_{Alloy\ 625(HAZ)} = (\dot{\epsilon}_s)_{Alloy\ 625(PM)} = 0$ gives:

$$(\dot{\epsilon}_s)_{1CrMoV(HAZ)} = \frac{1}{L_{1CrMoV(HAZ)}} \times [L_{DMW} \times (\dot{\epsilon}_s)_{DMW} - L_{1CrMoV(PM)} \times (\dot{\epsilon}_s)_{1CrMoV(PM)}] \quad (3.5.9)$$

Figure 3.5.14 presents the steady-state creep rate of 1CrMoV (PM/HAZ) and the corresponding model fits. The numerical values of the creep model parameters for 1CrMoV

Table 3.5.2: Sinh+N creep model parameters for 1CrMoV (PM/HAZ) at 550°C (Equation 3.5.7).

1CrMoV PM	Parameter	A_1	B_1	A_2	n_2
	Value	1.44×10^{-11}	0.55	2.37×10^{-14}	3.00
1CrMoV HAZ	Parameter	A_1	B_1	A_2	n_2
	Value	5.05×10^{-08}	0.43	2.91×10^{-12}	3.00

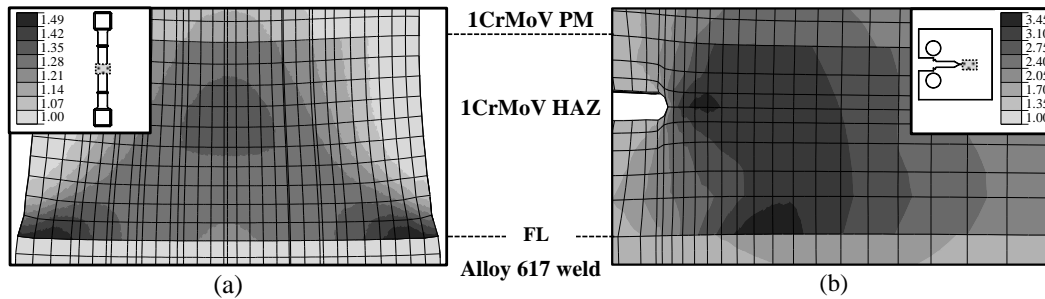


Figure 3.5.15: Stress multiaxiality factor distributions for (a) uniaxial and (b) CT DMW specimens (uniaxial specimen loaded at 200MPa to rupture time, CT specimen loaded at 8.0kN to CCI time).

(PM/HAZ) are summarised in Table 3.5.2

FE Results

Figure 3.5.15 shows the distributions of stress multiaxiality factor within (a) uniaxial and (b) CT DMW specimens.

Mismatch of the creep properties of different microstructural constituents of the DMW generates complicated multiaxial stress states within the specimens. Figure 3.5.15 shows two regions with high stress multiaxiality factors; one located in the vicinity of the FL and one in the middle of the HAZ. Similarly for the CT specimens, there are regions ahead of the notch tip and in the vicinity of the FL with high stress multiaxiality factors (3.5.15b).

Figure 3.5.16 shows crack development paths in (a) uniaxial and (b) CCI specimens. This reveals that for the CCI tests, cracking occurs ahead of the crack starter (1CrMoV IC/FGHAZ), and in the vicinity of the FL. For the uniaxially tested specimens, cracking occurs within the 1CrMoV IC/FGHAZ and at the FL. A comparison of Figure 3.5.15 with Figure 3.5.16 demonstrates the important role of generated stress multiaxiality in the determination of creep cracking patterns.

Figure 3.5.17 and 3.5.18 illustrate the FEA results for the distribution of von Mises stress and stress multiaxiality factor at mid-thickness of the DMW CT specimens loaded at 550°C to the corresponding CCI time. Figure 3.5.19 presents the radial distribution of stress multiaxiality factor at the FL of uniaxial specimens loaded at 550°C. The FE results presented in this section, in conjunction with the experimentally measured CCI times, are employed in the LICON method formulation to predict long term creep strength values for the DMW uniaxial testpieces in the next section.

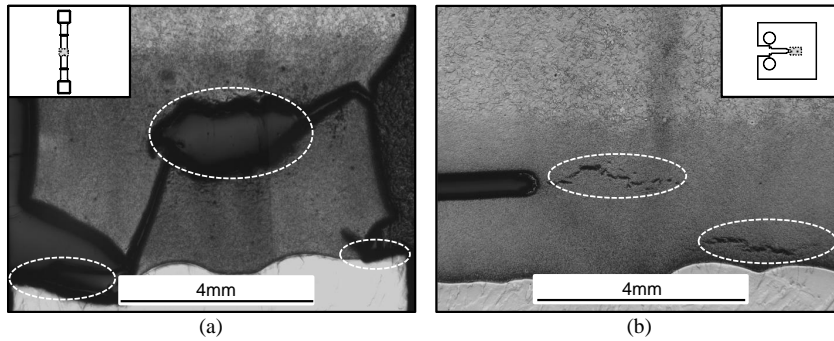


Figure 3.5.16: Typical creep cracking patterns in (a) uniaxial and (b) CT DMW specimens and loaded at 550°C (CCI: 8kN, uniaxial: 200MPa, Etchant: Nital).

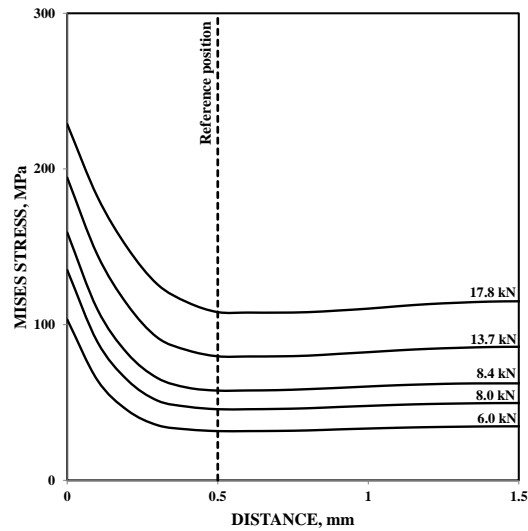


Figure 3.5.17: Distribution of von Mises stress at mid-thickness of the DMW CT specimens loaded at 550°C to the corresponding CCI times.

LICON Method Results

As explained in section 3.5.2, cracking in all the conducted CCI tests was due to grain boundary cavity nucleation, growth and coalescence (regime-2, Figure 3.5.11) where the LICON method adopts Equation 3.5.5 for interpretation of the observations.

Following the procedure proposed in [6], the FE calculated von Mises stress and stress mul-

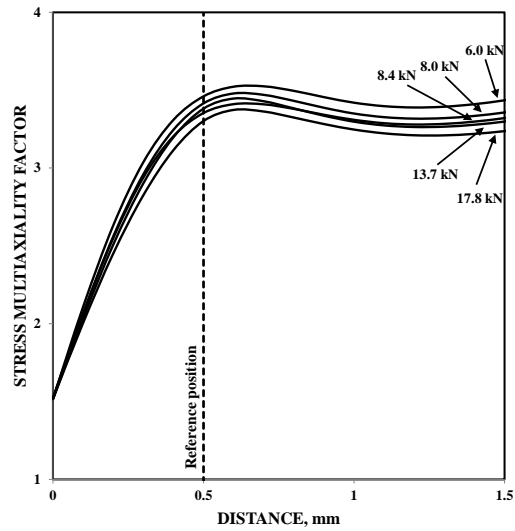


Figure 3.5.18: Distribution of stress multiaxiality factor at mid-thickness of the DMW CT specimens loaded at 550°C to the corresponding CCI times.

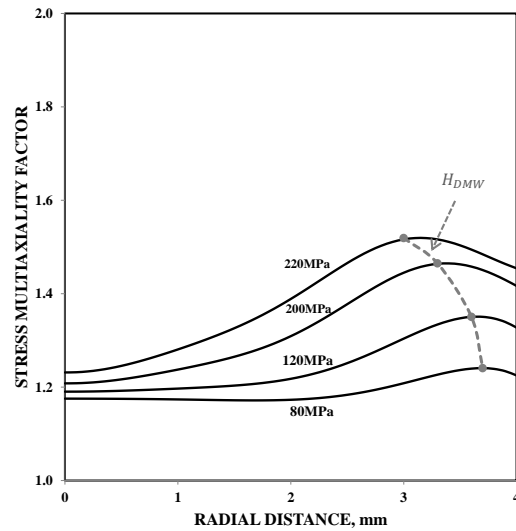


Figure 3.5.19: Radial distribution of stress multiaxiality factor at the FL of DMW uniaxial specimens loaded at 550°C to the corresponding rupture times.

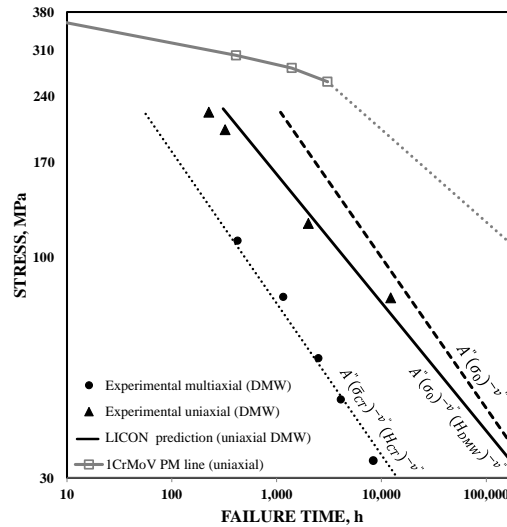


Figure 3.5.20: Presentation of the LICON predicted regime-2 uniaxial rupture strength for the DMW at 550°C.

triaxiality factor at 0.5mm from the notch root (in the mid-thickness plane of the testpiece) at the CCI time were adopted as the reference stress and stress multiaxiality factor ($\bar{\sigma}_{CT}$ and H_{CT}) used in the assessment.

Plotting $\log(t_{i,0.5})$ vs. $[\log(\bar{\sigma}_{CT}) + \log(H_{CT})]$ allows the identification of both ($-\nu''$) and $\log A''$, from respectively the slope and intercept of the straight line of best fit ($A'' = 4.0 \times 10^9$, $\nu'' = 2.8$). Finally, the LICON method employed the FEA calculated H_{DMW} (Figure 3.5.19) and the determined values for A'' and ν'' for prediction of the rupture strengths of the DMW uniaxial testpieces.

Figure 3.5.20 demonstrates the effectiveness of the LICON method for predicting the rupture behaviour DMW uniaxial testpieces. It also shows that adoption of $H=1$ in the LICON method formulation (Equation 3.5.4) significantly overestimates strength values for the uniaxial DMW specimens (dashed line). Consistent application of the LICON formulation, i.e. accounting for the multiaxial stress state in DMW testpieces, however provided an acceptable agreement between predicted uniaxial creep rupture behaviour and experimental observations for the DMW uniaxial testpieces. The approach is equally applicable for similar metal welds (SMW) and the use of Equation 3.5.6 instead of Equation 3.5.4 is recommended for predicting the long term creep strength of SMW uniaxial testpieces.

3.5.4 Concluding Remarks

This study examines the application of the LICON method to a dissimilar metal weld (DMW). The examined material is part of a weldment of 1CrMoV and Alloy 625 with filler metal of Alloy 617 which was considered as a candidate solution for rotor constructions in new advanced power plant (i.e. in the AD700 project).

The LICON methodology is an approach for predicting the lifetime of materials under creep loading conditions. The LICON method predicts long-time uniaxial creep strength using the results from several short duration creep crack incubation (CCI) tests in conjunction with the outcome of a mechanical analysis for the adopted multiaxial specimen geometry. Early findings confirmed the applicability of the methodology for the long term creep strength prediction of the martensitic 9%Cr pipe steels and 1CrMoV bainitic steels.

This study has demonstrated the feasibility of the approach for predicting creep rupture strength values for DMW uniaxial testpieces. Consistent application of the LICON formulation, i.e. accounting for the multiaxial stress state in DMW testpieces, provides an acceptable agreement between predicted uniaxial creep rupture behaviour and experimental observations for the DMW uniaxial testpieces.

References

- [1] P. Auerkari, W. Bendick, S. Holdsworth, J.H. Rantala, R. Hurst, C. Coussement, and R. Hack. Predicting long term creep behaviour using the LICON methodology. In *Proceedings of the 3rd International Conference of Advances in Material Technology for Fossil Power Plants*, pages 329–339, 2001.
- [2] V.M. Martins and S.R. Holdsworth. The LICON methodology for predicting the long term service behaviour of new steels. *Materials at High Temperatures*, 19(2):99–103, 2002.
- [3] S.R. Holdsworth and E. Mazza. Exploring the applicability of the LICON methodology for a 1CrMoV steel. *Materials at High Temperatures*, 25(4):267–276, 2008.
- [4] S.R. Holdsworth and E. Mazza. Using the results of creep crack incubation tests on 1CrMoV steel for predicting long-time creep rupture properties. *International Journal of Pressure Vessels and Piping*, 86(12):838–844, 2009.
- [5] E. Hosseini, S.R. Holdsworth, and E. Mazza. Experience with using the LICON methodology for predicting long term creep behaviour in materials. *International Journal of Pressure Vessels and Piping*, 92:70–76, 2012.
- [6] E. Hosseini, S.R. Holdsworth, and E. Mazza. The LICON methodology for predicting long-time uniaxial creep rupture strength of materials. *International Journal of Pressure Vessels and Piping*, doi: 10.1016/j.ijpvp.2013.04.033, 2013.
- [7] R. Blum and R.W. Vanstone. Materials development for boilers and steam turbines operating at 700°C. In *6th International Charles Parsons Turbine Conference*, pages 489–510, 2003.
- [8] R. Blum and J. Kjær, S. and Bugge. Development of a PF fired high efficiency power plant (AD700). In *Proceedings of the Riso International Energy Conference of Energy Solutions for Sustainable Development*, 2007.
- [9] A. Pirscher. Alstom steam turbine designs for AD700 power plant. In *AD700 Conference Milan*, 2005.
- [10] B.J. Cane. Creep cavitation and rupture in 2.5CrMo steel under uniaxial and multiaxial stresses. In *Proceedings of Conference on Mechanical Behaviour of Materials*, pages 173–182, 1979.
- [11] S.R. Holdsworth. Initiation and early growth of creep cracks from pre-existing defects. *Materials at High Temperatures*, 10(2):127–137, 1992.
- [12] A.G. Miller. Review of limit loads of structures containing defects. *International Journal of Pressure Vessels and Piping*, 32(1–4):197–327, 1988.
- [13] S. Al Laham, S.I. Branch, and R.A. Ainsworth. Stress Intensity Factor and Limit Load Handbook. *British Energy Generation*, 1999.
- [14] ABAQUS. User's Manual, Version 6.10, Hibbit, Karlsson and Sorenson, Pawtucket, RI, USA, 2011.
- [15] Inconel alloy 625, www.specialmetals.com, 2006.
- [16] E Hosseini, S.R. Holdsworth, and E. Mazza. Stress regime dependent creep constitutive model consideration in finite element continuum damage mechanics. *International Journal of Damage Mechanics*, doi: 10.1177/1056789513479810, 2013.
- [17] E. Hosseini, S.R. Holdsworth, and E. Mazza. Creep constitutive model considerations for high temperature finite element numerical simulations. *The Journal of Strain Analysis for Engineering Design*, 47(6):341–349, 2012.
- [18] W.E. White and I. LeMay. Strain time behaviour and second stage creep rate characterization in stainless steel weldments. In *Proceedings of International Conference on Engineering Aspect of Creep, Sheffield, Institute of Mechanical Engineers, London*, pages 89–94, 1980.
- [19] Y Monma, S Yokoi, and M Yamazaki. Creep strain time behavior of 304/308 weldments for fast breeder reactor vessel. In *Proceedings of the 5th International Conference on Pressure Vessel Technology*, volume 2, pages 1366–1392, 1984.

Chapter 4

Summary and Discussion

This chapter has provided a brief and continuous review of the research articles given in Chapter 3.

The primary aim of this research project has been to examine the applicability of the LICON methodology for predicting the long-time creep rupture strength of a dissimilar metal weldment of 1CrMoV and Alloy 625 with filler metal of Alloy 617.

The LICON methodology is an approach for predicting the lifetime of materials under creep loading conditions. The LICON method predicts long-time uniaxial creep strength using the results from several short duration creep crack incubation tests in conjunction with the outcome of a mechanical analysis for the testpiece. The applicability of this methodology for long term creep strength predictions for the martensitic 9%Cr and bainitic 1%Cr steels has already been demonstrated [1–4]. This study has examined the possibility of extending the applicability of this methodology to creep assessment of dissimilar metal welds (DMW).

Investigation of the applicability of the LICON methodology for welded joints requires an understanding of the previous applications of the method for other material types. The following first re-examines the application of the LICON method to bainitic 1%Cr and martensitic 9%Cr steels.

4.1 LICON Method Application for 1%Cr and 9%Cr steels

The LICON methodology is based on the formulation:

$$t_{i,x} = A(\bar{\sigma})^{-\nu}(H)^{-\gamma} \quad (4.1)$$

with $H = \sigma_1/\bar{\sigma}$, where σ_1 is the maximum principal stress and $\bar{\sigma}$ is the von Mises equivalent stress, and where A , ν and γ are constants determined for the material and temperature of interest and the associated multiaxial creep–rupture response. Typically γ varies between zero for $\bar{\sigma}$ –controlled rupture and ν for σ_1 –controlled rupture [3, 5].

The LICON method equations characterise the rupture behaviour in two mechanism regimes. For ferritic steels, in regime–1, the damage mechanism is typically void nucleation due to particle/matrix decohesion, and rupture is $\bar{\sigma}$ –controlled (i.e. with $\gamma' \rightarrow 0$) [3, 5], such that:

$$t_r = A'(\sigma_0)^{-\nu'} \quad \text{uniaxial} \quad (4.2)$$

$$t_{i,x} = A'(\bar{\sigma}_{CT})^{-\nu'} \quad \text{multiaxial (e.g. CT specimens)} \quad (4.3)$$

For the long term creep condition of ferritic steels however creep damage nucleates and develops at grain/lath boundaries and rupture is mainly σ_1 –controlled (i.e. with $\gamma'' \rightarrow \nu''$ for regime–2) [3–5], such that:

$$t_r = A''(\sigma_0)^{-\nu''} \quad \text{uniaxial} \quad (4.4)$$

$$t_{i,x} = A''(\bar{\sigma}_{CT})^{-\nu''}(H_{CT})^{-\gamma''} \quad \text{multiaxial (e.g. CT specimen)} \quad (4.5)$$

where t_r and $t_{i,x}$ are uniaxial rupture and multiaxial crack initiation times and $\bar{\sigma}_{CT}$ and H_{CT} are reference von Mises stress and reference stress multiaxiality factor for the compact tension (CT) testpiece [1–4].

Prediction of the long–time uniaxial rupture behaviour (i.e. defining the values of A'' and ν'') from the results of a series of creep crack incubation (CCI) tests needs determination of the values of $\bar{\sigma}_{CT}$ and H_{CT} using a mechanical analysis for the CT testpiece.

4.1.1 Reference Stress Solution Based LICON Methodology

The original concept for the mechanical analysis part of the LICON approach was to consider a reference stress solution for determination of von Mises equivalent stress and to use tabulated stress multiaxiality factors for the common multiaxial creep testing geometries characterised within the LICON project [1, 2]. The key idea of the reference stress approach is that for a multiaxial testpiece/structure under creep loading conditions, after instantaneous elastic-plastic deformation, creep begins, stresses redistribute and a stationary state is eventually reached. After this, reference stress solutions are applicable for representing the creep deformation/failure of the structure. However they may not be applied for transient creep conditions. Different formulations may be used as reference stress solutions with the most commonly used being based on limit load analysis. For example, the introduced formulation for determination of the reference stress of the CT specimen includes: $\bar{\sigma}_{CT} = P/(m^* B_n W)$ (where P is the applied load, B_n is the specimen net section, W is the specimen width and m^* is the yield load ratio) [1, 2].

Figure 4.1 shows the LICON long-time predictions resulting from consideration of the above solution with $H_{CT}=3.6$ [1, 2] for a 9%Cr steel (i.e. P91) at 600°C and for high creep strength (HCS) 1CrMoV alloy at 550°C. As can be seen, although consideration of such a solution is successful for P91, the resulting long-time LICON predictions for HCS 1CrMoV at 550°C are not acceptable [Section 3.4: *Article Four*].

Figure 4.2 shows the evolution of von Mises stress at the reference position of the CT testpieces made of P91 and HCS 1CrMoV (0.5mm from the notch root in the mid-thickness plane of the CT specimen is called reference position [1–4]). These results indicate that in contrast with 9%Cr steels which experience complete stress redistribution before the start of crack extension, HCS 1CrMoV does not achieve complete stress redistribution before crack initiation [Section 3.4: *Article Four*].

Reference stress solutions however may only be used for 'reference stress' materials (creep ductile and notch insensitive materials) which experience complete stress redistribution much earlier than crack initiation [6–8]. Therefore, application of the original LICON method procedure (based on reference stress solutions) for HCS 1CrMoV at 550°C is not appropriate. Application of the LICON method to this sort of materials requires to adopt a more advanced mechanical analysis tool.

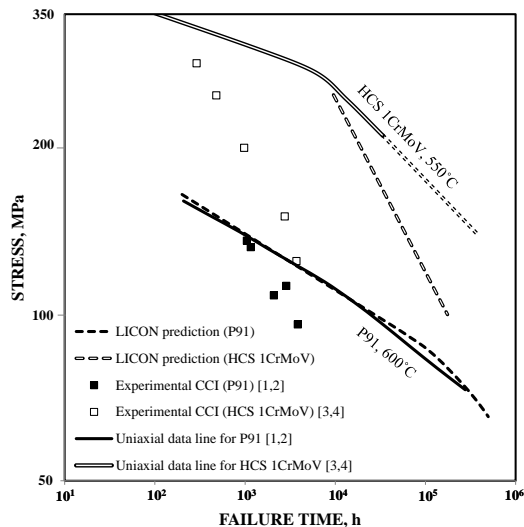


Figure 4.1: Comparison of experimental and LICON predicted uniaxial rupture strength for P91 at 600°C and HCS 1CrMoV at 550°C (predictions using consideration of reference stress solution and $H_{CT} = 3.6$ [1, 2]) [Section 3.4: *Article Four*].

4.1.2 Finite Element Analysis Based LICON Methodology

The representation of non-uniform creep redistributing stress states throughout a test-piece/component/structure is a challenging problem, and finite element analysis (FEA) is likely to be the most effective solution for this type of problem. This study therefore proposed FEA for the mechanical analysis part of the LICON method when it is to be applied to 'non-reference stress' materials (e.g. HCS 1CrMoV) [Section 3.4: *Article Four*].

An important consideration in creep FEA is the constitutive model used to represent the creep strain response of the component material. There are a variety of creep models which can be chosen by the analyst for implementation in FEA. This study has examined the sensitivity of creep FEA to the creep model consideration. Five different creep models have been fitted to a set of experimental uniaxial creep curves for HCS 1CrMoV at 550°C and subsequently, the derived constitutive equations have been implemented in finite element (FE) model representations of a series of CCI tests using CT testpiece manufactured from the same material and loaded at the same temperature. Observations on different predictions resulting from consideration of different creep constitutive models have clearly demonstrated the potential sensitivity of high temperature numerical analyses of structures to the type of creep model adopted, and to the scope of the experimental data from which the model is

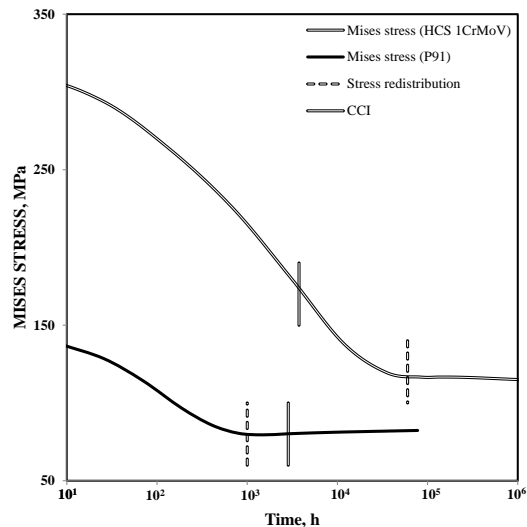


Figure 4.2: FEA calculated stress–state evolution at reference position of CT testpieces for P91 loaded at 9.8kN (600°C) and for HCS 1CrMoV loaded at 11.2kN (550°C) (creep constitutive model: 2RN) [Section 3.4: *Article Four*].

derived [Section 3.1: *Article One*, 3.2: *Article Two*].

For many engineering alloys, the creep deformation mechanism exhibited at high stresses is not the same as those at lower stresses [9, 10]. Typically, at relatively high temperatures, dislocation creep controlled by dislocation climb and glide occurs at higher stresses (when the stress exponent is ≥ 5), whereas diffusion creep controlled by volume or grain boundary diffusion occurs at lower stresses (when the stress exponent is around three or, in the limit, unity).

Some creep models (e.g. the conventional Norton [11] equation) involve a general single formulation to describe the behaviour of a material for all stress regimes (i.e. single regime models). The consideration of single regime creep models cannot represent the effect of creep mechanism transition due to a change of stress and ideally should not be used in applications with a wide range of redistributing stresses (e.g. analysis of CT specimen for the LICON method application) [3.2: *Article Two*, Section 3.3: *Article Three*].

Consideration of the conventional creep model formulations with different parameter sets for different stress regimes can be a solution to this problem (i.e. two–regime creep models) [10]. This study has shown that achieved FEA predictions based on consideration of stress regime dependent creep models are much more reliable than that of single regime models.

The difficulty of using stress regime dependent creep models however is that the parameter fitting for them requires experimental creep strain data from low stress (long duration) creep tests which are not usually available for most of materials (a potential solution to this challenge has been introduced in this study) [Section 3.4: *Article Four*].

This study has also evaluated the sensitivity of FEA outcomes to FE mesh condition. It was observed that certain parameters such as determined stress multiaxiality factor (H) are more sensitive to variations of the mesh configuration characteristics. The evidences from FEA of CT specimens have indicated that reproducible results are determined using hexahedral elements with quadratic interpolation, and an element size which has been optimized to give convergence of the stress multiaxiality factor [Section 3.1: *Article One*].

In general, creep FEA to determine the stress state in a high temperature testpiece/structure is a sensitive analysis and can result in non-unique numerical representations if the assessment procedure has not been carefully defined. Defining such a procedure for consideration of FEA for the mechanical analysis part of the LICON approach, in addition to describing the characteristics of the FE model to be used, involves defining the reference position and time for determining $\bar{\sigma}_{CT}$ and H_{CT} [3.4: *Article Four*].

The FEA calculated stress state (e.g. $\bar{\sigma}$ and H) in a loaded CT testpiece is a function of position and varies with time. Determination of $\bar{\sigma}_{CT}$ and H_{CT} from FEA calculations therefore needs to be specified for a reference position and reference time. The original assumption of the LICON approach, when the CT testpiece was first analysed, was to consider 0.5mm from the notch root as the reference position and the time to complete stress redistribution as the reference time. This consideration of reference position was coincident with the adopted crack initiation criterion of $\Delta a=0.5\text{mm}$.

As shown in Figure 4.2, complete stress redistribution for HCS 1CrMoV (and other 'non-reference stress' materials) does not occur until after crack initiation. Consideration of the stress redistribution time as the reference time in the LICON method application of such materials relates to a time-condition which cannot be achieved and an alternative assumption has to be introduced. The recommendation of this study was therefore to keep the coincidence of reference position and crack initiation criterion at 0.5mm, but to replace complete stress redistribution time with the CCI time as the reference time [Section 3.4: *Article Four*].

As a conclusion, the proposed procedure by this study for consideration of FEA as the mechanical analysis part of the LICON method for application to 'non-reference stress' materials includes [Section 3.4: *Article Four*]:

- the adoption of an elastic-plastic-(secondary) creep constitutive model, with the sec-

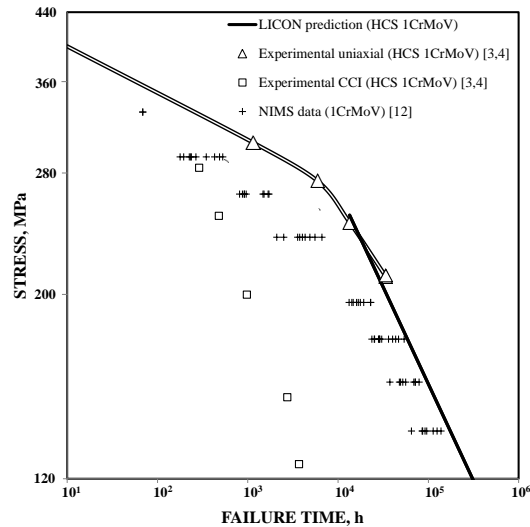


Figure 4.3: Comparison of experimental and FEA based LICON method predicted regime-2 uniaxial rupture strength for HCS 1CrMoV at 550°C (predictions using 2RN creep model). Note: The investigated heat of 1CrMoV in this part of the study is significantly more resistant to creep than the NIMS [12] heat of 1CrMoV and is hence referred to as HCS 1CrMoV [Section 3.1: *Article One*, Section 3.4: *Article Four*].

ondary creep model being representative of the material behaviour over a wide range of stresses, i.e. the adoption of a stress regime dependent secondary creep model.

- the adoption of 0.5mm from the notch root (in the mid-thickness plane of the CT testpiece) as the stress state reference position, and the CCI time as the reference time, with 0.5mm crack extension being the considered crack initiation criterion.
- the adoption of a sufficiently refined mesh configuration for the FE model (quadratic hexahedral elements with converged H_{CT} value).

Figure 4.3 presents the FEA based LICON long-time predictions for HCS 1CrMoV resulting from consideration of the above procedure.

The adopted FE code for the analysis of CCI tests employed the two-regime Norton (2RN) creep model equation as the stress regime dependent secondary creep model. The results of four uniaxial creep tests [3, 4] with reference to the published NIMS [12] low stress steady-state creep rate data for different heats of 1CrMoV at 550°C were used to underpin the 2RN creep model ($A_{1,2}$ and $n_{1,2}$ are constants and σ^* is the stress associated with deformation

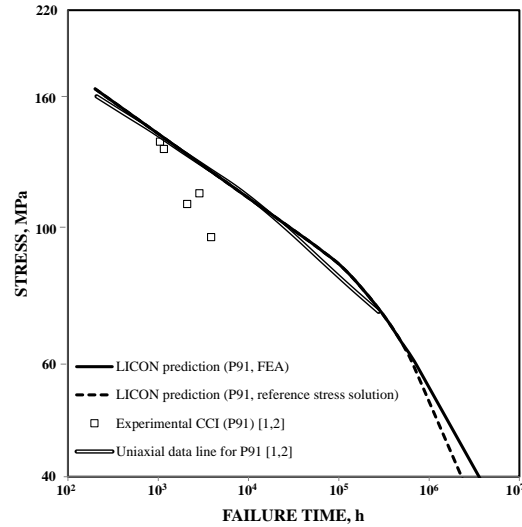


Figure 4.4: Comparison of experimental and LICON method predicted uniaxial rupture strength for P91 at 600°C (predictions using FEA and the reference stress solution [1, 2]) [Section 3.4: *Article Four*].

mechanism change).

$$\dot{\epsilon}_s = \begin{cases} A_1 \sigma^{n_1} & \text{if } \sigma \geq \sigma^* \\ A_2 \sigma^{n_2} & \text{if } \sigma < \sigma^* \end{cases} \quad \text{2RN model} \quad (4.6)$$

The conclusion was that the proposed procedure for the FEA application to the LICON approach is successful for HCS 1CrMoV at 550°C [Section 3.1: *Article One*, Section 3.4: *Article Four*].

Figure 4.4 compares the LICON method predictions for P91 at 600°C resulting from consideration of either FEA or reference stress solutions for the mechanical analysis part of the approach. The FEA implementation was according to the proposed procedure and considered a 2RN creep model equation as the stress regime dependent secondary creep model.

Successful application of the FEA based LICON method for P91 at 600°C indicates that although the newly proposed procedure is developed for application to 'non-reference stress' materials (e.g. HCS 1CrMoV), it is equally applicable for 'reference stress' materials (e.g. P91) [Section 3.4: *Article Four*].

Application of the LICON Method to Newly Developed Alloys This study has shown that successful implementation of the FEA based LICON approach for creep life assessment of a material requires a steady-state creep rate model for the material over a wide range of stresses. For the evaluated HCS 1CrMoV at 550°C and P91 at 600°C, the available uniaxial dataset [1–4] in conjunction with the published NIMS data [12, 13] provided the possibility to underpin stress regime dependent creep rate models.

In general, this is however a significant challenge for the LICON methodology, because the LICON method was originally developed to predict long term creep strength of materials with little existing creep data (e.g. for newly developed alloys). For such materials, the available creep data is usually limited to high stress (short duration) tests and developing an effective FE solution for LICON method application is not guaranteed [Section 3.4: *Article Four*].

This study has explored potential ways to resolve the problem and proposed a viable approximate method to estimate the creep rates of newly developed alloys in the viscous-glide stress regime. Literature reported experimental data on steady-state creep rate behaviour of different creep resistant alloys for stresses responsible for life durations up to 200–300kh were evaluated. Representations of steady-state creep rate vs. normalized stress (with respect to either 0.2% proof stress or limit of proportionality, σ_{LP} and $\sigma_{p0.2}$, respectively) for different alloys indicated that the creep rate behaviour of alloys in the viscous-glide stress regime can be estimated from their high stress creep and time-independent yield properties. This study has therefore proposed that for a newly developed alloy with only high stress creep and short term tensile data available, adoption of the 2RN creep model (i.e. Equation (4.6)) with $\sigma^* = 63\% \sigma_{LP}$ and $n_2 = 3.54$ can be used as an early approximation for the steady-state creep rate behaviour of the material in the viscous-glide stress regime. This is an important development which helps to formulate the stress regime dependent creep deformation behaviour of materials with limited available creep data. Consideration of this approximate method is a potential solution for the challenge involved in application of the LICON method for long-time creep strength prediction of newly developed alloys. This study has demonstrated the appropriateness of the presented approximation for application to creep life assessment of HCS 1CrMoV steel using a FEA based LICON approach where only a portion of available material data (high stress regime steady-state creep rates and time-independent yield properties) was used for creep constitutive model development. The study therefore introduces this approximate method as a potential solution for application of the LICON method to new materials with little/no existing low stress creep data, but also acknowledge the involved uncertainty. [Section 3.4: *Article Four*].

Creep Constitutive Model Development Before starting with examination of the LICON method applicability for the DMW, it is worth mentioning that this study, as a part of performed investigations on exploring the importance of using stress regime dependent creep models in FEA, has led to the introduction of a new primary–secondary–tertiary stress regime dependent creep constitutive model [Section 3.3: *Article Three*].

As shown earlier, some creep models like 2RN provide a bi-linear formulation with different parameter sets for high and low stress regimes to consider the stress regime dependency of materials creep deformation behaviour. The application of such formulations for a wide range of stresses is much more successful than that of conventional single regime models. However in reality, the stress dependent creep mechanism change is not a sharp transition and considering a step change of creep mechanism at a critical stress (as is considered in 2RN creep model) is not a realistic assumption. The more physically acceptable representation is a gradual and continuous change of creep deformation mechanism with stress variation (as is considered in the introduced creep model in Section 3.3: *Article Three*).

Stress regime dependency also exists for creep damage development. While in a high stress regime, creep damage arises mainly due to $\bar{\sigma}$ -controlled mechanisms, σ_1 -controlled mechanisms are responsible for creep damage in the low stress regime. For example, for ferritic steel at high stresses, the damage mechanism is predominantly void formation due to particle/matrix decohesion ($\bar{\sigma}$ -controlled) while at lower stresses, damage nucleates and develops at grain/lath boundaries (σ_1 -controlled) [3–5]. Consequently, as for creep deformation model equations, creep damage equations are therefore expected to cover multiple mechanism regimes and represent a gradual and continuous change of creep damage mechanism with stress variation.

In this study, a modification to the primary–secondary version of a single regime creep model proposed by Dyson and Osgerby [14] (originating from the Garofalo creep model equation [15]) has been presented. The new creep model considers a stress regime dependent creep deformation mechanism change with stress variation. Furthermore, influenced by the LICON method formulation, a stress regime dependent creep damage accumulation function is derived. This function is then introduced to the developed primary–secondary creep constitutive model to extend it for covering the tertiary creep regime [Section 3.3: *Article Three*].

The effectiveness of the developed creep constitutive model has been examined by applying the model in a finite element continuum damage mechanics (FECMD) implementation to predict deformation/damage accumulation for the series of CCI tests involving CT specimens made of the HCS 1CrMoV loaded at 550°C. The application of the new creep model formulation is shown to be successful, thus confirming the applicability of the proposed creep

constitutive model [Section 3.3: *Article Three*].

As mentioned, the creep damage accumulation part of the new constitutive model has been constructed based on the LICON method formulation and successful demonstration of that provided a new confirmation for the LICON formulation, and from a different point of view, i.e. FECDM.

4.2 LICON Method Application for Dissimilar Metal Welds

As the main objective of this research project, the applicability of the LICON method for the weldment of 1CrMoV and Alloy 625 with filler metal of Alloy 617 is examined. A set of experiments has been conducted to generate the required information for application of the LICON method to the DMW at 550°C (note: the 1CrMoV parent material (PM) heat is different from HCS 1CrMoV heat).

Uniaxial constant load creep tests at 550°C were conducted for cross-weld, 1CrMoV PM and Alloy 617 weld material (WM) testpieces to indicate the secondary creep deformation behaviour of the materials and to provide data for evaluation of the LICON method uniaxial creep strength predictions. Furthermore, CCI tests at 550°C were performed using DMW CT specimens with the crack starter located in the middle of the 1CrMoV heat affected zone (HAZ). These tests were used for identification of CCI behaviour of the under investigation DMW [Section 3.5: *Article Five*].

As a part of post test examination of the CCI tests, it was important to define the location of developed creep cavities with respect to the grain boundaries. Application of the CCI test results to the LICON methodology requires a knowledge of the corresponding creep failure mechanisms (e.g. particle/matrix decohesion or grain boundary cavitation). Different techniques were used to investigate the microstructure of crept specimens (i.e. optical microscopy, electron channelling contrast (ECC) imaging technique and electron backscatter diffraction (EBSD) analysis). The outcome was that the sites of creep cavity nucleation in the material for CCI tests were located at grain boundaries and the mechanism of creep failure, even for the shortest test, was grain boundary cavitation and this is the damage mechanism anticipated after long-time creep. The CCI test data can therefore be used by the LICON method formulation for predicting the long-time creep rupture behaviour of DMW uniaxial testpieces [Section 3.5: *Article Five*].

Figure 4.5 presents the evolution of von Mises stress at the reference position of the DMW

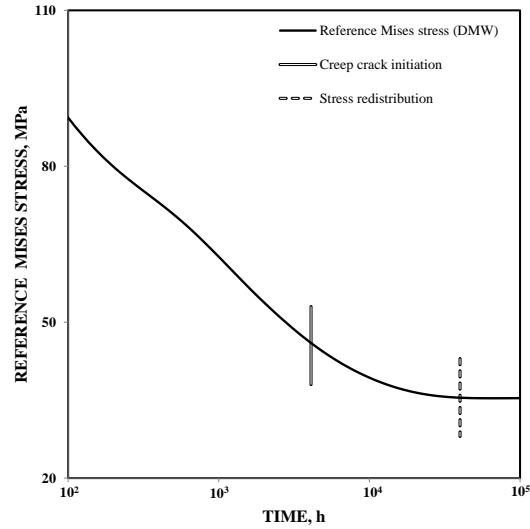


Figure 4.5: Reference von Mises stress evolution for DMW CT specimen loaded at 8.0kN and 550°C (FE calculation based on Sinh+N creep model consideration) [Section 3.5: *Article Five*].

CT testpiece (0.5mm from the notch root in the mid-thickness plane [1–4]).

As can be seen, similar to HCS 1CrMoV, the investigated DMW exhibits fast creep crack initiation and crack extension starts before complete stress redistribution. Therefore, the investigated DMW is an example of a 'non-reference stress' material condition and application of the original LICON method, based on a reference stress solution, is not appropriate. Application of the LICON method to the investigated DMW in this study has therefore followed the newly proposed procedure for FEA consideration in the LICON methodology [Section 3.5: *Article Five*].

FE models representing the conducted CCI (and uniaxial creep) tests have been designed. The models included five different material sections: 1CrMoV PM, 1CrMoV HAZ, Alloy 617 WM, Alloy 625 HAZ, Alloy 625 PM. While creep deformations of Alloy 617 and Alloy 625 (in comparison with that of 1CrMoV) were negligible, a secondary version of the newly developed stress regime dependent creep model was used to represent the creep deformation behaviour of 1CrMoV (PM/HAZ) [Section 3.3: *Article Three*]:

$$\dot{\epsilon}_s = A_1 \sinh(B_1 \sigma) + A_2 \sigma^{n_2} \quad \text{Sinh+N model} \quad (4.5)$$

The uniaxial creep test results for 1CrMoV PM were used to underpin this creep model

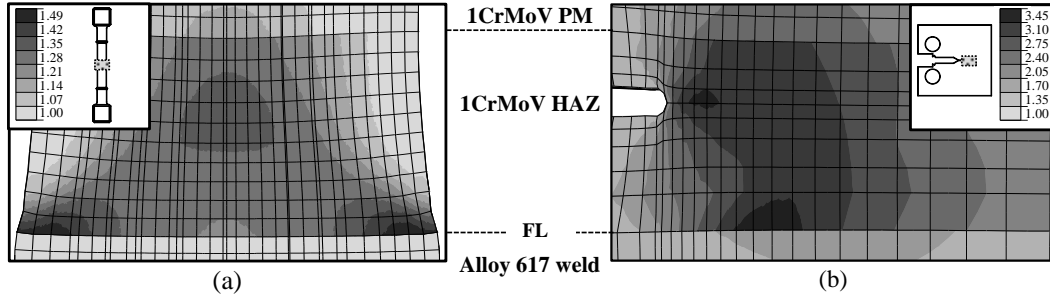


Figure 4.6: Stress multiaxiality factor distributions for (a) uniaxial and (b) CT specimens made of the DMW (uniaxial specimen loaded at 200MPa to rupture time, CT specimen loaded at 8.0kN to CCI time) [Section 3.5: *Article Five*].

for the parent material. Early effort using the small punch (SP) creep testing approach for underpinning the creep model for different sections of HAZ was unsuccessful (because it was difficult to extract SP specimen from specific HAZ locations of this particular weld). The uniaxial creep test results for the DMW were therefore used to underpin the secondary creep behaviour of 1CrMoV HAZ, as explained in Section 3.3: *Article Three*.

Figure 4.6 shows typical distributions of stress multiaxiality factors within (a) uniaxial and (b) CT specimens made of the DMW.

The original LICON method formula for long term uniaxial testing condition (Equation 4.4) considers a uniformly distributed stress state with $H=1$. As can be seen in Figure 4.6, different inelastic (creep) deformation behaviour of different sections (i.e. PM, HAZ, WM) generates a non-uniform multiaxial stress state within the DMW uniaxial testpiece and $H \neq 1$. The LICON method formulation for application to predict the creep rupture behaviour of DMW uniaxial specimens therefore required further development involving treatment of the testpieces as multiaxial structures (e.g. [3, 4]). Development of the LICON method formulation for predicting the creep rupture strength of a DMW uniaxial testpiece can then be rewritten as Equation 4.4, i.e.

$$t_{r,DMW} = A''(\sigma_0)^{-\nu''} (H_{DMW})^{-\gamma''} \quad \text{uniaxially loaded DMW} \quad (4.6)$$

where H_{DMW} is considered to be the maximum of FEA calculated stress multiaxiality factor within the DMW uniaxial testpiece which is function of σ_0 for a weld [Section 3.5: *Article Five*].

Figure 4.7 shows the crack development path originating from (a) uniaxial and (b) CCI tests. This reveals that for the CCI tests, cracking occurs ahead of the crack starter and in

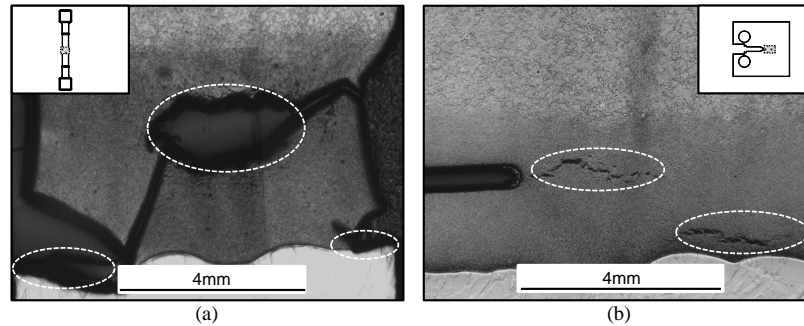


Figure 4.7: Typical creep cracking patterns in (a) uniaxial and (b) CT specimens made of the DMW and loaded at 550°C (CCI: 8kN, uniaxial: 200MPa, Etchant: Nital) [Section 3.5: *Article Five*].

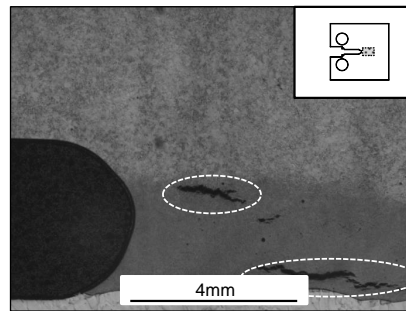


Figure 4.8: Creep cracking pattern in a CT specimen including 4mm wide crack starter made of the DMW loaded at 550°C and 17.8kN (Etchant: Nital).

the vicinity of the FL, and for the uniaxially tested specimens, cracking occurs within the 1CrMoV (HAZ) and at the FL. Comparison of Figure 4.7 with Figure 4.6 demonstrates the important role of generated stress multiaxiality in determination of creep cracking pattern [Section 3.5: *Article Five*].

Figure 4.8 shows the creep crack development pattern in a CT specimen incorporating a wide crack starter (crack starter width of 4mm in comparison with the other CT specimens with 0.4mm wide crack starter). The observation of similar cracking patterns for wide and narrow notched specimens (Figures 4.8 and 4.7b) demonstrated that the observed cracking pattern is not dominated by the CT specimen stress state and is a characteristic of the DMW under investigation.

A comparison of the LICON long term creep strength prediction and existed uniaxial creep rupture experience for the DMW is presented in Figure 4.9 proving the effectiveness of the

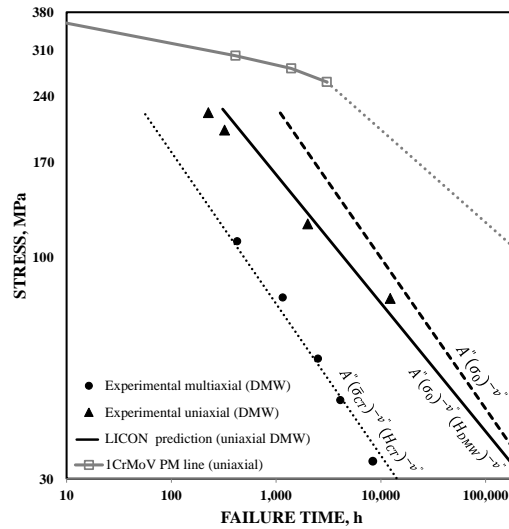


Figure 4.9: Presentation of the LICON predicted regime-2 uniaxial rupture strength for the DMW at 550°C [Section 3.5: *Article Five*].

LICON method for predicting the uniaxial rupture behaviour of the investigated DMW. It also shows that the adoption of $H=1$ in the LICON method formulation (i.e. Equation 4.4) significantly overestimates strength values for the DMW uniaxial specimens (dashed line). The proposed development in this study was therefore necessary for application of the LICON method to DMWs. This development is equally applicable for similar metal welds (SMW) and the use of Equation 4.6 instead of Equation 4.4 is recommended for predicting the long term creep strength of SMW uniaxial testpieces [Section 3.5: *Article Five*].

References

- [1] P. Auerkari, W. Bendick, S. Holdsworth, J.H. Rantala, R. Hurst, C. Coussement, and R. Hack. Predicting long term creep behaviour using the LICON methodology. In *Proceedings of the 3rd International Conference of Advances in Material Technology for Fossil Power Plants*, pages 329–339, 2001.
- [2] V.M. Martins and S.R. Holdsworth. The LICON methodology for predicting the long term service behaviour of new steels. *Materials at High Temperatures*, 19(2):99–103, 2002.
- [3] S.R. Holdsworth and E. Mazza. Exploring the applicability of the LICON methodology for a 1CrMoV steel. *Materials at High Temperatures*, 25(4):267–276, 2008.
- [4] S.R. Holdsworth and E. Mazza. Using the results of creep crack incubation tests on 1CrMoV steel for predicting long time creep rupture properties. *International Journal of Pressure Vessels and Piping*, 86(12):838–844, 2009.
- [5] B.J. Cane. Creep cavitation and rupture in 2.5CrMo steel under uniaxial and multiaxial stresses. In *Proceedings of Conference on Mechanical Behaviour of Materials*, pages 173–182, 1979.
- [6] T.H. Hyde. *Experimental Reference Stress Techniques for the Prediction of Creep Deformation Using Lead Alloy Models*. PhD thesis, University of Nottingham, 1976.
- [7] R.K. Penny and D.L. Marriott. *Design for Creep*. McGraw–Hill London, 1971.
- [8] D.J. Gooch, S.R. Holdsworth, and P.R. McCarthy. The influence of net section area on the notched bar creep rupture lives of three power plant steels. In *Proceedings of the 3rd International Conference on Creep and Fracture of Engineering Materials and Structures*, pages 441–457, 1987.
- [9] R.W. Evans and B. Wilshire. *Introduction to Creep*. Institute of Materials, London, 1993.
- [10] K. Naumenko, H. Altenbach, and Y. Gorash. Creep analysis with a stress range dependent constitutive model. *Archive of Applied Mechanics*, 79(6–7):619–630, 2009.
- [11] F.H. Norton. *The Creep of Steel at High Temperatures*. McGraw–Hill book company, 1929.
- [12] NIMS. *Data Sheet 9B, Data sheets on the elevated-temperature properties of 1Cr–1Mo–0.25V steel forgings for turbine rotors and shafts*. National Research Institute for Metals, Tokyo, Japan, 1990.
- [13] NIMS. *Data Sheet 43, Data sheets on the elevated-temperature properties of 9Cr–1Mo–V–Nb steel tubes for boilers and heat exchangers and 9Cr–1Mo–V–Nb steel plates for boilers and pressure vessels*. National Research Institute for Metals, Tokyo, Japan, 1996.
- [14] B. F. Dyson and S. Osgerby. *Modelling and Analysis of Creep Deformation and Fracture in a 1Cr0.5Mo Ferritic Steel*. NPL report. National Physical Laboratory, 1993.
- [15] F. Garofalo. *Fundamentals of Creep and Creep–Rupture in Metals*. Macmillan Series in Materials Science. Macmillan, 1965.

Chapter 5

Conclusions and Future Work

The primary objective of this research project has been to examine the applicability of the LICON methodology for predicting the long-time creep rupture strength of a dissimilar metal weld (DMW). Considerable experimental and analytical efforts have been undertaken to fulfil the requirements of this objective. Behind these, this study has dealt with several other subjects which have effectively helped the progress of this study (e.g. creep constitutive modelling, stress regime dependent creep deformation/damage accumulation, finite element continuum damage mechanics (FECDM), reference stress solutions and materials, etc). The outcomes of this research project have been published in five research articles which contribute to the fields of creep deformation and creep life assessment. The following presents the main findings of this research project and also indicates several interesting directions for future work.

5.1 Conclusions

This section provides findings, conclusions, and recommendations based on the investigations conducted within this research project.

5.1.1 Reference Stress Solutions/Materials

Reference stress solutions are approximate analytical solution which may be applied to multiaxial specimens (structures) for predicting creep deformation/failure behaviour from the results of uniaxial creep tests. Different formulations may be used as reference stress

solutions with the most commonly used being based on limit load analysis. The underlying requirement of the reference stress approach is that for a multiaxial testpiece/structure under creep loading conditions, after the instantaneous elastic-plastic deformation, creep begins, stresses redistribute and a stationary state is eventually reached. After this stage, reference stress solutions are applicable for representing the creep deformation/failure of the structure. However they may not be applied for transient creep conditions.

Numerical mechanical analysis for the creep loaded fracture mechanics compact tension (CT) specimen manufactured from different materials has shown that application of a reference stress solution for assessment of this specimen is limited to creep ductile, notch insensitive materials with long creep crack incubation (CCI) times (i.e. 'reference stress' materials). It has been shown that for CT specimens manufactured from creep brittle, notch sensitive materials (i.e. 'non-reference stress' materials) creep crack extension starts before complete stress redistribution and application of a reference stress solution to this sort of material is not appropriate. Mechanical analysis of such structures requires a more advanced mechanical evaluation, e.g. creep finite element analysis (FEA).

5.1.2 Creep Finite Element Analysis

The representation of non-uniform creep redistributing stress and strain states throughout a testpiece/component/structure is a challenging problem, and FEA is likely to be the most effective solution for this type of problem. The underlying premise of FEA is that an approximate analysis of any complex engineering calculation can be obtained by subdividing the problem into smaller (finite) elements. Careful use of FEA for analysis of multiaxial testpieces/structures made of 'non-reference stress' materials under creep loading conditions can be regarded as a powerful substitute for the application of reference stress solutions. Creep FEA to determine the stress/strain state in a high temperature testpiece/structure however is a sensitive analysis and can result in non-unique numerical representations if the assessment procedure has not been carefully defined. This study has examined the sensitivity of creep FEA outcomes to different assumptions/designs for creep constitutive models and finite element (FE) mesh configurations. The outcome has been reviewed in following.

Creep Constitutive Models

An important consideration in creep FEA is the constitutive model used to represent the creep strain response of the component material. There are a variety of creep models which can be chosen by the analyst for implementation in FEA. This study has demonstrated the

potential sensitivity of creep FEA to the type of creep model adopted, and to the scope of the experimental data from which the model is derived. It has also shown that the application of stress regime dependent creep constitutive models for applications involving a wide range of redistributing stresses is much more successful than that of conventional single regime creep models.

Stress Regime Dependent Creep Constitutive Models For many engineering alloys, the creep deformation mechanism exhibited at high stresses is not the same as those at lower stresses. Typically, at relatively high temperatures, dislocation creep is controlled by dislocation climb, and glide occurs at higher stresses (when the stress exponent is ≥ 5). At lower stresses diffusion creep is controlled by volume or grain boundary diffusion (when the stress exponent is around three or, in the limit, unity). Conventional single regime creep models imply a single creep deformation mechanism for all stresses and ideally should not be used in applications with a wide range of redistributing stresses (e.g. in the analysis of CT specimens for application in the LICON method). As an alternative, a two-regime form of the conventional models may be adopted with different parameter sets for high and low stress regimes. Application of two-regime creep models for analysis of structures with a wide range of redistributing stresses is much more reliable than that of single regime creep models. In reality, the stress dependent creep mechanism change is not a sharp transition and considering a step change of creep mechanism at a critical stress (as is considered in simple two-regime creep models) is not a realistic assumption. This study has introduced a creep model which considers a gradual and continuous change of creep deformation mechanism with stress variation. Successful application of the new creep model in creep FEA of fracture mechanics CT specimens for a series of CCI tests has been presented.

The difficulty of using stress regime dependent creep models however is that the parameter fitting for them requires experimental creep data from low stress (long duration) creep tests which are not usually available, in particular for newly developed materials. This study has proposed a viable approximate method applicable for newly developed alloys (with limited high stress creep and short term tensile data) which can estimate the steady-state creep rates of the alloy over a wide range of stresses.

Finite Element Model Mesh Design

As mentioned earlier in this section, this study has highlighted the sensitivity of FEA outcome to variations in FE model mesh configuration. It has been observed that the accuracy of FEA calculations for certain parameters is more sensitive to the configuration of the used

FE mesh. Examination of the creep FEA of CT specimens has shown that FE calculated stress multiaxiality factor (H) is much more sensitive to the adopted mesh design than von Mises stress ($\bar{\sigma}$) and load point displacement (LPD). Mesh convergence examinations should therefore give lower priority to the evaluation of less sensitive parameters (e.g. $\bar{\sigma}$ or LPD) and should focus on more sensitive parameters (such as H).

Finite Element Continuum Damage Mechanics

In addition to predicting creep deformation and state of redistributing stresses, creep FEA can also be used for representing creep damage accumulation in a creeping testpiece/structure. Such an application requires the implementation of a creep damage equation in FEA (e.g. FECDM). This study has shown a successful application of FECDM for predicting creep deformation/damage accumulation in a series of CCI tests involving CT specimens made of 1CrMoV. The FECDM calculations considered the primary–secondary–tertiary version of the newly developed creep constitutive model. While a combination of Garofalo and power law creep models has been used by the new model for representing the stress regime dependent creep deformation behaviour, the LICON formulation has been used in the development of the creep damage formulation. This is therefore a new application for the LICON formulation (i.e. FECDM).

5.1.3 LICON Method Application for Materials

As a pre-step for examination of the LICON method application for weldments of 1CrMoV and Alloy 625, this study has re-examined the previous applications of the LICON method for other materials (e.g. 1CrMoV and P91) and this revealed some details about the mechanical analysis part of the method which had not been previously considered. In the original LICON method development, it was aimed to use approximate reference stress solutions as the mechanical analysis part of the approach. This study revealed that application of the original LICON method (i.e. based on reference stress solutions) should be limited to 'reference stress' materials and that application of the LICON method to 'non-reference stress' materials required the adoption of a more advance mechanical analysis (e.g. creep FEA). Creep FEA for such an application is however a sensitive analysis and can result in non-unique LICON long term predictions if an optimized assessment procedure is not carefully followed. This study has described details of a proposed procedure for consideration of FEA in the LICON method. Careful evaluation has proved the applicability of the proposed procedure for not only high creep strength (HCS) 1CrMoV (as an example of a 'non-reference stress' material), but also for P91 as an example of a 'reference stress' material.

This demonstrates that although the new procedure was originally developed to use for LICON method applications to 'non-reference stress' materials, it is equally applicable for 'reference stress' materials.

5.1.4 LICON Method Application for Dissimilar Metal Welds

This study has reported details of experimental and analytical efforts made for examination of the LICON method applicability to a DMW. The investigated material is part of an existing weldment of 1CrMoV and Alloy 625 with filler metal of Alloy 617 which has been a candidate to use for rotor constructions in new advanced power plants (i.e. AD700). Beside the conducted analytical/numerical analyses, experimental examinations including uniaxial and multiaxial creep testing and microstructural investigations have been performed to provide the required information for examination of the LICON method application.

Mechanical analysis of the conducted CCI tests has shown that this joint (similar to HCS 1CrMoV) is an example of a 'non-reference stress' material condition. Analysis of this joint therefore followed the newly proposed procedure for application of the FEA based LICON method to 'non-reference stress' materials.

It has also been shown that the LICON method formulation for application to predict the creep rupture behaviour of uniaxially loaded DMWs requires further development. The original LICON method formulas assume a uniformly distributed uniaxial stress state for predicting long-time uniaxial strength values. This assumption is reasonable for homogeneous material conditions. In contrast, for a DMW, the inelastic (creep) deformation behaviour exhibited by different microstructural constituents (e.g. parent material (PM), heat affected zone (HAZ) and weld material (WM)) generates the evolution of a non-uniform multiaxial stress state.

This study therefore proposed a development for the LICON method formulation when applied for predicting uniaxial creep rupture strength of DMWs. This development considers a DMW as a multiaxial structure and accounts for the multiaxial stress state in DMW uniaxial testpieces. Application of the developed formulation for predicting creep rupture behaviour of the investigated DMW uniaxial testpieces showed an acceptable agreement with experimental observations which was not achievable without introducing the new development. It is worth mentioning that this approach is equally applicable for similar metal welds (SMW) and consideration of the developed multiaxial stress fields in SMW uniaxial testpieces is recommended for predicting the long term creep strength of SMW uniaxial testpieces using the LICON method.

5.2 Future Work

The work presented in this dissertation points to several different directions for future work. As the most important topics, the following can be mentioned:

LICON Method Application to other Materials/Joints Details of a new procedure for the consideration of FEA as the mechanical analysis part of the LICON method has been presented. Examinations for HCS 1CrMoV and P91 steels indicate that the FEA based LICON method considering the proposed procedure is successful for predicting the long term creep rupture strength of 'reference/non-reference stress' materials. Furthermore, this study proposes a new development for the LICON method formulation when it is to be applied for predicting the uniaxial creep rupture strength of DMWs (and similar metal welds, SMW). Application of the developed formulation for predicting uniaxial creep rupture behaviour of the weldment of 1CrMoV and Alloy 625 with filler metal of Alloy 617 showed an acceptable agreement with experimental observations. Examination of the proposed procedure/formulation in the LICON method application for other materials/joints in future studies can provide more confidence for the proposed procedure/formulation (or highlight a need for revision).

Revising Previous Creep Calculations This study has shown the importance of consideration of a stress regime dependent creep constitutive model for creep FEA of structures with a wide range of redistributing stresses. Consideration of the stress regime dependency of a material creep behaviour is an issue which has often been neglected in the past. Creep calculations involving the use of single regime creep models and their application to a structure exhibiting a wide range of redistributing stresses at elevated temperatures can result in non-conservative creep deformation/failure predictions, and their re-consideration is therefore important.

The same attention is required for the re-examination of calculations involving a reference stress solution for the analysis of testpieces/structures manufactured from 'non-reference stress' materials.

Estimating Low Stress Creep Behaviour of Materials The importance of consideration of a stress regime dependent creep constitutive model for analysis of structures with a wide range of redistributing stresses has been highlighted in this study. Development of a multi-regime creep model however requires creep data from both high and low stress regimes. This is a challenge for materials with limited available creep data, only from a number of

high stress (short duration) tests. This study has introduced a viable approximate solution to this challenge and described a method for the development of a multi-regime creep model (i.e. 2RN creep model) based on high stress creep and time-independent yield properties of a material. This is an important development which helps to formulate the stress regime dependent creep deformation behaviour of materials with limited available creep data (e.g. newly developed alloys). Application of the introduced approximate method for predicting the low stress creep behaviour of a 1CrMoV steel has been successfully demonstrated. Further investigation including examination of the introduced approximation for other materials is an important direction for future work.

Finite Element Continuum Damage Mechanics A successful application of FECDM for reproducing the creep deformation/damage accumulation in a series of CCI tests involving CT specimens made of a HCS 1CrMoV has been presented in this study. The introduced formulation has improved the state of the art for FECDM in the field of creep by considering stress regime dependent creep deformation/damage accumulation behaviours. FECDM has a high potential for solving complicated creep failure problems and applying the introduced formulation to other problems or its improvement is an interesting possibility for further work.

Appendix

ABAQUS/Standard Solver Scheme¹

Basic Equations for Displacement Based Finite Element Analysis

This section describes the basic equations for standard displacement-based finite element analysis. It begins with the equilibrium statement, written as the virtual work principle. Let V denote a volume occupied by a part of the body in the current configuration, and let S be the surface bounding this volume. Also, let the surface traction at any point on S be the force \mathbf{t} per unit of current area, and let the body force at any point within the volume of material under consideration be \mathbf{f} per unit of current volume. For a virtual velocity field of $\delta\mathbf{v}$ and the corresponding symmetrical virtual velocity gradient of $\delta\mathbf{D}$:

$$\int_V \boldsymbol{\sigma} : \delta\mathbf{D} \, dV = \int_S \mathbf{t}^T \cdot \delta\mathbf{v} \, dS + \int_V \mathbf{f}^T \cdot \delta\mathbf{v} \, dV \quad (\text{A.1})$$

The left-hand side of this equation (the internal virtual work rate term) is replaced with the integral over the reference volume of the virtual work rate per reference volume defined by any conjugate pairing of stress and strain rates, i.e. $\boldsymbol{\sigma}$ and $\dot{\boldsymbol{\epsilon}}$, respectively:

$$\int_{V^0} \boldsymbol{\sigma} : \delta\dot{\boldsymbol{\epsilon}} \, dV^0 = \int_S \mathbf{t}^T \cdot \delta\mathbf{v} \, dS + \int_V \mathbf{f}^T \cdot \delta\mathbf{v} \, dV \quad (\text{A.2})$$

The finite element interpolator can be written in general as:

$$\mathbf{u} = \mathbf{N}_N u^N \quad (\text{A.3})$$

¹The material in this section is adapted from ABAQUS Theory Manual, Version 6.10, 2011. Hibbit, Karlsson and Sorenson, Pawtucket, RI, USA.

where \mathbf{N}_N are interpolation functions that depend on some material coordinate system and u^N are nodal variables.

The virtual field, $\delta \mathbf{v}$, must be compatible with all kinematic constraints. Introducing the above interpolation, constrains the displacement to have a certain spatial variation, so $\delta \mathbf{v}$ must also have the same spatial form:

$$\delta \mathbf{v} = \mathbf{N}_N \delta v^N \quad (\text{A.4})$$

Now $\delta \dot{\boldsymbol{\varepsilon}}$ is the virtual rate of material strain associated with $\delta \mathbf{v}$, and because it is a rate form, it must be linear in $\delta \mathbf{v}$. Hence, the interpolation assumption gives:

$$\delta \dot{\boldsymbol{\varepsilon}} = \boldsymbol{\beta}_N \delta v^N \quad (\text{A.5})$$

where $\boldsymbol{\beta}_N$ is a matrix that depends, in general, on the current position of the material point being considered. The matrix $\boldsymbol{\beta}_N$ that defines the strain variation from the variations of the kinematic variables is derivable immediately from the interpolation functions once the particular strain measure to be used is defined. With this notation, the equilibrium equation is approximated as:

$$\delta v^N \int_{V^0} \boldsymbol{\beta}_N : \boldsymbol{\sigma} dV^0 = \delta v^N \left[\int_S \mathbf{N}_N^T \cdot \mathbf{t} dS + \int_V \mathbf{N}_N^T \cdot \mathbf{f} dV \right] \quad (\text{A.6})$$

since the δv^N are independent variables, we can choose each one to be non-zero and all others zero in turn, to arrive at a system of nonlinear equilibrium equations:

$$\int_{V^0} \boldsymbol{\beta}_N : \boldsymbol{\sigma} dV^0 = \int_S \mathbf{N}_N^T \cdot \mathbf{t} dS + \int_V \mathbf{N}_N^T \cdot \mathbf{f} dV \quad (\text{A.7})$$

This system of equations forms the basis for the displacement-based finite element (static) analysis procedure and is of the form:

$$F^N(u^M) = 0 \quad (\text{A.8})$$

For the Newton algorithm used in ABAQUS/Standard, the Jacobian of the finite element equilibrium equations is required. For a material with constitutive behaviour in the form of $\boldsymbol{\sigma} = \mathbf{H} : d\boldsymbol{\varepsilon}$, the Jacobian is:

$$\frac{\partial F^N}{\partial u^P} = \int_{V^0} \boldsymbol{\beta}_N : \mathbf{H} : \boldsymbol{\beta}_P dV^0 + \int_{V^0} \boldsymbol{\sigma} : \frac{\partial \boldsymbol{\beta}_N}{\partial u^P} dV^0 - \int_S \mathbf{N}_N^T \cdot \mathbf{Q}_P^S dS - \int_V \mathbf{N}_N^T \cdot \mathbf{Q}_P^V dV \quad (\text{A.9})$$

where assuming $A_r = \left| \frac{dS}{ds_0} \right|$ and $J = \left| \frac{dV}{dV_0} \right|$:

$$\mathbf{Q}_P^S = \frac{\partial \mathbf{t}}{\partial u^P} + \mathbf{t} \frac{1}{A_r} \frac{\partial A_r}{\partial u^P} \quad (\text{A.10})$$

$$\mathbf{Q}_P^V = \frac{\partial \mathbf{f}}{\partial u^P} + \mathbf{f} \frac{1}{J} \frac{\partial J}{\partial u^P} \quad (\text{A.11})$$

Thus, equation A.7 and equation A.9 provide the basis for the Newton incremental solution, given specification of the interpolation function and constitutive theories to be used.

Nonlinear Solution Method in ABAQUS/Standard

The finite element models generated in ABAQUS are usually nonlinear and can involve from a few to thousands of variables. In terms of these variables, the equilibrium equations obtained by discretizing the virtual work equation can be written symbolically as:

$$F^N(u^M) = 0$$

where F^N is the force component conjugate to the N^{th} variable in the problem and u^M is the value of the M^{th} variable. The basic problem is to solve the equation for the u^M throughout the history of interest.

ABAQUS/Standard generally uses the following method for solving the nonlinear equilibrium equations. Many of the problems to which ABAQUS will be applied are history-dependent, so the solution must be developed by a series of 'small increments'.

Let $\{^1u^M, ^2u^M, \dots, ^{n-1}u^M\}$ be the solution for equilibrium equation in increments $\{1, 2, \dots, n-1\}$. As an initial guess for the first iteration, ABAQUS assumes $^n u^{M,1} = ^{n-1}u^M$. The force residual for this approximation is:

$$^n F^N(^n u^{M,1}) = ^n F^{N,1} \quad (\text{A.12})$$

The difference between $^n u^{M,1}$ and the exact solution to the discrete equilibrium equation can be approximated from the first order Taylor series:

$$\begin{aligned} c^{M,1} &= - \left[\frac{\partial ^n F^N}{\partial ^n u^P} \right]^{-1} ^n F^{N,1} \\ &= - \left[^n K^{NP,1} \right]^{-1} ^n F^{N,1} \end{aligned} \quad (\text{A.13})$$

If all force residuals, ${}^n F^{N,1}$, and all corrections to the displacements, $c^{M,1}$, are sufficiently small, the solution converges for increment n and a new increment can start, otherwise further iterations for the current increment are required where:

$${}^n u^{M,i+1} = {}^n u^{M,i} + c^{M,i} \quad (\text{A.14})$$

The determination of the Jacobian matrix inverse, $[K^{NP}]^{-1}$, is usually an expensive process. Therefore, while the Newton's method forms and solves it at each iteration, the modified-Newton method recalculates it only occasionally and Quasi-Newton method approximates the inverse Jacobian by an iterational process. The approximation involved in Jacobian calculations does not affect the accuracy of the numerical analysis and only determine the rate of convergence to the solution.

The issue of choosing suitable increment size is also a difficult problem. ABAQUS/Standard provides both 'automatic' choice and direct user control. The automatic schemes in ABAQUS/Standard are based on extensive experience with a wide range of problems and, therefore, generally provide a reliable approach. ABAQUS/Standard uses a scheme based predominantly on the maximum force residuals following each iteration. By comparing consecutive values of these quantities, ABAQUS/Standard determines whether convergence is likely in a reasonable number of iterations. If convergence is deemed unlikely, ABAQUS/Standard adjusts the increment size to a smaller value. If convergence is deemed likely, ABAQUS/Standard continues with the iteration process. In this way excessive iteration is eliminated in cases where convergence is unlikely, and an increment that appears to be converging is not aborted because it needed a few more iterations (there are several other ingredient based on empirical testing in this algorithm controlling the increment size).

Mechanical Constitutive Models

From a numerical viewpoint, the implementation of a constitutive model involves the integration of the state of the material at an integration point over a time increment during a nonlinear analysis. An estimate of the kinematic solution to the problem at the point under consideration (i.e. the strain increments, $\Delta\varepsilon$) is passed to the constitutive routine. The constitutive routine obtains the state at the point under consideration at the start of the increment from the 'material point data base' (i.e. stress or accumulated inelastic strains). The function of constitutive routine then is to update the state to the end of the increment. The mechanical constitutive models that are provided in ABAQUS often consider elastic and inelastic response. The inelastic response is most commonly modelled with rate-independent

and rate-dependent plasticity (with and without yield surfaces models).

Rate Independent Isotropic Plasticity with Yield Surface

This material model is very commonly used for metal plasticity calculations and has a particularly simple form. Because of this simplicity, the algebraic equations associated with integrating the model are easily developed in terms of a single variable.

From the estimated kinematic solution, it is possible to define the volumetric and deviatoric strain components:

$${}^n \varepsilon_{\text{vol}}^i = \text{Trace}({}^{n-1} \varepsilon + {}^n \Delta \varepsilon^i) \quad (\text{A.15})$$

$${}^n e^i = ({}^{n-1} \varepsilon + {}^n \Delta \varepsilon^i) - \frac{1}{3} {}^n \varepsilon_{\text{vol}}^i \mathbf{I} \quad (\text{A.16})$$

with a knowledge of the material bulk modulus, K , and the shear modulus, G , hydrostatic and deviatoric stress components are:

$${}^n \sigma_h^i = K {}^n \varepsilon_{\text{vol}}^i \quad (\text{A.17})$$

$$\begin{aligned} {}^n S^i &= 2G {}^{n-1} e_{el}^i \\ &= 2G ({}^n e^i - {}^{n-1} \varepsilon_{pl} - {}^n \Delta \varepsilon_{pl}^i) \end{aligned} \quad (\text{A.18})$$

While hydrostatic stress can be explicitly calculated in equation A.17, the determination of the deviatoric part of stress matrix requires defining the increment of plastic strain. The flow rule can be written as:

$$d\varepsilon_{pl} = \frac{3S}{2q} d\bar{\varepsilon}_{pl} \quad (\text{A.19})$$

where $q = \sqrt{\frac{3}{2} S : S}$ and $\bar{\varepsilon}_{pl}$ are the von Mises effective stress and plastic strain. Application of the backward Euler method to the flow rule gives:

$${}^n \Delta \varepsilon_{pl}^i = \frac{3 {}^n S^i}{2 {}^n q^i} {}^n \Delta \bar{\varepsilon}_{pl}^i \quad (\text{A.20})$$

Combination of equations A.18 and A.20 gives:

$$\left(1 + \frac{3G}{{}^n q^i} {}^n \Delta \bar{\varepsilon}_{pl}^i\right) {}^n S^i = 2G {}^n e^i \quad (\text{A.21})$$

where ${}^n\tilde{\epsilon}^i = {}^n\epsilon^i - {}^{n-1}\epsilon_{pl}$. Taking the inner product of this equation with itself gives:

$${}^nq^i + 3G {}^n\Delta\tilde{\epsilon}_{pl}^i = 3G {}^n\tilde{\epsilon}^i \quad (\text{A.22})$$

where ${}^n\tilde{\epsilon}^i = \sqrt{\frac{2}{3}} {}^n\hat{\epsilon}^i$. The von Mises equivalent stress, ${}^nq^i$, must satisfy the yield function in the form of ${}^nq^i = {}^n\bar{\sigma}_{pl}^i = \bar{\sigma}({}^n\tilde{\epsilon}_{pl}^i)$:

$$3G ({}^n\tilde{\epsilon}^i - {}^n\Delta\tilde{\epsilon}_{pl}^i) - {}^n\bar{\sigma}_{pl}^i = 0 \quad (\text{A.23})$$

This is a nonlinear equation for ${}^n\Delta\tilde{\epsilon}_{pl}^i$ and the solution with the Newton's method is:

$$\{{}^nc_i^{pl}\}^j = \frac{3G ({}^n\tilde{\epsilon}^i - \{{}^n\Delta\tilde{\epsilon}_{pl}^i\}^j) - \{{}^n\bar{\sigma}_{pl}^i\}^j}{3G + \{{}^nH^i\}^j} \quad (\text{A.24})$$

$$\{{}^n\Delta\tilde{\epsilon}_{pl}^i\}^{j+1} = \{{}^n\Delta\tilde{\epsilon}_{pl}^i\}^j + \{{}^nc_i^{pl}\}^j \quad (\text{A.25})$$

where $H = \frac{d\bar{\sigma}}{d\tilde{\epsilon}_{pl}}$. These are local material point iterations and are not the same as the global equilibrium iterations. The iteration should continue until convergence is achieved. Once ${}^n\Delta\tilde{\epsilon}_{pl}^i$ is known, the solution for current (global) iteration is fully defined.

Rate Dependent Isotropic Plasticity without Yield Surface

The rate-dependent plasticity models provided in ABAQUS/Standard are used to model inelastic straining of materials that are rate sensitive. High temperature creep in structures is one important class of examples of the application of such material models.

Explicit Formulation Because creep problems generally involve relatively small amounts of inelastic straining (otherwise the structure is not a suitable design), the explicit, forward Euler method is often satisfactory as an integrator for the flow rule. This method is only conditionally stable, but the stability limit is usually sufficiently large compared to the time history of interest. In such cases that the explicit method is very economical.

In the explicit scheme the creep strain rate for any iteration during the time increment is defined in terms of (known) quantities at the beginning of the increment. Thus, an explicit integration would lead to the following incremental form:

$${}^nS^i = D^{el} : \left[{}^n\epsilon^i - {}^{n-1}\epsilon_{pl}^i - {}^n\Delta t \quad {}^{n-1}\dot{\epsilon}_{pl}^i \right] \quad (\text{A.26})$$

All of the terms on the right-hand side of this equation are known when the constitutive integration is done, so these equations define ${}^n S^i$ explicitly and no local iterations are needed.

Implicit Formulation There also exist many problems involving rate-dependent plastic response in which it can be more economical to use the implicit method. ABAQUS always uses the implicit method for high strain rate applications and in all geometrically nonlinear problems and in problems for which rate-independent plasticity is active simultaneously. The followings describe implicit formulation used by ABAQUS/Standard for rate-dependent (only) isotropic plasticity.

From the last section:

$$\begin{aligned} {}^n \sigma_h^i &= K {}^n \varepsilon_{\text{vol}}^i \\ {}^n S^i &= 2G ({}^n e^i - {}^{n-1} \varepsilon_{pl} - {}^n \Delta \varepsilon_{pl}^i) \end{aligned}$$

For incompressible creep with von Mises stress potential assumption:

$$\dot{\varepsilon}_{pl} = \frac{3S}{2q} \dot{\varepsilon}_{cr} \quad (\text{A.27})$$

where $\dot{\varepsilon}_{cr}$ is the 'equivalent creep strain rate'. Backward Euler integration gives:

$${}^n \Delta \varepsilon_{pl}^i = \frac{3 {}^n S^i}{2 {}^n q^i} {}^n \Delta \varepsilon_{cr}^i \quad (\text{A.28})$$

where ${}^n \Delta \varepsilon_{cr}^i = {}^n \Delta t {}^n \dot{\varepsilon}_{cr}^i$. Considering ${}^n \Delta \varepsilon_{cr}^i = h_c({}^n q^i, {}^n \varepsilon_{cr}^i, \dots)$, the implicit integration scheme leads to a nonlinear equation for the creep strain increment, ${}^n \Delta \varepsilon_{cr}^i$, that is solved by ABAQUS iteratively at each material point. The solution with the Newton's method is:

$$\{ {}^n c_i^{cr} \}^j = \left[\frac{\partial h_c}{\partial \Delta \varepsilon} |_{{}^n q^i, {}^n \varepsilon_{cr}^i, \dots} \right]^{-1} \{ h_c({}^n q^i, {}^n \varepsilon_{cr}^i, \dots) \}^j \quad (\text{A.29})$$

$$\{ {}^n \Delta \varepsilon_{cr}^i \}^{j+1} = \{ {}^n \Delta \varepsilon_{cr}^i \}^j + \{ {}^n c_i^{pl} \}^j \quad (\text{A.30})$$

These are local material point iterations and are not the same as the global equilibrium iterations. The iteration should continue until convergence is achieved. Once ${}^n \Delta \varepsilon_{cr}^i$ is known, the solution for current (global) iteration is fully defined.

Irrespective of the integration scheme used to integrate the rate form of the creep equation,

the creep constitutive routine is called at each material point once at the beginning and once at the end of each increment. These calls are for the purpose of getting the creep strain increment based on the creep strain rate at the beginning and at the end of the increment, respectively.

$$|{}^n\dot{\epsilon}_{cr} - {}^{n-1}\dot{\epsilon}_{cr}| {}^n\Delta t \leq \text{CETOL} \quad (\text{A.31})$$

The difference between these two creep strain increment values measures the accuracy of the integration scheme and must be less than the value specified with the CETOL parameter on the relevant analysis step option.

Curriculum Vitae

Ehsan Hosseini

Date of birth May 2nd 1985
Citizen of Iran



Education

2003–2007 BSc, Faculty of Metallurgical and Materials Engineering, Semnan University, Semnan, Iran

2007–2009 MSc, Department of Materials Science and Engineering, Sharif University of Technology, Tehran, Iran

2009 Internship, School of Architecture, Civil and Environmental Engineering, , École Polytechnique Fédérale de Lausanne (EPFL), Lausanne, Switzerland

2009–2013 PhD, Department of Mechanical and Process Engineering, Eidgenössische Technische Hochschule Zürich (ETHZ), Zürich, Switzerland

Department of Mechanics for Modelling and Simulation, High Temperature Integrity, Eidgenössische Materialprüfungs und Forschungsanstalt (Empa), Dübendorf, Switzerland

Refereed Journal Publications

1. E. Hosseini, S.R. Holdsworth, E. Mazza. Exploring the applicability of the LICON methodology for the creep assessment of a dissimilar metal weld. *International Journal of Pressure Vessels and Piping*, doi: 10.1016/j.ijpvp.2013.07.003, 2013.
2. E. Hosseini, S.R. Holdsworth, E. Mazza. The LICON methodology for predicting long time uniaxial creep rupture strength of materials. *International Journal of Pressure Vessels and Piping*, doi: 10.1016/j.ijpvp.2013.04.033, 2013.
3. E. Hosseini, S.R. Holdsworth, E. Mazza. Stress regime dependent creep constitutive model consideration in finite element continuum damage mechanics. *International Journal of Damage Mechanics*, doi: 10.1177/1056789513479810, 2013.
4. E. Hosseini, S.R. Holdsworth, E. Mazza. Creep constitutive model considerations for high temperature finite element numerical simulations. *The Journal of Strain Analysis for Engineering Design*, 47(6):341–349, 2012.
5. E. Hosseini, S.R. Holdsworth, E. Mazza. Experience with using the LICON methodology for predicting long term creep behaviour in materials. *International Journal of Pressure Vessels and Piping*, 92:70–76, 2012.
6. E. Hosseini, M. Kazeminezhad. A new microstructural model based on dislocation generation and consumption mechanisms through severe plastic deformation. *Computational Materials Science*, 50(3):1123–1135, 2011.
7. E. Hosseini, M. Kazeminezhad. Implementation of a constitutive model in finite element method for intense deformation. *Materials and Design*, 32(2):487–494, 2011.
8. E. Hosseini, M. Kazeminezhad. Integration of physically based models into FE analysis: homogeneity of copper sheets under large plastic deformations. *Computational Materials Science*, 48(1):166–173, 2010.
9. M. Kazeminezhad, E. Hosseini. Optimum groove pressing die design to achieve desirable severely plastic deformed sheets. *Materials and Design*, 31(1):94–103, 2010.
10. M. Kazeminezhad, E. Hosseini. Modelling of induced empirical constitutive relations on materials with FCC, BCC, and HCP crystalline structures: severe plastic deformation. *The International Journal of Advanced Manufacturing Technology*, 47(9–12):1033–1039, 2010.
11. E. Hosseini, M. Kazeminezhad. A dislocation based model considering free surface theory through HPT process: nanostructured Ni. *Scientia Iranica Transaction F: Nanotechnology*, 17(1):52–59, 2010.
12. E. Hosseini, M. Kazeminezhad. Nanostructure and mechanical properties of 0–7 strained aluminium by CGP: XRD, TEM and tensile test. *Materials Science and Engineering: A*, 526(1–2):219–224, 2009.
13. E. Hosseini, M. Kazeminezhad. ETMB model investigation of flow softening during severe plastic deformation. *Computational Materials Science*, 46(4):902–905, 2009.

14. E. Hosseini, A. Habibollahzadeh, M. Erfanmanesh, H. Mostajabodave, M. Kazeminezhad. Influence of deformation during T10 treatment on microstructure/hardness/electrical conductivity of Cu–Cr alloy produced in non protected atmosphere. *Materials Science and Technology*, 25(10):1283–1288, 2009.
15. E. Hosseini, A. Mani, E. Rafizadeh, M. Kazeminezhad. On the evolution of flow stress during constrained groove pressing of pure copper sheet. *Computational Materials Science*, 45(4):855–859, 2009.
16. E. Hosseini, M. Kazeminezhad. Dislocation structure and strength evolution of heavily deformed tantalum. *International Journal of Refractory Metals and Hard Materials*, 27(3):605–610, 2009.
17. E. Hosseini, M. Kazeminezhad. Stress based model on work hardening and softening of materials at large strains: corrugation process of sheet. *Journal of Materials Science*, 44(5):1212–1218, 2009.
18. E. Hosseini, M. Kazeminezhad. A hybrid model on severe plastic deformation of copper. *Computational Materials Science*, 44(4):1107–1115, 2009.
19. E. Hosseini, M. Kazeminezhad. The effect of ECAP die shape on nanostructure of materials. *Computational Materials Science*, 44(3):962–967, 2009.
20. M. Kazeminezhad, E. Hosseini. Coupling kinetic dislocation model and Monte Carlo algorithm for recrystallized microstructure modeling of severely deformed copper. *Journal of Materials Science*, 43(18):6081–6086, 2008.

Nomenclature

Terms	Meanings
2RN	Two-regime Norton creep model
2RSinh	Two-regime hyperbolic sine creep model
3D	Three-dimensional
Δa	Crack extension
a_0	CT testpiece crack length
a_1, a_2	Constant values in creep models
A, A', A''	Constant values in the LICON method formulation
A_1, A_2	Constant values in creep models
\bar{b}	Burger's vector
b, b_1, b_2, b_3	Constant values in creep models
b_{Cob}, b_{N-H}	Constant values in creep models
B, B_1, B_2	Constant values in creep models
B_n	CT testpiece net section
BSD	Backscatter diffraction
BSE	Backscattered electron
$c, c_0, c_1, c_2, c_3, c_4, c_5$	Constant values in creep models
C, C_1, C_2, C_3, C_4	Constant values in creep models
C^*	Parameter characterising creep stress and strain rate fields at the tip of crack
CDM	Continuum damage mechanics
CCI	Creep crack incubation
CCG	Creep crack growth
CGHAZ	Coarse grained HAZ
CT	Compact tension (specimen)
d	Grain size
D_{gb}, D_l	Coefficients for grain boundary and lattice diffusions
DC	Direct current
DMW	Dissimilar metal weld
DCPD	Direct current potential drop
E, E_0	Elastic moduli
EBSD	Electron backscatter diffraction
ECC	Electron channelling contrast
ECCC	European creep collaborative committee
F	Force
FE, FEA	Finite element, finite element analysis
FECDM	Finite element continuum damage mechanics
FGHAZ	Fine grained HAZ
FL	Fusion line
H, H_{CT}, H_{DMW}	Stress multiaxiality factor ($\sigma_1/\bar{\sigma}$), for CT specimen, for DMW uniaxial specimen
$\mathcal{H}, \mathcal{H}^*$	State variable representing primary creep, saturated value for \mathcal{H}
HAZ	Heat affected zone
HCS	High creep strength
HL	Hexahedral linear (element)

Terms	Meanings
HP	High pressure
HQ	Hexahedral quadratic (element)
IP	Intermediate pressure
ISM	Initial strain method
k	Boltzmann's constant
k_1	Constant value in Wilshire–Scharning model
K	Stress intensity factor
K_{ro}, K'_{ro}	Constant values in Ramberg–Osgood model
l, l_0	Interparticle distance, initial interparticle distance
l_g	Gauge length
L_i	Length of different material sections in DMW
LMP	Larson–Miller parameter
LP	Limit of proportionality
LPD	Load point displacement of CT specimen
MHP	Manson–Haferd Parameter
m	Exponent in Monkman–Grant relationship
m^*	Yield load ratio of the CT testpiece
n, n_1, n_2	Stress exponents in creep models
n_{ro}	Constant value in Ramberg–Osgood model
N	Constant value in creep models
NB	Norton–Bailey creep model
OSDP	Orr–Sherby–Dorn Parameter
p	Constant in creep damage equation
P	Load
P_L	Collapse load
PM	Parent material
PWHT	Post weld heat treatment
q	Constant value in creep damage equation
Q	Activation energy
Q_c	Activation energy for creep
Q_{BD}, Q_{CD}, Q_{SD}	Activation energies for grain boundary, dislocation core and self diffusion
R	Universal gas constant
$R_{p0.2}$	0.2% proof stress
R_m	Tensile strength
RVE	Representative volume element
S	Surface
SEM	Electron scanning microscopy
SM	Soviet model
SMCM	Simplified minimum commitment model
SMW	Similar metal weld
SP	Small punch (test)
S_{ij}	Deviatoric stress tensor components
Sinh+N	Hyperbolic sine + Norton creep model
$t, t_r, t_{i,x}$	Time, time to rupture, time to crack initiation (for crack initiation criterion x)

Terms	Meanings
$t_f, t_{f1}, t_{f2}, t_{fi}$	Times to failure (rupture)
t_{red}	Redistribution time
T, T_m	Temperature, melting temperature
TQ	Tetrahedral quadratic (element)
TL	Tetrahedral linear (element)
u	Constant value in Wilshire–Scharning model
V	Atomic volume
V_P	Volume fraction of precipitates
W	CT testpiece width
WM	Weld material
WSF	Weld strength factor
x-weld	Cross-weld
α	Constant value in creep models
δ	Effective width of grain boundary for vacancy diffusion
$\gamma, \gamma', \gamma''$	Stress multiaxiality exponents in the LICON method formulation
γ_2	Constant value in creep models
ε_0	Instantaneous strain in constant load uniaxial tensile test
$\varepsilon, \varepsilon_r$	Accumulated creep strain, creep rupture strain
ε_p	Accumulated plastic strain
$\dot{\varepsilon}, \dot{\varepsilon}$	Creep strain rate, von Mises equivalent creep strain rate
$\dot{\varepsilon}_0$	Stress independent strain rate coefficient
$\dot{\varepsilon}_{ij}$	Creep strain rate tensor components
$\dot{\varepsilon}_{Cob}, \dot{\varepsilon}_{Dis}, \dot{\varepsilon}_{N-H}$	Creep strain rates corresponding to Coble, dislocation climb/glide and Nabarro-Herring creep mechanisms
$\dot{\varepsilon}_s$	Steady-state creep strain rate
θ_{1-4}	Constants in Theta projection method
ν_1, ν_2, ν_i	Constant values in creep models
ν, ν', ν''	Stress exponents in the LICON method formulation
σ	Stress
σ_0	Initial stress (in constant load uniaxial test)
σ_1	Maximum principal stress
σ^*	Stress associated with deformation mechanism change in creep constitutive models
σ_i	Internal stress
σ_{LP}	Limit of proportionality (stress)
σ_{ref}	Deformation reference stress
σ_{ref}^r	Rupture reference stress
σ_y	Yield stress
$\bar{\sigma}, \bar{\sigma}_{CT}$	Von Mises equivalent stress, for CT specimen
φ	State variable representing interparticle distance
$\Phi, \Phi_i, \Phi_c, \Phi_s, \Phi_t$	General, initial, creep, stationary and transient deformation parameters
χ	Stress concentration factor
ω, ω_{max}	State variable representing creep damage (cavitation), ω value for a failed material
Ω	Constant in Omega method formulation

